University of Bath

PHD

On-line monitoring and control of the injection moulding process

Fronimidis, Dimitris

Award date:
2007

Awarding institution:
University of Bath

Link to publication

Alternative formats
If you require this document in an alternative format, please contact:
openaccess@bath.ac.uk

Copyright of this thesis rests with the author. Access is subject to the above licence, if given. If no licence is specified above, original content in this thesis is licensed under the terms of the Creative Commons Attribution-NonCommercial 4.0 International (CC BY-NC-ND 4.0) Licence (https://creativecommons.org/licenses/by-nc-nd/4.0/). Any third-party copyright material present remains the property of its respective owner(s) and is licensed under its existing terms.

Take down policy
If you consider content within Bath's Research Portal to be in breach of UK law, please contact: openaccess@bath.ac.uk with the details. Your claim will be investigated and, where appropriate, the item will be removed from public view as soon as possible.

Download date: 05. May. 2023

ON-LINE MONITORING AND CONTROL OF THE INJECTION MOULDING PROCESS

Dimitris Fronimidis
A thesis submitted for the degree of Doctor of Philosophy
University of Bath
Department of Mechanical Engineering
January 2007

COPYRIGHT

Attention is drawn to the fact that copyright of this thesis rests with its author. This copy of the thesis has been supplied on condition that anyone who consults it is understood to recognise that its copyright rests with its author and no information derived from it may be published without the prior written consent of the author. This thesis may be made available for consultation within the University library and may be photocopied or lent to other libraries for the purposes of consultation.

UMI Number: U221340

All rights reserved

INFORMATION TO ALL USERS
The quality of this reproduction is dependent upon the quality of the copy submitted.

In the unlikely event that the author did not send a complete manuscript
and there are missing pages, these will be noted. Also, if material had to be removed,
a note will indicate the deletion.

UMI U221340
Published by ProQuest LLC 2013. Copyright in the Dissertation held by the Author.
Microform Edition © ProQuest LLC.
All rights reserved. This work is protected against
unauthorized copying under Title 17, United States Code.

ProQuest LLC
789 East Eisenhower Parkway
P.O. Box 1346
Ann Arbor, MI 48106-1346

UNIVERSITY OF BATH
LIBRARY
65 - 4 JUL 2007
PhD

Abstract

Production of quality injection moulded parts is a complex task that requires a deep understanding of the interaction between machine settings and in-mould parameters. This thesis reports on the monitoring of the polymer dynamics during the injection cycle and proposes an effective control scheme for the process.

The study is focused on an Arburg 25-tonne injection moulding machine which is hydraulically-actuated. For the modelling and simulation of the filling and packing phases, the dynamics of both the machine's hydraulic circuit and the polymer (polypropylene) behaviour were investigated. The simulations were validated on a modified version of the injection moulding machine in which a specially instrumented mould was used.

To assess the extent of solidification of the part and identify phase changes during the cycle, two monitoring methods were studied. One makes use of ultrasound transducers while the other utilizes fast-response thermocouples. Both methods were found to enhance the control of the process. The ultrasound feedback provided sufficient information for quick set up of the controller in real time.

A hybrid minimal controller synthesis (MCS) controller was developed and evaluated experimentally for the closed-loop control of flow and pressure trajectories. The algorithm does not require a priori information about the plant dynamics. To reduce the MCS sensitivity to noise in the feedback signals, a modification of the MCS is proposed and validated. This approach is shown to enhance the performance of the machine.

A major disadvantage in conventional moulding is the difficulty in influencing the molecular orientation at the core. Vibration of the melt polymer has been applied by previous researchers, by means of additional injection cylinders, because control of fast-acting screw dynamics could not be achieved with conventional control methods. A new method is proposed here, where vibration of the screw in a conventional moulding machine is controlled by the hybrid MCS algorithm.

The mechanical properties of tensile specimens produced with vibration were compared with parts produced by conventional moulding. They show significant improvements; part warpage is reduced by up to 30% and tensile modulus is increased by around 10%.

Acknowledgements

The pursuit of this PhD has been a remarkable experience. Looking back in time, it can be realised that this work was the result of a team effort, involving coordination of many groups of people. Without their help and dedication to academics, it would not be possible to accomplish this target. There were happy and difficult moments during this project, but the support of my friends and supervisors helped me to overcome these problems. It was an experience that matured me as a person, through the interaction with people from different countries. Apart from the academic knowledge that I gained during my PhD, there were many other joyful things to remember from the academic life. I believe that a PhD is a remarkable experience which you have to go through, in order to appreciate the rewarding for your effort.

First of all I would like to thank all my supervisors, Professor Kevin Edge, Professor Tony Mileham, Professor Kim Stelson and Dr. Matija Sokola for their advice, input and support during my PhD.

I would like personally to thank my principal supervisor Professor Kevin Edge for his professional guidance and advice in the direction of the Thesis. I am really grateful to him for the understanding and patience that he showed during the years of my PhD. I would like to thank him again for reading my PhD thesis and giving me very constructive comments.

My sincere thanks to my supervisor, Professor Kim Stelson from University of Minnesota for his guidance on setting up the foundations of this research project, in the first year of my PhD.

I am grateful to my supervisor, Professor Tony Mileham for his support and input as an expert in the manufacturing systems.

In particular, special thanks go to my supervisor, Dr. Matija Sokola for his guidance and support during my years as a MSc and PhD student. Without his encouragement this PhD journey would have not started. I am grateful to him.

I would like to thank Steve Nightingale from *Moog Inc.* for supplying us with the P-Q Servo-

Proportional Valve for the injection moulding machine.

I am grateful to Professor Victor Humphrey and his team, from the Physics Department, for the provided ultrasound equipment and technical advice.

I would like to thank all the instrumentation team and especially Vijay Rajput and Jeffrey Brewster, for their input for building the data acquisition systems. Without their help it would not be possible to carry out the experimental part of this project.

I would like to thank the manufacturing lab team, Andrew Green and Robert Pepler for their help and assistance with the injection moulding machine.

My sincere thanks to my colleague, Mr Andrey Gizatullin who introduced me to the MCS control. Andrey has been a wonderful colleague and friend to all of us here at the department. I wish him great success in his life and career.

I would like to thank Yiannis Vassilopoulos from the Electrical Engineering Department, for his guidance with the Matlab Signal Processing Toolbox.

I am grateful to my uncle Dimitris and my auntie Anita, for their support and encouragement during my PhD. My uncles advice, helped me to get through many difficult situations.

My sincere thanks to Mother Sarah from the Chaplaincy Centre for her spiritual support and guidance. I would like to thank her for her advice, she has been a really good friend during my PhD.

I am really grateful to my fiancee Ellada for her determination and support during the writing of my PhD thesis.

My sincere gratitude to all the staff members of the department of the Mechanical Engineering and the University, including librarians, security, accommodation and catering staff.

Last but not least, I would like to thank my parents for being next to me during my journey as a PhD student. My sincere thanks to my mother for her encouragement, love and affection. I believe that my parents deserve to be honored for what I have achieved in my life up to this moment. Therefore I would like to dedicate this PhD thesis to my parents Lia and Yiannis.

Contents

List of Figures

List of Tables

Abbreviations

Chapter 2

A_1	Effective piston area 1
A_2	Effective piston area 2
A_s	Injection screw area
A_1, A_2, D_1	Cross - WLF model constants
D, D_3	Cross - WLF model constants
A_b	Area of injection barrel
β	Hydraulic Oil bulk Modulus
β_p	Bulk modulus of polymer
b_{3m}, b_{4m}	Constant parameters for the Tait pvT equation
b_{3s}, b_{3m}	Constant parameters for the Tait pvT equation
b_5, b_6	Constant parameters for the Tait pvT equation
C	Consistency factor of power law model
C_{Tait}	Universal constant - Tait pvT equation
γ_α	Apparent shear rate
ΔP	Pressure drop at a flow path section
ΔP_T	Pressure drop across the geometrical sections of mould and nozzle
F_{frict}	Friction force
F_c	Filter coefficient of first order filter
h	Thickness of flow path channel
K_{sv}	Servo-valve gain
K_{QX}	Valve's flow spool displacement coefficient
K_{QP}	Valve's flow pressure coefficient
K_{Plant}	Hydraulic plant gain
K_{fb}	Inner feedback loop coefficient
K_v	Servo-valve flow gain
K_{body}	Flow gain for the servo-valve body
K_{man}	Flow gain for the manifold body

k_s	Spring load stiffness (equivalent stiffness of the system)
k_{visc}	Viscous friction coefficient
L	Length of flow path channel
M_{pist}	Hydraulic actuator piston mass
M_{load}	Load mass
η_a	Apparent viscosity
η_0	Zero-shear rate viscosity
n	Power law index
P	Pressure
P_L	Load pressure
P_s	Supply line pressure
P_R	Return pressure line
P_S	System pressure
P_{L_0}	Load Pressure at linearization point
P_n	Pressure drop along the nozzle
p	Pressure
P_1, P_2	Pressures at the inlet and outlet of flow path channel
Q	Injection polymer flow rate
Q_1, Q_2	Inlet and outlet hydr. actuator ports flow rates
Q_r	Rated valve flow
Q_{leak}	Cylinder cross piston leakage flow
Q_{cpb}	Cross port bleed flow
Q_p	Polymer flow in the cavity
Q_{leak}	Polymer leakage past the screw
Q_{cav}	Additional flow of polymer in the cavity during packing
R, R_1, R_2	Radius of flow path channels
R_x	Instantaneous value of radius
T_g	Glass transition temperature
T_{sp}	Servo-valve time constant
T	Width of flow channel
τ	Shear stress
τ_w	Shear stress at the wall
$\bar{u}$	Dimensionless servo-valve control signal
V_1	Trapped fluid volume in cylinder chamber 1
V_2	Trapped fluid volume in cylinder chamber 2
V_0	Trapped fluid volume in cylinder chamber ($V_1 = V_2$)
V_t	Volume in the cavity at the end of packing phase
V_{cav}	Volume in the cavity at the end of filling phase
V_{pack}	Additional volume injected during the packing phase
V_b	Volume of polymer inside the barrel
V_{b_0}	Initial volume of polymer inside the barrel

$V(T,p)$	Specific volume - Tait pvT equation
X_f, X_{in}	Output and input signals from/to first order filter
x_{max}	Screw maximum stroke
x_0	Screw initial position at the start of injection
x_{sp_0}	Spool displacement at linearization point
x_{sp}	Dimensionless spool position
X_{ff}	Flow-front position
x	length
y	Road position
ζ_{sp}	Damping ratio of servo-valve
ζ_p	Hydraulic plant damping ratio
ω_{sp}	Natural frequency of the servo-valve
ω_p	Hydraulic plant natural frequency

Chapter 3

A_p	Area of the moulded plate (cavity)
A_m	Area of the mould
α	Thermal diffusivity of material
A_{cav}	Area of the cavity
α_m	Thermal diffusivity of the mould material
A	Attenuation coefficient of sound waves
β	Volumetric thermal expansion coefficient
b_{pen}	Coefficient of Heat Penetration
b_{pen_m}	Coefficient of Heat Penetration for mould
b_{pen_p}	Coefficient of Heat Penetration for polymer
b	Half thickness of the moulded part
c	Velocity of sound
c_{av}	Average wave velocity
c_l	Longitudinal wave velocity
c_m	Specific Heat of mould
c_p	Specific Heat
C	Constant for isothermal surfaces
C_l	Thermal Capacitance of the lamped mass
Δx	Depth of Heat Penetration
Δx_m	Half thickness of the mould
ΔT	Temperature Difference
d	Thickness of the media that waves propagate through

D	Transmission coefficient of sound waves at the interface
E	Modulus of Elasticity
f	Sound frequency
G	Shear Modulus of the material
Gr	Grashof Number
g	Acceleration of gravity
h	Convection heat transfer coefficient
k	Thermal Conductivity
k_m	Thermal Conductivity of the mould
K	Bulk Modulus of material
λ	Wave length of sound wave
L	Characteristic length
L_H	Latent Heat of crystalline polymers
L_1, L_2	Lamped masses one and two
M	Mass
m	Constant for isothermal surfaces
Nu	Nusselt Number
p	Sound pressure of the wave
Pr	Prandtl Number
q	Heat Flux
Q	Heat transferred
Q_{ov}	Overall free convection heat loss
R_{L1-L2}	Thermal resistance between the two lumps masses
R_{m-L1}	Thermal resistance between the mould and the first lump mass
R_c	Thermal convective resistance at mould-polymer interface
R	Reflection coefficient of sound waves at the interface
ρ	Density of material
ρ_m	Density of mould
Ra	Rayleigh Number
T_f	Film temperature
T_∞	Quiescent temperature
T_e	Part ejection temperature
T_m	Temperature of the melt polymer
T_s	Temperature of the solidified polymer
T_w	Temperature at the mould wall
t_{cool}	Cooling time of the part
T_i	Temperature at the mould-polymer interface
t_t	Transient time for the heat to penetrate at depth
T_{solid}	Temperature at the solidified layer of the polymer
T_{liquid}	Temperature at the liquid layer of the polymer
t	Time for the sound wave to propagate through media of thickness d

t_{al}	Time for the sound wave to propagate through the aluminium mould
t_{cav}	Time for the sound wave to propagate through the mould cavity
t_{var}	Variation of sound wave speed through the mould during the injection cycle
t_{max}	Time of sound to propagate through mound at the beginning of cycle
t_{min}	Time of sound to propagate through mound at the end of cycle
T_1	Temperature data from thermocouple close (5mm depth) to the cavity surface
T_2	Temperature data from thermocouple close (15mm depth) to the cavity surface
u_s	Specific internal energy at the solidified layers of the polymer
u_l	Specific internal energy at the liquid layers of the polymer
u	Velocity of particles in the media
U_T	Total internal energy of the moulded part
v	Kinematic Viscosity
v	Poisson's Ratio
z_s	Thickness of solidified layer of polymer
Z_i	Acoustic impedance of sound wave

Chapter 6

α	Integral adaptive weight
$\mathbf{A_m}$	Reference model state matrix
$\mathbf{A_p}$	Plant state matrix
β	Proportional adaptive weight
$\mathbf{B_m}$	Reference model state matrix
$\mathbf{B_p}$	Plant state matrix
$\mathbf{B_e}$	Error dynamics input state matrix
$\mathbf{C_e}$	Error output matrix
d	Unknown disturbance vector
K_M	Reference model gain
K_P	Linearised plant gain
$\mathbf{K}$	State feedback gain vector
K_1, K_2	Plant state feedback adaptive gains
$K_{\alpha,\beta}$	Adaptive weight ratio
K_R	Feed-forward adjustable gain
K_i	Integral of output error adjustable gain
$\underline{\mathbf{r}}$	Reference signal vector
$\mathbf{P}$	Symmetric positive-definite solution to a Lyapunov equation
$\mathbf{Q}$	Symmetric positive-definite term in a Lyapunov equation
$\underline{\mathbf{u}}$	Control signal vector

u	Control drive signal
$\underline{\mathbf{x}}$	Plant state variable vector
$\underline{\mathbf{x}}_\mathbf{e}$	Model-following state error
x_i	Integral state error
$\mathbf{x_m}$	Reference model state vector
$\bar{x}$	Normalised state
y_e	Output error scalar
$\underline{\mathbf{y}}_\mathbf{e}$	Output error vector
ζ_M	Damping ratio of reference model
ζ_P	Linearised plant damping ratio
ω_M	Natural frequency of the reference model
ω_P	Linearised plant natural frequency

Subscripts and Superscripts

inc	Incident Wave
$trans$	Transmitted Wave
$refl$	Reflected Wave
ad	Wave energy loss expressed in nepers (Np)
est	Estimated parameters from plant identification
ID	Identification parameters
0	First estimated parameters
M	Model
P	Plant

Chapter 1

Introduction

1.1 Background

The injection moulding of thermoplastics is a widely used manufacturing process for the production of low cost and lightweight material products. Parts are moulded efficiently on a mass production scale with mechanical properties which often surpass those of metals. The products range from low-quality simple-geometry parts to very complex ones with strict dimensional tolerances. Economic constrains have raised the need to increase productivity and improve the automation of the injection moulding process. These parameters alongside with the use of multi-cavity moulds have perplexed further the control of the process, where advanced control methods are necessary to meet the new specification tolerances. Therefore a better understanding of the polymer melt behaviour during the process could aid the control of the polymer viscosity in order to produce consistent parts with desired properties. Advanced monitoring methods could be used to visualize in-mould parameters such as the melt polymer dynamics and identify phase changes, estimate the extent of solidification of the part and alert for process variations in real time.

Machine process parameters and polymer processing conditions are very interlinked and together have a great impact on the quality of the produced part. For the injection moulding process, parameters of great importance are: injection speed, holding pressure, polymer processing temperature, mould temperature and part cooling rate. Precise control of these parameters during the injection cycle, helps to control the polymer's molecular structure in the cavity and part final properties, that determine the physical appearance of the mouldings, such as residual stresses, shrinkage and warpage. However in order to control the filling and packing phases, the profile of the injection velocity and holding pressure should be optimized, while maintaining the processing temperature of the polymer and mould temperature nominally con-

stant. Therefore fast adaptation of the process control when other parameters change (mould geometry, material) is essential in order to achieve good quality of products. A deeper insight into the process enables the design of a robust controller be realised.

1.2 Description of the Injection Moulding Process

Injection moulding is one of the most important processes for the manufacturing of plastics. It is an automated sequential process where raw material is converted into a moulding in a single operation. The mould is the heart of the injection moulding machine where the melt polymer is injected to take the form of the cavity. Injection moulding machines are hydraulically driven which provides a very compact and efficient method of power transmission with the in-line screw. Injection moulding is a cyclical process which involves a number of auxiliary equipments to assist the productivity, such as mould temperature control, polymer dryers, robots for moulding handling and moving lines. The process has been extensively described in the literature, in [1, 2, 3, 4]. A schematic of the injection moulding machine is shown in Figure 1.1.

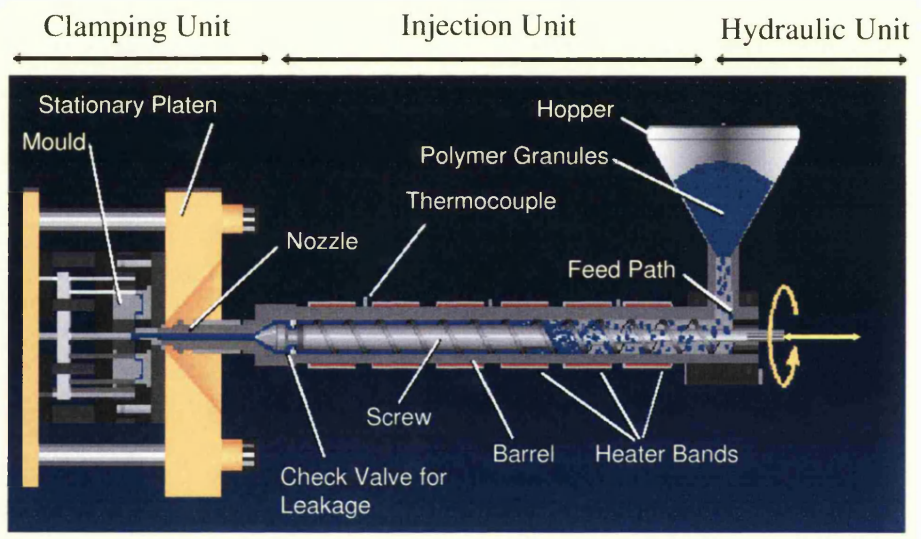

Figure 1.1: Schematic diagram of the Injection Moulding Machine

Three units can be identified: the hydraulic unit, the injection unit and the clamping unit. The hydraulic unit involves the actuation of the screw and is linked with the injection unit. Inside the injection barrel the melt material is prepared while the screw provides the means for forcing the melt to enter the mould cavity. The clamping unit applies a considerable force to keep the mould closed as the cavity pressure rises during the injection cycle. A sequential operation of

all units is necessary in order to transform the raw material into the final product. There are four main phases associated with the moulding process: the plasticization phase, the filling phase, the packing phase and the cooling phase. During these phases it is important to efficiently control a number of process parameters [5].

Initially in the *plasticization phase*, a certain amount of molten plastic is prepared, according to the required volume (Appendix A.1). The material is fed through the hopper inside the barrel in the form of granules. The barrel temperature is maintained at the necessary level, according to the material specifications. The material is melted and mixed as the screw rotates. The melt polymer gets accumulated at the front section of the barrel where the build up of pressure forces the screw to move backward. At this period a back-pressure is applied to the screw motion to achieve a homogeneous blend of polymer. The screw rotation speed is set accordingly, to reduce excessive shear, which can result in degradation or scorched resin. The parameters associated with the plasticizing phase are shown in Figure 1.2.

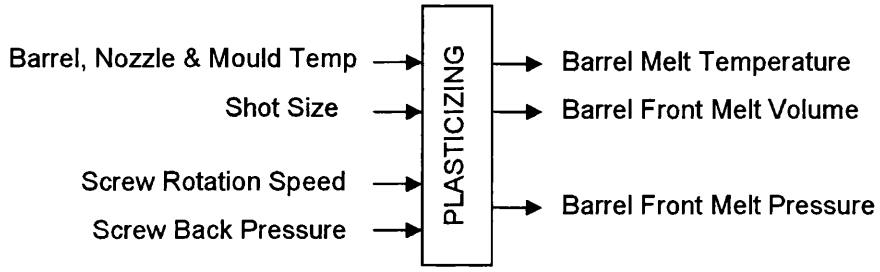

Figure 1.2: Schematic diagram of the Plasticization Phase

Next the *filling phase* commences, where the mould is closed and the injection unit is advanced forward. The nozzle of the barrel is pushed against the sprue bushing of the mould, where a preset hydraulic pressure ensures a firm contact during the filling and packing phases. The prepared shot size from the plasticization phase is injected as the screw moves forward. The screw velocity can be constant [6] or can follow a varying velocity profile. When the velocity trajectory is profiled, the polymer flow-front velocity is kept nominally constant throughout the different cavity cross sections. In this way the control of the molecular orientation and skin structure is achieved, avoiding the creation of flow marks. Moreover the flow front velocity could be reduced at critical sections, such as gates to avoid shear heating and increase again when filling the cavity. The point of injection in the cavity is important since it influences the flow orientation and mechanical properties of the part. The parameters associated with the filling phase are shown in Figure 1.3.

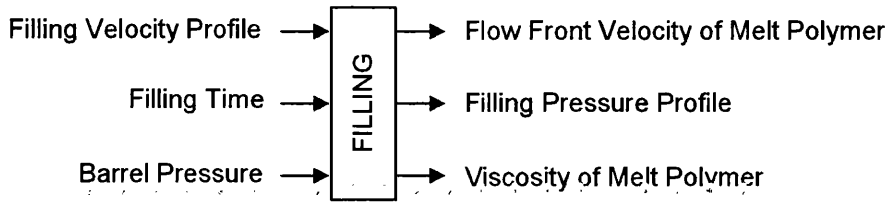

Figure 1.3: Schematic diagram of the Filling Phase

When the cavity is filled the transition to *packing phase* occurs and the melt polymer density changes. Additional material is packed into the cavity to compensate for the polymer shrinkage during part solidification. The transition from filling to packing phase should be closely controlled; otherwise the cavity pressure can reach excessive levels which would affect the dimensional stability of the part. In the packing phase the pressure inside the cavity should be either maintained constant or made to follow a specified pressure trajectory. Effective control of the pressure reduces the sink marks, and maintains the part weight constant. Depending on the pressure profile, flow-induced residual stresses can be formed and may cause part warpage if not allowed to relax during the cooling phase. It is important to allow sufficient time for the gate to solidify to avoid melt material flowing back to the barrel. When the gate is solid the volume inside the cavity is constant and no further material can be injected. The parameters associated with the packing phase are shown in Figure 1.4.

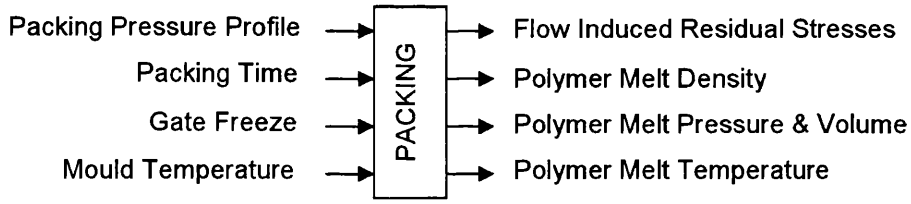

Figure 1.4: Schematic diagram of the Packing Phase

The solidification of the gate marks the beginning of the *cooling phase* where the molecules could relax to their initial state of equilibrium, depending on the cooling time and mould cooling rate. As the part solidifies it shrinks from the outer surface layer towards the centre, where the polymer is still in a liquid state. Consequently, the outer surface layers have a prime solidification that prevents the inner layers cooling freely. This can result in thermally induced residual stresses with a compressive profile at the surface and tensile at the core. The parameters associated with the cooling phase are shown in Figure 1.5.

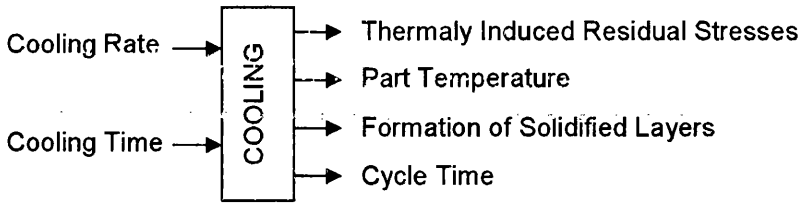

Figure 1.5: Schematic diagram of the Cooling Phase

The cooling phase lasts typically 70% of the injection cycle time and the part must be ejected as soon as it is solid. Premature ejection of the part should be avoided when the cavity is still under pressure, otherwise part distortion may occur. Usually the part is ejected at a higher temperature than the mould temperature, to increase productivity. In order to reduce the overall cycle time, the plasticization phase in the barrel commences at the start of the cooling phase. Therefore the next material dosage is prepared for the next cycle. Often the plasticization finishes before the end of the cooling phase. While the screw is stationary the heat conducted to the polymer (from barrel heaters) improves the thermal uniformity and homogeneity of the melt.

1.3 Current Problems in Injection Moulding

In this section an introduction is given for the work that has been published for the monitoring and control of the injection moulding process. A more detailed literature review of the melt polymer dynamic behaviour and methods that could enhance quality of products and improve their mechanical properties is given in Chapter 4. Moreover, the literature review of modern control strategies for controlling the injection moulding process is given in Chapter 5.

1.3.1 Complexity of Process Control

The injection moulding of plastics is a very complex and time dependent process. There are many parameters involved in each phase which require precise control in order to maintain part quality. Even when process parameters do not change, small variations exist between the parts. However the level of control can be further improved to minimise the tolerances and maintain repeatability throughout the injection cycles. Generally the control of the injection process is categorised to: phase-dependent, cycle-to-cycle and all-phase control [7]. The phase-dependent control is the most pragmatic approach as each phase can be separately controlled and a bumpless transfer algorithm can be utilised to maintain the control signal con-

tinuous. Cycle-to-cycle control is quite attractive as injection moulding is a repetitive process and information from the previous cycle could be used to improve the next one. However as parameters do change from cycle to cycle and disturbances occur, more iterations would be necessary in order to improve the performance of the machine. Finally, all-phase control is a very difficult and demanding task for the moulding process as it requires a deep understanding of the process dynamics (hydraulics and rheology). So far such an effective approach to all-phase control has not yet been realised [8].

Generally the most efficient approach would be the one combining information about the process machine parameters and the in-mould parameters during the process. Advance instrumentation techniques, including non-invasive methods are available to use, therefore information about the polymer behaviour in the cavity would enable the controller in real time to take corrective actions to optimise product quality. For these reasons over the last decade researchers have tried to simulate the injection process [9, 10, 11] in detail and apply various control methods [12, 13, 14] to manipulate the process parameters. Sophisticated software programs such as *C-Mold* and *Moldflow* contributed to a better understanding of the process parameters and allowed prediction of the final mechanical and physical properties of the products. On the other hand, control methods such as expert systems, neural networks, adaptive control, etc., help to improve the dynamic performance of the moulding machine, in order to maintain part dimensional accuracy and part weight nominally constant from cycle to cycle. The strengths and the weaknesses on each control method have been reviewed in [15, 16]. Modification to aid the (flow and pressure, P-Q) controllability of the hydraulic circuit has been realised in [17] with the use of a proportional flow control valve and a proportional pressure control valve. Some of the areas where progress needs to be done are the repeatability in the part quality, mechanical properties, the design of energy efficient moulding machines and achievement of faster cycle times to increase the production output and reduce the cost [8]. In order to achieve these targets, efficient monitoring methods should be applied to aid the control of the process in real time.

1.3.2 Polymer Melt Flow Behaviour

Polymers have several properties that need to be considered when designing a product or setting up the injection moulding process. When plastics are in their melt state are compressible and their viscosity can change depending on flow-gradients and processing temperature. On the other hand, plastics shrink during solidification and their volume changes considerably. Bearing these properties in mind enables for a better understanding of the moulding process. At the start of the filling phase, as the polymer melt enters the cavity, a frozen layer is formed from the contact with the cold wall. The initial temperature of the mould wall and polymer affects the thickness of the frozen layers, which increases during the filling phase. There are

two distinctive flow regions inside the mould cavity affecting the melt flow rate and viscosity:

- In the mould cavity - *Hele-Shaw Flow*. This type of flow refers to morphological instabilities such as non-equilibrium growth of crystals and differential solidification that occur. Often a less viscous fluid displaces the more viscous fluid.
- At the advancing front, *Fountain Flow*. The fountain flow continuously splits along the mid-plane allowing the polymer molecules on this interface (melt-air interface), to acquire a velocity component that forces the fluid element down the channel.

High injection speeds reduce the cooling rates resulting in thinner frozen layers at the end of filling. Usually the frozen layers are formed in the direction of the flow and have a parabolic shape, as seen in Figure 1.6.

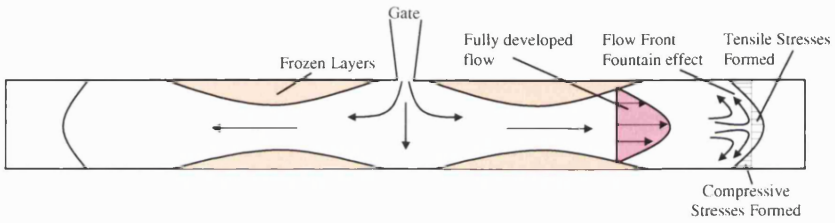

Figure 1.6: Polymer Melt Flow Behaviour in a Rectangular Cavity

Close to the gate, due to the high shear stresses developed, the temperature is high and very thin (frozen) layers are formed [18]. In the direction of polymer flow, the elongational molecular orientation is higher close to the cavity walls due to the high shear friction that occurs. This is affected by the flow-front velocity profile (fountain effect). At the same time, in the skin layer, the orientation is reduced by the molecular relaxation that occurs [1]. At the centre of the flow channel the degree of orientation is minimum (molecule at rest) as there is no shear effect [18]. All of this can be seen in Figure 1.7.

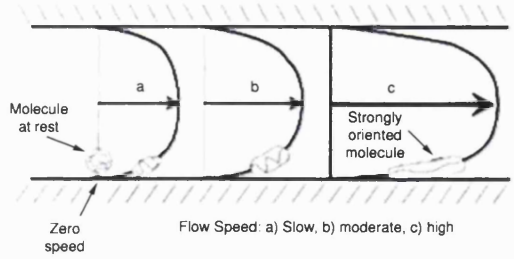

Figure 1.7: Molecular Orientation during the Filling Phase

For this reason the packing and holding pressure can influence the orientation at the core of the part. When the holding pressure is extended at constant temperature, the specific volume is smaller due to a higher compression of the polymer melt. The weight of the produced part increases and the percentage of shrinkage is smaller [18].

In the cooling phase, residual stresses are formed with a tensile profile at the core and compressive at the surface (Figure 1.6). The lower the wall temperature is, the sharper is the stress profile [18]. However, if the cooling time is shorter, lower residual stresses are formed. The part relaxation process takes place after ejection, when shrinkage and warpage are no longer mechanically restricted. If the holding pressure exceeds the limits and the part is highly pressurised, the possibility of ejecting a part being still under pressure is possible. In this case the stresses are tensile at the surface and compressive at the centre of the part [18].

Another important factor, which is influenced during the cooling phase, is the degree of crystallinity of the polymer (semi-crystalline). The slower the cooling rates are, the more time is available for the molecules to relax and return to their initial state. The structure of the molecules is called spherulites and is composed from crystalline and amorphous regions. As the polymer cools, the spherulites grow until they are constrained from others close to them [18], as seen in Figure 1.8. The number and the size of the created spherulites greatly affects the mechanical behaviour of the produced part (improved crystallinity results in a higher Young Modulus, etc.). However, high degree of crystallinity reduces the impact resistance of the part.

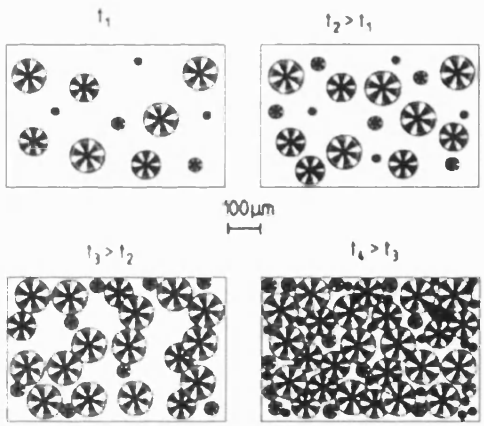

Figure 1.8: Spherulitic Growth during Part Solidification, from [18]

Finally due to the flow orientation, the mechanical properties of the produced part are enhanced in the direction of flow rather in the perpendicular direction. In general, before the moulding of a part is planned, there are many factors to consider.

1.3.3 Effects of Processing Parameters during the Injection Moulding Process

Precise control of flow, pressure and solidification during injection would allow final properties of parts such as shrinkage, warpage and residual stresses to be tailored to meet part specifications. Flow and pressure trajectories should be carefully designed in order to maintain an optimum level of control in the repeatability of dimension and mechanical properties of the moulded parts.

1.3.3.1 Screw Velocity

The injection screw linear velocity determines the flow pattern in which the polymer melt is injected in the cavity. It has a great influence on the molecular orientation and thickness of the frozen layers during the filling phase. It is dependent on the material (viscosity) being used, flow path geometry and processing conditions (barrel-mould-material temperature, etc). Since the polymer's behaviour is viscoelastic, a certain filling profile must be followed to ensure that the cavity is filled before gate solidification. Some researchers believe that the optimum velocity profile is to maintain the screw velocity constant in order to keep flow-front velocity constant [6]. This ensures good part quality and repeatability in each cycle. A schematic illustration of the flow front velocity including the primary and secondary flows is presented in Figure 1.9.

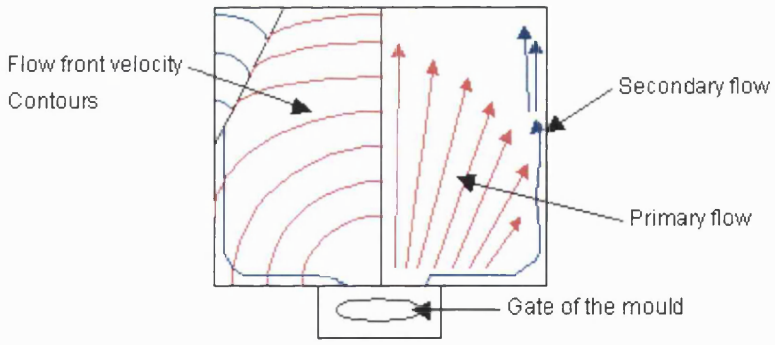

Figure 1.9: Schematic of Flow Front Velocity including the Primary and Secondary Flows

However, it is very difficult to maintain a constant flow-front velocity due to the complexity of the moulds geometry and the velocity dynamics, which is non-linear and time varying [19]. For these reasons, in the moulding of complex parts it is necessary to use multiple gates to maintain an even orientation throughout the part.

The injection speed at the beginning and at the end of the filling phase must be set low, to

improve the orientation of the melt polymer and ensure a smooth transition to the packing phase [18]. A bumpless transfer control algorithm is normally used to ensure a smooth transition [13]. This prevents excessive packing that could result in material flashing and high residual stresses (if inadequate relaxation takes place). The flow-front velocity should be high at less critical flow paths such as sprue and runners and low at gates and other critical areas [20]. In addition, the velocity profile should be selected to minimise the filling time while at the same time maintaining a uniform flow front velocity & temperature [20]. Careful design of the mould runner and gate is also crucial to avoid excessive shear heating which can damage the polymer melt. Because the polymer flow rate and flow front position are difficult to measure, other process parameters such as screw velocity and cavity pressure can provide this information (by assuming no leakage past the screw and no compressibility of the melt polymer).

High injection speeds could increase the shear heating at the gate, reduce the Young Modulus and increase the injection pressure [21]. Inevitably the initial temperature of the melt being injected will increase due to the shear heating effect. Flow marks, sink marks (on the moulded part surface) and variability in part weight may occur. On the other hand, *low injection speeds* may produce a poor molecular orientation in the produced part and a decrease in the Young modulus [21]. In addition, the flow front velocity could become unstable (secondary flows develop) if premature solidification of the polymer melt takes place. This would result in a partially filled cavity (short shot). A solution to this problem would be the use of hot runners where no solidification (of runner) takes place; only the moulded part is ejected from the mould. This reduces the scrap material (that needs to be recycled under normal conditions) up to 20% [8]. Overall, an *average injection speed* must be selected (results in even molecular orientation and mechanical properties) which does not require excessive injection pressure to fill the cavity.

Lower injection pressure during the filling phase ensures low residual stresses and optimum part quality [22]. A good combination would be a fast filling rate followed by high packing pressure and rapid freezing of the gate. This is mainly because the thickness of the frozen skin formed during the filling phase will affect the packing phase especially when a thin gate is used [23].

In addition, if cooling & viscosity variations occur during the filling phase inside the mould, these will affect the flow front and the pressure drop at that particular path. As a consequence the flow may eventually stop (due to the high pressure drop) and continue elsewhere where the conditions allow. Therefore, instead of having a smooth flow, a chaotic unstable condition (flow hesitation) is formed which in turn can lead to poor surface finish and small short shots [22].

During filling the melt core temperature changes continuously as the flow front travels along the length and width of the cavity. The solidification rate varies at different sections of the cavity, hence the shear stress varies as well. Near the gate the shear stress is maximum and the

melt temperature rises as high shear heating takes place. Due to the shear heating effect the melt temperature could rise up to $40°C$ (depending on the processed polymer) above the barrel temperature [24] during injection. Therefore an optimum melt temperature should be adopted to avoid burn marks at elevated temperatures or melt ripples at low ones [22].

1.3.3.2 Holding Pressure

For the packing phase information of the hydraulic pressure is necessary in order to profile the holding pressure. The holding pressure is applied at the end of the filling phase when the mould cavity is almost full. The feedback signal of the hydraulic pressure transducer could be used as an accurate indication for the transition from filling to packing phase [25]. The pressure will force the melt polymer to compact and follow the shape of the cavity in order to produce parts with high dimensional accuracy and free from surface defects. A high packing pressure reduces the shrinkage in all directions (cavity pressure increases), however shrinkage is always higher in direction perpendicular to flow and lower in the flow direction [26]. During packing phase an elastic strain is developed in the skin layer, which is removed at the end of the packing phase (as pressure drops to atmospheric level). This improves the surface appearance of the part, reducing surface defects such as sink marks, etc. In addition, extension of the holding pressure prolongs the duration in which the additional polymer can enter the cavity.

The pressure profile has a clear effect on the viscosity which can shift up the glass transition temperature, T_g. An increase in the T_g during the packing phase will allow the melt material to solidify faster, thus reducing the cycle time [27]. The increase in the T_g and injection pressure will result in a more uniform part with smaller molecular structure (spherulites) throughout the part. This enhances the optical transparency and tensile strength in amorphous polymers where fast cooling is desirable to obtain small uniform grain sizes [27].

A stepped pressure profile (downward) at the end of packing can reduce the variation in the thickness of the part (especially in direct sprue cases) as the risk of melt material coming out of the unsolidified gate is reduced [23]. Different packing profiles affect the weight of the part, and over-packing should be avoided especially in cases where the fill rate is low. This is because low fill rates allows for higher thickness of frozen skin to form during filling phase (result in higher weight parts). Once the gate is solidified, packing pressure has no further effect and unnecessary energy is wasted. Internal pressure and stress relaxation take place depending on the percentage of the core still in a molten phase.

1.3.3.3 Cavity Pressure

To control the injection moulding process and tune the process parameters effectively, continuous monitoring of the cavity pressure is required. Valuable information can be extracted about the part weight, degree of forming, possible flash and morphology of the part [28]. In the filling phase the cavity pressure is very low (1-3bar) and rises suddenly at the end of the phase. A sudden peak indicates the transition to the packing phase. The position of the cavity pressure transducer is critical for monitoring the transition. For control purposes the change in the derivative of the cavity pressure (dPc/dt) can optimise a good switching point from flow to pressure control [29]. A more detailed analysis of the cavity pressure profile can be found in Appendix A.2. In the packing phase the cavity pressure should have a constant profile for a period of time. This can ensure a uniform packing of the cavity and constant part weight. However, research has shown that many factors such as hydraulic oil temperature, packing pressure and polymer-cavity bulk temperature affect the part weight [30]. During the cooling phase the part starts to solidify and the cavity pressure is decreasing (from the peak value). This happens after the gate is solidified and the volume in the cavity is constant. An indication of this fact is a change in the pressure slope. If the pressure sensor is very close to the gate, the solidification of the gate occurs at the moment that the pressure is maximum [30]. Sometimes, after the solidification of the gate, a second peak may occur due to the flow halt effect (at the nozzle).

The solidification process can no longer be controlled by the actuation system, but only by manipulation of the temperature of the mould and heat transfer rate. In a research study it was shown that a mould coolant temperature control system is effective for this purpose [31]. Another study was concerned with the dynamics of the cavity pressure where a self-tuning controller was used for both flow and pressure control. A nonlinear and time-varying behaviour was found in relation with the hydraulic servovalve opening. Due to this nature a forgetting factor was used with the self-tuning regulator to function properly [29]. In another study [30], two control methods were proposed. The first approach was concerned with the control of the peak cavity pressure via a self-tuning control and the bulk temperature via a cascade strategy for the coolant temperature control. The second approach, which gives better experimental results, is focused on the control of the cavity pressure. This is used to compensate for bulk temperature fluctuations from cycle-to-cycle [30]. Mould temperature control is not used in this research.

1.3.3.4 Polymer & Mould Temperature

The processing temperature of the polymer and mould temperature are two parameters that determine the injection cycle time to a great extent. A low mould temperature could reduce

the cycle time as rapid solidification occurs when the melt polymer comes in contact with the cold wall [5]. However, higher filling rates and holding pressure are necessary in order to mould the part successfully. On the other hand, a higher processing temperature improves the disentanglement of the molecules lowering the shear viscosity level [32]. For semi-crystalline polymers and particularly for polypropylene a low melt temperature may result in a low Young modulus due to the formation of β-phase spherulites. However, the impact resistance of the produced part is greater. To increase the Young modulus in such a case, a high molecular orientation is required followed by a rapid cooling of the part, where less time is available for molecular relaxation [21].

The melt polymer and mould temperature have also a great effect in the profile of the holding pressure. When the mould temperature is higher, the cooling rates are lower and it takes more time for the gate to solidify; further manipulation of the holding pressure can be achieved. In addition, when the melt temperature is higher, the viscosity is lower and the pressure drops at the flow path sections are lower too. However, the shear heating that occurs near the gate will raise the temperature of the melt. If the temperature reaches excessive limits a chemical degradation of the polymer may occur [18].

Generally, the temperature control of the mould during the injection cycle is very crucial to ensure the production of parts with constant quality. The mould heat transfer rate and efficiency of the cooling system are the primary parameters that can be used for control of part solidification. Some suggested controlled variables are, the cycle average surface temperature, cycle average mould metal temperature, cycle peak temperature and partial cooling time. Based on these variables a control algorithm is proposed in [33], for the control of the cycle average surface temperature based on experimental data. Another approach provides a good methodology to estimate the part weight through the bulk temperature of the part for control purposes [34]. Temperature measurements close to the cavity wall with heat conduction model are used. In another study, simulation of the injection mould cooling process was developed with the use of a modified boundary element technique. The surface temperature of the cavity was estimated on a cycle average basis [35]. The algorithm used provides a good description of the cyclic transient characteristics of the mould cavity surface temperature. This was achieved within three iterations. Hence the temperature of polymer and mould should be controlled at an appropriate level.

1.3.4 Monitoring of Product Quality

The monitoring of the product quality in the injection moulding process occurs in two stages. In the first stage tunning of the process parameters ensures to produce parts of an acceptable quality level. In the second stage a monitoring system is set to identify parameter variations

and take appropriate control actions. *Traditionally* this has been performed manually by trial and error were the commissioning engineer would set the machine depending on his level of expertise. Afterwards the moulded parts would be visually inspected and dimensions would occasionally be measured to evaluate the level of quality. This process should be repeated for a few times in successive injection cycles until an acceptable level of quality is attained. On-line equipment to monitor material properties such as polymer viscosity and melt flow index are used as well to feed back this information to the process controller. However these equipments are expensive and require highly skilled personnel. A more efficient method is the *empirical approach* where a model is build by performing a regression analysis. In this Design Of Experiment (DOE) approach, data are acquired from a series of experiments where the input data that produce the best quality attributes are taken as the optimum. The empirical model is then used to map the input parameters to the output variables to predict product quality. A number of researchers [36, 37] have used DOE approach in order to define an optimum operating process window for the process. However this method is time consuming and requires a large number of parameters to be studied. Another approach widely used in manufacturing is the *Statistical Process Control* (SPC) approach where measured variables, such as part weight, etc. [38] are sampled and compared with the process mean values. Variation within certain limits classify parts as acceptable. A more promising approach is the application of Neural Networks which can be used to "learn" the complex relationship between input and output parameters in order to predict part quality. Neural Networks have been used to predict part quality in injection moulding with promising results [39, 40].

An alternative approach is proposed here, where instead of monitoring process parameters based on empirical models, information for the melt behaviour is extracted by the use of two non-invasive methods. Determination of the extent of solidification of the moulded parts, detection of flow-oriented defects (such as short-shots and flashing) as well as identifying phase changes in real time is believed to be the key issues in controlling quality.

1.3.5 Monitoring of Part Solidification

The extent of solidification of the moulded part is a critical in-mould parameter which, if monitored, could ensure repeatability in part quality and reduction in the running costs. If the part is ejected on time, a considerable reduction in the cycle time can be achieved, considering that cooling corresponds to 70% of the injection cycle. For this reason establishing a direct relationship between the polymer properties and the solidification rate of the part would be a challenging task. The manipulated variables which could be used for possible control techniques include:

- The reduction in cavity pressure during cooling and its variation after reaching the datum

level (atmospheric).

- The average mould surface temperature variation during cooling due to the reduction of the internal energy of the part.
- The speed variation of ultrasound waves (longitudinal), that propagate through the melt polymer during cooling.

With the use of ultrasound (non-invasive) monitoring, researchers have tried to characterise the polymer behaviour during injection moulding and extrusion using different methods. The velocity and the amplitude change in the transmitted and reflected signals are used for the interpretation of the solidification rate of the part. Continuous variations in process parameters has been experimentally observed during the injection process. These include the flow front position in [41], cavity pressure in [42], degree of crystallinity in [43], polymer temperature in [44], polymer density in [45] and transition signs to packing phase including the monitoring of gap formation between the part and the cavity wall, in [46].

Therefore ultrasound seems to be a very attractive way to monitor the melt polymer behaviour during the injection cycle. Due to the large amount of data that needs to be processed off-line, a fast data acquisition system would be necessary. Therefore it would be beneficial to develop an efficient and cost effective way in order to extract critical information for the extent of solidification of the part in real time and use this information for control and quality monitoring purposes. So far most researchers have used theoretical models based on an average surface temperature of the cavity (theoretical) to estimate the ejection time of the part [47, 48]. Recently a more efficient method has been proposed and developed by co-worker Stelson [49] (during the first year of this PhD study), where real time data acquired from thermocouples embedded close to the mould cavity surface are used to estimate the extent of solidification of the part based on a linear algorithm. This particular heat transfer model [49] was used in the experimental work curried out in this study to estimate the extent of part solidification. More details can be found in section 3.6.1.

1.3.6 Methods for Improving Part Quality

So far it was emphasised that maintaining repeatability in part quality during the moulding process is a very important task where extensive research has been conducted. However, implementing methods that could enhance quality and tailor the melt polymer properties according to the design specifications is of utmost importance. Two methods that have been lately under investigation for improving part quality during injection and enhancing the mechanical properties are:

- Controlled flow-induced crystallization, which influences the degree of crystallinity, level of shrinkage in order to manipulate residual stresses and reduce warpage [50].
- Application of melt vibration, where shear-controlled orientation is achieved under continuous pulsating flow and/or pressure. Improvements in the molecular structure, surface appearance and processability of the produced parts are reported [51].

So far in conventional injection moulding machines, melt vibration has been applied by oscillating the injection screw in open-loop control. Good results have been reported with improvements in the mechanical properties. However it is believed that closed-loop control of the screw motion could further improve the melt vibration effect which relates to part quality. Application of melt vibration with a conventional moulding machine was one of the goals pursued in this research. More details are given in Chapter 4.

A good overview of the injection moulding process and its parameters has been presented. Modern methods for monitoring melt polymer behaviour and part quality as well as ways to control properties of the material during injection are reviewed. It is believed that there is a great potential in combining these methods with an advanced control scheme to enhance the quality of the parts. It is likely that the new generation injection moulding machines in the near future will combine these features to stay competitive in the manufacturing market. This area of research has a great potential and needs further development.

1.4 Aims and Objectives

The aims of this PhD research study were the following:

- Investigate the relation of the moulding machine process parameters and in-mould parameters.
- Monitor the melt polymer dynamics during the injection cycle with the use of a cost effective method.
- Achieve self-commissioning of the process parameters eliminating the need for a skillful operator.
- Enhance the mechanical properties of the final moulded products by modifying the conventional injection method.

In order to achieve these targets the performance of a hybrid adaptive controller is considered in this work for the control of the injection moulding filling and packing phases. The

phase changes during the cycle and the extent of part solidification, knowledge which is difficult to extract empirically, are estimated with the use of a non-invasive monitoring method. Integrating the developed monitoring strategy with the adaptive control scheme enables rapid optimization of the process as well as monitoring quality parameters in real time. During the injection process, melt vibration is applied to manipulate the viscosity of the polymer and improve the mechanical properties of the final products. The proposed (adaptive) control and (non-invasive) monitoring system is expected to demonstrate additional benefits and advantages over traditional forms of control for the injection moulding process.

The objectives of this research were the following:

- **Investigate the relationship between machine process parameters and in-mould parameters in the injection moulding process**. This would lead to a deep understanding of the key variables that need to be controlled during the injection cycle in order to enhance product quality and improve productivity. This task requires simulation of the injection moulding process for the filling and packing phases. Simulation studies in combination with a thorough literature review would be necessary for a sound theoretical understanding of the melt polymer dynamic behaviour during the process. Thereafter, experimental investigations could be carried out in an injection moulding machine.

- **Control the injection moulding process from a personal computer in real time**. The hydraulic circuit of the moulding machine would need a modification as the current configuration limits the control of the screw motion and profile parameters can only be preset. A single flow and pressure (P-Q) control valve could enable precise control of the screw, while it would simplify the set-up/commissioning time of the machine as one control signal is necessary. A proposed controller could be implemented in a discrete form, from a Matlab-Simulink model.

- **Develop an on-line quality control system with the aid of a specially instrumented mould**. For the instrumentation of the mould, non-invasive methods [52] could be utilised to monitor the melt polymer dynamic behaviour under the effect of flow and pressure. The information extracted during the injection cycle could be used to detect the polymer flow-front position (in the cavity), determine the extent of solidification of the part and identify phase changes in real time. However the development of an efficient and cost effective data acquisition system would be necessary, to process the data during injection and extract critical information to aid the controllability and repeatability in part quality.

- **Apply a modern control strategy such as an adaptive algorithm which requires no a priori information about the plant dynamics**. Simplify the need for a complex mathematical model to describe the injection moulding process, which is non-linear and time-varying. Combine the developed quality control system with a phase-dependent

control scheme for the filling and packing phases. This would enable fast optimization of the initial process setup without the need of trial and error cycles or iterations to reach an optimum level of control. The development of an adaptive controller would necessitate the use of a linearised plant model for velocity and pressure control. In addition, the use of a bumpless transfer algorithm would be necessary to maintain a continuous control signal to the P-Q valve at the transition from flow to pressure control.

- **Enhance the part quality and tailor the mechanical properties of the injection moulded parts by application of the melt vibration method in a conventional injection moulding machine**. Use a closed-loop control for the process and force the screw to oscillate to transmit the vibrational energy to the melt polymer, to lower its viscosity and improve the processability. A precise level of control and tracking performance would be necessary, in order to vibrate the screw and investigate the effect of different (screw) profiles in melt polymer viscosity and final part quality. Carry out mechanical tests to evaluate the improvements in the mechanical properties of the parts.

1.5 Thesis Structure

A brief overview of the six major sections of this thesis follows.

In Chapter 2, the modelling of the filling and packing phases of the injection moulding is presented. The non-linear model is used in simulation to analyse the hydraulic system response and to investigate the role of processing conditions.

Chapter 3 presents a specially instrumented mould that was designed and manufactured. Experimental work is carried out on an *Arburg* injection moulding machine with two different polymers, to investigate the effect of processing parameters on part weight and surface defects. To predict the extent of solidification of the part and to identify phase changes during the cycle, two non-invasive monitoring methods are presented.

In Chapter 4, a thorough literature review on process parameters that influence the crystallization and solidification of the melt polymer is presented, to give a better insight into the injection moulding process. Processing methods that could manipulate polymer rheology during the cycle and enhance the mechanical properties of the final products are reviewed.

Chapter 5 presents a new design to the original hydraulic circuit that is implemented in order to enable real time control of the process. An efficient data acquisition system which processes data of the proposed non-invasive method in real time is described. A literature review on modern control strategies for the control of the process follows. The strategy which could

adapt to plant uncertainties and unknown disturbances is selected.

Chapter 6 discusses the selected hybrid controller for the closed-loop control of flow and pressure trajectories, with a bumpless transfer algorithm. The hybrid controller is implemented experimentally in the moulding machine with the fully instrumented mould. The established non-invasive method is used for quick set up of the process parameters. Issues with stability of the hybrid controller are dealt with a proposed modification.

In Chapter 7, a new processing method is proposed to manipulate the melt polymer during injection, in order to enhance the molecular orientation of the moulded parts. The mechanical properties of tensile specimens produced with this method are compared with parts produced by conventional moulding process.

Chapter 8 presents a summary of achievements in this work. Suggestions for future work are given with particular emphasis on the proposed melt polymer processing method and commercialization of the non-invasive data acquisition system.

Chapter 2

Modelling and Simulation of the Injection Moulding Process

2.1 The Thermo-mechanical Environment

To model and simulate the filling and packing phase of the injection moulding process two aspects were considered. The first was to model the hydraulic circuit where integrated directional valves control the successive operations of the cycle (mould clamp, injection unit motion, screw motion). The most important machine operation associated with the two phases is the screw motion controlled by a directional control valve connected in series with a set of flow and pressure cartridge valves. To simplify the modelling and improve the efficiency of the hydraulics it is assumed that a servo-proportional valve is used to control the flow and pressure in the two actuators (connected in parallel). Since the servo-proportional valve has sufficiently fast dynamics, different velocity and force profiles can be simulated (as directional valve has slow response). The modelling of the hydraulic plant is presented in section 2.2.

The second aspect to model was the polymer melt behaviour through mould flow sections during the injection cycle. This is presented in section 2.3. This modelling involves the dimensions of the flow paths as well as the characteristics of the polymer used which is subjected to a complex thermo-mechanical environment during the cycle. The flow of the melt polymer into the cavity is often unsteady and is subjected to non-isothermal conditions. This often occurs due to the high temperature difference between the cavity wall and processing temperature of the polymer. The viscoelastic nature of the polymer makes it compressible throughout the cycle and particularly during the packing phase where the cavity is packed with additional material. At the beginning of the filling phase the melt polymer is forced to flow through (mould) flow paths with different cross sections and temperatures (hot runners, cold cavity). Under such

conditions the polymer is subjected to different shear rates that influence its viscosity history and consequently final properties of the moulded part. Therefore the velocity profile of the melt flow-front is of particular importance and greatly affects the thickness of the solidifying layers with impact on (moulded) part dimensions and weight. The formed solidifying layers (thickness wise) during filling determine to a great extent the pressure (force) profile of the screw during packing. Depending on how effective the cavity is packed, properties such as shrinkage, part weight and residual stresses are affected. Therefore to mould parts with strict dimensional tolerances and free from defects the effect of processing conditions must be investigated thoroughly.

For the above reasons the role of simulation can be a powerful tool to analyse the hydraulic system response, investigate the role of processing conditions and predict the final properties of the part. In order for the overall system model to be sufficiently accurate it is essential to describe the physical laws, the polymer model behaviour, processing conditions and mould geometry. Simulation of the filling and packing phases is presented in section 2.4.

2.2 Hydraulic System

A schematic diagram of the injection moulding hydraulic circuit is shown in Figure 2.1.

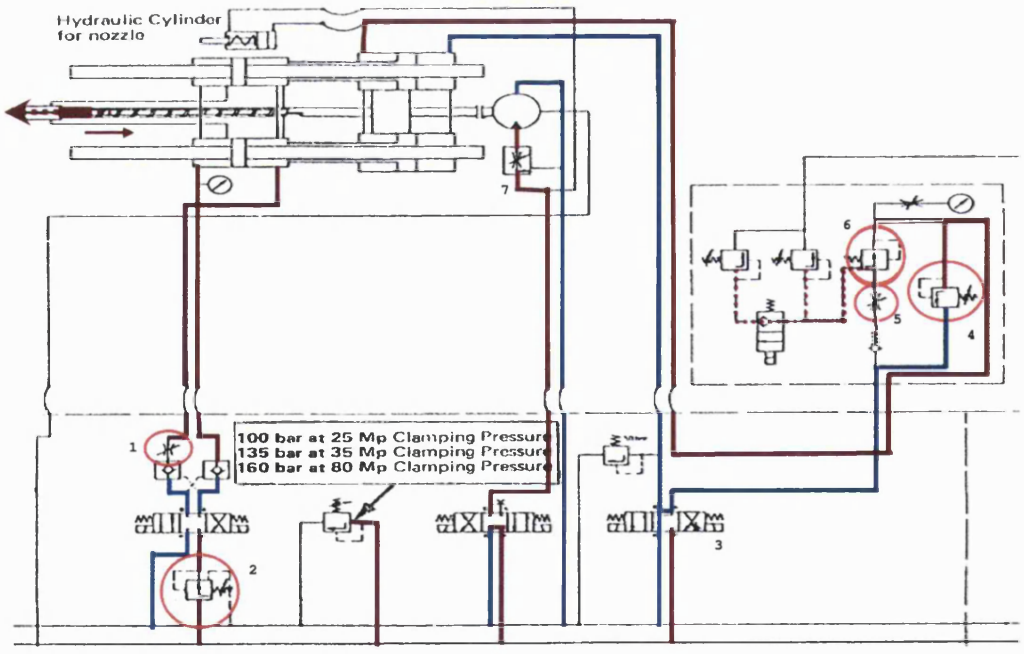

Figure 2.1: Schematic diagram of the hydraulic circuit

The main components are: the hydraulic actuators that control the movement of the screw, the hydraulic motor that rotates the screw during plasticization and a set of directional control valves that control the machine operations during the injection cycle. In the hydraulic circuit there is a central manifold with directional control valves (1,2) that control the clamping mechanism and the injection unit. The screw motion is controlled by a directional control valve (3) which is connected in series with the side manifold. This manifold is located on the right hand side of the Figure, with an arrangement of cartridge valves (4,5,6) that preset the flow rate and maximum packing pressure for the injection cycle. A main relief valve sets the maximum system pressure for the circuit, set at 100bar pressure.

The machine control settings that need to be set prior to injection are the following:

- the polymer processing temperature inside the barrel
- the polymer shot size prepared during plasticization
- the duration of the filling phase to fill the cavity
- the screw velocity setpoint during filling
- the screw stroke point to switch from the filling to the packing phase
- the maximum hydraulic pressure to sufficiently pack the cavity
- the duration of the cooling phase for complete solidification of the moulded part

To correctly adjust these process parameters and guarantee the successful moulding of the part an experienced commissioning engineer is required. In addition, a few trial and error cycles would be necessary for fine tunning of the parameters. In the event of a disturbance to the process (variation in polymer viscosity due to selection of a different grade, fluctuation in processing or mould temperature, contamination in the hydraulics oil, wear of mechanical components, etc.) the process parameter may change or drift as no adjustments can be made during the process. During inspection of the batches, variations in the dimensional tolerances of the parts could indicate deviation from the mean values, however it would be costly and time consuming (with no guaranteed result) to stop the production and try to identify the fault. In order to overcome these drawbacks and be able to take corrective actions during the injection cycle, efficient control of the injection screw would be required, with monitoring methods in place to alert for process changes. Therefore it was decided in this project to modify the existing hydraulic circuit and use a servo-proportional valve to control both flow and pressure during the cycle. This valve would be controlled in real time, via a personal computer, to change hydraulic flow and pressure trajectories to compensate for variations in process parameters. Details for the modification of the hydraulic circuit are given in Chapter 5.

2.2.1 Mathematical Model of Hydraulic Plant

In this section an approximate mathematical model of the injection moulding hydraulic plant (excluding mould) is presented. The section of the hydraulic plant that is examined consist of a pair of two unequal area hydraulic cylinders controlled by the servo-proportional valve, while the casing of the actuators is linked with the injection screw. The servo-proportional valve used in the modelling was also used in the test rig to replace the function of the side manifold and simplify the hydraulic circuit. It provides accurate control for a wider bandwidth of flow and pressure trajectories during the cycle. The actuators rods are fixed on the structure of the machine. Due to the unequal area cylinder, the flow rate has a nonlinear relationship with the servo-proportional valve's spool displacement, and pressure in the two hydraulic actuators which control the load during the packing phase. The load has a nonlinear nature due to the stiffness of the melt polymer inside the injection barrel and mould (solidifying melt) and the polymer leakage past the screw (viscosity dependent). A typical representation of the of the hydraulic circuit with the friction forces acting on the rod is shown in Figure 2.2. For convenience in the modelling of the system the two hydraulic cylinders can be represented by a single cylinder with appropriate area adjustments. Good literature for modelling hydraulic systems can be found in [53].

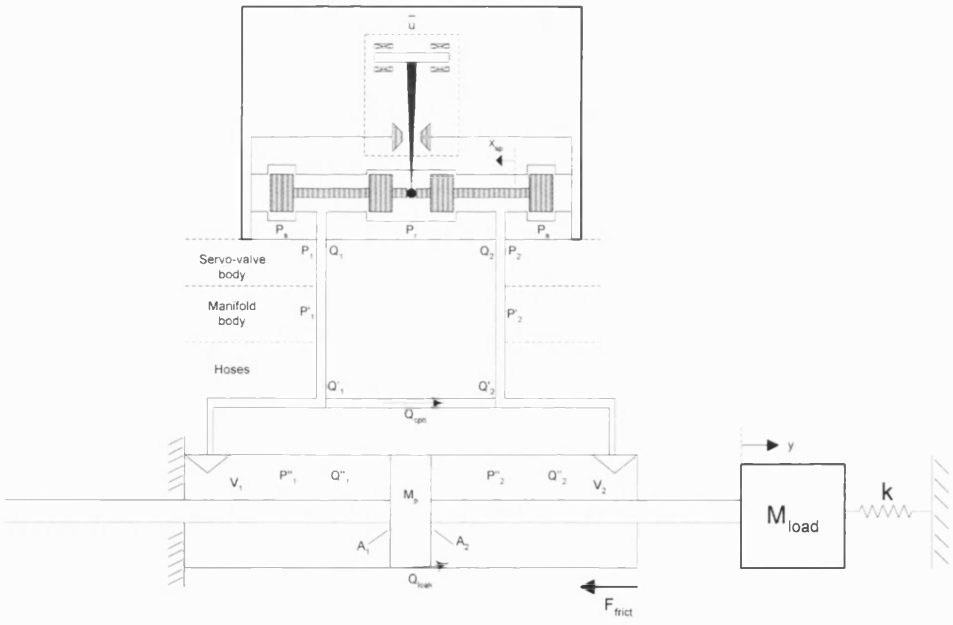

Figure 2.2: Schematic diagram of the hydraulic circuit

1. The dynamics of the servo-valve can be approximated by a second-order differential

equation where [54]:

$$\bar{u}(t) = T_{sp}^2 \cdot \ddot{\bar{x}}_{sp}(t) + 2\zeta_{sp} \cdot T_{sp} \cdot \dot{\bar{x}}_{sp}(t) + \bar{x}_{sp}(t) \tag{2.1}$$

where by substitution of $\bar{u}(t) = K_{sv} \cdot u \cdot \omega_{sp}^2$ and $\frac{1}{\omega_{sp}} = T_{sp}$

$$K_{sv} \cdot u \cdot \omega_{sp}^2 = \ddot{x}_{sp} + 2\zeta_{sp} \cdot \omega_{sp} \cdot \dot{x}_{sp} + x_{sp} \cdot \omega_{sp}^2 \tag{2.2}$$

where,
K_{sv} is the servo-valve gain ($K_{sv} = 1$ for normalised I/O signals),
x_{sp} is the dimensionless spool position [-1... +1],
$\bar{u}$ is the dimensionless servo-valve control signal [-1... +1],
ζ_{sp} is the damping ratio,
T_{sp}, ω_{sp} the time constant and natural frequency of the servo-valve.

2. The servo-valves spool slew limit can be set as:

$$-\dot{\bar{x}}_{sp}^{max} \leqslant \dot{\bar{x}}_{sp} \leqslant \dot{\bar{x}}_{sp}^{max} \tag{2.3}$$

where, $\dot{\bar{x}}_{sp}^{max} = \frac{1000}{Ts}$ (obtained from valve catalogue).

3. The servo-valve spool position limit is set as:

$$-\bar{x}_{sp}^{max} \leqslant \bar{x}_{sp} \leqslant \bar{x}_{sp}^{max} \tag{2.4}$$

For the shake of simplicity the spool used in simulation is assumed to be straight cut, critically damped and symmetric.

4. The flow from the servo-valve to the actuator when the spool displacement is $(+ve)$ is described as:

$$Q_1 = K_v \cdot \bar{x}_{sp} \cdot \sqrt{|P_s - P_1|} \cdot sign(P_s - P_1) \tag{2.5}$$

$$Q_2 = K_v \cdot \bar{x}_{sp} \cdot \sqrt{|P_2 - P_R|} \cdot sign(P_2 - P_R) \tag{2.6}$$

5. The flow from the servo-valve to the actuator when the spool displacement is $(-ve)$ is described as:

$$Q_1 = K_v \cdot \bar{x}_{sp} \cdot \sqrt{|P_1 - P_s|} \cdot sign(P_1 - P_s) \tag{2.7}$$

$$Q_2 = K_v \cdot \bar{x}_{sp} \cdot \sqrt{|P_R - P_2|} \cdot sign(P_R - P_2) \tag{2.8}$$

where, for both cases, $\bar{x}_{sp}(+ve)$ & $\bar{x}_{sp}(-ve)$, flow gain $K_v = Q_{rated} \cdot \sqrt{\frac{\Delta P}{2}}$.

6. The pressure drop at servo-valve body of the injection moulding machine is modelled by assuming turbulent flow:

$$Q_1 = K_{body} \cdot \sqrt{|P_1 - P_1'|} \cdot sign\left(P_1 - P_1'\right) \tag{2.9}$$

$$Q_2 = K_{body} \cdot \sqrt{|P_2' - P_2|} \cdot sign\left(P_2' - P_2\right) \tag{2.10}$$

to set values for P_1 and P_2 the following expressions can be used:

$$P_1 = \left(\frac{Q_1}{K_{body}}\right)^2 \cdot sign(Q_1) + P_1' \tag{2.11}$$

$$P_2 = \left(\frac{Q_2}{K_{body}}\right)^2 \cdot sign(Q_2) + P_2' \tag{2.12}$$

where, K_{body} is the flow gain for the servo-valve body, $K_{body} = \frac{Q_{body-rated}}{\sqrt{\frac{\Delta P_{body-rated}}{2}}}$.

7. The flow to and from the actuator is:

$$Q_1' = Q_1 - Q_{cpb},\ Q_2' = Q_2 - Q_{cpb} \tag{2.13}$$

$$Q_1'' = Q_1' - Q_{leak},\ Q_2'' = Q_2' - Q_{leak} \tag{2.14}$$

$$Q_1''(t) = A_1 \cdot \dot{y}(t) + \frac{V_1 + A_1 \cdot y(t)}{\beta} \cdot P_1''(t) \tag{2.15}$$

$$Q_2''(t) = A_2 \cdot \dot{y}(t) - \frac{V_2 - A_2 \cdot y(t)}{\beta} \cdot P_2''(t) \tag{2.16}$$

therefore,

$$Q_1(t) = A_1 \cdot \dot{y}(t) + \frac{V_1 + A_1 \cdot y(t)}{\beta} \cdot P_1''(t) + Q_{leak} + Q_{cpb} \tag{2.17}$$

$$Q_2(t) = A_2 \cdot \dot{y}(t) - \frac{V_2 - A_2 \cdot y(t)}{\beta} \cdot P_2''(t) + Q_{leak} + Q_{cpb} \tag{2.18}$$

where,
y is the position of the rod,
$Q_{leak} = K_{leak} \cdot \left(P_1'' - P_2''\right)$ is the cylinder cross piston leakage which is usually quite small $(0.01L/min/bar)$,
$Q_{cpb} = K_{cpb} \cdot \sqrt{|P_1'' - P_2''|} \cdot sign\left(P_1'' - P_2''\right)$ is the cross port bleed flow.

8. The pressure drop at the manifold of the injection moulding machine is again modelled by assuming turbulent flow:

$$Q_1' = K_{man} \cdot \sqrt{|P_1' - P_1''|} \cdot sign\left(P_1' - P_1''\right) \tag{2.19}$$

$$Q_2' = K_{man} \cdot \sqrt{|P_2'' - P_2'|} \cdot sign\left(P_2'' - P_2'\right) \tag{2.20}$$

to set values for P_1' and P_2' the following expressions can be used:

$$P_1' = \left(\frac{Q_1'}{K_{man}}\right)^2 \cdot sign\left(Q_1'\right) + P_1'' \tag{2.21}$$

$$P_2' = \left(\frac{Q_2'}{K_{man}}\right)^2 \cdot sign\left(Q_2'\right) + P_2'' \tag{2.22}$$

where K_{body} is the flow gain for the servo-valve body, $K_{body} = \frac{Q_{body-rated}}{\sqrt{\frac{\Delta P_{body-rated}}{2}}}$.

9. The force balance equation for the hydraulic system can be derived as:

$$M_{pist} \cdot \ddot{y} = P_1'' \cdot A_1 - P_2'' \cdot A_2 - k_s \cdot y - F_{frict} \tag{2.23}$$

where, the F_{frict} includes the components of the stiction force, stick-slip region [55], coulomb friction and viscous friction. The actuator's stick friction occurs in the zero velocity region ($\approx 0.001m/s$). As long as the stick friction force is not exceeded, the mechanical friction of the seals counteracts the hydraulic force. When the hydraulic force is greater than the stick force, the slip force arises where the actuator's velocity

is greater than the zero velocity region. The stick friction especially at low velocities affects the tracking error of the system in position control.

2.2.2 Linearized Model

The model derived in section 2.2.1 is a highly nonlinear model and a simplified is required to investigate the system performance and stability for various control algorithms. A linearised model in Figure 2.3 is derived for the case of flow and pressure control during the filling and packing phase of the injection cycle.

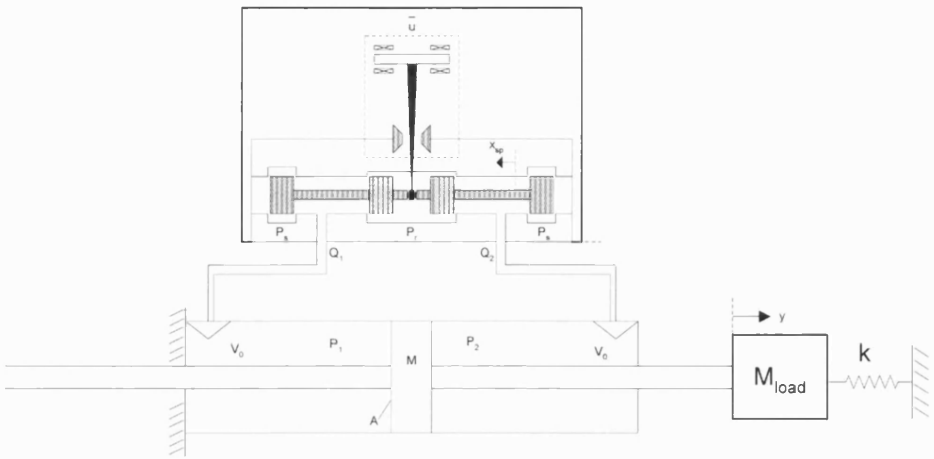

Figure 2.3: Simplified Hydraulic Circuit

For the analysis the following assumptions were made:

- the actuator areas are equal, $A_1 = A_2 = A$
- the trapped volume at each side of the actuator is the same, $V_1 = V_2$
- there are no leakages, $Q_{leak} = 0$, $Q_{cpb} = 0$ or pressure losses
- the piston friction is pure viscous

The guiding differential equations are the following:

$$Q_{sp} = K_v \cdot x_{sp} \cdot \sqrt{\frac{|P_S - P_L|}{2}} \cdot sign(P_S - P_L) \tag{2.24}$$

$$Q_{sp} = A \cdot \dot{y} + \frac{V_0}{2\beta} \cdot \dot{P}_L \tag{2.25}$$

$$M \cdot \ddot{y} = A \cdot P_L - k_{visc} \cdot \dot{y} - k \cdot y \tag{2.26}$$

where P_S and P_L are the system pressure and load pressure.

The differential equations that describe the system are given by equations 2.2, combination of 2.24-2.25 and 2.26:

$$\ddot{x}_{sp} = K_{sv} \cdot u \cdot \omega_{sp}^2 - 2\zeta_{sp} \cdot \omega_{sp} \cdot \dot{x}_{sp} - x_{sp} \cdot \omega_{sp}^2 \tag{2.27}$$

$$\dot{P}_L = \frac{2\beta}{V_0} \cdot K_v \cdot x_{sp} \cdot \sqrt{\frac{|P_S - P_L|}{2}} \cdot sign(P_S - P_L) - \frac{2\beta \cdot A}{V_0} \cdot \dot{y} \tag{2.28}$$

$$\ddot{y} = \frac{A \cdot P_L}{M} - \frac{k_{visc}}{M} \cdot \dot{y} - \frac{k}{M} \cdot y \tag{2.29}$$

When the flow pressure dependence equation is linearised for an operating point the following linear relationship yields:

$$Q_{sp} = K_{Q_x} \cdot x_{sp} - K_{Q_p} \cdot P_L \tag{2.30}$$

where K_{Q_x} and K_{Q_P} are the valve's flow-spool displacement coefficient and valve flow-pressure coefficient respectively.

$$K_{Q_x} = \left| \frac{\partial Q}{\partial x_{sp}} \right|_{x_{sp}=x_{sp_0}, P_L=P_{L_0}} = K_v \cdot \sqrt{\frac{|P_S - P_{L_0}|}{2}} \tag{2.31}$$

$$K_{Q_P} = \left| \frac{\partial Q}{\partial p_{sp}} \right|_{x_{sp}=x_{sp_0}, P_L=P_{L_0}} = \frac{K_v \cdot x_{sp_0}}{2 \cdot \sqrt{2 \cdot |P_S - P_{L_0}|}} \tag{2.32}$$

where x_{sp_0} and P_{L_0} is the spool position and load pressure at the linearization point.

The new set of differential equation from equations 2.27, 2.29 and combination of 2.25 with 2.30 can describe the linearised hydraulic system:

$$\ddot{x}_{sp} = K_{sv} \cdot u \cdot \omega_{sp}^2 - 2\zeta_{sp} \cdot \omega_{sp} \cdot \dot{x}_{sp} - x_{sp} \cdot \omega_{sp}^2 \tag{2.33}$$

$$\ddot{y} = \frac{A \cdot P_L}{M} - \frac{k_{visc}}{M} \cdot \dot{y} - \frac{k}{M} \cdot y \tag{2.34}$$

$$\dot{P}_L = \frac{2\beta \cdot K_{Qx}}{V_0} \cdot x_{sp} - \frac{2\beta \cdot A}{V_0} \cdot \dot{y} - \frac{2\beta \cdot K_{Qp}}{V_0} \cdot P_L \tag{2.35}$$

Conversion of the system by Laplace transform action using zero initial conditions yields the following open-loop transfer function for the hydraulic plant, where the input is the drive signal to the servo-valve and output the position of the rod:

$$\frac{s \cdot \left(s^2 + 2\zeta_P \cdot \omega_P + \omega_P^2\right)}{K_{Plant} \cdot \omega_P} \cdot y(s) + K_{fb} \cdot y(s) = \frac{s^2 + 2\zeta_{sp} \cdot \omega_{sp} + \omega_{sp}^2}{K_{sp} \cdot \omega_{sp}} \cdot u(s) \tag{2.36}$$

where the plant parameters, K_{Plant}, ω_P and ζ_P are defined as:

$K_{Plant} = \frac{K_{Qx}}{A}$

$\omega_P = \sqrt{\frac{2A^2 \cdot \beta}{M \cdot V_0}}$

$\zeta_P = \left(\frac{K_{Qp} \cdot M}{A^2} + \frac{k_{visc} \cdot V_0}{2A^2 \cdot \beta}\right) \sqrt{\frac{A^2 \cdot \beta}{2M \cdot V_0}}$

The feedback loop gain K_{fb} is from the spring load opposing the rod's motion and is defined as, $K_{fb} = \frac{K_{Qp} \cdot k}{K_{Qx} \cdot A}$. In the case that the load is only inertial, $k = 0$ and the feedback loop is emitted. To further simplify the model the servovalve dynamics can be assumed to be sufficient fast to be neglected to represent the system with a third order transfer function.

2.2.2.1 Linearised Equations for Velocity Control

The new set of the linearised equations yields from equations 2.25, 2.26 and 2.30. Combination of 2.25 & 2.30 yields:

$$K_{Qx} \cdot x_{sp}(s) = A \cdot y(s) \cdot s + \frac{V_0}{2\beta} \cdot P_L(s) \cdot s + K_{Q_p} \cdot P_L(s) \tag{2.37}$$

From equation 2.26 it yields that:

$$P_L = \frac{1}{A}\left\{Ms^2 + k_{visc}s + k\right\} y(s) \tag{2.38}$$

Substitution of equation 2.38 to 2.37 yields that:

$$\frac{x_{sp}(s) \cdot K_{Qx}}{\frac{V_0 \cdot M}{2\beta A}} = y(s)\left[s^3 + \left\{\frac{k_{visc}}{M} + K_{Q_P} \cdot \frac{2\beta}{V_0}\right\} s^2 + \left\{\frac{2\beta A^2}{V_0 M} + \frac{2\beta K_{Q_P} k_{visc}}{V_0 M} + \frac{k}{M}\right\} s + \frac{2\beta K_{Q_P} k}{V_0 M}\right] \tag{2.39}$$

If we substitute the s^2, s coefficients and constant parameter with a_2, a_1 and a_0 equation 2.39 simplifies to:

$$x_{sp}(s) \cdot \mathbf{K} = y(s)\left[s^3 + a_2 s^2 + a_1 s + a_0\right] \tag{2.40}$$

For the case of *velocity control* there is an additional s term in the numerator which gives a system with a relative degree of 2:

$$\frac{\dot{y}(s)}{x_{sp}(s)} = \frac{\mathbf{K} \cdot s}{s^3 + a_2 s^2 + a_1 s + a_0} \tag{2.41}$$

where,

$\mathbf{K} = \frac{K_{Qx} \cdot 2\beta A}{V_0 \cdot M}$, $a_2 = \frac{k_{visc}}{M} + K_{Q_P} \cdot \frac{2\beta}{V_0}$, $a_1 = \frac{2\beta A^2}{V_0 M} + \frac{2\beta K_{Q_P} k_{visc}}{V_0 M} + \frac{k}{M}$ and $a_0 = \frac{2\beta K_{Q_P} k}{V_0 M}$.

2.2.2.2 Linearised Equations for Pressure Control

For the case of pressure control of the hydraulic system, manipulation of equation 2.37 and 2.38 yields:

$$K_{Qx} \cdot x_{sp}(s) = A \cdot y(s) \cdot s + \left[\frac{V_0}{2\beta} \cdot s + K_{Q_p}\right] \cdot P_L(s) \tag{2.42}$$

and

$$y(s) = \frac{A \cdot P_L}{Ms^2 + k_{visc}s + k} \tag{2.43}$$

Substitution of equation 2.43 to 2.42 gives:

$$K_{Qx} \cdot x_{sp}(s) = \frac{\left[\frac{V_0 \cdot M}{2\beta}s^3 + \left\{\frac{V_0 \cdot k_{visc}}{2\beta} + K_{Q_P} \cdot M\right\}s^2 + \left\{A^2 + \frac{V_0 \cdot k}{2\beta} + K_{Q_P} \cdot k_{visc}\right\}s + K_{Q_P} \cdot k\right]}{Ms^2 + k_{visc}s + k} \cdot P_L(s) \tag{2.44}$$

By close inspection of equation 2.44 it can be seen that the numerator (in brackets) is identical with the second part of equation *eq.*2.39 times $\frac{1}{A}$. Therefore equation 2.44 can be rewritten as:

$$x_{sp}(s) \cdot \mathbf{K} = \frac{A \cdot \{s^3 + a_2s^2 + a_1s + a_0\}}{Ms^2 + k_{visc}s + k} \cdot P_L(s) \Leftrightarrow \frac{P_L(s)}{x_{sp}(s)} = \frac{\mathbf{K}}{A} \cdot M \cdot \frac{s^2 + \frac{k_{visc}}{M}s + \frac{k}{M}}{s^3 + a_2s^2 + a_1s + a_0} \tag{2.45}$$

Therefore the linearised system for *pressure control* is of relative degree of 1:

$$\frac{P_L(s)}{x_{sp}(s)} = \frac{\mathbf{K} \cdot M}{A} \cdot \frac{s^2 + b_1s + b_0}{s^3 + a_2s^2 + a_1s + a_0} \tag{2.46}$$

where, $b_1 = \frac{k_{visc}}{M}$, $b_0 = \frac{k}{M}$, $\mathbf{K} = \frac{K_{Qx} \cdot 2\beta A}{V_0 \cdot M}$, $a_2 = \frac{k_{visc}}{M} + K_{Q_P} \cdot \frac{2\beta}{V_0}$, $a_1 = \frac{2\beta A^2}{V_0 M} + \frac{2\beta K_{Q_P} k_{visc}}{V_0 M} + \frac{k}{M}$ and $a_0 = \frac{2\beta K_{Q_P} k}{V_0 M}$.

2.2.2.3 Parameters of Linearised Hydraulic Model

In Table 2.1 the hydraulic plant parameters are presented. The linearization parameters are derived from experimental data from a hydraulic cycle of the injection moulding screw ($v_s = 0.01\,m/s$) with no polymer viscous load (empty barrel).

Hydraulic Parameters	Values
Physical Parameters	
Piston Area, A_1	$0.0043\,m^2$
Piston Area, A_2	$0.0058\,m^2$
Half Stroke	0.045 m
Volume, V_1	0.798 L
Volume, V_2	0.766 L
Piston Mass (each), M_p	30 kg
Bulk Modulus, β	$\approx 0.1\,GPa$
Rated Valve Flow, Q_r	$55\,\frac{L}{min}$
Flow Gain, K_v	$1.83 \cdot 10^{-6} m^3/s/\sqrt{Pa}$
Linearization Parameters	
Load Pressure at linearization point, P_{L_0}	$2.5\,MPa$
Spool displacement at linearization point, x_{sp_0}	0.05
Flow spool displacement coefficient, K_{Q_X}	$3.6 \cdot 10^{-3} m^3/s$
Flow load pressure coefficient, K_{Q_P}	$1.18 \cdot 10^{-11} m^3/s$
Hydraulic plant natural frequency, ω_p	343 rad/s (55 Hz)
Hydraulic plant damping ratio, ζ_p	0.25

Table 2.1: Hydraulic Model Parameters

In the case where the polymer viscous friction is neglected the Bode plot (open-loop response, no position feedback) for the hydraulic system (pure inertial load) with (5th order system) and without (3rd order system) servo-proportional valve dynamics (represented by 2nd order model) is presented in the Figure 2.4.

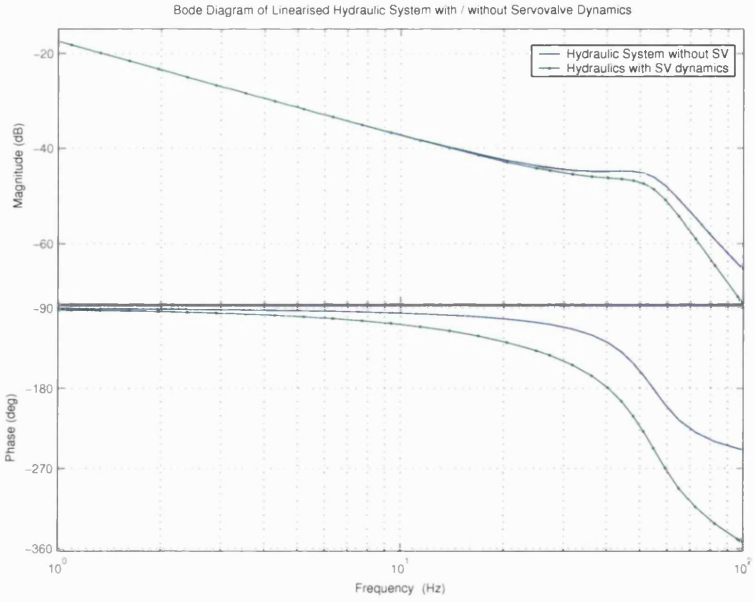

Figure 2.4: Bode Plot of Linearised Hydraulic System - Simulation

To compare the theoretically estimated plant dynamics (natural freq.) the frequency response of the hydraulic injection screw was derived experimentally (using a chirp signal of $0.01m/s$ amplitude and frequency range from $0.1 to 100Hz$). The frequency response of the hydraulic plant and servo-proportional valve were estimated by monitoring and logging input and output signals of screw velocity and valve spool position. The data were processed in Matlab's plant identification routine with a spectral model using a smooth Fourier transform method, as seen in Figure 2.5.

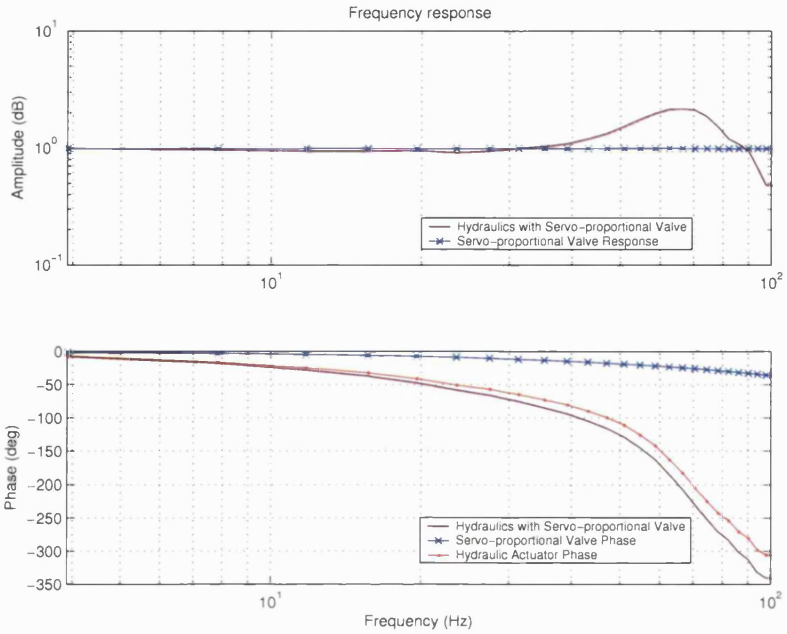

Figure 2.5: Bode Plot of Hydraulic System - Experimental

The phase of the actuator's frequency response was calculated as the difference of the measured phase lag of the system and servo-proportional valve. The natural frequency of the actuator system (pair) was obtained at $-90°$ phase shift between the excitation source and response of the actuator. It was found to be 44Hz. However by observation of the amplitude plot it can be seen that instead of having the resonance at 44Hz it occurs at 65Hz indicating that another phase effect is coming either from the stationary pair of actuators (which move the injection unit forward and backward before injection) that may vibrate as well during excitation or from another component of the hydraulic system. To locate the additional effect one accelerometer was attached on the stationary pair of actuators and another on the actuator's rod which is attached to the injection moulding machine structure. When the acceleration signals were processed both signals were found to be identical and in phase as can be seen in Figure 2.6.

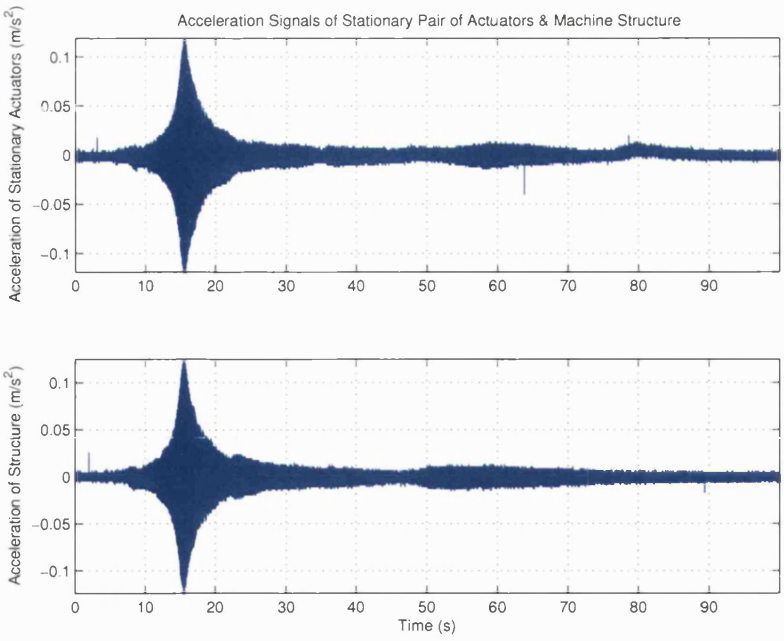

Figure 2.6: Input and Output Plant Signals of Hydraulic System - Experimental

This indicates that the stationary pair of actuators have not any significant effect on the active pair of actuators. Moreover both acceleration signals indicate a resonance at 16 seconds (16Hz), most likely the resonance frequency of the injection moulding machines structure. Another important phenomenon which was observed, was a mechanical noise occurring during excitation of the hydraulics around 60-65Hz. It was concluded that this noise comes from the injection screw which at that frequency starts vibrating inside the barrel where a small clearance exists. This frictional contact with the barrel wall, acts as an additional load and disturbance to the hydraulic system. Therefore the resonance occurring at 65Hz (in Figure 2.5) is most likely caused by the screw and can be assumed to be the main reason for not having the resonance at 44Hz. Overall the discrepancy between the theoretical (55Hz) and experimental estimation (44Hz) arises from the selection of parameters in the linearised model and simplification of the model. Although the parameters of the linearised model could be tuned to minimise the error, this was not done as the linearised model was not used for the adaptive controller (more details in Chapter 6).

2.3 Polymer Rheology & Material Characterization

The processing parameters during the injection moulding cycle strongly influence the final properties of the parts. In polymer processing the formed molecular structure has a direct effect on the properties of the material. The most important is the viscosity which is a fluid

property that represents the material's internal resistance to deform. Mathematically, viscosity is defined as the ratio of shear stress and shear rate. Most polymeric liquids are non-Newtonian fluids as their viscosity varies with the shear rate. Viscosity behaviour of materials is important in determining the flow length and the amount of viscous heating generated during the melt flow. Most melt polymer exhibit shear-thinning behaviour (Figure 2.7), which translates to lower viscosity with higher shear rate.

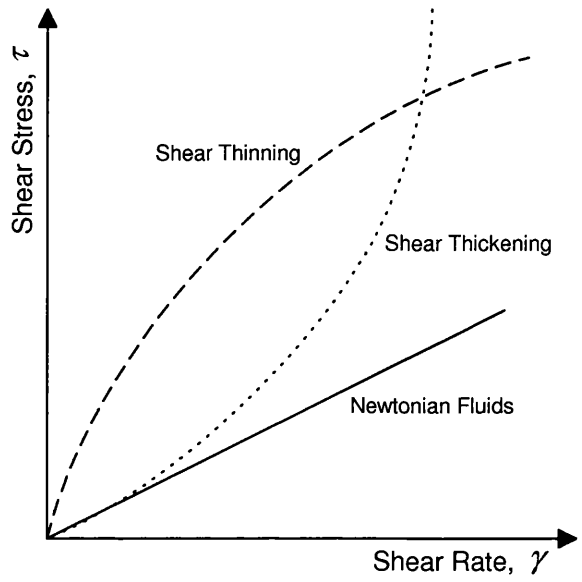

Figure 2.7: Shear Thinning Behaviour of non-Newtonian Polymers

Therefore in an injection moulded part the viscosity of the melt polymer can vary throughout the product. Melt viscosity decreases with temperature but the sensitivity varies among different thermoplastics. The viscosity is critical for determining the injection pressure with a given rate or the flow length with a given maximum pressure [56, 57].

2.3.1 Mould Dimensions and Volumes

In order to investigate experimentally the behaviour of the polymer melt during injection a new mould was designed and manufactured. A preliminary analysis was made to estimate the pressure drop at each of the flow paths. This is always required to ensure that the machine is capable (within limits of max injection pressure) of filling the mould at a certain speed. A schematic illustration in Figure 2.8 shows the flow paths, including the barrel and nozzle of the injection-moulding machine.

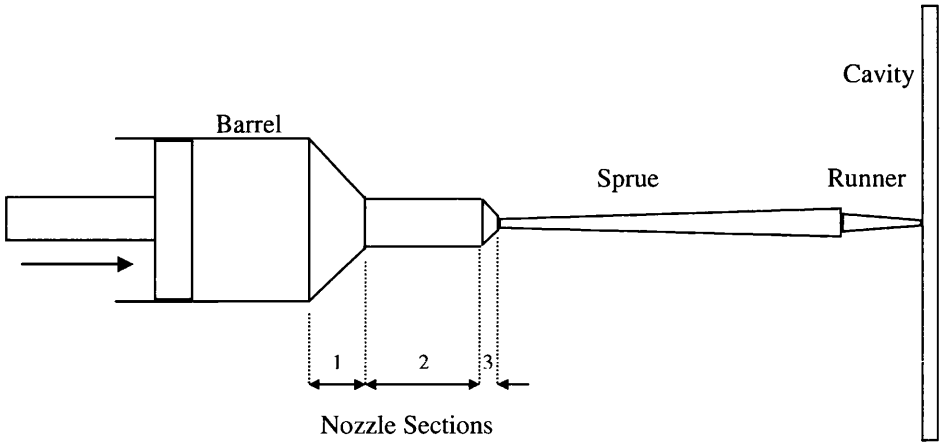

Figure 2.8: Mould Flow Paths

The convergence angle of the nozzle contributes to the shear of the polymer (viscosity decreases) before entering the mould cavity. The mould cavity is of an oblong shape with constant thickness. The dimensions of the nozzle and mould sections are presented in Table 2.2.

Sections (all dimensions in m)	Length	Radius R1	Radius R2	Volume (m^3)
1. Nozzle tapered section 1	0.032	0.0125	0.004	$7.45 \cdot 10^{-6}$
2. Nozzle cylindrical section 2	0.082	0.004	-	$4.12 \cdot 10^{-6}$
3. Nozzle tapered section 3	0.006	0.004	0.00085	$1.26 \cdot 10^{-7}$
4. Sprue reverse tapered section	0.080	0.001	0.004	$1.76 \cdot 10^{-6}$
5. Runner tapered section	0.011	0.0025	0.001	$1.12 \cdot 10^{-7}$
6. Mould Cavity $(0.160 \times 0.044 \times 0.004)$		-	-	$2.82 \cdot 10^{-5}$

Table 2.2: Mould Dimensions and Volumes

2.3.2 Behaviour of Polymer Viscosity under Flow Restrictions

To estimate the injection pressure requirements for the filling of the new mould, the pressure drop at each flow paths must be calculated. In the following analysis, mathematical models (of a non-Newtonian polymer - polypropylene) for the pressure drop at different geometries are presented. Most polymers exhibit a non-Newtonian behaviour where the apparent viscosity decreases as the shear rare increases (shear thinning). This decrease in viscosity occurs over many decades of shear rate while the viscosity at high shear rates can be of several orders of magnitude smaller than at lower shear rates [58]. To describe this pseudo-plastic behaviour (shear thinning) of the polymer over a certain range of shear rates, a power law model is used. In this power law the flow curve of log shear stress versus log shear rate is a straight line for a certain shear rate range [57] and is defined as:

$$\tau = C(\dot{\gamma}_\alpha)^n \tag{2.47}$$

where τ is the shear stress $\left(N/m^2\right)$, $\dot{\gamma}_\alpha$ is the apparent shear rate and n is the power law index which indicates the degree of the non-Newtonian behaviour (between values $0 < n < 1$). Most polymers follow a pseudo-plastic behaviour ($n < 1$) where n decreases with increasing shear rate. When $n = 1$ the fluid is Newtonian. Term C is the consistency factor, a measure of the Newtonian viscosity at low shear rates. The development of this empirical constitutive relationship (power law model) is a curve fitting process where for calculation purposes is only sufficiently accurate for one decade of shear stress. For more than one decade the apparent viscosity, η_α does not follow a linear relationship with the shear stress or strain rate [32].

$$\eta_\alpha = \frac{\tau}{\dot{\gamma}_\alpha} = C(\dot{\gamma}_\alpha)^{n-1} \tag{2.48}$$

2.3.2.1 Polymer Flow between Parallel Plates - Cavity Section

For the polymer flow between parallel plates (Figure 2.9) the pressure drop, shear rate (at the wall) and shear stress (at the wall) can be mathematically described [32] as follows:

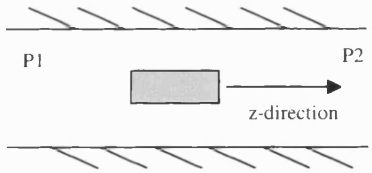

Figure 2.9: Flow between parallel plates

The pressure drop at the flow path is :

$$\Delta P = \frac{2\tau_w \cdot L}{h} = -2C \cdot \frac{L}{h}\left[\frac{(2n+1)\cdot 2Q}{n \cdot T \cdot h^2}\right]^n \tag{2.49}$$

The shear stress at the wall is:

$$\tau_w = \frac{h}{2}\left(\frac{dP}{dz}\right) = -C\left[\frac{(2n+1)\cdot 2Q}{n \cdot T \cdot h^2}\right] \tag{2.50}$$

The strain rate at the wall is:

$$\dot{\gamma}_w = -\frac{(2n+1)\cdot 2Q}{n\cdot T\cdot h^2} \tag{2.51}$$

2.3.2.2 Polymer Flow in a Circular Channel - Nozzle Section 2

For the polymer flow in a circular channel (Figure 2.10) the pressure drop, shear rate (at the wall) and shear stress (at the wall) can be mathematically described [32] as follows:

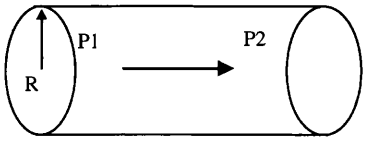

Figure 2.10: Flow in a circular channel

The pressure drop at the flow path is :

$$\Delta P = \frac{2\tau_w \cdot L}{R} = -2C\cdot\frac{L}{R}\left[\frac{(3n+1)\cdot Q}{n\cdot\pi\cdot R^3}\right]^n \tag{2.52}$$

The shear stress at the wall is:

$$\tau_w = \frac{R}{2}\left(\frac{dP}{dz}\right) = -C\left[\frac{(3n+1)\cdot Q}{n\cdot\pi\cdot R^3}\right]^n \tag{2.53}$$

The strain rate at the wall is:

$$\dot{\gamma}_w = -\frac{(3n+1)\cdot Q}{n\cdot\pi\cdot R^3} \tag{2.54}$$

2.3.2.3 Polymer Flow in a Reverse Tapered Channel - Sprue Section

For the polymer flow in a reversed tapered channel (Figure 2.11) the pressure drop, shear rate (at the wall) and shear stress (at the wall) can be mathematically described [32] as follows:

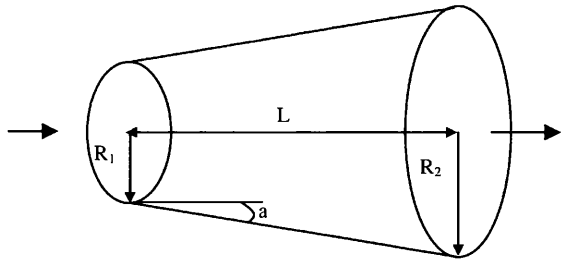

Figure 2.11: Flow in a reversed tapered channel

The pressure drop is:

$$\Delta P = \frac{2\tau_{1w}}{3n \cdot tan\alpha} \cdot \left[1 - \left(\frac{R_1}{R_2}\right)^{3n}\right], \quad \alpha = tan^{-1}\left[\frac{(R_2 - R_1)}{L}\right] \tag{2.55}$$

$$\Delta P = -2C \cdot \frac{1}{3n \cdot tan\alpha} \cdot \left[1 - \left(\frac{R_1}{R_2}\right)^{3n}\right] \cdot \left[\frac{(3n+1) \cdot Q}{n \cdot \pi \cdot R_1^3}\right]^n \tag{2.56}$$

The shear stress at the wall is:

$$\tau_{1w} = \frac{R_1}{2}\left(\frac{dP}{dz}\right) = -C\left[\frac{(3n+1) \cdot Q}{n \cdot \pi \cdot R_1^3}\right]^n \tag{2.57}$$

The strain rate at the wall is:

$$\dot{\gamma}_{1w} = -\frac{(3n+1) \cdot Q}{n \cdot \pi \cdot R_1^3} \tag{2.58}$$

To estimate during simulation the flow front position of the polymer inside the reversed tapered channel the following method was adopted. In Figure 2.12 the initial radius of the reversed tapered channel is R_1 and increases linearly with the length depending on the the converging angle α.

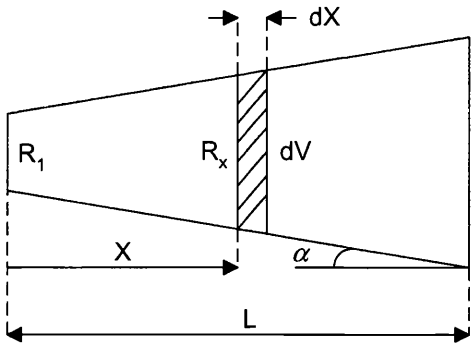

Figure 2.12: Geometry of a reversed tapered channel

The instantaneous value of the radius R_x for length x can be realised using the following formula.

$$R_x = R_1 + x \cdot tan\alpha \tag{2.59}$$

Assuming that the radius of the flow channel remains constant for a small volume dV, the horizontal displacement dX, can be defined as the following ratio.

$$dX = \frac{dV}{\pi \cdot R_x^2} \tag{2.60}$$

The instantaneous length can be defined as the sum of each individual dX.

$$X = \sum dX \tag{2.61}$$

2.3.2.4 Polymer Flow in a Tapered Channel - Nozzle 1 & 3 and Runner Sections

For the polymer flow in a tapered channel (Figure 2.13) the pressure drop, shear rate (at the wall) and shear stress (at the wall) can be mathematically described [32] as follows:

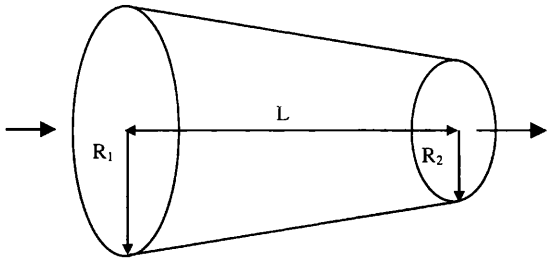

Figure 2.13: Flow in a tapered channel

The pressure drop is:

$$\Delta P = 2C \cdot \frac{L}{3n(R_1 - R_2)} \cdot \left[\frac{(3n+1) \cdot Q}{n \cdot \pi} \left(\frac{1}{R_1^3} - \frac{1}{R_2^3} \right) \right]^n \tag{2.62}$$

The shear stress at the wall is:

$$\tau_{1w} = \frac{R_1}{2} \left(\frac{dP}{dz} \right) = -C \left[\frac{(3n+1) \cdot Q}{n \cdot \pi \cdot R_1^3} \right]^n \tag{2.63}$$

The strain rate at the wall is:

$$\dot{\gamma}_{1w} = -\frac{(3n+1) \cdot Q}{n \cdot \pi \cdot R_1^3} \tag{2.64}$$

For the case of the tapered channel the flow front position can be estimated in simulation using the integration method described in previous section with the only difference that the the instant value of the radius R_x for length x can be realised using the following formula.

$$R_x = R_1 - x \cdot tan\alpha \tag{2.65}$$

2.3.3 Pressure Drop in Nozzle Runners and Mould

With the use of the mathematical expressions previously described, the pressure drops along the mould have been estimated. The viscosity of polypropylene (PP) versus shear rate is shown in Figure 2.14. The processing temperature of the polymer is within the region of $200 - 210°C$,

so the chart of PP viscosity versus shear rate can be used for calculation of the power law constants.

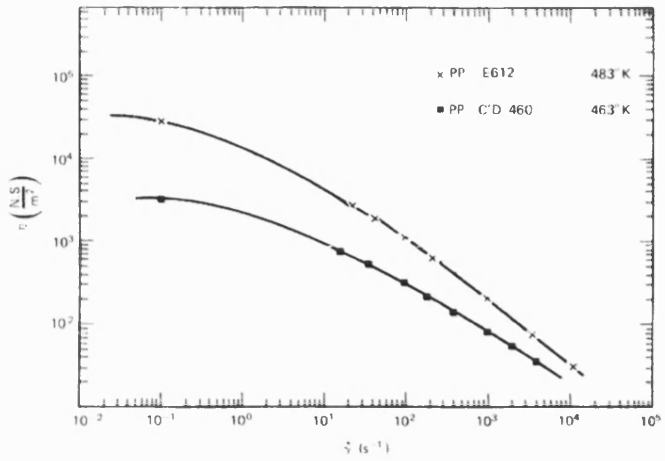

Figure 2.14: Polypropylene Viscosity Chart, After [1]

The following data presented in Table 2.3 were extracted from Figure 2.14 and can be used to identify the viscosity power law constants C and n.

η_α(Viscosity)	$log(\eta_\alpha)$	$\dot{\gamma}_\alpha$	$log(\dot{\gamma}_\alpha)$
10450	4.019	100	0
4250	3.628	101	1
1100	3.041	102	2
215	2.332	103	3
22	1.342	104	4

Table 2.3: Power Law Constants

By taking logs in (2.48), the apparent viscosity η_α can be described as:

$$log(\eta_\alpha) = log(C) + (n-1)\, log\dot{\gamma}_\alpha \tag{2.66}$$

Therefore the plot of $log(\eta_\alpha)$ versus $log\dot{\gamma}_\alpha$ will have the *gradient* $(n-1) = \frac{1.342-3.628}{4-1} = -0.762 \Rightarrow n = 0.238$.

If one point $\left(\dot{\gamma}_\alpha = 10^3\right)$ is taken to find C, then:

$$log(215) = log(C) + (-0.762)\,log\left(10^3\right) \Leftrightarrow C = 41.5 \cdot 10^3 \tag{2.67}$$

Now the viscosity for all the shear rate range $\left(10^1 - 10^4\right)$ is estimated as:

$$\eta_\alpha = 41.5 \cdot (\dot{\gamma}_\alpha)^{-0.762} \tag{2.68}$$

The polymer's flow rate in the mould is proportional to the screw velocity during the filling phase. A typical injection velocity such as $v_s = 0.012m/s$ gives a flow rate of:

$$Q = v_s \cdot A_s = 0.012 \times 4.9 \cdot 10^{-4} = 5.89 \cdot 10^{-6} m^3/s \tag{2.69}$$

Using the equations of strain rate at the wall for each section of the nozzle and mould in combination with the above estimated coefficients (η_α, C, n) the shear rate can be theoretically calculated. The estimated shear rate for each flow section is shown in Table 2.4.

Sections	Shear Rate (s-1)	Decade
Nozzle tapered section 1	6.9	$\left(10^0 - 10^1\right)$
Nozzle cylindrical section 2	211	$\left(10^2 - 10^3\right)$
Nozzle tapered section 3	211	$\left(10^2 - 10^3\right)$
Sprue reversed tapered section	$13.5 \cdot 10^3$	$\left(10^4 - 10^5\right)$
Runner tapered section	864	$\left(10^2 - 10^3\right)$
Mould Cavity	104	$\left(10^2 - 10^3\right)$

Table 2.4: Shear rate at the inlet wall of the mould flow path sections

Once the shear rate is known, it is more accurate to estimate the power law constants again, for each particular decade (to avoid mistakes). For this reason four power laws have been estimated in Table 2.5.

Decade	Law Constant c	Law Constant C	Power Laws
$\left(10^0 - 10^1\right)$	0.609	$10.5 \cdot 10^3$	$\eta_\alpha = 10.5 \cdot 10^3 \cdot (\dot{\gamma}_\alpha)^{-0.391}$
$\left(10^1 - 10^2\right)$	0.0414	$16.4 \cdot 10^3$	$\eta_\alpha = 16.4 \cdot 10^3 \cdot (\dot{\gamma}_\alpha)^{-0.586}$
$\left(10^2 - 10^3\right)$	0.291	$28.8 \cdot 10^3$	$\eta_\alpha = 28.8 \cdot 10^3 \cdot (\dot{\gamma}_\alpha)^{-0.709}$
$\left(10^3 - 10^4\right)$	0.01	$200 \cdot 10^3$	$\eta_\alpha = 200 \cdot 10^3 \cdot (\dot{\gamma}_\alpha)^{-0.99}$

Table 2.5: Viscosity Power Law Constants & Power Laws valid for One Decade

Using the equations (2.51,2.54,2.58,2.64) and the new coefficients calculated in Table 2.5, the pressure drop (at flow path), shear stress (at inlet wall) and shear rate (at inlet wall) for each section of the mould have been theoretically calculated in Table 2.6. The total pressure drop at the flow path sections is predicted to be 400bar.

Sections, $i = 1,...,6$	$\Delta P\ (bar)$	$\tau_w\ (N/m^2)$	$\dot{\gamma}_w\ (s^{-1})$
1. Nozzle tapered section 1	8.4	$2.59 \cdot 10^4$	4.45
2. Nozzle cylindrical section 2	54.3	$1.32 \cdot 10^5$	188.6
3. Nozzle tapered section 3	22.3	$1.32 \cdot 10^5$	188.6
4. Sprue reversed tapered section	164.1	$2.27 \cdot 10^5$	$1.93 \cdot 10^5$
5. Runner tapered section	73.1	$1.99 \cdot 10^5$	772.4
6. Mould Cavity	78	$9.75 \cdot 10^4$	73.9
Total Pressure Drop for PP	$\approx 400\,bar$		

Table 2.6: Pressure Drop, Shear Stress and Shear Rate at Flow Paths when Injecting Polypropylene

This total pressure drop of 400 bar corresponds to a hydraulic pressure of about 34.5 bar (1 bar in hydraulic circuit = 11.6 bar in injection barrel). For the case where Polycarbonate is used for injection, following the same procedure, the total pressure drop at the flow path sections is calculated to be 683 bar. This corresponds to a hydraulic circuit pressure of about 58.9bar. The maximum injection pressure of the injection-moulding machine used is 100 bar, so this product can be moulded.

2.3.4 Modelling Polymer Viscosity

At the beginning of the process the viscosity due to the high temperature of the melt is quite low with amorphous regions. As more and more crystals are formed during crystallization the viscosity increases with a sharp change. The most accurate model that can be used to describe the polymer viscosity for the injection moulding process is the Cross-WLF model. This model is specified by *seven constants*, which account for the effect of temperature, shear rate, and pressure on the viscosity over a wide temperature range [59]. The Cross-WLF model is currently used by most commercial simulation packages such as *C-Mould* and *Moldflow*.

The region between the Newtonian and shear thinning behaviour is defined by the τ^* factor that represents the shear stress at which the onset of the shear thinning behaviour occurs. The zero-shear rate viscosity (as the shear rate approaches infinity) is represented by the WLF model. Constants A_1, A_2, D_1, D_2 and D_3 are used to describe the zero-shear rate viscosity η_0.

$$\eta(T,\dot{\gamma},p) = \frac{\eta_0(T,p)}{1+\left[\frac{\eta_0(T,p)\cdot\dot{\gamma}}{\tau^*}\right]^{(1-n)}} \tag{2.70}$$

When, $T \geq T_g$, $\eta_0(T,p) = D_1 \cdot exp\left\{\frac{-[A_1(T-T_g)]}{[A_2+(T-T_g)]}\right\}$

When, $T < T_g$, $\eta_0(T,p) = \infty$

Where, $A_2 = \tilde{A}_2 + D_3 \cdot p$ and $T_g = D_2 + D_3 \cdot p$.

The full expression of the zero shear rate viscosity is defined as:

$$\eta_0(T,p) = D_1 \cdot exp\left\{\frac{-A_1 \cdot [T-(D_2+D_3 \cdot p)]}{\tilde{A}_2 + D_3 \cdot p + [T-(D_2+D_3 \cdot p)]}\right\} \tag{2.71}$$

where the units of the constant parameters are given in Table 2.7.

τ^*	D_1	$\tilde{A}_2, D_2$	D_3	A_1, n
Pa	$Pa-s$	K	K/Pa	dimensionless

Table 2.7: Units of zero-shear rate viscosity

The constant parameters of the Cross-WLF model for Polypropylene and Polycarbonate are summarised in Table 2.8.

Parameters	**PP**	**PC**	**Units**
n	0.29	$0.17-0.2$	-
τ	$25.23 \cdot 10^3$	$716.5 \cdot 10^3$	Pa
D_1	$168 \cdot 10^{12}$	$2.68 \cdot 10^{12}$	$Pa \cdot s$
D_2	263	417.15	K
D_3	$5 \cdot 10^{-7}$	$2 \cdot 10^{-7}$	$K \cdot Pa^{-1}$
A_1	34.67	30.22	-
A_2	51.6	51.6	K

Table 2.8: PP & PC parameters for Cross-WLF model, from [60]

2.3.5 Governing Equations for the Filling Phase

The following state equations describe the polymer melt behaviour during the filling phase of the injection cycle. The polymer flows due to the physical movement of the screw and the rise of pressure inside the injection barrel. The pressure drop along the nozzle is assumed to be the same as the barrel pressure since the pressure drop along the barrel is insignificant. From the continuity equation for a compressible polymer the conservation of the polymer mass inside the barrel is described as:

$$\frac{dP_n}{dt} = \frac{\beta_p}{V_b}\left(A_b \cdot \frac{dx}{dt} - Q_p - Q_{leak}\right) \tag{2.72}$$

Hence, the pressure drop along the nozzle is defined as:

$$P_n = \int \frac{\beta_p}{A_b \cdot (x_{max} - x_0)} \cdot \left(A_b \cdot \frac{dx}{dt} - Q_p - Q_{leak}\right) \tag{2.73}$$

The volume of the polymer left inside the barrel with respect to the position of the screw is:

$$V_b = V_{b_0} - \int_{x_{min}}^{x_{max}} (Q_p - Q_{leak})\, dt \tag{2.74}$$

To estimate the viscous friction load opposing the actuator, the pressure drop along the mould flow path sections must be determined. The viscous shear force is estimated as the product of the overall pressure drop across the flow path sections times the area ($4.9087 \cdot 10^{-4} m^2$) of the injection barrel :

$$F_{viscous} = \Delta P_T \cdot A_b \tag{2.75}$$

To determine the pressure drop across (ΔP) the geometrical sections of the nozzle and mould equations (2.49,2.52,2.56,2.62) were used. As the polymer solidifies during the packing and cooling phase the flow cross section changes as well, however this effect is not considered in the simulation. To derive the consistency factor C_i (2.48) in these equations, the seven constant Cross-WLF viscosity model (2.70) was used to account for temperature and pressure variations that occur in the polymer melt viscosity during the cycle.

$$C_i = \frac{\eta_{\alpha_i}}{(\dot{\gamma}_{\alpha_i})^{n-1}} = \frac{\eta_{\alpha_i}(T,\gamma,p) = \frac{\eta_{0_i}(T,p)}{1+\left[\frac{\eta_{0_i}(T,p)\cdot\dot{\gamma}_{\alpha_i}}{\tau^*}\right]^{(1-n)}}}{(\dot{\gamma}_{\alpha})^{n-1}} \tag{2.76}$$

The overall pressure drop is described as the sum of the pressure drops at the nozzle ($i = 1,2,3$) and mould sections ($i = 4,5,6$):

$$\Delta P_T = \sum_{i=1}^{6} \Delta P_i \tag{2.77}$$

where the pressure drop at each section is a function of the flow rate of the melt polymer. Since the flowrate and the geometry of the cross sections are known the flow-front position X_{ff}, can be determined by integration of the flow area where $X_{ff} = \sum dX$ (eq:2.61).

During the filling phase the volume of the melt inside the cavity changes continuously due to the compressibility of the polymer. The modified Tait equation describes the pvT behaviour of the polymer and is based on measurements of isothermal compression volume changes starting at each temperature from atmospheric pressure [60]. The two-domain Tait pvT equation is described as:

$$V(T,p) = V_0(T) \cdot \left[1 - C_{Tait} \cdot ln\left(1 + \frac{p}{B(T)}\right)\right] + V_t(T,p) \tag{2.78}$$

where $V(T,p)$ is the specific volume inside the cavity at temperature T and pressure P while V_0 is the specific volume at zero gauge pressure. C_{Tait} is a universal constant equal to 0.0894 and B describes the pressure sensitivity of the polymer. The $V_t(T,p)$ term is applicable only for crystalline materials, and in the case of amorphous materials this term is omitted. By differentiating the Tait pvT equation assuming constant temperature [61] the nonlinear nature of the polymer bulk modulus can be approximated as:

$$\beta_p = \frac{P_n + B(T)}{C_{Tait}} \left(1 - C_{Tait} \cdot log\left[1 + \frac{P_n}{B(T)}\right]\right) \tag{2.79}$$

In the case where the material temperature is greater than the glass transition temperature, $T > T_g$:

$$B(T) = b_{3m} \cdot exp\left[-b_{4m}(T - b_5)\right] \tag{2.80}$$

while when the material temperature is lower than the glass transition temperature, $T < T_g$ it follows that:

$$B(T) = b_{3s} \cdot exp\left[-b_{4s}(T - b_5)\right] \tag{2.81}$$

The subscripts m and s refer to the molten and solid state of the polymer. The transition temperature is assumed to be a linear function of the pressure where b_5 is the transition temperature at zero gauge pressure and b_6 the linear increase in the transition temperature with pressure.

$$T_t(p) = b_5 + b_6 \cdot p \tag{2.82}$$

The constant parameters for Polypropylene and Polycarbonate for the two-domain Tait pvT model which are applicable for eq. (2.79) are summarised in Table 2.9.

Parameters	PP	PC	Units
b_5	428.15	417.15	K
b_6	$0.715 \cdot 10^{-7}$	$3.48 \cdot 10^{-7}$	K/Pa
b_{3m}	$0.866 \cdot 10^{8}$	$1.82 \cdot 10^{8}$	Pa
b_{4m}	$5.181 \cdot 10^{-3}$	$4.041 \cdot 10^{-3}$	K^{-1}
b_{3s}	$1.47 \cdot 10^{8}$	$2{,}99 \cdot 10^{8}$	Pa
b_{4s}	$4.589 \cdot 10^{-3}$	$1.71 \cdot 10^{-3}$	K^{-1}

Table 2.9: PP & PC parameters for pvT - Tait equation, from [60]

2.3.6 Governing Equations for the Packing Phase

For the case of the packing phase, the volume of the melt inside the cavity changes continuously as additional material is injected to compensate for shrinkage effects. The overall pressure inside the cavity was simply estimated by considering the pressure drop due to the shear flow and the compressibility effect with respect to volume change:

$$P_{cav.} = \Delta P_{cav.} + \int \frac{Q_{cav.} \cdot \beta_p}{V_t} \tag{2.83}$$

where the final cavity volume is the initial volume at the beginning of packing plus the additional volume injected during packing:

$$V_t = V_{cav} + V_{pack} \tag{2.84}$$

The packing phase model provides an approximation of the cavity pressure behaviour during the packing phase under normal operating conditions, which is sufficient for simulation purposes regarding the controller's evaluation. To account for temperature changes that occur in the polymer melt during the simulation (fill & pack), experimental data from thermocouples embedded near the mould surface were used (details in Chapter 4). The heat transfer rate from the melt to the mould was approximated using a heat transfer model under normal moulding conditions and found to be, $6°C/s$ during filling, $1.25°C/s$ during packing and $0.5°C/s$ during cooling. A look up table with different heat transfer rates was developed for a set of pressure levels adopted during the packing phase. It must be noted that the low heat transfer rates during packing and cooling were due to the insulation between the mould and the machine's platens as no cooling method was used. The insulation was introduced on purpose to prolong the solidification of the melt and to allow for various packing profiles to be implemented and test their effect. Generally solidification times vary and are dependent on the cooling rate and insulation of the mould.

Overall the developed mould model provides an approximate representation for the nonlinear viscous friction load that counteracts the actuator's motion during the filling and packing phase where pressure and temperature variations vary the viscoelastic behaviour of the melt polymer. It can be used as a simulation model in the design and development of new velocity and load (P-Q) controllers.

2.3.7 Polymer Leakage

The injection moulding machine used for experimental purposes was equipped with a screw but without a check valve. Therefore leakage past the screw was a parameter that should be considered in modelling and simulation. Depending on the viscosity of the polymer and processing temperature, leakage varies and reduces the amount of polymer injected in the cavity, It also acts as a damping factor in the motion of the screw. The amount of leakage was estimated experimentally with [62]. To estimate the leakage a small cavity was over-packed while packing was further extended for a period of time. At the same time the screw velocity was observed to reduce gradually close to zero. The experiments were held at three different processing temperatures of $200°C$, $220°C$ and $240°C$. A linear approximation is shown in Figure 2.15, was derived by [62] to describe the polymer leakage in relation with the barrel pressure.

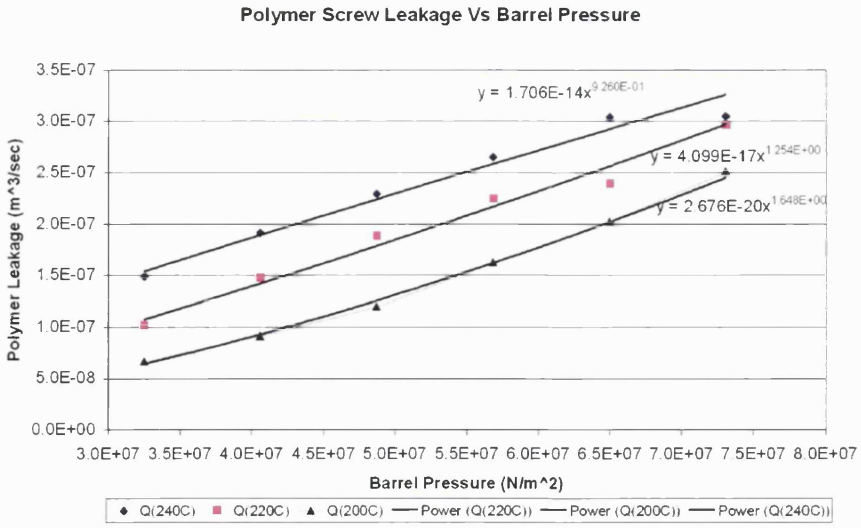

Figure 2.15: Linear approximation of the polymer leakage, from [62]

2.4 Simulation Study

For the numerical simulation of the filling and packing phase the nonlinear model of the plant (hydraulics & mould) was used. A discrete time PI and PID controllers were used for the flow and pressure control respectively. The discrete controllers could also at a later stage be implemented experimentally in the injection moulding machine. Due to the nature of the process the control parameter changes from flow to pressure during the transition to packing phase. Traditionally the screw stroke is used to initiate the switch of the controlled parameter. However this method is not reliable and requires many trial and error cycles to reach an optimum level (switching when the mould is almost full). Therefore to guarantee an accurate transition in simulation, the derivative of the hydraulic circuit or cavity pressure should be used. The reason for using the derivative of the pressure is because it gives a sharp increase at the time of switching as the pressure changes abruptly. In the case of a premature commencement of the pressure controller it is very likely that the system will go unstable due to the low damping of the load.

2.4.1 Anti-windup & Bumpless Transfer Algorithm

During the switch from flow to pressure control it is necessary to maintain a continuous command signal to the servovalve (which controls the screw) otherwise any considerable fluctuation could cause pressure and velocity perturbations. These can be high enough to saturate the active controller (pressure controller) interrupting the injection cycle. Moreover if the output of the pressure (load) controller is outside the servovalve's bandwidth it can act as a nonlinear saturation element to the plant. This phenomenon has been extensively studied with PID controllers and is classified as *integral windup* where the controller continuously integrates the plant's error saturating the plant [63]. To avoid this undesirable situation it is important to match the the output of the pressure controller with that of the flow (velocity) controller. Two anti-windup and bumpless transfer (AWBT) approaches have been successfully used so far in the literature [64, 65]. The first scheme assumes that the controller's states are known so that they can be manipulated to maintain a continuous control signal during the transition. Therefore the states of the flow controller are adjusted so that immediately after the switching the output of the plant is identical with that of the pressure controller just before the transition [64]. However this approach is not always applicable as the controllers states are not always computable. The second scheme is of a model based approach as the output of the second controller is constrained to track that of the first. This approach is of an input-output model and does not require the controller's states to be known.

In this work a modification of the second scheme was used. The pressure controller (2nd) was forced to track a first order pressure reference model while the initial condition was the differential pressure of the plant (controlled variable) at the time of switching. In addition, the integrator of the controller was reset to match the initial condition set by the reference model to avoid integral windup. In this way the output of the second controller was matching that of the first providing a smooth transition.

2.4.2 PID Control

The two controllers (PI and PID) were coupled under the proposed bumpless transfer algorithm avoiding major velocity transients when switching from flow to pressure control. Both feedback states, velocity and pressure were normalised. A schematic illustration is presented in Figure 2.16.

In the z-domain the PID controller is described as:

$$G_c(z) = K_p + \frac{K_i}{1-z^{-1}} + K_d\left(1-z^{-1}\right) \tag{2.85}$$

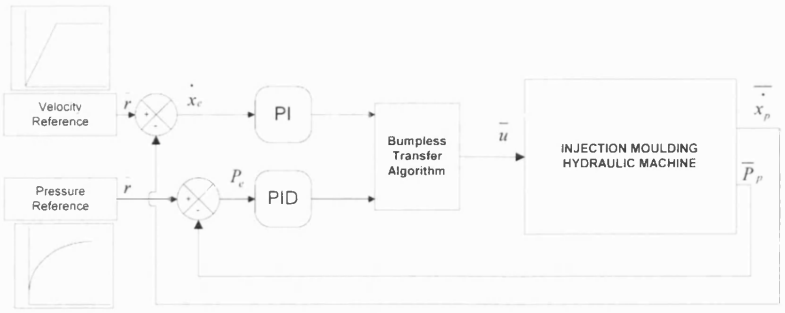

Figure 2.16: Hydraulic Pressure and Flow during Filling and Packing Stage

To cancel out noise in the feedback state (either velocity or pressure) the PID controller was realised with an approximate first order filter. The filter coefficient F_c and filter equation follow where, X_f and X_{in} are the output and input signals while TF and T_s are the filter and model time constants.

$$F_c = e^{-\frac{T_s}{TF}} \approx \frac{TF}{TF + T_s} \tag{2.86}$$

$$X_f(n) = X_f(n-1) + \left(\frac{T_s}{T_s + TF}\right) \cdot (X_{in}(n) - X_f(n-1)) \tag{2.87}$$

In $Matlab_{\circledR}$ Simulink the filter was implemented using a discrete time integrator with an initial condition, as seen in Figure 2.17.

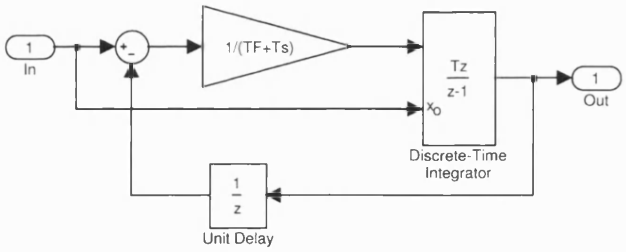

Figure 2.17: Hydraulic Pressure and Flow during Filling and Packing Stage

The tuning of both PI and PID controllers was performed using the *Ziegler-Nichols* method [66] where the proportional, integral and derivative gains are given in Table 2.10 for both cases.

Control	Gains		
	P	I	D
PI (flow control)	0.35	0.01	0
PID (pressure control)	2	0.04	0.005

Table 2.10: Discrete PI and PID Controller Gains

Two reference models (1st order) were used where the plant had to follow a specific velocity setpoint and a pressure trajectory. Some of the reference model parameters are summarised in Table 2.11.

Reference Model Parameters		
	Rise Time	Setpoint
Velocity Reference Model	0.075 s	0.02 m/s
Pressure (ΔP) Reference Model	4 s	33 bar

Table 2.11: Parameters of Flow & Pressure Reference Models

The setpoint of the velocity reference model can be adjusted accordingly (from 0.01 - 0.08 m/s) to influence the final properties of the part (residual stresses, part weight, etc). For the pressure reference model the rise time and setpoint can be altered depending on the dimensions of the flow paths that determine the minimum hydraulic pressure required to fill and pack the mould cavity.

2.4.3 Simulink Model of Hydraulics

In the initial simulation studies the actuator was set to start from the end providing a full stroke of material dosage to fill the cavity. The processing temperature of the melt was set at 200°C. The derivative of the differential hydraulic pressure was used as the trigger signal to switch to the packing phase. The PI and PID controllers where used to control the hydraulic system's response at various velocity setpoints and pressure profiles with an overall stable performance. The end of packing was initiated once the cavity volume was 5% more than its actual capacity and/or the screw velocity dropped close to zero.

The screw position and velocity during filling and packing for a typical case is shown in Figure 2.18. When switching to pressure control the bumpless transfer algorithm ensures a smooth transfer in the hydraulic pressure while a small perturbation occurs in the screw velocity that decays fast. Apart from keeping the control signal continuous at the time of switching, the response of the controlled parameters is also dependent in the velocity setpoint at the time of

switching. The lower the screw velocity is the more pronounced the perturbations can be.

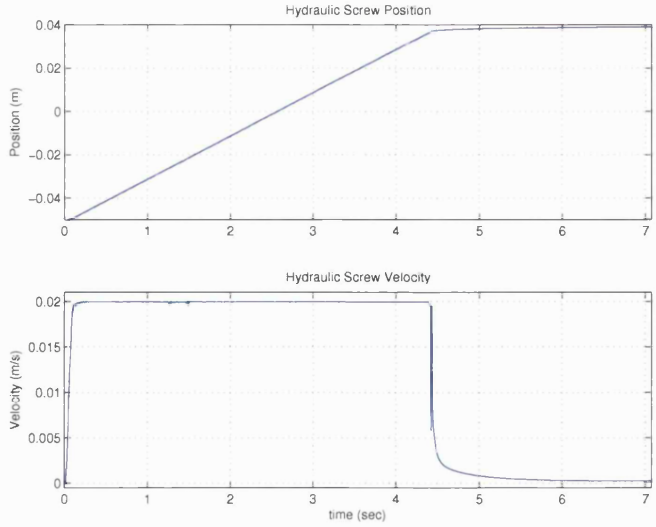

Figure 2.18: Hydraulic Screw Position and Velocity during Filling and Packing Stage

In Figure 2.19 the hydraulic flow, relief valve flow and pressure in the annulus chambers A and B are shown. During the filling phase as the viscous friction increases the hydraulic pressure changes to meet the load demand. When the packing phase commences the largest part of the flow is throttled through the relief valve as the velocity drops gradually to zero.

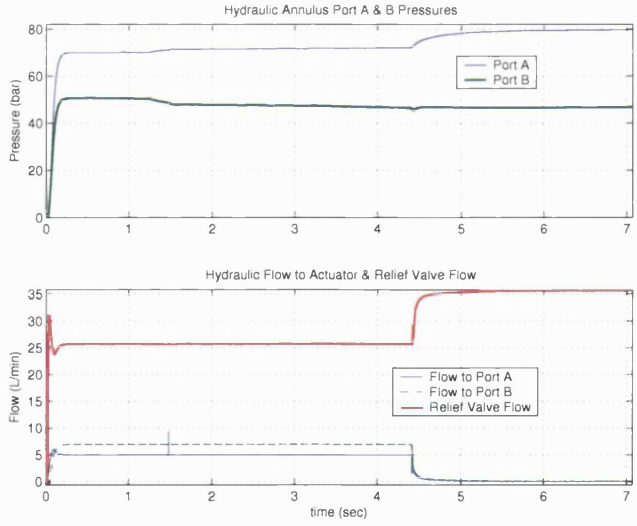

Figure 2.19: Hydraulic Pressure and Flow during Filling and Packing Stage

The velocity and pressure of the hydraulic system are presented in Figure 2.20 (top window). In this case the screw leakage factor is not included in the simulation.

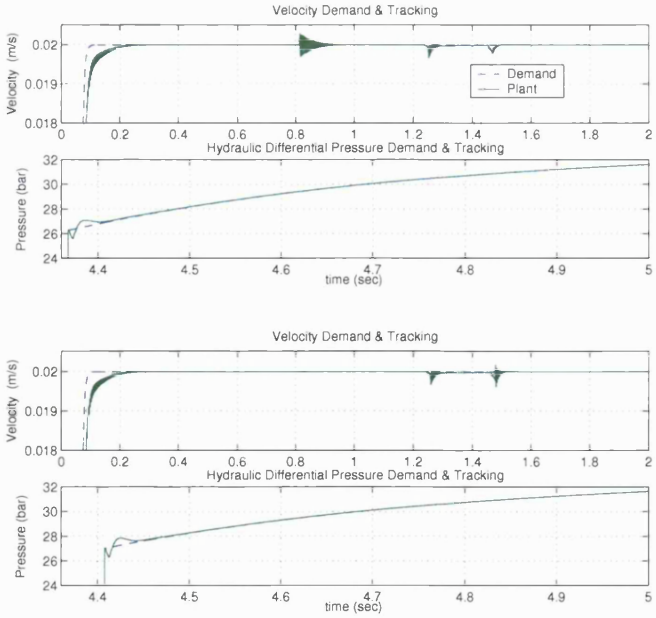

Figure 2.20: Screw Velocity and Hydraulic Differential Pressure Demand and Tracking without and with Polymer Leakage past the Screw

The plant velocity follows sufficiently well the velocity setpoint with the aid of the PI controller while some oscillatory behaviour occurs at 0.8 seconds as the viscous load increases due to the increasing pressure drop as the polymer flow-front progresses through the flow path sections. On the other hand the PID controller achieves good tracking of the pressure reference signal with a small error at the time of switching (4.35 to 4.4seconds). Overall a good pressure tracking is achieved. In the lower window of the figure the same simulation results are presented with the leakage factor past the screw included. It can be seen that the velocity response of the system is very good while the previously described oscillatory behaviour at 0.8seconds has been suppressed. This is a result of the polymer leakage, which acts as a damping factor in the screw motion. Moreover it can be seen that due to leakage the switch to packing phase is delayed (from 4.36 at 4.41seconds) as it takes longer to fill the cavity.

2.4.4 Simulink Model of Mould

In this section the simulation results for the mould model are presented. In Figure 2.21 (1st window) the hydraulic differential pressure rises to counteract the polymer viscous friction (2nd window) that follows a nonlinear behaviour. This is due to the different pressure drops at the flow path sections. In the third window as the packing phase commences, the cavity pressure rises abruptly and the hydraulic differential pressure is controlled to reach the level of 33bar. This corresponds to a cavity pressure of 260bar.

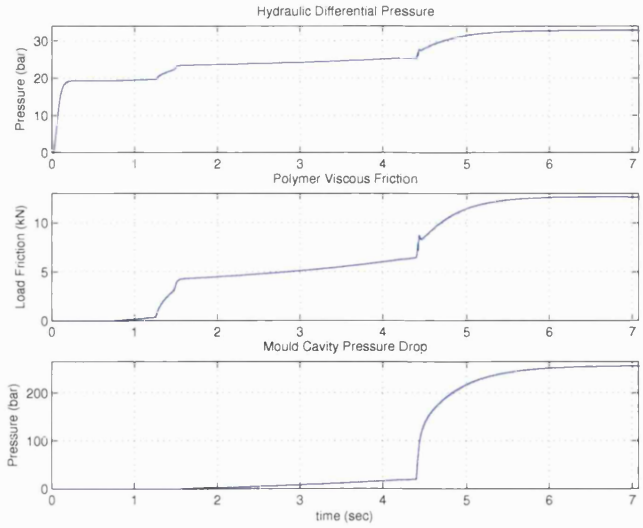

Figure 2.21: Hydraulic Differential Pressure, Polymer Viscous Friction Load and Mould Cavity Pressure

Some further details about the polymer flow into the cavity, polymer leakage past the screw and polymer bulk modulus are given in Figure 2.22.

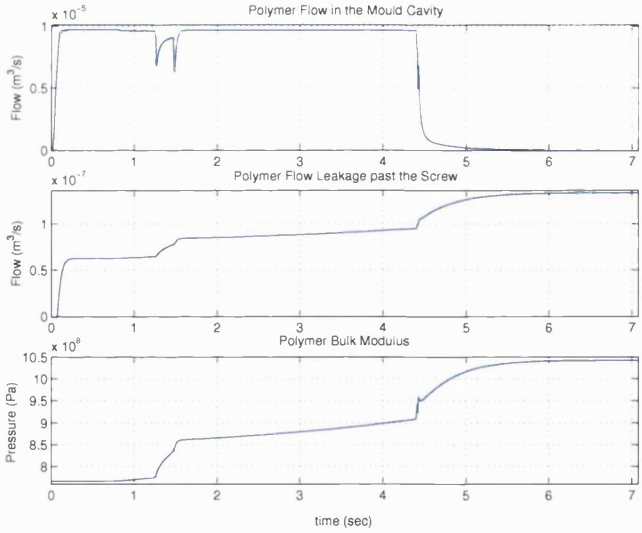

Figure 2.22: Polymer Flow & Volume in the Cavity and Polymer Bulk Modulus

By close inspection of the upper window, it can be seen that the amount of polymer injected during packing is very small as a low injection rate is maintained to fill the final sections of the cavity and pack the mould. This additional material compensates for the shrinkage effect that takes place during the cooling phase as the melt polymer solidifies completely before

it is ejected from the mould. In the second window the polymer leakage past the screw is shown. The polymer leakage increases linearly during filling (staying at low levels) as the cavity pressure is low while increases suddenly during the packing phase. In cases where the polymer used has a very low viscosity the packing phase could be compromised as the required cavity pressure might not be reached to to excessive leakage. In the third window of the figure, the polymer bulk modulus dependence on the melt pressure and temperature inside the cavity is shown. The bulk modulus according to the model parameters used, starts from a value of 7680bar reaching a maximum value of 10475bar at the end of the packing phase. These values are in good agreement with experimental values measured in melt viscometers [56].

During the simulation the polymer viscosity is described by the seven constant Cross-WLF model and changes continuously, due to shear rate, temperature and pressure changes. In Figure 2.23 the polymer's apparent viscosity at the end of the filling phase is plotted versus the shear rate at the cross sections of the mould.

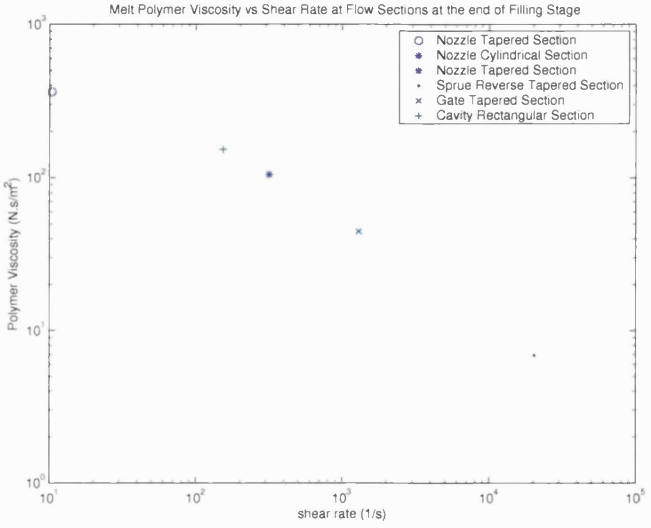

Figure 2.23: Polymer Apparent Viscosity vs Shear Rate at Flow-path Sections at the end of the Filling Stage

The graph provides a good indication in identifying flow paths that increase considerably the pressure drop during the cycle. For example in the sprue reversed tapered section (marked with a dot) the viscosity drops considerably due to the high shear rate and shear heating that takes place. In this region the pressure drop is considerably larger than other flow sections. If this cross section could be increased without compromising the part quality, the pressure drop could be reduced and the overall efficiency of the injection cycle would improve.

2.5 Concluding Remarks

In this Chapter a methodology was adopted to interpret the viscosity-behaviour of non-Newtonian polymers in different flow geometries and under various dynamic processing conditions (flow-rate, mould temperature). This methodology is then utilised to estimate the pressure drops at the various mould cross sections and check that their aggregate will not exceed the maximum injection pressure of the moulding machine. Two materials were considered, polypropylene and polycarbonate. The flexible design of the mould allows the location of the gate in the cavity to be positioned either at the centre or at the side of the part. Depending on the position of the gate, the moulded parts could have a different flow orientation and different final mechanical properties.

An experimental plant identification was performed without polymer load to further investigate the response of the hydraulic system and compare it with a linearised model. Linearised models for the control of the filling and packing phase were also derived and will be discussed in Chapter 5 in the context of different control strategies.

A detailed nonlinear dynamic simulation model was derived for the hydraulic and mould systems of the injection moulding machine. In simulation PI and PID controllers regulated the demanded flow and pressure trajectories, respectively. The simulation results enable a deep insight into the injection moulding process and reveal the complexity of relations between machine and mould parameters.

Chapter 3

Monitoring of the In-Mould Parameters

3.1 Introduction

In this chapter, an investigation of the injection moulding process parameters is presented. Preliminary experiments were carried out with polypropylene, in order to distinguish the phases of the process and become familiar with the operation of the injection moulding machine. These are presented in section 3.2. The effects of injection speed, packing pressure and material dosage on the quality of the product were investigated for a simple square cavity mould. The aim of these experiments was to optimise the injection process parameters to produce parts free from surface defects.

Following on a new mould was designed, manufactured and instrumented with a series of transducers to monitor the behaviour of the polymer (temperature, pressure) during the moulding of the part as presented in section 3.3. A heat transfer analysis was made with co-worker Stelson [67] to estimate the heat losses from the mould during one injection cycle, described in section 3.4. To overcome the heat losses and warm up the mould sufficiently quickly four cartridge heaters were selected, capable of heating up the mould and maintain its temperature at a nominally constant level. The heating time for the mould to reach the requisite temperature was estimated. Subsequently, a one-dimensional heat conduction model was used to estimate the cooling time of the part (used in the experimental set-up).

Once a good understanding of setting up the process was gained, two polymers, polypropylene and polycarbonate, were used to carry out a set of experiments and mould parts with different mechanical properties and flow orientation. During the injection cycle the behaviour of the

hydraulic pressure, cavity pressure and screw displacement were recorded. These experiments enabled the capabilities of the moulding machine to be explored and compared with information supplied by the manufacturer [68]. The limitations in the control features were identified. The experimental analysis and the results are presented in section 3.5.

In order to adjust the control parameters efficiently it is important to monitor and detect changes in the morphology of injection moulded parts during the manufacturing process. Knowledge of the extent of solidification of the part during the packing and cooling phase could enable better control of the process and good repetition of product quality. A novel way of extracting process information from two existing non-invasive methods was investigated, described in detail in section 3.6. The first method uses piezoelectric transducers generating/recording ultrasound waves that propagate through the polymer melt, while the other utilizes fast-response thermocouples embedded close to the mould cavity. The ultrasound wave speed variation and amplitude attenuation have been monitored. These were then utilized, with the aid of an off-line data processing algorithm to identify phase changes during the injection cycle (rather than monitoring variations in cavity pressure), as well as to predict accurately the extent of solidification of the produced part. The extent of solidification was also predicted with the thermocouple method.

3.2 Preliminary Experiments

To observe the effect the process parameters have on the dimensional accuracy and surface appearance of the moulded part, a preliminary set of experiments was carried out with different processing settings. A mould with a square cavity with embossed patterns was used with the gate located at the centre of the part. The material used for injection was low-density grey polypropylene and the process settings that were used are presented in Table 3.1.

Injection time	1.6s
Injection Velocity Range	0.01m/s to 0.085m/s
Packing time	7s
Packing Pressure Range	10bar to 66bar
Cooling time	6s
Mould Temperature	20°C
Average nozzle and barrel temperature	200°C

Table 3.1: Processing Parameters Settings for the Moulding of Square Cavity

Before injection, the material was dried for two hours at 80°C to remove any moisture content which can degrade the polymer melt during injection (details are given in section 4.4.8.1). The

dosage slider on the control panel of the moulding machine was set accordingly to the mould volume requirement. To investigate the effect of the melt flow-front velocity the injection speed was altered for each experiment by adjusting manually the appropriate hydraulic cartridge valves. A typical set of the experimental results is shown in Figure 3.1, where the four phases of the process phases can be distinguished.

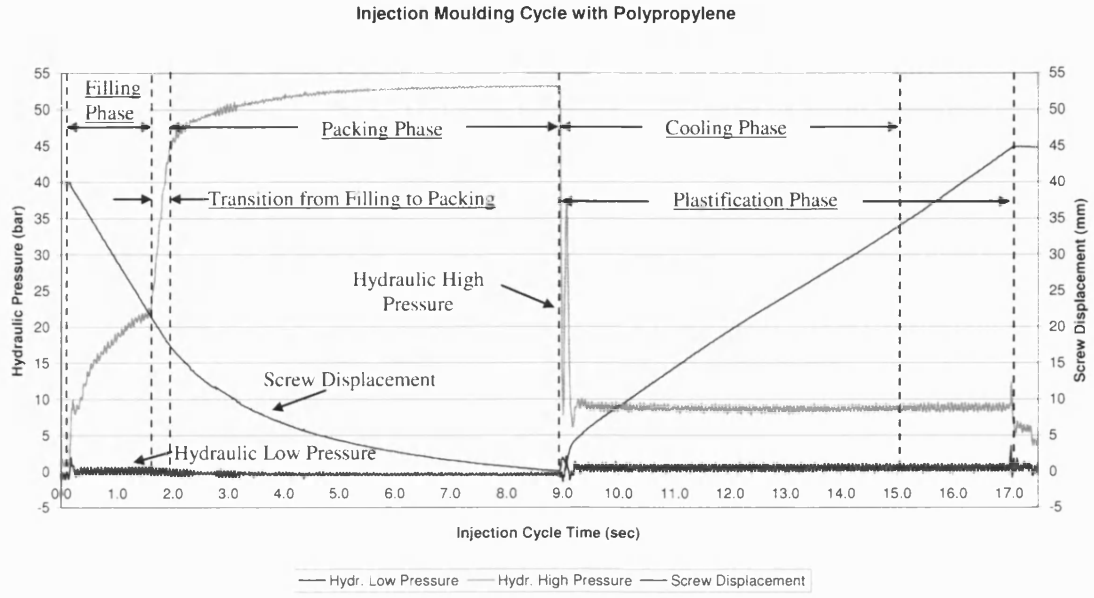

Figure 3.1: Injection Moulding Cycle of the Square Cavity Mould

At the beginning of the injection cycle the hydraulic circuit pressure rises from atmospheric up to 21bar as the cavity is filled. During this period the velocity of the screw is maintained constant. When the cavity is full the moulding machine stops controlling the flow and regulates the hydraulic pressure to a preset level. The profile that the hydraulic pressure will follow relies completely on the geometry of the cavity and the time of switching (from filling to packing) as no closed loop control of the process is available. During the transition the hydraulic pressure rises rapidly from 21bar to 45bar indicating that the cavity is full. As the packing phase continues additional melt polymer is injected to further pack the cavity and compensate for the shrinkage effect that takes place during part solidification. At this stage the hydraulic pressure rises exponentially from 45bar to 53bar. During this phase the screw velocity decreases until it drops to zero at the end of the packing phase. This is attributed to the gradual solidification of the cavity gate after which no polymer can enter or escape from the cavity. Following on from the packing phase the plasticization phase commences where the new material dosage is prepared for the next cycle. A back-pressure is applied to the screw motion to obtain a more homogeneous mixing of the melt. At the same time the part is allowed to cool down before its ejection from the mould.

3.2.1 Preliminary Experimental Results

After numerous experiments with a range of settings for shot size, injection speed and packing pressure, the dimensions and weight of the produced parts were measured. The parts were also examined to observe any sink marks or flash of material. The thickness of the part at the two corners, the edges and centre (where black dots are identified in Figure 3.2) was measured with a micrometer for high accuracy.

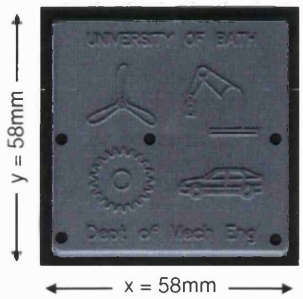

Figure 3.2: Produced Part from the Square Mould Cavity

1. In the first set of experiments, the injection speed was altered from 0.01m/s to 0.085m/s. The following results were obtained as presented in Figure 3.3.

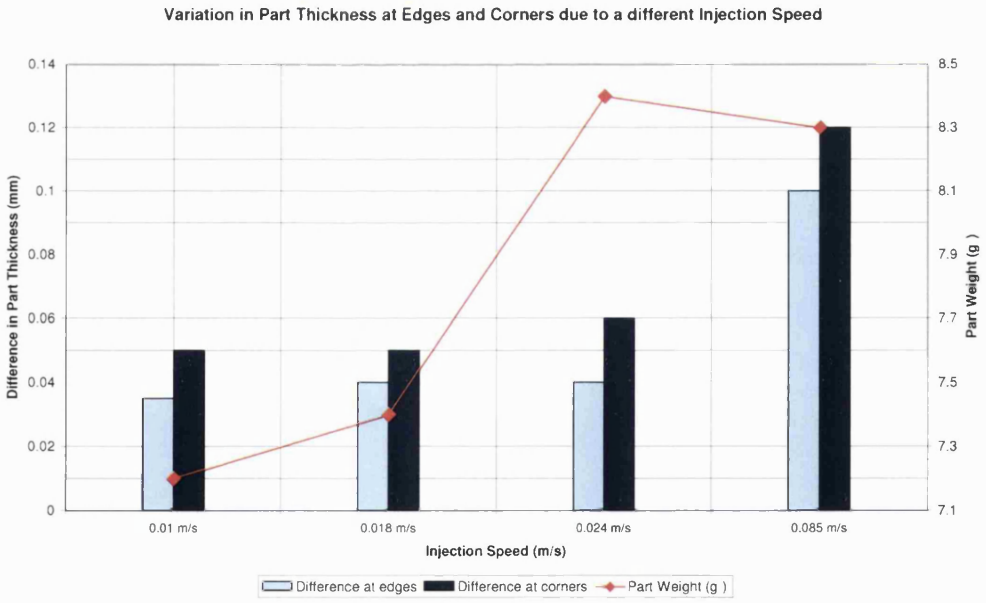

Figure 3.3: Variation in Thickness and Weight of the Parts

It can be seen from the graph that the increase in injection speed results in an increase in the part weight. The main reason is that more material is injected during filling into the cavity before the polymer starts to solidify. In the first three cases, the difference between thicknesses at the edges and corners was maintained almost constant. In the last case, the injection velocity was too high and the part weight drops due to material flash. The flash occurred because the cavity separation force exceeded the maximum clamping force (per cavity area) and the mould opened slightly, allowing melt polymer to escape out of the cavity, as shown in Figure 3.4.

Figure 3.4: Flashing of the Part due to a High Injection Speed

2. In the second set of experiments, the dosage shot (Appendix A.1) size was altered. The injection velocity was set at $0.01 m/s$. The results are shown in Figure 3.5.

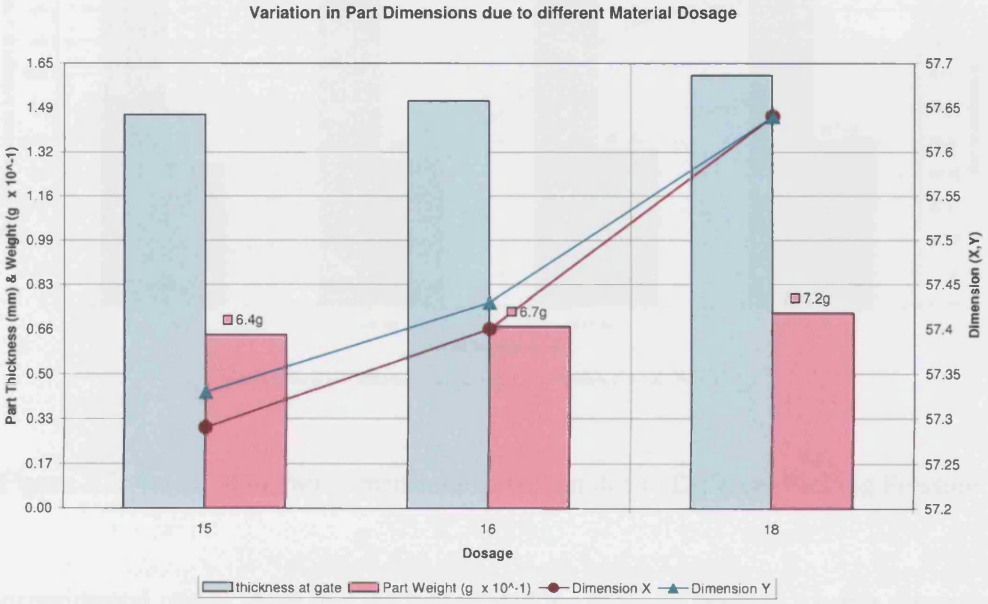

Figure 3.5: Variation in Part Dimensions due to Different Material Dosage

It can be seen that the higher the injected dosage results in an increase in the thickness close to the gate and the (x,y) dimensions of the part. Similarly, the part weight increases from 6.4gm up to 7.2gm. When the shot size was reduced considerably, a partially filled part was produced (short shot). An example is given in Figure 3.6, where the shot sizes were decreased to the shot size scale of 12 and 13 (Appendix A.1). The first short shot part is shown on the left hand side. It can be seen that the advancing flow front follows a radial pattern.

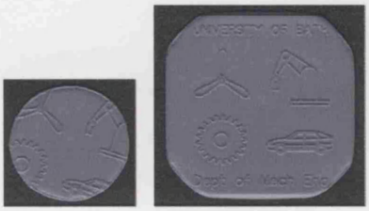

Figure 3.6: Partially Filled Cavity due to Insufficient Material Dosage

3. In the third set of experiments, the packing pressure was altered. The screw velocity and shot dosage were set at normal levels. The following results were obtained and presented in Figure 3.7.

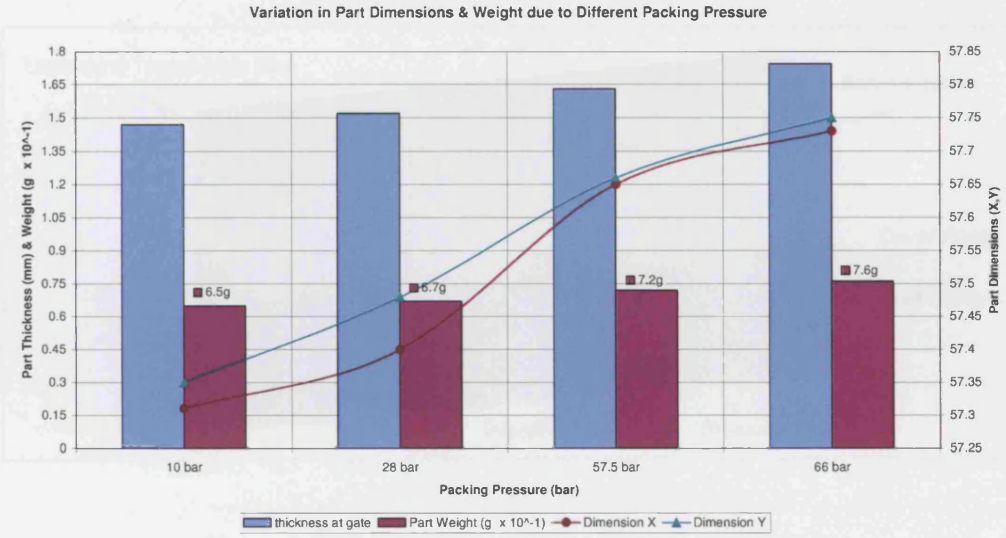

Figure 3.7: Variation in Part Dimensions & Weight due to Different Packing Pressure

The experimental results show that the higher packing pressure leads to a better dimensional accuracy with less variations (Last case 57.75mm for both x,y dimensions). The thickness close to the gate changes considerably from 1.47mm to 1.75mm. In addition, when a small variation in packing pressure occurs, from 57.5bar to 66bar, there is a change in thickness (0.12mm) as well as in part weight (0.4gm). This dimensional difference could be important in applications

where tight tolerances are required. Moreover the effect of the packing pressure also has a significant effect in the appearance of the part. The higher the packing pressure (but up to a limit), the less sink marks appeared on the surface area of the part during the experiments.

3.3 New Mould Design

To further investigate the effect of the processing parameters on the quality of the parts a new mould was designed, which allowed a set of transducers to be embedded close to the cavity surface and monitor the variation in the polymer flow behaviour. To monitor the in-mould parameters, the new mould was instrumented with pressure and temperature transducers. A rectangular cavity shape was adopted, to keep the geometry simple, to understand more readily the flow behaviour of the polymer melt (flow-orientation, etc.) during the injection process. Using a suitable cavity insert, tensile specimens could be moulded in order to carry out mechanical tensile tests and explore the impact of the processing conditions.The mould cavity was positioned at the centre of the mould to achieve symmetrical cooling and a uniform heat transfer from the part to the mould body. A half-section of the mould shown in Figure 3.8 illustrates the geometry of the mould and the position of the transducers.

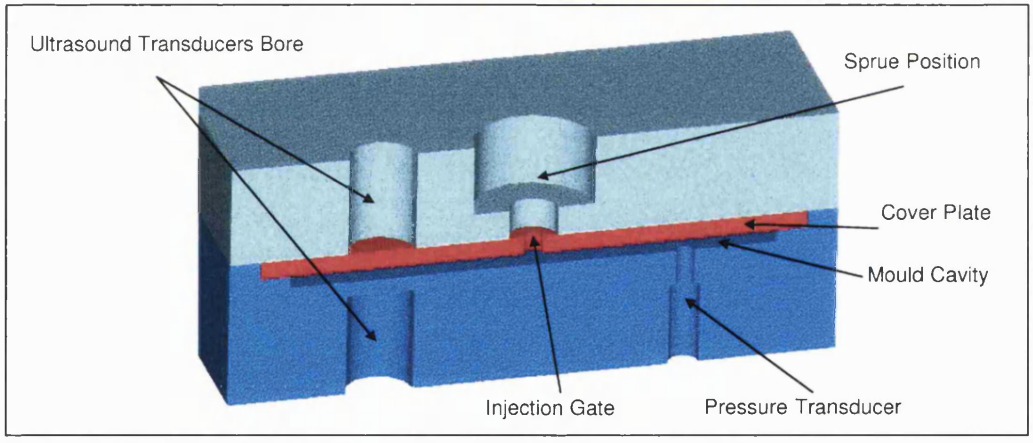

Figure 3.8: Half Section of the Mould when Clamped

Two cover plates were machined, each with a single injection gate, one in the centre and the other at the side of the part. This design gives flexibility in the number and position of injection gates that can be used. For example, a cover plate with more than one gate could be used to investigate the formation of weld lines (the line where two polymer melt flows join) at the surface of the parts. The two sections of the mould and the cover plate are shown in Figure 3.9.

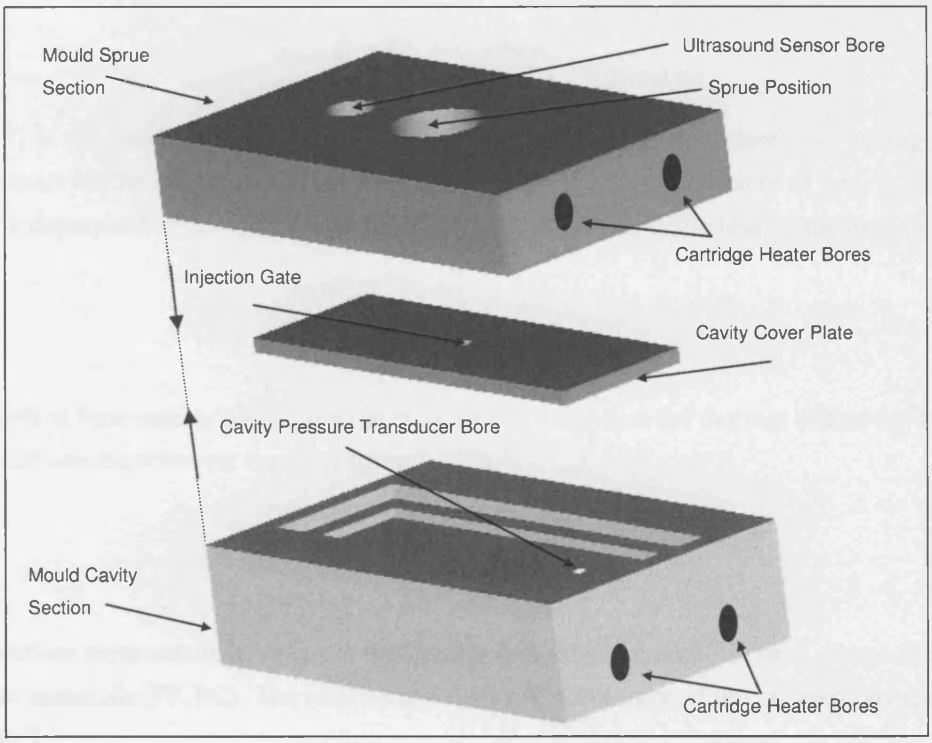

Figure 3.9: Mould Sections Assembly

The two materials used for the experiments were transparent polycarbonate (amorphous) and both grey and white polypropylene (crystalline) polymers. These materials have a different flow behaviour and solidify at a different rate. Therefore the processing conditions should be optimised to meet the flow and pressure characteristics guideline for the polymers. The processing parameters of the polymers require a preset mould temperature much higher than the ambient ($40°C$ for PP and $100°C$ for PC). Two cartridge heaters were installed in each mould section and controlled separately by temperature controllers (K-type thermocouples sense the feedback temperature). To improve the performance of the cartridge heaters and reduce the heating time, insulation was used between the machine platens and the mould surface. However to improve the cooling rate of the moulded part (since insulation reduces the heat transfer rate) an aluminium alloy 7075-T6 (Appendix A.3) was used for the mould, with very high thermal conductivity (10 times higher than steel).

3.3.1 Mould Material & Insulation

The heat penetration in the aluminium mould is much greater than for steel. At the polymer-mould interface, a perfect thermal contact is assumed, where the temperature can be approximated as:

$$\frac{T_i - T_w}{T_s - T_w} = \frac{b_{pen_p}}{b_{pen_m} + b_{pen_p}} \tag{3.1}$$

where T_i is the interface temperature and T_w the mould wall temperature. An average value can be used for the solidification polymer temperature T_s. The coefficient of heat penetration (b_{pen}) is dependent on the thermal conductivity, density and specific heat of the material:

$$b_{pen} = \sqrt{k\rho c_p} \tag{3.2}$$

The depth of heat penetration within the mould is dependent on the thermal diffusivity (α_m) of the mould and the transient time (t_t) taken:

$$\Delta x = \sqrt{\alpha_m t_t} \tag{3.3}$$

The interface temperature has been estimated for two different moulds (steel, aluminium) and polymer materials (PP, PC). The parameter values and the results of the calculations are given in Table 3.2.

Material	Aluminium Mould	Steel Mould	PP	PC
Thermal Diffusivity $\alpha = k/\rho c_p$	$4.83 \cdot 10^{-5}$	$3.93 \cdot 10^{-6}$	$7.30 \cdot 10^{-8}$	$1.49 \cdot 10^{-7}$
Heat Penetration $J/m^2\,°Cs^{\frac{1}{2}}$	18694	7566	481	543
Aluminium / Steel Mould Temp. ($°C$)	-	-	20	100
Polymer Solid. Temp.($°C$)	-	-	200	300
Interface Temp. Aluminium ($°C$)	-	-	24.6	105.7
Interface Temp. Steel ($°C$)	-	-	30.8	113.4

Table 3.2: Mould Interface Temperatures, from [69, 70, 71]

As expected in the aluminium mould the temperature at the interface (24.6°C for PP and 105.7°C for PC) is lower than that in steel (30.8°C for PP and 113.4°C for PC) for both polymers. This is mainly due to the high thermal conductivity of the aluminium mould when compared with that of steel (8 times higher). The depth of heat penetration for the (Aluminium / Steel) mould has been estimated (theoretically) for the first 40 seconds of the cycle (maximum cooling time) as shown in Figure 3.10:

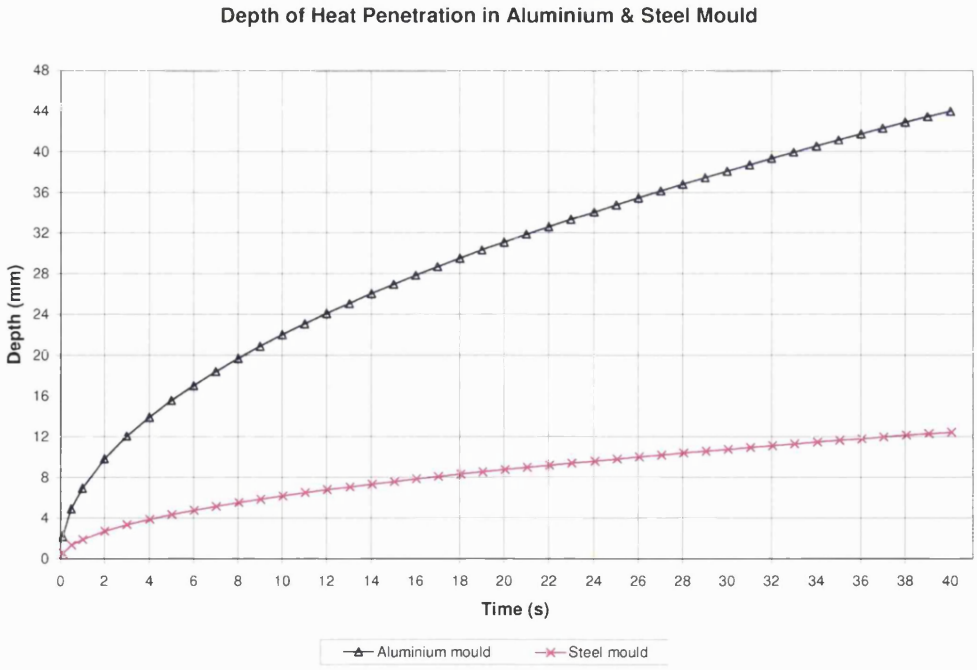

Figure 3.10: Depth of Heat penetration in Aluminium and Steel Mould

As expected the depth of heat penetration in the aluminium mould is greater than that in steel. This allows two thermocouples to be embedded close to the cavity wall to monitor the heat transients (during the injection cycle) without making the depth from the heat source critical (as it would be in steel).

3.4 Mould Heat Transfer Analysis

In order to estimate the heat-up and cooling time of the mould as well as the solidification rate of the moulded part, a theoretical heat transfer mould analysis was carried out. Depending on the mould heat loss to the surroundings appropriate insulation material was selected. To minimise the heat-up time of the mould the cartridge heaters needed to be of sufficient capacity. To accurately estimate these parameters three cases were considered in the heat transfer analysis:

- Free convection from the mould surface
- Conduction through the insulation
- Radiation between the mould and machine platens

The problem is treated as one with constant heat flux on the surface. The mould was heated and maintained at constant temperature. As previously mentioned the new designed mould consists of two sections, one that includes the cavity and one that includes the flow runner and sprue. At the rear of each section, insulation material was used to reduce the heat conduction to the injection moulding machine platens. The dimensions of the two blocks when in contact are $0.204\,(L) \times 0.094\,(W) \times 0.125\,(H)$. In Figure 3.11 the mould sections with the insulation on each side are shown.

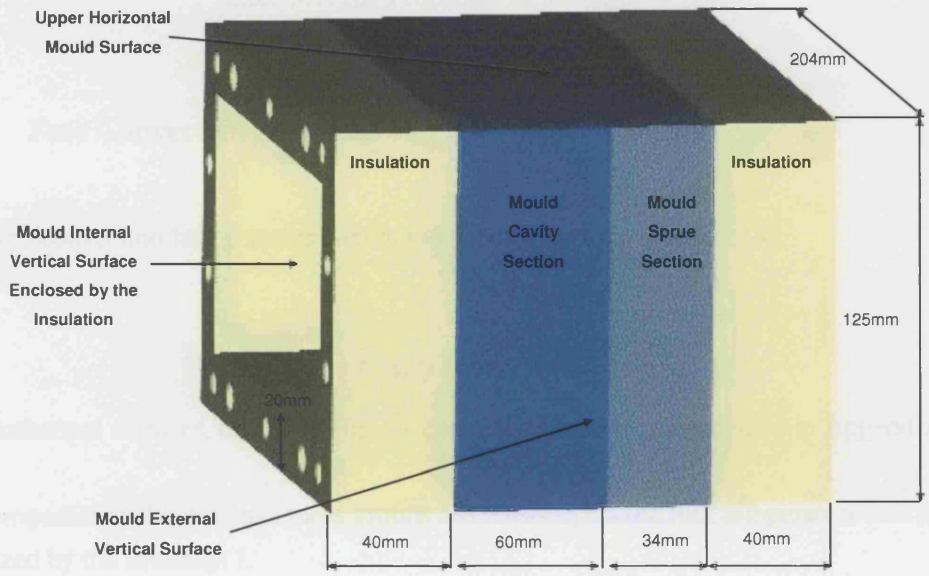

Figure 3.11: Mould with Insulation Bars

Before every injection cycle, the mould is raised at the appropriate material temperature and thereafter maintained constant. The worst situation (for natural convection and conduction), considered in this heat transfer analysis, is during the injection of polycarbonate material. In this case the mould temperature should be maintained at $100°C$ with the ambient temperature at $20°C$. For the case of polypropylene the mould temperature should be maintained at $40°C$. The physical properties of the mould material and the air are presented in Tables 3.3 and 3.4.

Nominal Density $\rho\,(Kg/m^3)$	2800
Specific Heat $c_p\,(J/KgK)$	960
Thermal Conductivity $k\,(W/mK)$	130
Ambient Temperature $(°C)$	20
Mould Temperature $(°C)$	100

Table 3.3: Aluminium Mould properties, from [72]

Film Temperature $T_f\,(K)$	333
Density $\rho\,(Kg/m^3)$	1.0589
Specific heat $c_p\,(J/KgK)$	1059
Kinematic Viscosity $v\,(m^2/s)$	19.04×10^{-6}
Temperature Coefficient $\beta\,(1/K)$	3.0×10^{-3}
Thermal Conductivity $k\,(W/mK)$	0.0287
Prandtl number (Pr)	0.7007

Table 3.4: Air Properties at $333K$, from [72]

3.4.1 Free Convection Analysis

The free-convection heat transfer coefficient can be approximated as [72]:

$$\overline{Nu_f} = C\,(Gr_f \times Pr_f)^m\,, \overline{Nu_f} = \frac{hL}{k} \tag{3.4}$$

For isothermal surfaces, the values for the constants C and m are provided in Appendix A.4.

The properties in the dimensionless groups are estimated at the film temperature and are characterized by the subscript f.

$$T_f = \frac{T_\infty - T_w}{2} \tag{3.5}$$

The Grashof number is expressed by the following equation:

$$Gr_L = \frac{g \cdot \beta\,(T_\infty - T_w)\,L^3}{T_f \cdot v^2},\ \beta = \frac{1}{T_f} \tag{3.6}$$

The Prandtl number is expressed by the following equation:

$$Pr = \frac{v}{\alpha} \tag{3.7}$$

The product of Grashof and Prandtl numbers defines the Rayleigh number:

$$Ra = Gr \cdot Pr \tag{3.8}$$

With the use of the formulas for free convection and the constants provided for isothermal

surfaces, the overall heat loss from the mould vertical and horizontal surfaces was estimated to be 48W. Some more details are given in Table 3.5.

Estimation of Free Convection Heat Loss from Mould Surfaces	
Free Convection from Mould External Vertical Surfaces, Fig. 3.11 (L=0.125m, $A = 0.125m \times 0.094m$, C=0.59, m=1/4)	Q=13.9W
Free Convection from Mould Internal Vertical Surfaces Enclosed by the Insulation Bars, Fig. 3.11 (L=0.085m, $A = 0.085m \times 0.164m$, C=0.59, m=1/4)	Q=18.2W
Free Convection from Mould Upper Horizontal Surface, Fig. 3.11 (L=0.149m, $A = 0.204m \times 0.094m$, C=0.15, m=1/3)	Q=11W
Free Convection from Mould Lower Horizontal Surface, Fig. 3.11 (L=0.149m, $A = 0.204m \times 0.094m$, C=0.27, m=1/4)	Q=4.99W
Overall Free Convection Heat Loss	$Q_{ov} = 48W$

Table 3.5: Free Convection from Mould Surfaces

3.4.2 Conduction Analysis through Insulation

For the conduction analysis, the heat transfer from the mould through the insulation material to the platens was estimated. The insulation material was carefully selected to have a low thermal conductivity and high shear strength to withstand the clamping force. An epoxy glass fabric, TUFNOL (grade 10G/40) was used with the following specification, Table 3.6:

Young's Modulus (MPa)	17.7
Compressive strength (edgewise MPa)	300
Maximum continuous working temperature ($°C$)	130
Thermal Conductivity through laminate (W/mK)	0.42

Table 3.6: Mechanical and Thermal Properties of TUFNOL, from [73]

The total heat conducted through the four horizontal and four vertical insulating bars of the

mould was estimated to be 19.1W.

3.4.3 Radiation Heat Loss from Mould to Platens

In this analysis, both the mould and the platen surface were treated as black bodies. By making this simplification it is assumed that all the heat been radiated from the mould is absorbed by the platen neglecting any heat reflected (back and forward). The mould temperature is taken to be $100°C$ and the injection moulding machine platens were assumed to be at $20°C$. The radiation shape factor between parallel rectangles was used [72]. The total amount of heat being transferred from both sides of the mould was estimated to be 8.9W.

3.4.4 Overall Heat Loss

The overall heat loss from the mould is equal to the amount lost from convection (to air), conduction and radiation to the platens. The total amount of energy lost was estimated to be, $Q_{ov} = 76W$. This amount of heat loss is very small when compared with the case of no insulation, where the overall heat loss to the moulding machine platens would be, $Q_{ov} = 910W$.

3.4.5 Mould Heating

Based on the estimated overall heat loss from the mould (76W), four custom made cartridge heaters with a capacity of 150W each were used. These would be capable of heating up the mould sufficiently fast to the required operating temperature. To achieve a uniform heating each pair is located at an equal distance from the cavity (two in each mould section). Temperature controllers in conjunction with thermocouples at each section were set to adjust separately the mould temperature. Each heater is assumed that it has a perfect thermal contact with the mould. The time required to heat up the mould at each section has been calculated based on the mass (M), specific heat (c_p) and temperature difference (ΔT).

$$Q_h = \frac{Mc_p\Delta T}{t} = \frac{A\Delta x\rho_m c_p\Delta T}{t} \tag{3.9}$$

The heat-up times for the sprue and cavity mould sections for the moulding of polypropylene and polycarbonate materials are presented in Table 3.7.

Estimation of Heat-up Time for Mould Sections	PP at 40°C	PC at 100°C
Heat-up time for Sprue Mould Section	5min	20min
Heat-up time for Cavity Mould Section	3min	12min
Heat-up time when Mould Clamped	4min	16min

Table 3.7: Mould Heat-up Times for the Moulding of Polypropylene and Polycarbonate

3.4.6 Part Cooling

For the cooling analysis of the part, the following assumptions were made.

- One-dimensional heat conduction
- There is no mass transfer.
- No heat transfer during the filling phase.
- The polymer is incompressible and its density is independent of pressure and temperature.
- The polymer heat capacity and thermal conductivity are independent of temperature.
- The polymer is isotropic and its properties (c_p, k, ρ) are the same at all points within the material.
- There is a perfect thermal contact between the cavity wall and polymer

The cooling time model to estimate the solidification of the (rectangular) part has been extensively reviewed in the literature [40,41]. The polymers temperature T_m, when entering the cavity is assumed to be the same as the melt temperature. The mould wall temperature T_w, at that instant is maintained constant [67]. The ejection temperature can be estimated using the mid-plane or average temperature of the part. The former is more often used for the estimation of the cooling time, while the latter for the sealing (polymer has changed state from liquid to solid polymer) time of the cavity. Cooling time based on an average part temperature (ejection temperature of polymer) is expressed by the following formula:

$$t_{cool} = \frac{h^2}{\pi\alpha^2} \times \left[\frac{8}{\pi^2}\left(\frac{T_m - T_w}{T_e - T_w}\right)\right] \tag{3.10}$$

where h is the maximum thickness of the part and a is the thermal diffusivity of the polymer. The mould wall temperature, the melt polymer temperature and the ejection temperature are

represented by T_w, T_m, and T_e respectively. Cooling time based on a mid-plane part temperature (sealing temperature of polymer) is expressed by the following formula:

$$t_{cool} = \frac{h^2}{\pi\alpha^2} \times \left[\frac{4}{\pi^2}\left(\frac{T_m - T_w}{T_s - T_w}\right)\right] \tag{3.11}$$

where T_s denotes the sealing temperature (when part is solid).

Average values (for polymer melt temperature - ejection temperature) for the theoretical model were taken based on the material properties [69]. For the sealing temperature, a value was chosen slightly below the glass transition temperature for the amorphous Polycarbonate. The cooling time based on the mid-plane or average temperature of the part has been estimated in Table 3.8.

Material	PP	PC
Thermal Diffusivity $\alpha = k/\rho c_p$	$7.3 \cdot 10^{-8}$	$1.5 \cdot 10^{-7}$
Mould Temp. $(°C)$	20	100
Melt Temp. $(°C)$	200	300
Ejection Temp. $(°C)$	60	110
Sealing Temp. $T_s\,(°C)$	-	145
Cooling Time Mid-temp (sec)	-	7.7
Cooling Time Average-temp (sec)	29	30

Table 3.8: Theoretical Cooling Time Data [69, 70] and Estimated Cooling Times

The results for the cooling time represent an estimate. However, they are very similar to those found in the experiments with errors of around ± 5 seconds. Depending on the processing conditions a longer time might be required, however for more precision a transient heat transfer analysis from the melt part to the mould would be required.

3.5 Main Experimental Set-up and Results

Based on the heat transfer analysis of the previous section the new designed mould was manufactured and assembled for testing. The experimental results that are presented in this section were carried out with the standard configuration of the hydraulic system. The velocity and pressure setpoints for the filling and packing phase of the cycle were preset before injection. Two materials were tested, polypropylene (white & grey) and polycarbonate.

3.5.1 Injection of Polypropylene

For the moulding of polypropylene two tests were performed; one with the gate at the centre of the part and the other at the side (to obtain parts with different flow orientation). The transient behaviour of the hydraulic and cavity pressure were investigated. The machine process settings for the injection of polypropylene are presented in Table 3.9.

Injection time Range	4s to 4.6s
Injection Velocity	0.01m/s to 0.012m/s
Packing time	7s
Packing Pressure	66bar
Cooling time	40s
Mould Temperature	$20°C$
Average nozzle and barrel temperature	$200°C$

Table 3.9: Process Settings for the Moulding of Rectangular Part with Polypropylene

In these experiments the transition to the packing phase was triggered by the end of the filling phase (timed). Before injection the material was dried for two hours at $80°C$ to remove any moisture content present. The material dosage for the plasticization phase was adjusted to meet the cavity volume size and the back-pressure was set at 8bar to achieve uniform plasticizing of the melt.

3.5.1.1 Flow Visualization

In the first two sets of experiments, grey Polypropylene was used. The gate was properly sized to lower the viscosity and fill efficiently the cavity while maintaining the shear heating low to avoid degradation of the polymer melt. Because of the gate position change, two parts were produced with a different flow path orientation, as shown in Figure 3.12.

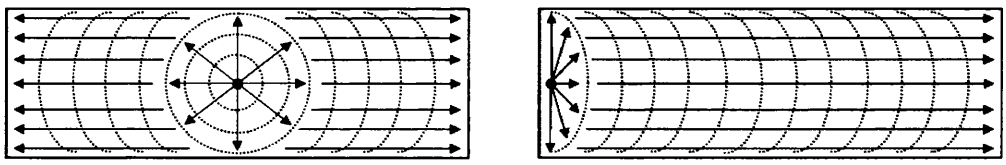

Centre Gate *Side gate*

Figure 3.12: Flow Path Orientation of Polymer with Centre or Side Location of the Gate

In the first case the flow follows a radial pattern until the polymer reaches the cavity's wall. After that, two flow-front contours develop which progressively move towards the edges of the part. This flow behaviour was verified experimentally, with the aid of a mixture of polymers. In Figure 3.13 the flow orientation of a centre gated, injected part is shown.

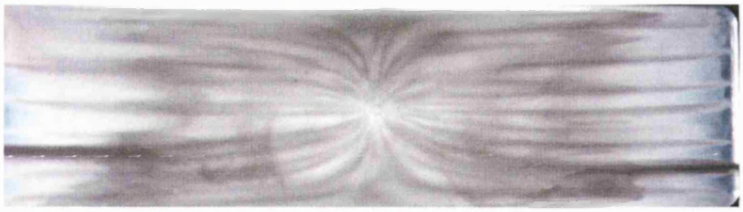

Figure 3.13: Experimentally Observed Radial and Linear Flow Orientation

The location of the gate is important since it controls the polymer flow into the cavity. The narrow gate design at both cavity cover plates helped for an easy separation of the part and quick solidification to isolate the cavity after the packing phase. Side gated parts were found to be stiffer, and having a less tendency to warp (bend) after a premature ejection. However, the location of the gate should rely on the application of the part to ensure that the direction of flow orientation corresponds to the axis that the part will be mostly stressed.

In Figure 3.14 below, the first (centre gate injection) set of experimental results is presented.

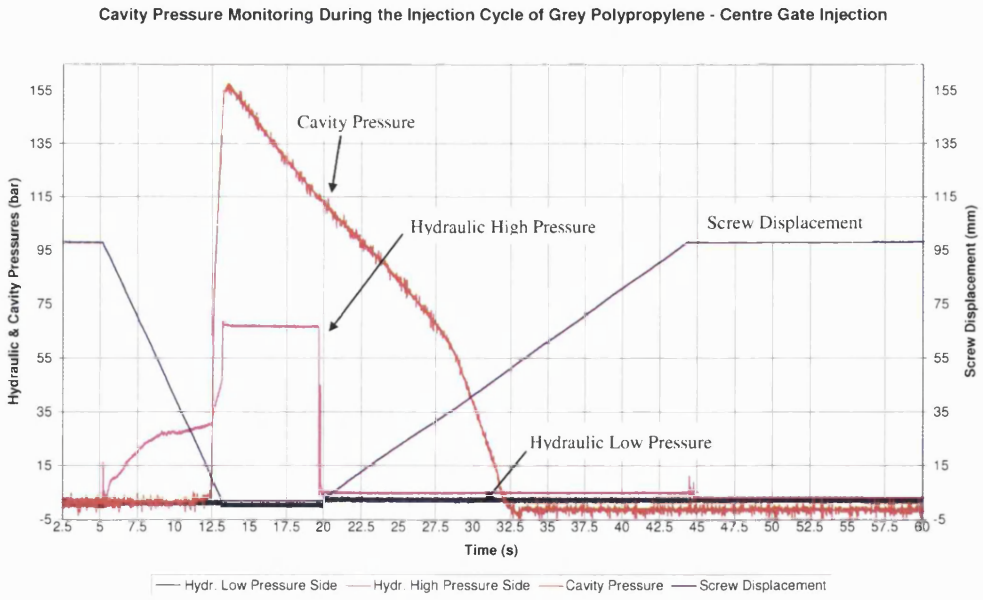

Figure 3.14: Cavity Pressure Monitoring during the Injection of Grey Polypropylene from Centre Gate

Before injection, a predetermined volume of material is being plasticized, while the screw retracts due to the material volume been build at the front part of the barrel. As soon as the cycle starts, the hydraulic pressure rises smoothly, and the screw is pushed forward at a constant velocity. The hydraulic pressure reaches a level (28bar at 11s) where it stays constant for a certain period. This marks the end of the filling phase where the cavity is almost full. At that instant the cavity pressure rises from atmospheric and peaks suddenly to 155bar as the transition to the packing phase occurs (sensor is 0.05m away from the gate). It is important for the packing phase to commence immediately after the end of the filling to avoid the cavity pressure reaching excessive pressure. Therefore a good time synchronization was set to provide a smooth transition to the packing phase. At this point the control of the screw motion changes from flow pressure control. The maximum hydraulic pressure level is preset before the injection and no alteration can be made during the injection cycle. The screw continues to move forward until it comes in contact with the nozzle where it stops. At that instant the cavity pressure is 157bar while the plasticization phase is delayed for a few seconds (screw is not moving) until the polymer at the gate solidifies (to avoid any polymer flowing out of the cavity). As the cooling phase commences the cavity pressure drops linearly with time and changes slope at 24s. This marks a change in the heat transfer rate from the solidifying part to the mould, until the cavity pressure reach an atmospheric level. The plasticization phase continues (until 43s) for the preparation of the next material dosage.

The second set of experimental results is presented in Figure 3.15, where the polymer is injected from the side to mould a part with a different flow orientation.

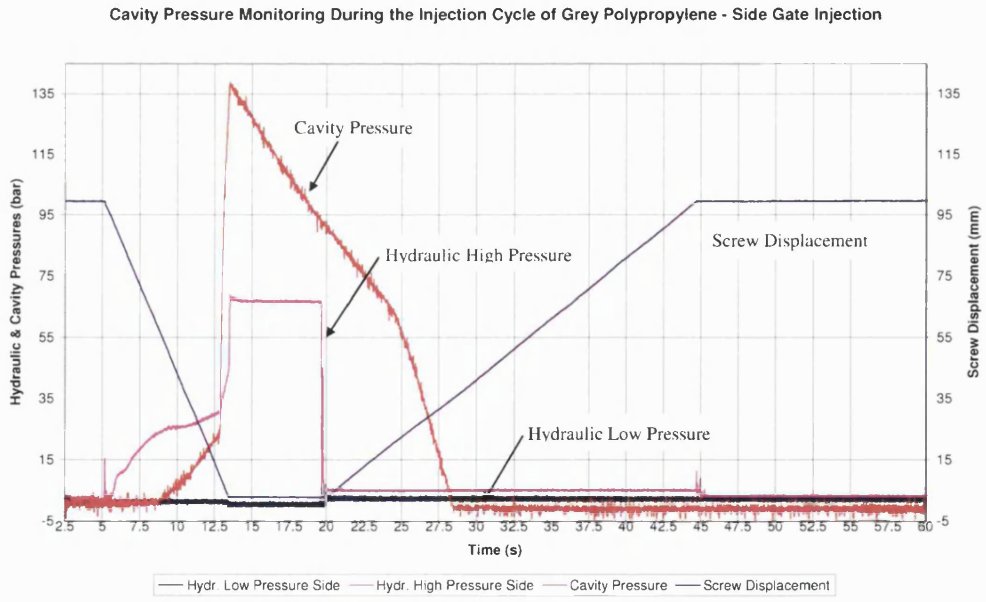

Figure 3.15: Cavity Pressure Monitoring during the Injection of Grey Polypropylene from Side Gate

The cycle characteristics are very similar with the first experimental set, with the only difference in the cavity pressure dynamics. This time the gate is located at the edge of the part, very close to the cavity pressure sensor diaphragm (2.5cm away). The sensor detects the rise in pressure earlier (at 8.5s), than in the first case (at 11.5s in Figure 3.14) where a considerable delay of three seconds occurs. The cavity pressure increases linearly during the filling phase up to the transition region (at 12.6s), where both hydraulic and cavity pressures peak together at the same time. The change at the slope of the cavity pressure plot (at 24.5s) marks the sealing of the gate. Afterwards the cavity pressure profile cannot be affected by the machine process parameters and the melt polymer orientation at the core remains unchanged. Only the cooling rate profile can affect the crystallization of the polymer, therefore the size and number of crystals and thermally-induced residual stresses.

A comparison of Figure 3.14 & 3.15 shows the relation between the cavity gate and the pressure transducer location. When the cavity pressure signal is used as a feedback in the control loop, the position of the transducer becomes critical. To monitor the extent of filling the transducer should be placed in the cavity at the end of the flow channel. On the other hand, when the transducer is close to the gate more information can be extracted about the solidification of the gate, which is very useful for estimating the completion of the packing phase.

The third set of experimental results is presented in Figure 3.16. In this case, the polymer used was a low viscosity polypropylene (white) and was injected from the centre of the cavity.

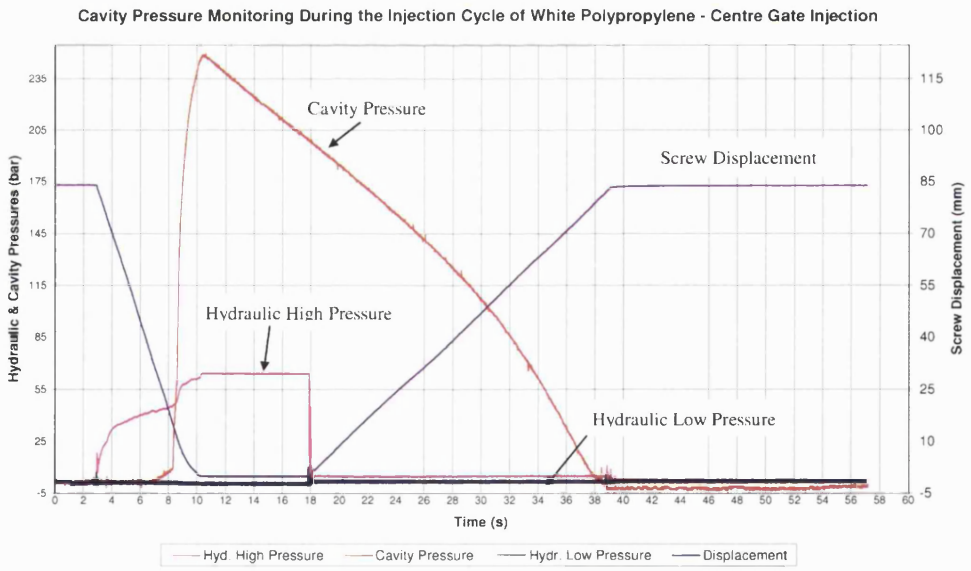

Figure 3.16: Cavity Pressure Monitoring during the Injection of White Polypropylene from Centre Gate

The cycle characteristics are similar with the two previously described cases. The cavity pres-

sure reached a higher level due to the lower viscosity (the processing settings were kept the same with the previous experiment). A lower screw velocity would still fill the cavity efficiently (due to the lower viscosity) and control the cavity pressure at a lower level. Again little control was available to manipulate further the holding pressure profile. During packing the screw moves at a low velocity (position slope changes) as additional material is injected to compensate for the part shrinkage in the cooling phase. The injection pressure was also higher (around 42bar) as a result of leakage past the screw due to the lower viscosity of the polymer.

3.5.2 Injection of Polycarbonate

For the injection of the transparent Polycarbonate, the gate was located in the centre of the part. Again, the dynamics of the hydraulic and cavity pressure were examined. The machine process settings that were used for the injection of polycarbonate are presented in Table 3.10.

Injection time	6.1s
Injection Velocity	0.012m/s
Packing time	13.4s
Packing Pressure	66bar
Cooling time	40s
Mould Temperature	115°C
Average nozzle and barrel temperature	300°C

Table 3.10: Process Settings for the Moulding of Rectangular Part with Polycarbonate

In Figure 3.17, the fourth set of experimental results is presented. Transparent polycarbonate material was used which was dried (before use) for four hours at 100°C to remove any moisture content. For the injection of polycarbonate the cover plate with the gate positioned at the centre of the cavity was used. Overall similar process characteristics and trends were obtained as with the previous experiments. As the polycarbonate is more viscous, a higher injection pressure was necessary during the filling and packing phase. In an attempt to inject from the side, (using the same settings) it was found that the gate solidified very quickly (the flow path was longer) and the cavity was partially filled.

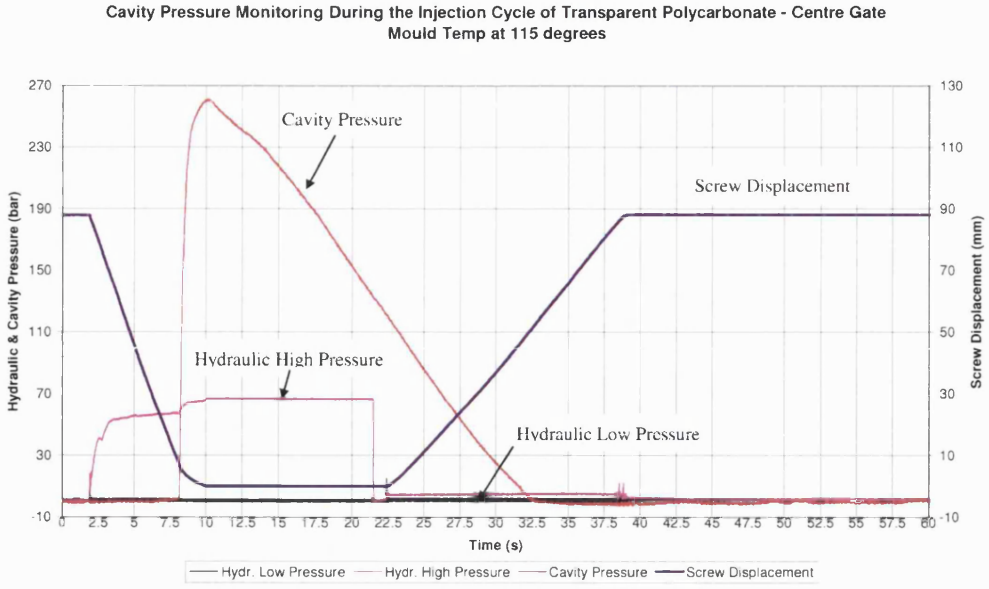

Figure 3.17: Cavity Pressure Monitoring during the Injection of Polycarbonate from Centre Gate

A higher injection speed in such a case is required to fill the cavity on time before the solidification of the flow front, or melt polymer at the gate/runner. Alternatively temperature controlled runners could be used to prevent solidification of the polymer and maintain the temperature of the melt higher. The produced parts with the gate, runner and sprue flow paths are shown in Figure 3.18.

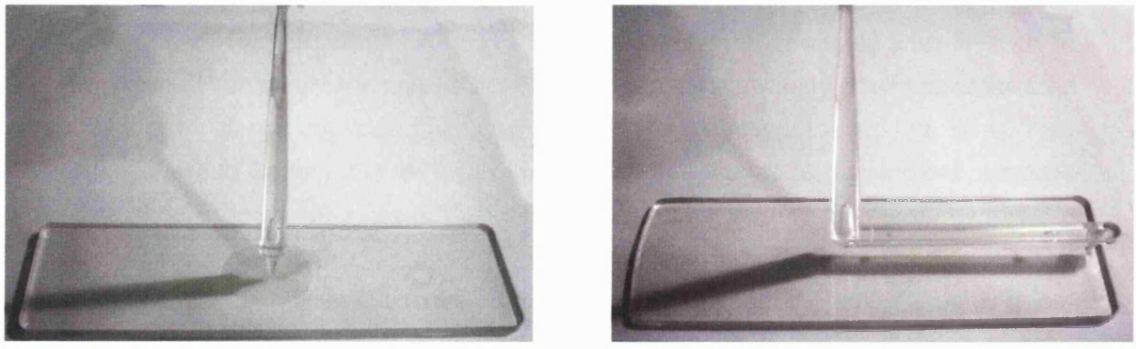

1) Centre Gate Injected PC Plate *2) Side Gate Injected PC Plate*

Figure 3.18: Centre and Side Gate Injected Plates with Polycarbonate

3.5.3 Comparison of Theoretical and Experimental Injection Pressure

The theoretical prediction for the required injection pressure to mould PP and PC plates including the experimental mean values (of 5 consecutive experiments for each case) are summarised in Table 3.11. During the experiments the necessary injection pressure varied according to the type of polymer being used from 28bar up to 57bar for the same flow paths and cavity shape. For the theoretical estimation of the injection pressure for PP, catalogue data where used (for a commercial PP grade) which did not correspond to the properties of the grey and white polypropylenes that were used for the experiments. Therefore a comparison between the theoretical estimation and experimental mean values could only be made for the PC where the material properties (of the experimental PC) were known. A good agreement was found between the mean experimental value of PC with the theoretical.

Polymer	**Injection Pressure**	
	Experimental Mean Value	**Theoretical Estimation**
Grey Polypropylene	28 bar	-
White Polypropylene	42 bar	-
Plain Polypropylene	-	34.5 bar
Transparent Polycarbonate	57 bar	58.9

Table 3.11: Comparison between Theoretical and Experimental Injection Pressure Levels

The viscosity of the grey polypropylene used in the experiment was higher than that of the white polypropylene. However, the white PP produced a higher (experimental) injection pressure drop than the grey PP. The main reason was that the same injection speed and packing pressure were used for both white and grey PP, where lower settings should have been sufficient (for white PP) to mould the part successfully. As a result the cavity pressure reached the level of 238bar which was considerably higher than the previous case (158bar, Fig. 3.14). This was attributed also to the fact that the lower viscosity white PP allowed higher local pressures to be reached near the pressure sensor diaphragm. This is also verified by the cavity pressure that rises a few bar (about 8bar, Figure 3.16) before the transition to the packing phase. For the moulding of polycarbonate due to the higher viscosity from both PP grades a higher injection pressure was required. Moreover the first three sets of experimental results were in good agreement with simulation results derived in Chapter 2, in regard with filling time, injection and packing pressure level.

3.5.4 Conclusions

Overall a thorough experimental programme was conducted with the aid of the newly designed mould in which a series of polymers with different viscosities were used for the moulding of the parts. Different part orientation was obtained by changing the position of the gate from the centre to the side of the cavity. The flow orientation was verified experimentally to confirm that the flow is radial initially and as it progresses spreads to two flow contours when injecting from the centre of the cavity. Depending on the viscosity of material used a different injection pressure was necessary for the filling and packing phase.

There is little that can be done to control screw motion during injection as all settings must be preset before the commence of the cycle. For the above reasons it would be beneficial to enhance the hydraulic control of the moulding machine such that the process parameters can be altered in real time. In order to do this efficiently a better insight into the melt flow behaviour is required during the injection phases. Once appropriate information is obtained, different control strategies can be considered with a view to influencing the orientation of the polymer and mechanical properties of the parts. As a first attempt, two methods are proposed in the next section with the aim of monitoring the extent of solidification of the parts during moulding.

3.6 Part Solidification

In order to optimise the injection cycle while at the same time retaining the quality in the parts it is important to monitor and control the process efficiently. Information about the dynamics of melt polymer inside the cavity could provide information about variations in the material properties due to processing conditions. In addition, the injection cycle time could be reduced, provided that information regarding the extent of part solidification is available. Depending on the cooling time and rate, residual stresses form while the degree of crystallinity of the polymer changes. Therefore the mechanical properties can be manipulated in order to meet specifications for the particular application.

The first method makes use of real-time temperature measurements at two different depths from the cavity surface. The high thermal conductivity of aluminium enables the thermocouples to detect rapidly the heat transients while these are logged with the aid of a custom made data acquisition unit. The thermocouples are assumed to be in the centre of a lumped thermal section. An algorithm was developed by co-worker Stelson [49] to take into account the heat conducted from the first lumped thermal section to the second section and relate it to the growth of solid layers within the molten part. Information about the polymer properties, and dimensions of the cavity, are used to estimate the reduction in the internal energy and solidification rate of the

part. The decrease in the internal energy of the polymer and the cavity surface temperature are estimated as linear functions of the extent of solidification.

The second method makes use of a non-intrusive method with the use of ultrasound waves generated by piezoelectric transducers operating at high frequencies. These waves propagate through the mould sections and polymer melt in the cavity. As the state of the polymer changes during the solidification, a variation in the wave speed and its amplitude (attenuation) occurs. These real-time data are captured and analysed to identify the trajectories and transitions of the phases, variation in process parameters and solidification rate of the part. In Figure 3.19 the instrumented mould is presented.

Figure 3.19: Specially Instrumented Mould with Embedded Thermocouples, Cavity Pressure and Ultrasound Transducers

3.6.1 Prediction of Part Solidification via Temperature Transients

The following mathematical analysis of part solidification in the next two sections is attributed to previous work by Stelson [49]. This analysis is used for the prediction of the extent of solidification of the moulded part during the cooling phase. Temperature data from thermocouples embedded close to the cavity wall, are logged and processed by an algorithm, which interprets the reduction in the internal energy of the part and the heat being transfered to the mould.

3.6.1.1 Liquid and Solid Part Layers

To predict the extent of solidification of the part during cooling for modelling purposes, the cavity is divided in two sections. These are the solidified layer (close to the walls surface) and the liquid layer up to the centre of the part as shown in Figure 3.20. The spatial temperature distribution within the mould follows a linear relationship in the solid layer and assumed constant for the liquid layers [49, 74]. The mould is designed to be symmetrical, therefore the part solidifies uniformly from the wall towards the core.

The boundary conditions are set such as: $T = T_w$ when $z = 0$ and $T = T_s$ when $z = z_s$.

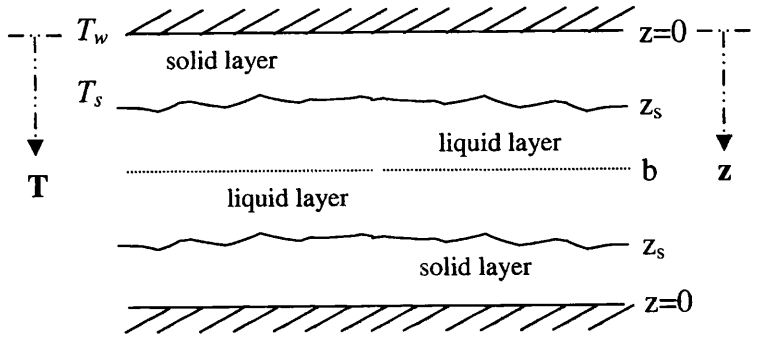

Figure 3.20: Extend of solidification of the part (0.004m thick) and boundary conditions

The following formulas describe the temperature distribution behaviour:

$$T_{solid}(z,t) = \frac{T_s - T_w}{z_s(t)} z + T_w \tag{3.12}$$

where $0 \leq z \leq z_s(t)$

$$T_{liquid}(z,t) = T_s \tag{3.13}$$

where $z_s(t) < z \leq b$

The specific internal energy (u) in the solid and liquid layers, including the latent heat of the polymer, is described by the following formulas.

$$u_s = c_p (T - T_w) \tag{3.14}$$

where $T_w \leq T < T_s$

$$u_l = c_p (T - T_w) + L_H \tag{3.15}$$

where $T_s \leq T$

If the temperature distribution in each layer is combined with its internal energy, the spatial distribution can be obtained.

$$u_s (z) = c_p (T_s - T_w) \frac{z}{z_s} \tag{3.16}$$

where $0 \leq z \leq z_s (t)$

$$u_l (z) = c_p (T_s - T_w) + L_H \tag{3.17}$$

where $z_s (t) < z \leq b$

Next by integrating the specific internal energy over the volume of the polymer, the total internal energy in the part can be defined as a function of the solidified layer thickness z_s.

$$U_T = \rho A_p \left[c_p (T_s - T_w) \left(b - \frac{z_s}{2} \right) + L_H (b - z_s) \right] \tag{3.18}$$

3.6.1.2 Monitoring of the Thermal Transients

To monitor the thermal transients during the injection cycle, two copper-constantan thermocouples (T-type with bead diameter of $2.54 \cdot 10^{-4} m$ and time constant, $\tau = 0.11 s$) were used, embedded at a depth of 0.005m and 0.015m from the cavity respectively. The mould is symmetrical and the model applies for both sides. Each thermocouple is treated as being in the centre of a lumped thermal mass (L1 and L2 close to the cavity wall) with thickness d, at depths $\frac{1}{2}d$ and $\frac{3}{2}d$.

The schematic illustration in Figure 3.21 shows the thermocouple configuration in the mould.

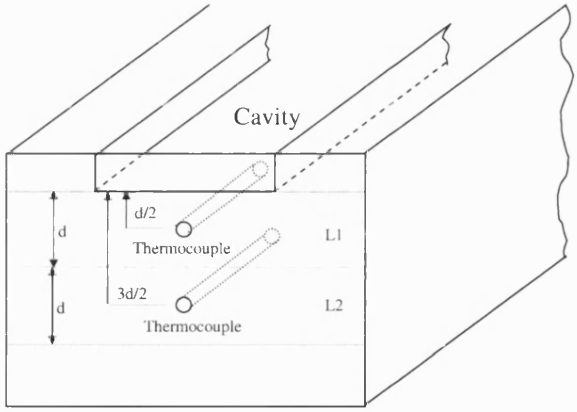

Figure 3.21: Lumped Thermal Mass L1 and L2 located close to the cavity wall

The thermal capacitance of each lump is equal to:

$$C_l = \rho_m c_m A_p d \tag{3.19}$$

The heat transferred (by conduction) from the cavity's wall to the mould is related to the thermal resistances, between the two lumps (L_1, L_2) and between the mould and the first lump. These can be respectively expressed by:

$$R_{L1-L2} = d \times \frac{1}{kA} = R_c \tag{3.20}$$

$$R_{m-L1} = \frac{d}{2} \times \frac{1}{kA} = \frac{R_c}{2} \tag{3.21}$$

During the cooling phase, a perfect thermal contact is assumed at the polymer/mould interface and the thermal convective resistance is neglected. Therefore, all the heat flux from the polymers surface is transferred to the mould with no energy being lost. The heat flow rate into the mould is proportional to the extent of the solidified layers of the polymer.

$$q(t) = -\frac{dU}{dt} = \rho A \left(c_p \frac{T_s - T_w}{2} + L_H \right) \frac{dz_s}{dt} = w \frac{dz_s}{dt} \tag{3.22}$$

Consequently, the temperature change in the mould will be detected first from the first lump and next from the second one. This is expressed by the state equation for the first lump:

$$\frac{dT_1}{dt} = \frac{T_2(t) - T_1}{R_c C_l} + \frac{q(t)}{C_l} \tag{3.23}$$

where T_2 and $q(t)$ are the inputs.

The time constant for the lumped system will be:

$$R_c C_l = \frac{\rho_m c_m d^2}{k_m} = \frac{(2800)(960)(0.01^2)}{130} = 2.07s \tag{3.24}$$

Finally, by combination of equations 3.22 and 3.23 the extent of solidification of the part can be estimated by entering the temperatures (experimental data - T_1 and T_2) from the lumped parameters as inputs.

$$\frac{dz_s}{dt} = \frac{q(t)}{w} = \frac{C_l}{w} \times \frac{dT_1}{dt} + \frac{1}{wR_c}(T_1 - T_2) \tag{3.25}$$

By integration of the above equation the solidified layer profile z_s, is expressed by:

$$z_s(t) = \frac{C_l}{w}[T_1(t) - T_w] + \frac{1}{wR_c}\int_0^t [T_1(\tau) - T_2(\tau)]d\tau \tag{3.26}$$

The equation 3.26 enables the prediction of the extent of solidification from the experimental temperature data.

3.6.1.3 Experimental Setup and Findings

To validate the theoretical model experimentally a series of tests were carried out with the thermocouples monitoring the thermal transients during the injection cycle. The mould was insulated and the cavity cover plate had the gate located at the centre of the cavity. The temperature readings in the lumped masses L_1 and L_2 were monitored and logged for off-line analysis. A cavity insert was used to mould tensile testing specimens. The material used for injection was low-density polypropylene with the following process settings, presented in Table 3.12.

Injection time	1.5s
Injection Velocity	0.012m/s
Packing time	15s
Packing Pressure	66bar
Cooling time	25s
Mould Temperature	$50°C$
Average nozzle and barrel temperature	$200°C$

Table 3.12: Process Settings for the Moulding of Rectangular Part with Grey Polypropylene

Before injection the polymer was dried for two hours at $80°C$ to remove any moisture content present. The dosage slider setting was set depending on the volume requirement. The back-pressure was set at low pressure (8bar) to achieve uniform plasticizing. In Figure 3.22 below the recorded experimental cavity pressure and temperature transients are presented.

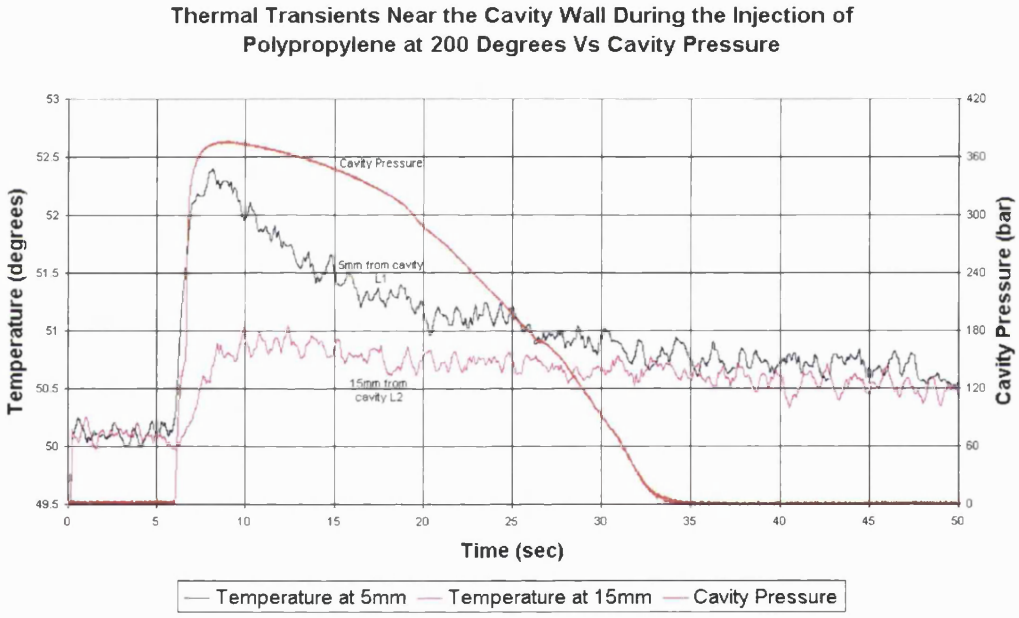

Figure 3.22: Temperature and Cavity Pressure Monitoring during Injection

In the filling stage the molten plastic enters the cavity and a thermal shock is created at the mould walls. This is tracked by thermocouples embedded close to the cavity at the centre of L_1 and L_2 lumped masses. The first thermocouple that is closer to the interface, (wall / PP) receives the thermal flow transient first. The second thermocouple captures the thermal transient, with a certain delay, since it is further away from the cavity wall (embedded 0.015m away). As the internal energy of the mould increases, the heat conducted from the first to the second lump decreases as the heat is dissipated through insulation to the platens. The heat flow rate from

the part to the mould is increased when the cavity pressure reaches its peak value at 380bar (neglecting thermal resistance at the interface). At the end of the packing phase (19s, gate is frozen), as the cavity pressure starts to decrease, (the cooling of the part starts) the temperature slope (L_1) at 25s decreases (resulting from poor thermal contact). The cavity pressure confirms this effect with the change of slope at 27s. This indicates the degree of the part solidification. After 32s the part can be safely ejected as the cavity pressure is back to atmospheric.

At the end of every injection cycle, it was observed that the temperature of the mould rose by no more than half degree. The insulation between the platens and the mould prevents any major heat loss, to maintain the mould at a nominally constant temperature. These experimental temperature data are processed in real time and the extent of solidification is predicted. The heat transfer model developed by Stelson in equation 3.26 assumes that both thermocouple readings start from the same temperature. The real time temperature data from the lumped thermal masses L_1 and L_2 were processed during the process in a Matlab Simulink model. In Figure 3.23 the extent of solidification z_s for the injection moulding of polypropylene is shown for different mould temperatures.

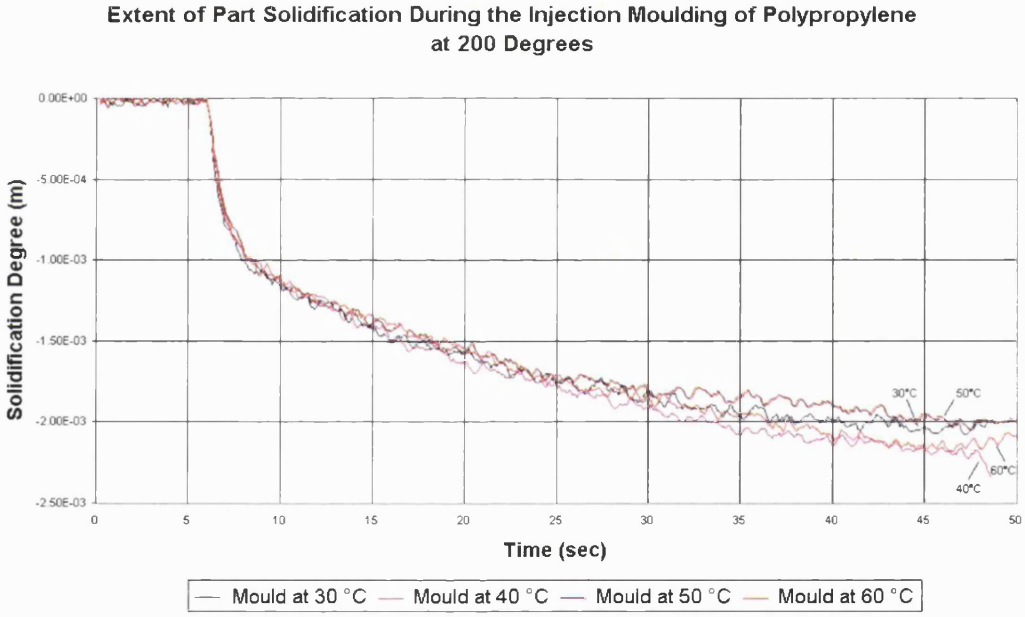

Figure 3.23: Extent of Solidification of the Half Part

The pattern of the extent of solidification for most cases (mould at 30°C up to 60°C) is mainly the same since no external cooling was used for the mould. Given that the mould is symmetrical the model predicts the solidification of the half part (2 mm). The part can be safely ejected when:

- The extent of solidification will reach 100% of part thickness.
- The temperature gradient of the mould reaches the steady state condition of the preset temperature level (30°C up to 60°C).

The actual solidification starts around 5.5s and finishes around 40s when the half part is solid. Hence, the time taken for the part to solidify is about 35s. This is a very good result considering that parameters such as density, specific heat and thermal conductivity are assumed constant in the model. In addition, the resolution in the data acquisition system was about $0.5°C$, which introduces a small error in the results.

The reduction in the internal energy (U) of the part can also be estimated using equation 3.18. It was found that the internal energy of the half part decreases in an exponential manner from 1440Joule to 56 Joule before ejection. In the case that all the heat flow from the part is conducted to the mould, the temperature at the interface can be approximated as well using the following formula:

$$T_i = q \times \frac{\Delta x_m}{k_m A_m} + T_w \tag{3.27}$$

where Δx_m, k_m and A_m are all mould constants ($\Delta x_m = 0.047\,m$, $A_m = 0.0255\,m^2$).

3.6.1.4 Conclusions

This adopted approach is simple to apply and provides a good approximation of the actual thermal conditions. As a result a major reduction can be achieved in the initial trial and error iterations required to set-up the machine and mould, since only a few parameters are required for the model to estimate the solidification time of the part. In the case of a complex mould, it would be appropriate for the pair of thermocouples to be embedded close to the cavity section where the part takes longer to solidify.

3.6.2 Prediction of Part Solidification via Ultrasound Wave Speed Variation

Ultrasound is a non-intrusive method for the prediction of the melt polymer behaviour (state) inside the cavity. No sensors are placed in direct contact with the moulded part. The waves propagate through the mould interfaces and the polymer melt. The variation in the speed of flight and attenuation of the signals amplitude, are a result of polymer solidification. The transducers can be used in a simple or complex mould at critical sections where information

is required about the solidification rate of the polymer. There are two methods for receiving the signal being transmitted. The first is the echo-pulse method, where one sensor sends and receives the signals reflected from the mould interfaces. The second one is the pulse and receiver method, where one sensor sends and the other one receives. Both approaches have been used in this study.

3.6.2.1 Ultrasound Theory

The velocity of sound for most waves is defined [75] by the formula,

$$c = f \times \lambda \tag{3.28}$$

were (f) is the frequency of the sound wave and (λ) the wave length. The propagation of sound through a fluid transmits both kinetic and potential energy through the movement of particles and stresses that are formed in the fluid (elastic) [75]. In a fluid these motions are parallel to the direction of propagation and include pressure fluctuations within the fluid. These are known as compression and rarefaction. An expression that relates the instantaneous pressure (p) and velocity (u) in the media is:

$$p = \rho c u \tag{3.29}$$

The longitudinal plane wave velocity (c_l) can also be defined by the time taken (t) to propagate through a media of a certain length (d),

$$c_l = \frac{d}{t} \tag{3.30}$$

For longitudinal waves the sound velocity is expressed by the elastic parameters of the material.

$$c_l = \sqrt{\frac{E}{\rho} \times \frac{(1-\nu)}{(1+\nu)(1-2\nu)}} \; or \; c_l = \sqrt{\frac{1}{\rho}\left(K + \frac{4}{3}G\right)} \tag{3.31}$$

Variables v, E, K, G are the Poisson's ratio, modulus of elasticity, Bulk modulus and Shear modulus of the material respectively. With the use of equation 3.31, the theoretical speed of sound propagating through solid polypropylene has been calculated with the following mechanical properties, shown in Table 3.13.

Polypropylene	Range	Average Value
Young's Modulus (Pa)	$0.7 \times 10^9 - 1.9 \times 10^9$	1.9×10^9
Density (kg/m3)	890	8.9×10^2
Poisson's Ratio	0.36 - 0.4	0.4
Speed of Sound (m/s)		≈ 2139

Table 3.13: Parameters used for determining Theoretical Speed of Sound through Solid Polypropylene

In order to characterise the material as sonically 'soft' or 'hard', the acoustic impedance is used. It is a function of the product of density (ρ) and ultrasound velocity (u). It is measured in Rayles, where $1\,Rayle = \frac{m}{s} \times \frac{kg}{m^3}$:

$$Z_i = \rho \times u \tag{3.32}$$

The speed of longitudinal waves through various media and their acoustic impedance are given in Table 3.14.

Different Media Properties	Velocity (m/s)	Density (kg/m^3)	Acoustic Impedance $(kg/m^2 \times s)$
Air (20°C)	344	1.247	4.29×10^2
Water	1480	1000	0.148×10^7
Steel (mild)	5000	7800	4.7×10^7
Aluminium (7075-T6)	6400	2800	1.78×10^7
Polypropylene (white)	2660	890	0.237×10^7
Polycarbonate (clear)	2270	1180	0.268×10^7

Table 3.14: Speed of Longitudinal Waves through different Media, from [76]

The sound pressure (amplitude) of a wave is a function of velocity (u) and acoustic impedance (z).

$$p = u \times z \tag{3.33}$$

When a wave that propagates through a media reaches an interface (for example Aluminium / Solid Polymer) part of the signal is transmitted through the material (polymer) and the rest is reflected back by the interface. In the case of a cavity filled with molten plastic, the velocity of the wave depends on the pressure and temperature of the plastic.

The amount of energy being reflected is characterized by the reflection coefficient. There are four cases that can be distinguished, depending on the interface [77].

- Sonically hard boundary, the signal is reflected without a change in the phase, $R \leq 1$ when $z_2 \gg z_1$
- Sonically soft boundary, the signal is reflected with a 180 degree phase change, $R \geq 1$ when $z_2 \ll z_1$
- No reflection, 100% of the signal is transmitted through the media, $R = 0$ when $z_2 = z_1$
- Small reflection, a slight phase change in the reflected signal, $-1 \ll R \ll 1$ when $z_2 \approx z_1$

3.6.2.2 Experimental Setup

For this experimental investigation the rheological behaviour of the molten polymer (PP) during the injection moulding cycle was monitored and analysed. Two ultrasound transducers (3.25MHz longitudinal piezoelectric with 21mm diameter) were used. A generator was used to produce the excitation pulse (burst) and a Lecroy Oscilloscope with a sampling rate of 100MHz monitored and logged the transmitted and reflected signals. Data acquisition was carried out using a National Instrument A/D card and LabView software program. The ultrasonic transducers were positioned in such a way that the waves are perpendicular to the direction of polymer flow. The first transducer was placed in the mould cavity section and the second one in the mould sprue section, as shown in Figure 3.24. The first arrival time of the transmitted signal, its amplitude and the attenuation coefficient will be used to identify the solidification rate of the part and identify phase transitions. In the following experiment the insulated mould was used with the cover plate diverting the polymer flow to the centre of the cavity (4mm thickness).

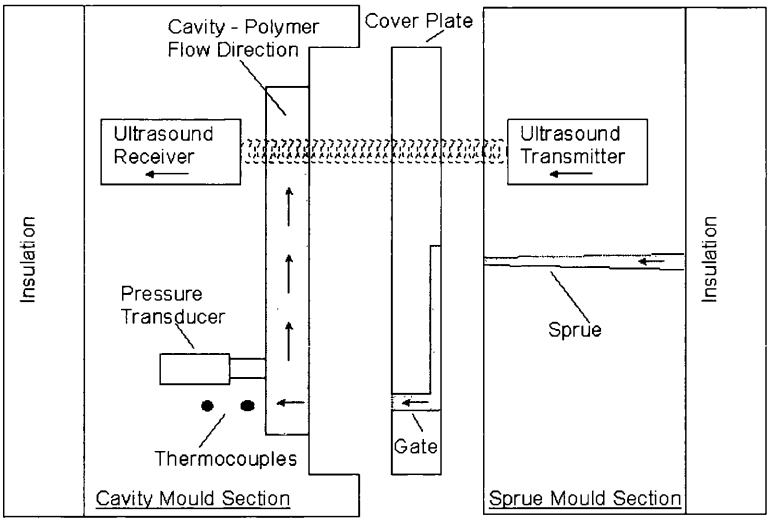

Figure 3.24: Position of Thermocouples and Ultrasound Sensors in the Mould

The material used for injection was low-density polypropylene (white) with the following machine (process) settings in Table 3.15.

Injection time	4.6s
Injection Velocity	0.012m/s
Packing time	10s
Packing Pressure	66bar
Cooling time	40s
Mould Temperature	41°C
Average nozzle and barrel temperature	200°C

Table 3.15: Process Settings for the Moulding of Rectangular Part with Polypropylene

Before injection the material was dried for two hours at 80°C to remove any moisture content. The dosage slider was set according to the volume requirement. The back-pressure was set at low pressure (8bar) to achieve uniform plasticizing.

3.6.2.3 First Arrival Time of the Ultrasonic Signal

Based on the experimental arrangement in Figure 3.24, the first transducer transmits a signal burst, which the second transducer receives with a certain time delay. The signal has to travel through the mould sections and the polymer in the cavity. Therefore the first arrival time, (time of signal flight, TOF) and attenuation of the signal can be estimated if the properties of the

interfacing material are known. Assuming that the properties of the aluminium stay the same during the process (temperature assumed constant) the only parameter that will alter the TOF will be the polymer's behaviour inside the cavity. Its properties are pressure and temperature dependent and will vary throughout the injection cycle. The following assumptions were made.

- In the plasticization phase there is no transmission as the presence of air in the cavity does not allow for any acoustic coupling to form.
- In the filling phase when the cavity is progressively filled, there is an acoustic coupling between the cavity walls (by the polymer). Therefore at the wall-polymer interface the signal can be transmitted through the mould.
- In the packing phase the cavity pressure increases, affecting the density of the melt polymer and improves the coupling at the wall-polymer interface.
- In the cooling phase the part starts to solidify symmetrically from the surface walls towards the core. As the part continues to solidify, solid layers replace the liquid while the speed of sound will vary in each layer. A major variation in the TOF is expected.

To estimate the TOF from the experimental data (transmitted ultrasound signal), the zero-crossing detection is used for the wave signal. The TOF results along with the amplitude of transmitted and reflected signal are presented in Figure 3.25.

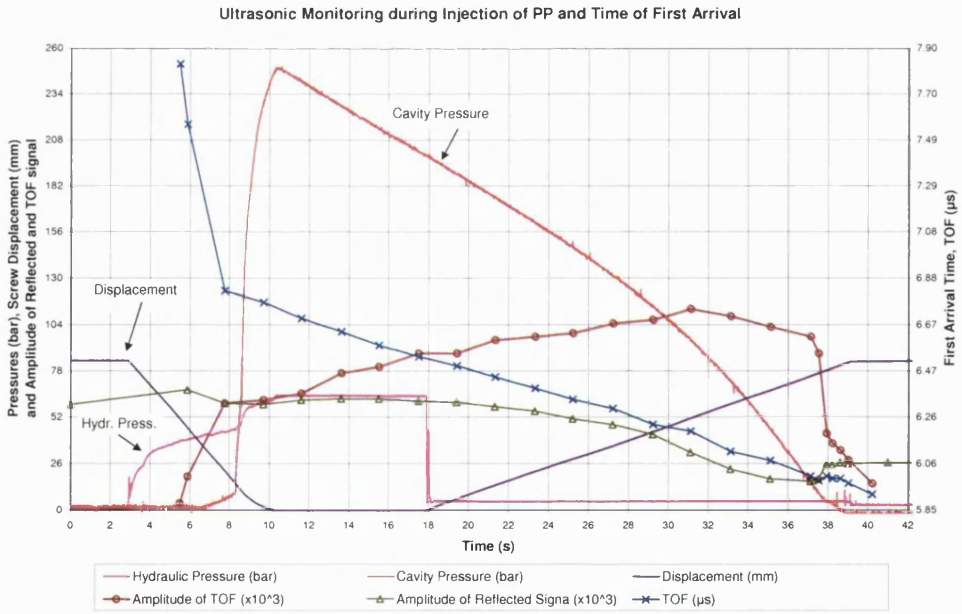

Figure 3.25: Ultrasonic Monitoring during Injection of PP and Time of first Signal Arrival

3.6.2.4 Analysis of Experimental Results

The rise in the hydraulic pressure (at 3s) indicates the start of the filling phase. No ultrasound signal is transmitted through the cavity before an ultrasound coupling is created (by the melt polymer) and all the air escapes. The speed of longitudinal waves in air is very low (18 times less than in aluminium), and the entire signal is reflected back to the medium (aluminium). As the cavity gets filled both cavity walls come in contact with the melt polymer through which the ultrasound wave starts to propagate (1st transmission). The TOF starts to reduce as the hydraulic pressure rises while the amplitude (sound pressure) of the reflected signal decreases. At the transition from the filling to packing phase there is a major reduction (from 7.56μs to 6.82μs) in the TOF as the cavity pressure rises (from 1-10bar). This increase in the cavity pressure improves the coupling (at the interface Al-PP) between the first solidified polymer skin at the aluminium wall with the wall itself. The amplitude of the transmitted signal increases as well. However, a further increase in the cavity pressure (from 10-250bar) does not have any significant effect in the TOF. Another parameter that influences the response of the TOF is the density (Appendix A.5) of Polypropylene which decreases in a very narrow region close to the melting temperature.

During the cooling phase the cavity pressure decreases linearly with time, a dominant factor keeping a good coupling at the polymer-aluminium interface. As the part further solidifies the waves travel through solid and liquid layers of polymer. Figure 3.26 illustrates the different layers inside the cavity.

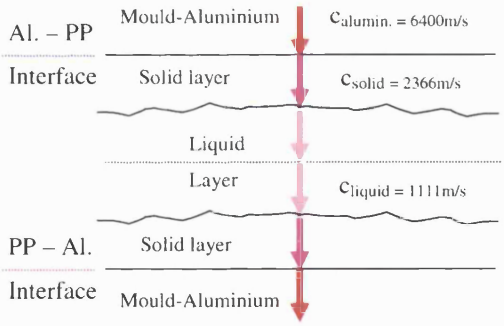

Figure 3.26: Solid and Liquid Layers Inside the Cavity Section

The speed of sound in the solid and liquid layers has been estimated experimentally using the difference in TOF at the beginning and at the end of the process. The TOF is about 2366m/s in a solid layer and 1111m/s in the liquid. At these interfaces (solid-liquid polymer) a certain amount of sound pressure is transmitted through, and some reflected back and forward in the solid medium (in the solidified polymer until it is completely attenuated). As the part solidifies towards the core of the cavity, the amplitude of the transmitted and reflected signal increases

and decreases respectively (TOF decreases linearly with time). At the end of the cycle the part further shrinks and the amplitude of the transmitted signal is gradually reduced to zero. This is an indication that the part is detached from the wall and a small layer of air is introduced at the interface. The entire transmitted signal is reflected back to the mould at the cavity wall-air interface.

The same experiment was repeated for the moulding of tensile test specimens for mould temperatures varying from 30°C to 60°C degrees. The TOF results are presented in Figure 3.27.

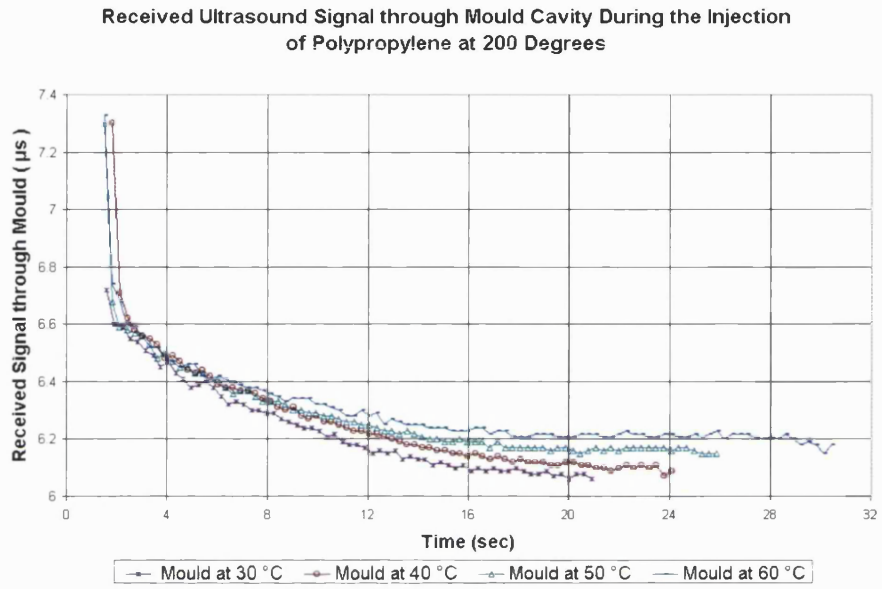

Figure 3.27: Received Ultrasound Signal through the Mould Cavity during the Injection of PP at 200°C

Parameters such as mould temperature and pressure affect the crystallization kinetics and consequently the way that the polymer chains are formed. As expected the higher the temperature of the mould the longer it takes for the part to solidify and detach from the mould wall. The sudden change in propagation delay at the beginning of the injection (falling from 7.3μs to 6.6 μs) cycle indicates that nearly half of the part solidifies when the polymer comes in contact with the mould wall. The core solidifies less rapidly and during this phase the packing pressure plays an important role in the core orientation of the produced part. The differences in propagation delay were also correlated with the measured thickness of the produced parts. For a mould temperature varying from 30 to 60 degrees the increase in thickness ranged from 4.00 to 4.01mm.

In Figure 3.28 the amplitude of the received ultrasound signal at the start of the filling phase exhibits a near linear rise for the first 5s. It approaches then a steady state level immediately

after the packing phase and remains roughly constant for most of the cooling phase.

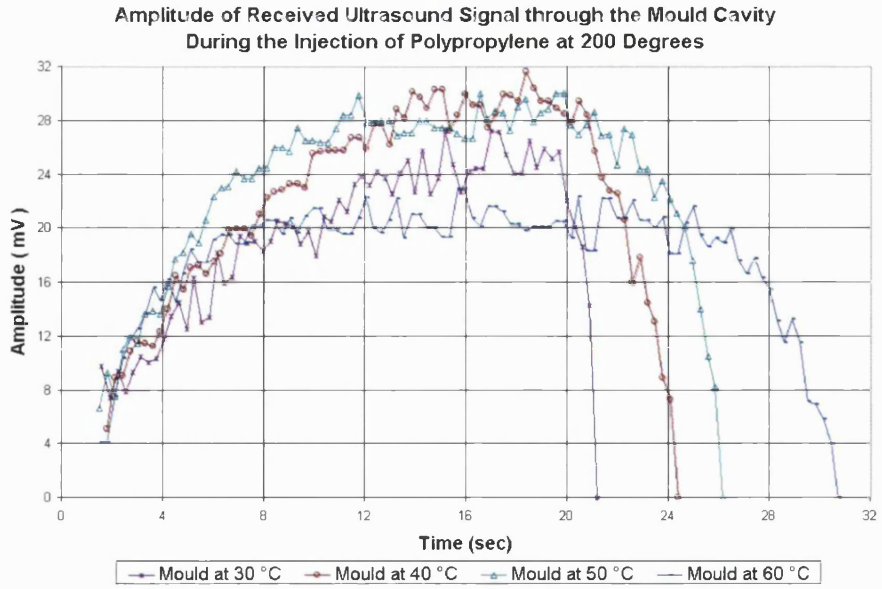

Figure 3.28: Amplitude of received ultrasound signal through the Mould Cavity during the Injection of PP at 200°C

During the cooling phase small changes occur in the molecular orientation of the polymer. At the end of that phase the sudden attenuation of the received signal indicates that the part has detached from the mould wall. Similar behaviour in the propagation delay and amplitude variation was also observed in the moulding of polycarbonate. However changes in propagation delay were less observable (<0.015 μs compared to PP moulding which where around 0.05μs) at mould temperatures of 80 up to 110 degrees. The amplitude of the received signal follows a different pattern during solidification, which reflects the cooling behaviour of amorphous materials. Cooling time is much shorter compared with moulding of polypropylene since no crystal formation takes place in amorphous polymers.

In Figure 3.29 the correlation coefficient between successive reflected signals during the injection cycle of polycarbonate is plotted alongside the cavity pressure profile.

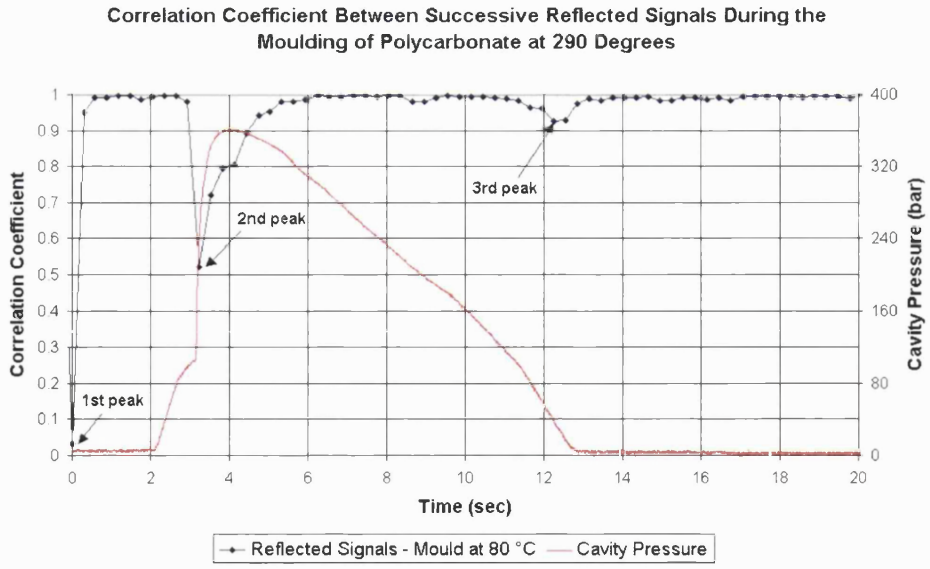

Figure 3.29: Correlation Coefficient between Successive Reflected Signals during the Moulding of PC at 290°C

Major variations in the correlation coefficient that occur during the injection cycle characterize most of the phases, such as:

- Mould closing (1st peak - interfaces change).
- End of filling and transition to packing phase (2nd peak).
- Packing phase (coefficient rises to 1).
- End of cooling part detachment from wall (3rd peak).

The major changes in the reflected signals are due to the molecular changes that take place early in the packing phase.

3.6.2.5 Reflection coefficient

All the energy generated by the transducer is sent in a form of sound pressure through the media. This will be either transmitted or reflected at different mould interfaces. Figure 3.30 schematic illustrates these interfaces.

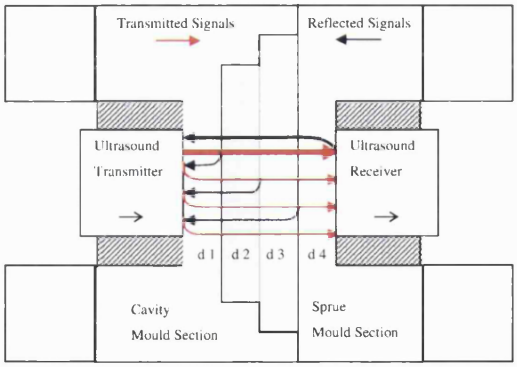

Figure 3.30: Transmitted and Reflected Signals at the Interfaces

In the first analysis of the experimental results, it was seen that during the injection process, the amplitude of the sound waves changed continuously. Initially when air was in the cavity the transmitted signal is reflected back to the transducer. This can be mathematically verified by the reflection and transmission coefficients. In this case the waves are normally incident to the boundary, the reflection (R) and transmission (D) coefficients are a function of the acoustic impedance of the material Z_i at the two faces [49].

$$R = \frac{A_{refl.}}{A_{inc.}} = \frac{Z_2 - Z_1}{Z_2 + Z_1}, \; D = \frac{A_{trans.}}{A_{inc.}} = 2 \times \frac{Z_2}{Z_1 + Z_2} = 1 - R \tag{3.34}$$

- So at the aluminium - air interface the coefficients will be:

$$R = -99.99\%, \; D = 0.01\% \tag{3.35}$$

The transmitted signal is obviously insignificant, 0.01% and virtually the entire signal, 99.99% is reflected.

- In the filling phase as the cavity volume is progressively increased the interface changes to aluminium - melt polymer interface. The coefficients at the new interface will be:

$$R = -78.84\%, \; D = 21.16\% \tag{3.36}$$

The transmitted signal now is about 21% while the rest 79% is still reflected back to the medium.

- As the longitudinal wave travels through the melt polymer, it will reach the aluminium interface at the cavity wall. Consequently at the melt polymer - aluminium interface the coefficients will be:

$$R = 78.84\%,\ D = 178.84\% \tag{3.37}$$

In this case +78.84% of the wave is reflected while a 178.84 % is transmitted. The (+ve) sign indicates that both waves (incident and reflected) are in phase. Because the sound pressure exceeds the 100% (sound pressure), it does not mean that the energy law is not valid. In this case the intensity of the transmitted wave is much smaller in Aluminium than in Polypropylene in spite of the higher sound pressure, where:

$$p_{inc} + p_{refl} = p_{trans}\ or\ 1 + R = D \tag{3.38}$$

Usually a phase reversal described by a (-ve) value of R occurs in the situation of reflection on the sonically softer medium (Al/PP interface, as described in equation 3.34).

3.6.2.6 Further Analysis of Ultrasound Data

In the analysis of the experimental ultrasound data it is very difficult to identify the interfaces (Al/Melt PP, Al/Solid PP, Solid PP/Melt PP, Melt PP/ Solid PP, Solid PP/ Al) that form during the solidification of the part. For this reason the nature of the reflection and transmission coefficient can be approximated using the average ultrasonic speed. The transmission coefficient incorporates the signal that passes through the mould interfaces. The reflection coefficient incorporates the reflected signal from the 2nd cavity wall. This means that the signal has to travel through the polymer and back to be received by the transmitter-receiver.

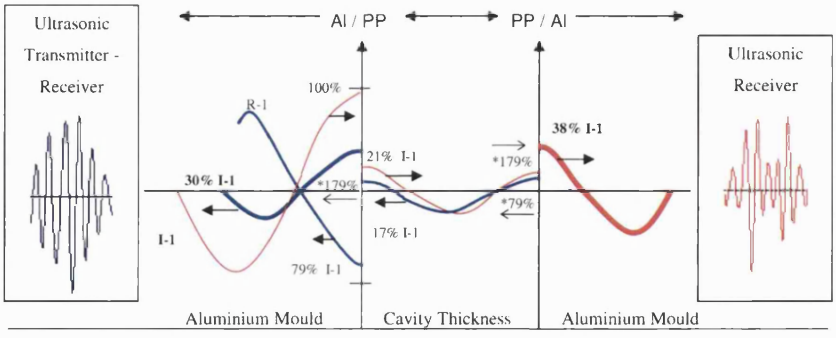

Figure 3.31: Amplification and Attenuation of Waves at the Mould Interfaces

Figure 3.31 schematically illustrates the signals, and their attenuation-amplification (of sound pressure) at the interfaces when the part is solid ($C_{av} = 2366m/s$). Based on the average (experimental) ultrasonic speed through the polypropylene the nature of the reflection and transmission coefficient can be plotted as in Figure 3.32.

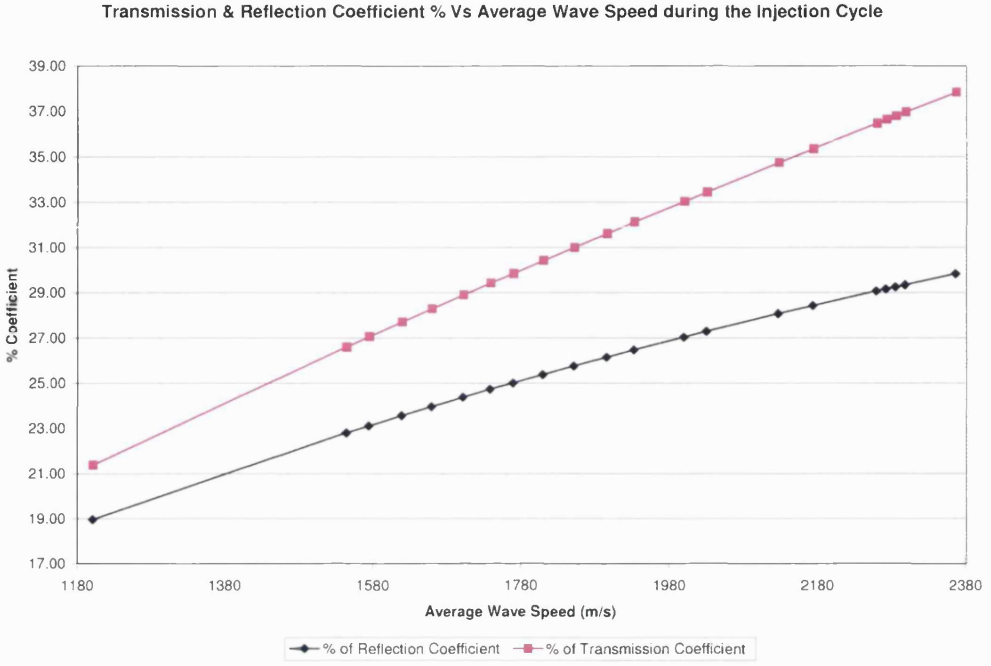

Figure 3.32: Theoretical Transmission and Reflection Coefficient % Vs Average Wave Speed

Both coefficients increase almost linearly with time during the solidification of the part. These results have a good correlation with the amplification of the (real time) transmitted and reflected signals.

3.6.2.7 Analysis of Sound Pressure Attenuation

During the solidification of the part, the amplitude of the signal (sound pressure of the plane wave) decreases as a result of attenuation, following an exponential form of:

$$p = p_0 e^{-ad} \tag{3.39}$$

The attenuation (a) over a distance (d), of the ultrasonic wave in the solid and liquid media is the energy loss expressed in nepers (Np), $ad = ln\frac{p_0}{p}Np$ or $ad = 20log\frac{p_0}{p}dB$ where $1Np =$

8.686dB. To estimate the attenuation coefficient, the amplitude of two successive (transmitted) signals must be compared. For example if in the second signal the energy being lost is less, this verifies that the polymer has changed state (solidified more) providing a better transmission media. Two sets have been used (17μs - 7.72μs and 17μs - 12.45μs) and the results are compared in Figure 3.33. The second transmitted signal (at 17μs) is delayed due to a set of multiple reflections at the mould interfaces (more attenuated).

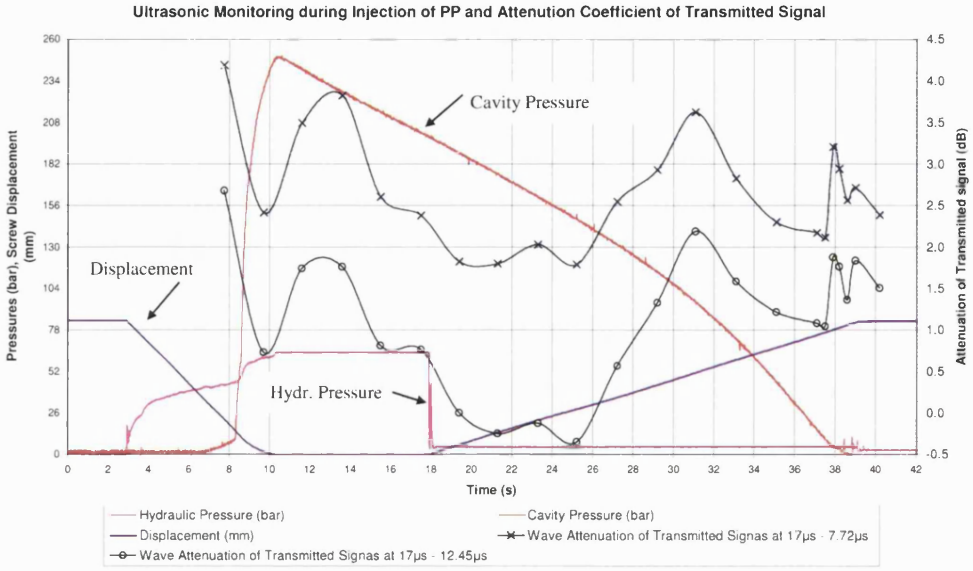

Figure 3.33: Experimental Attenuation Coefficient of Transmitted Signals

Both attenuation coefficients follow the same trend during the injection cycle. Initially the attenuation is high (4.18dB & 2.68dB at 7.74s) but decreases rapidly as the cavity pressure increases (at 230 bar). This is because the coupling at the cavity wall is improved. Afterwards as the part solidifies and the melt temperature drops, both slopes decrease almost linearly (from 14s up to 19s), and remain roughly constant from 19s up to 25s. The constant region could correspond to the crystallisation of the polymer. However to verify this hypothesis, temperature readings from the surface of the cavity would be required. As the cavity pressure changes slope again at 31s (verifying that the part shrinks) the attenuation coefficient increases again (3.63dB & 2.19dB) as the coupling between the mould wall and the part becomes weaker. Immediately after it reduces again indicating that the largest section of the part is solid. The rms (root mean square) attenuation in the second set ($17\mu s - 12.45\mu s$) was estimated to be $1.36dB$ while with the rms attenuation of the first set ($17\mu s - 7.72\mu s$) was $2.68dB$. The reduction in the attenuation coefficient is an additional indication that the part solidifies and less wave energy is lost as most of the transmitted signal propagates through the cavity with a minimum amount been reflected.

3.6.2.8 Predictive Analysis of the Extent of Solidification

To estimate the extent of the solidification of the part the average ultrasound speed was used. Based on the cavity thickness (4mm) the time required for the sound to propagate through the polymer can be theoretically calculated.

$$c = \frac{d_c}{t_{cav}} \Leftrightarrow \tag{3.40}$$

$$t_{cav} = \frac{d_c}{c} = \frac{0.004}{2366} = 1.69\mu s$$

The variation of the wave speed during the injection cycle will be:

$$t_{var} = t_{max} - t_{min} \Leftrightarrow \tag{3.41}$$

$$t_{var} = 7.83 - 5.92 = 1.91\mu s$$

The time taken to propagate through the aluminium sections (assumed constant) will be:

$$t_{al} = t_{min} - t_{cav} \Leftrightarrow \tag{3.42}$$

$$t_{al} = 5.92 - 1.69 = 4.23\mu s$$

Hence the time required for the wave speed to propagate through the solidifying part will vary from, $3.6\mu s$ to $1.69\mu s$. Based on the time variation, the average wave speed can be estimated as follows:

$$c_{av} = \frac{d_{cav}}{t_{var}} \tag{3.43}$$

The average wave speed during the injection cycle is shown in Figure 3.34:

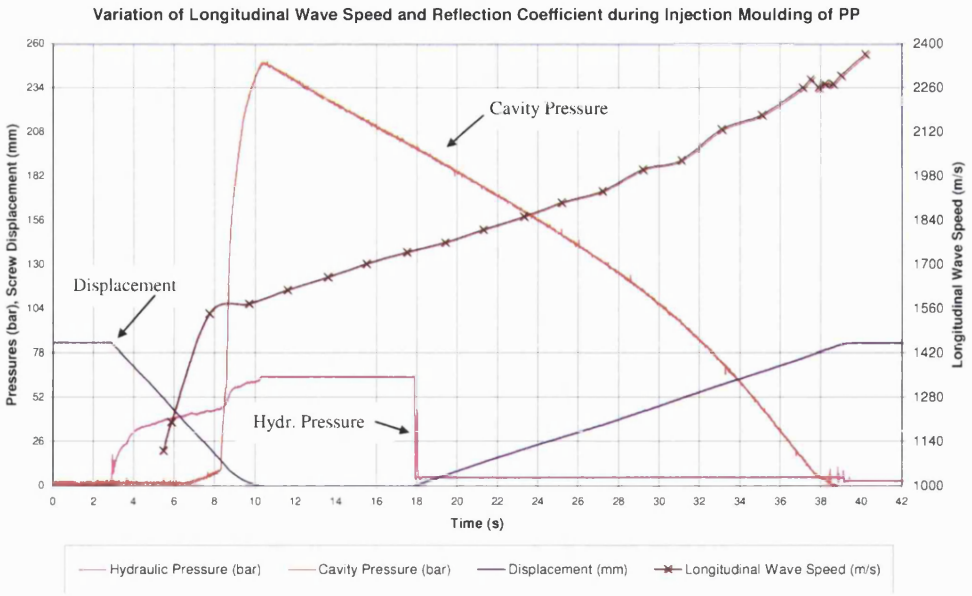

Figure 3.34: Variation of Longitudinal Wave Speed during Injection Moulding of PP

The average wave speed through the mould cavity varies from 1111m/s up to 2367m/s during the process. It is assumed that the first value (1111m/s) represents the wave speed through the molten Polypropylene. A sudden variation in the wave speed occurs at the beginning of the injection indicating that part of the melt polymer solidifies rapidly near the wall surface when it comes in contact with the cold wall. During the packing phase the wave speed increases linearly while around 31s the slope changes and the wave speed increased more rapidly (indicating a better transmission through the polymer). This change in the slope, can be explained by observing the attenuation of the transmitted signal in Figure 3.33 which peaks at 31s while it reduces again.

Moreover the extent of solidification can be defined by the average wave speed through the thickness of the cavity:

$$TOF_{cav} = \frac{2b}{c_{av}} \tag{3.44}$$

The cavity model incorporates a solid layer close to the wall and a liquid layer up to the centre. Figure 3.35 schematic illustrates the cavity model.

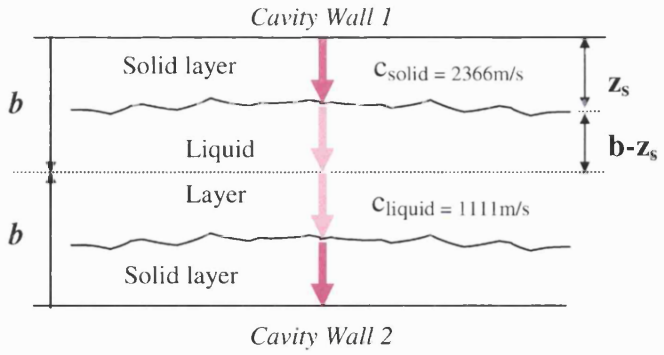

Figure 3.35: Cavity Model for the Determination of Extent of Solidification

Analysing the left hand side of equation 3.44 reveals that the $TOF_{cav.}$ is equal to the wave propagation through the two solid and liquid layers.

$$\frac{2b}{c_{av}} = 2 \times \frac{z_s}{c_s} + 2 \times \frac{(b - z_s)}{c_l} \Leftrightarrow$$

$$z_s = \frac{b\left(\frac{c_l}{c_{av}}\right) - 1}{\left(\frac{c_l}{c_s}\right) - 1} \tag{3.45}$$

Based on equation 3.45 the extent of solidification of a half part is plotted in Figure 3.36.

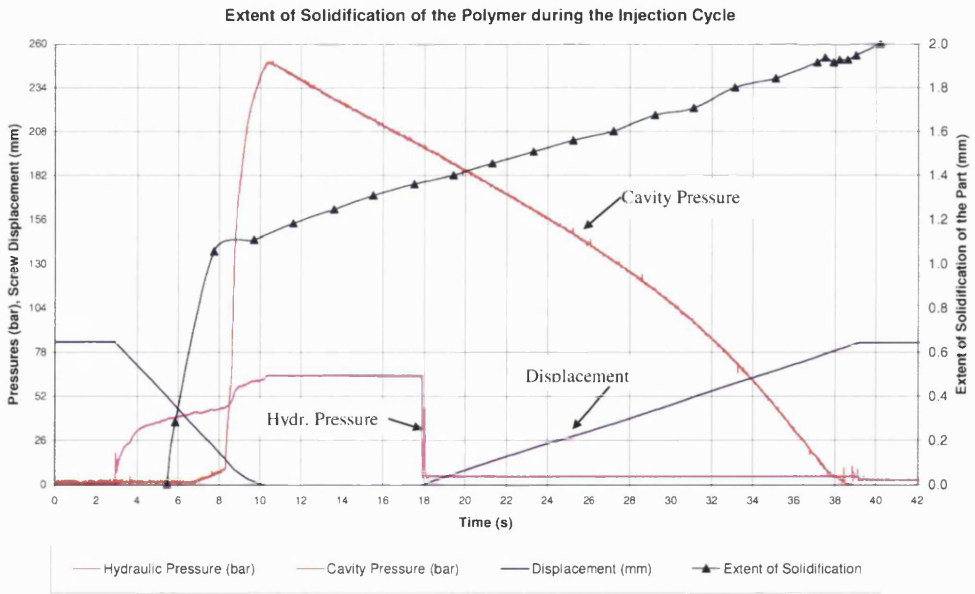

Figure 3.36: Extent of Solidification of the Polymer during the Injection Cycle

By observation of the solidification rate it is evident that the polymer layers which are close to the cavity walls, solidify very quickly during the filling phase. Nearly 50% of the part (at the measurement area where the transducers are) has solidified by the end of the filling phase. Thereafter the extent of solidification trend follows a 'linear' relationship as the cavity pressure decreases until the end of the cooling phase.

3.6.2.9 Comparison of the two Methods for Monitor Solidification

The ultrasound and thermocouple methods used to monitor the in-mould parameters and track the phase changes were both very reliable. In Figure 3.37 the extent of solidification (PP at 200°C mould at 50°C) is estimated using a) the average ultrasound speed, b) thermal changes that predict the heat being transferred to the mould.

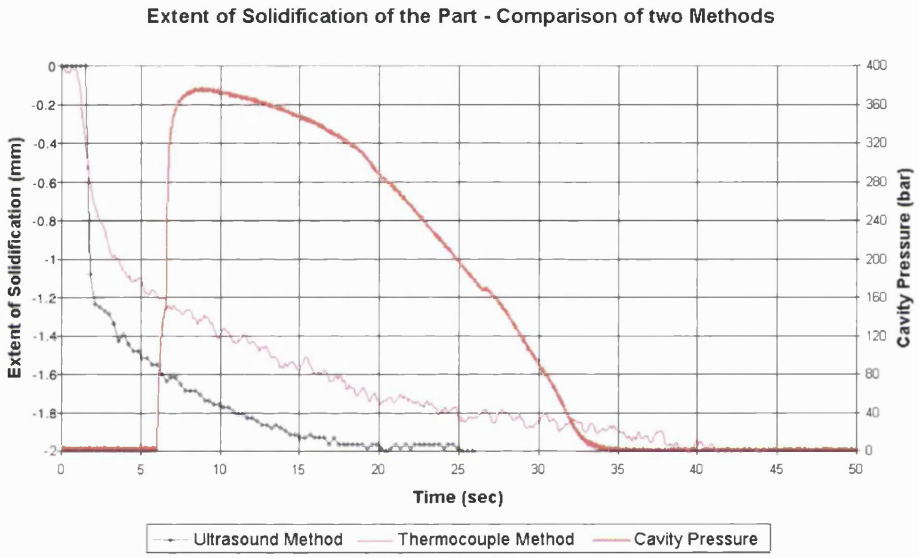

Figure 3.37: Thermocouple and Ultrasound Sensing of the Extent of Solidification of the Part

The solidification results of the two predictions show a small disparity due to the position of the sensors (Figure 3.24) in each method. The thermocouples were placed near the gate at the injection point while the ultrasound sensors were in the other side. Consequently the part side, which is near the hot gate, takes longer to cool compared with the other side, which has no thermal influence. However the trends are broadly similar.

3.7 Concluding Remarks

This chapter commences with the evaluation of the processing parameters and their effect in the quality of the produced parts. Two different materials are used, semicrystalline polypropylene and amorphous polycarbonate. Settings such as injection screw velocity, dosage size and packing pressure were altered in numerous mouldings of a square product, to investigate changes is surface appearance, weight and dimensional accuracy of the parts. Misadjustments of these parameters resulted in short shots, flash and surface defects in the parts. Both injection rate and hydraulic packing pressure influenced the cavity pressure profile, cooling rate of the part and cycle time. Proper adjustment of these two parameters is critical to maintain the overall hydraulic pressure drop low (low power consumption), while still maintaining the moulding process, e.g. not allowing premature solidification.

A new mould with embedded transducers was designed and manufactured in order to monitor temperature and pressure variations in the cavity during the injection cycle. Insulation between the mould and the machine platens was used to to minimise the heat loss and maintain the mould temperature nominally constant during the cycle. In preliminary tests the flow behavior of the melt polymer was investigated by changing the gate position in the cavity. It was observed that flow is initially radial until the melt polymer reaches the cavity walls. Thereafter a flow-front contour is developed that progressively moves towards the two ends of the flow path. The gate position should be placed thoughtfully in a mould in order to enhance flow orientation and avoid the formation of secondary flows that results in surface defects (weld lines).

Next the polymer molten behaviour during the injection cycle was evaluated based on real time ultrasound and temperature data. Ultrasound measurement were used to identify phase changes (Figure 3.29), determine the extent of solidification of the part as well as the product thickness before ejection. These data can be monitored from cycle to cycle with a statistical process control analysis to identify variations in the production. Selection of these data could provide a valuable feedback to the process controller to take corrective actions when necessary. For example if a delay occurs in the switching from filling to packing phase, the controller can reduce the cooling time of the part (for this delay period) to maintain the production rate constant. These particular batches which were moulded with process variations could be examined thoroughly after ejection to minimise the reject rate. On the other hand, the use of thermocouples proved to be an economic and reliable method, which provides sufficient information for determining the extent of solidification of the produced part in real-time (Figure 3.23).

However, the existing controls of the machine did not allow selecting a desired profile for the injection velocity, which remained constant throughout the filling process. In addition, the injection pressure could only be preset at the beginning of the cycle, thus preventing any

further manipulation of the cavity pressure. This control limitation urges the need for a modification in the hydraulics of the moulding machine that will enable control of some process parameters during injection. As a result of these considerations the hydraulic circuit of the injection-moulding machine was modified. The details of these modifications will be presented in Chapter 5.

In order to better interpret the experimental findings it is necessary to undertake a more detailed review of the polymer structure and behaviour under changing injection moulding conditions. Therefore the following chapter gives a more theoretical insight into the behaviour of the melt polymer during the process.

Chapter 4

Effects of Process Parameters on Rheology and Part Quality

4.1 Introduction

Nowadays the surface appearance of injection moulded parts has become a standard quality criterion of great importance. Plastics are increasingly used in both the aerospace and automotive industries to increase productivity, minimise costs and weights while at the same time improve aesthetics. Plastics are often used in the interior of passenger cabins or as external components. Year by year market competition is raising the standards and surface defects that used to be acceptable no longer meet the quality control requirements. Therefore it is of prime importance to understand the moulding process and identify the parameters that can optimise the cycle and enhance part quality. Especially in cases with materials sensitive to degrade, tight moulding conditions (temperature, injection rate) should be kept otherwise variations in their mechanical, thermal and physical properties (sink marks, weld lines and warpage, etc.) will occur.

This chapter describes the melt polymer behaviour during the crystallization and solidification phase of the injection moulding cycle. The need for a thorough literature review was important, for a better understanding of the experimental results (monitored during the cycle) and a further insight in methods influencing the molecular structure of polymers. Process parameters (such as flow and pressure) that affect the molecular orientation and degree of crystallinity of semi-crystalline polymers (polypropylene) were studied, as presented in section 4.3. Fibre reinforced materials where orientation of fibres has a more dominant effect than the molecular orientation where not investigated due to time constraints. Next various parts defects were studied and factors that can cause part failure in service-life were reviewed in section 4.4. A

sound understanding and knowledge of process parameters that should be carefully controlled during injection, was gained, in order to enhance product quality and mechanical properties. It is believed that theoretical models to predict the solidification time of the products are of less value, if ways to control crystallization and orientation of molecules are overlooked. To manipulate polymer rheology further, melt vibration method was investigated in section 4.5, as it is reported in [78, 79, 50, 27] to enhance the properties of the final products.

4.2 Structure of Polymers

4.2.1 Polymerization of Molecules

At the molecular level, polymers consist of long repeating molecular units which are coupled together to constitute chains. These polymer chains are free to rotate and orient themselves about the carbon atoms to intertwine with other molecular chains. These chains are held together by strong ionic or covalent bonds. When molecules polymerize, they usually form straight lines of carbon linkages. These linkages can be primary carbon-carbon (C-C bonds) linkages and secondary cohesive attractive energies known as the *Van der Waals forces* [27]. However these chains during polymerisation processing often form nonlinear or branched structures. In these cases carbon atoms branch out to form new polymeric chains[27]. Depending on the oriented structure, the material is very strong in the direction of flow and weak in the along flow direction [27]. This is attributed to the stronger links between the molecular chains by the primary C-C bonds when compared with the Van der Waals bonds as mentioned previously.

4.2.1.1 Degree of branching

The degree of branching varies depended on the manufacturing process. Higher branching (low density material) is usually achieved when the polymer is processed under high pressure. On the other hand polymers processed under low pressure are more linearly oriented and have a low branching (high density material) [27].

4.2.1.2 Elongation effects

Polymers ability to elongate is also related to its molecular structure. For instance, lower density polymers with many branches will exhibit under a load (parallel to the direction of the

polymer chains) a smaller percentage of elongation compared high density polymers. This is due to the properties of the molecular branches that resist sliding of one chain over another, thus prohibiting material strain effects [27]. On the other hand high-density polymers that have a linear oriented structure, will oppose a small resistance under (axial) loads. This is attributed to the unrestricted relative sliding (of one chain over another) resulting in higher elongation effects [27].

4.2.1.3 Material tensile strength

The structure of high density polymers is such that a greater intermolecular force of attraction is exerted between the chains when compared with low density polymers that have many branches. The higher the intermolecular force is, the higher the tensile strength of the polymer will be. On the same basis, low-density polymer that exhibit high-branching have a low tensile strength [27].

4.2.2 Molecular Structure of Polypropylene

Two types of polymers were investigated in this thesis. Amorphous polycarbonate and semi-crystalline polypropylene. In amorphous polymers the chains order is not well defined neither in the melt nor the solid state. In contrast semi-crystalline have a well defined crystal structure form. For the case of polypropylene upon polymerisation, the CH_3 groups can be incorporated in the macromolecule in spatially different ways. The final molecular structure of the resulting products alters the properties of the parts that can be classified as follows [50]: isotactic, syndiotactic and atactic. In the *isotactic* arrangement the CH_3 groups are positioned on the same side of the carbon chain. In Figure 4.1 the isostatic chain of isotactic polypropylene (PP) is shown.

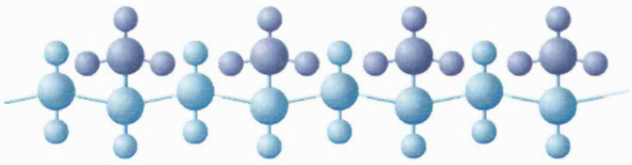

Figure 4.1: Isotactic Polypropylene, from [80]

In *syndiotactic*, the CH_3 groups are oriented alternately on each side of the polymer chain while in *atactic*, the CH_3 groups are distributed randomly at either side of the polymer chain. The chains have the tendency to crystallize efficiently in isotactic regions (in spherulite forms)

where molecules pack themselves very closely or stay amorphous in atactic regions [80]. On the other hand syndiotactic may crystallize under specific processing conditions and atactic can not crystallize at all (stay amorphous). Although the molecular orientation of the polymers is mainly random, it can be greatly influenced by flow gradients (shearing).

4.2.3 Molecular Orientation

The orientation during the moulding process is very important since it determines the alignment of the molecules with respect to the melt flow direction. High flow rates provide parts with a highly oriented structure in contrast with elevated melt temperatures that increase the molecular relaxation (this reduces the molecular orientation). The orientation is measured across the thickness of the moulded parts, where usually two maxima near the external surfaces and a minimum at the core are found [81]. The orientation of layers formed during injection moulding can be categorised into two forms [82]:

- orientation with complete random chain
- orientation with stretched (oriented) chain

There are no intermediate stages and the transition from one state to the other is rapid. As the elongation rate increases the chain conformation starts to change until the critical elongation rate is reached where the chain will switch to a fully stretched stage of the conformation. This critical elongation rate must be maintained for a certain period to allow the deformation to take place [50].

Manipulating the orientation can to a great extent determine the final properties of the moulded part. When the material is in the melt state, any applied force (parallel to flow) will start stretching the molecules and align them in the direction of flow (confined by the boundaries). Moreover during the injection moulding process the melt material is subjected to high flows and pressures, where shear stresses force the entangled molecular chains to untangle (up to a certain degree depending on the flow-pressure profile) and become more oriented [27]. During the filling phase both shear and extensional stresses are present where their variation and intensity determines the degree of orientation. The melt is forced to enter the cavity through a small gate where shear-heating takes place and turbulent flow randomizes the first molecular layer upon contact with the cold mould wall. Due to high temperature difference the molecules freeze rapidly without having time to orient themselves and the first 'skin layer' is formed. The higher the mould temperature the thinner the skin will be. Next the adjacent layer is formed upon contact with the skin layer where the molecules are stretched (with high shear stresses taking place) in the direction of flow giving a highly oriented layer. This phenomenon

is attributed to the poor thermal conductivity of the polymers [83]. As the process continues, the subsequent layers are formed towards the core of the part and as the melt flow is less and less sheared, the layers become less oriented. At the core of the part the molecules chains are insulated from the above layers and have the ability to relax and become randomised [27]. Therefore variation in the structure and crystallinity occurs through the section thickness. A cross section of an injection moulded part in Figure 4.2 shows these distinct areas.

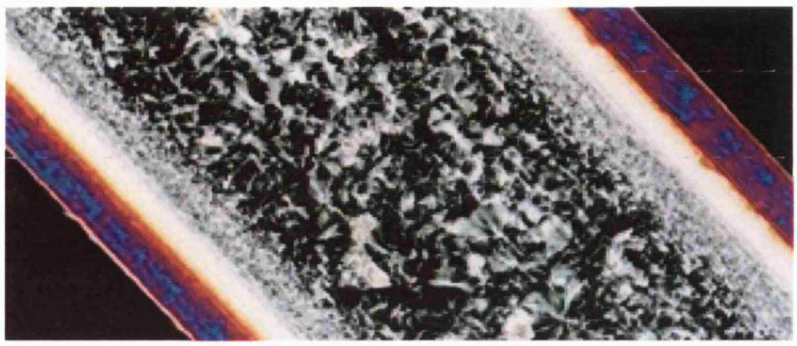

Figure 4.2: Cross section of injection moulded product, from [84]

4.2.4 Effect of Injection Speed & Mould Temperature on Morphology Distribution

Processing conditions during injection moulding have a decisive impact on the crystallinity and morphology distribution in semi-crystalline polymer layers. The effect of the injection speed and mould temperature influences the morphology of the layers and their orientation along the thickness and along the flow direction. In a recent experimental investigation by [85] the morphology of the layers was analysed by the use of Scanning Electron Microscopy (SEM) and Atomic Force Microscopy (AFM). It was reported that in the along the thickness direction of a semi-crystalline moulded polymer three distinct regions were identified (skin-core morphology):

- A thin oriented skin layer ($\approx 10\mu m$)
- A highly oriented non-spherulitic zone (darker region often mentioned as the shear layer)
- A spherulitic core with no preferred orientation

The author in the analysis of the micro-graphs denoted the thickness of the oriented region (skin layer & shear zone) as δ as seen in Figure 4.3.

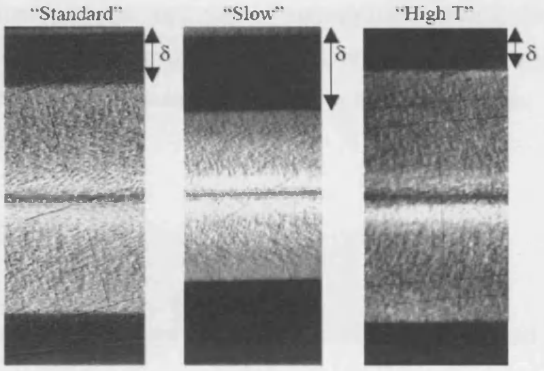

Figure 4.3: Micro-graphs in Optical Polarised Light, from [85]

In the experiment with slow injection speed $(5cm^3/s,\ 30°C)$ δ was found to have the largest thickness, compared to the standard speed $(15cm^3/s,\ 30°C)$. In the case where the mould temperature was increased $(15cm^3/s,\ 70°C)$ δ decreased. Both the SEM and AFM methods were in agreement with optical microscopy [85]. For the morphology orientation along flow direction it was reported that the flow thickness plane were investigated by [85] using optical microscopy. It was observed that the thickness of the shear layer increases when moving further from the gate (along the flow direction) reaching a maximum value at an intermediate section and decreasing again towards the end of the cavity [85]. Again at low injection speed there was a high molecular deformation with a developed highly oriented crystallite micro-structure on a thicker layer. On the other hand low injection speed can have disadvantages such as: premature solidification of the flow front prior to end of the packing phase and formation of secondary flows that result in surface defects.

4.3 Crystallinity of Polymers

Crystallinity is the ability of molecules to assemble into highly ordered structure which confer properties such as thermo-mechanical resistance, chemical resistance, as well as strength and toughness. If a crystalline polymer does not crystallize to the degree required, failure may occur. Processing conditions have to allow time for the crystallization to progress adequately. A nucleating agent may be needed to accelerate the rate of crystallization. If a pigment unintentionally acts as a nucleating agent, a high degree of undesired crystallinity may result and cause failure [86, 87].

In semicrystalline polymers the overall morphology is dictated in a large extent by the number, size, type and distribution of the crystallites been formed during the cooling phase [79]. The crystallinity is enhanced by prolonged packing while the higher the degree of crystallinity is

it increases the relaxation modulus and size of spherulites while it decreases impact strength and creep compliance above T_g. During cooling the crystallinity designates a sharp transition in the viscosity that occurs when crystallinity reaches a critical value.

4.3.1 Degree of Crystallinity

The degree of crystallinity determines the mechanical behaviour and fracture toughness of a polymer due to the crystallites acting as points of reinforcement and constraining the amorphous regions domains between crystallites [88]. In the case of PP which is a semicrystalline polymer a mix of crystalline and amorphous area forms. High crystallinity is associated with high rigidity, high strength properties, high temperature and chemical resistance. In addition, the properties are influenced by the size of the spherulites, which is affected by the nucleation and the cooling rate, and by the molecular weight. High molecular weight products are flexible and tough. On the other hand low molecular weight products are hard, stiff and brittle [80]. The transparency of the PP will be dependent on the spherulites size. Spherulites of a size smaller than the wavelength of light do not absorb the light, which improves transparency [80].

In semi-crystalline polymers where both amorphous and crystalline regions are formed the degree of crystallinity determines the specific volume. The structure is influenced by the pressure, thermal history, orientation of the polymer chains (their order depends on shear rate) and cooling rate [50]. Normally crystallization takes place during the cooling phase and can be enhanced by accurate control of the processing parameters. The most important are the cooling rate, strain rate in shear or elongation flow and pressure [89]. In the case of isostatic polypropylene (iPP) that requires a low cooling rate, crystallization can be initiated at low temperature. Rapid crystallization occurs at $125°C$ (where high crystallinity products can be obtained) in contrast with $150°C$ where crystallization might take up to 24 hours. This is one of the major reasons why iPP is extensively used in the industry [90].

4.3.2 Polymer Crystallization

There are two stages in polymer crystallization: *nucleation* and *growth.* Classical nucleation theory [91] describes that at any melt temperature during the process either in a stable ($T \geq T_m$) or metastable ($T \leq T_m$) state, thermal variations within the melt can create zones (nuclei) from which crystals can form.

Nucleation can be homogeneous *(isotropic crystals form)* and heterogeneous (anisotropic crystals form) [89]. Usually nucleation is heterogeneous where nuclei appear spontaneously due to the thermal variations in the liquid state. The amount of nuclei formed and the way they

are scattered during solidification affect the orientation and properties of the materials. Two critical temperature regions during crystallization are the glass transition temperature, T_g and the crystalline melting point, T_m. Below the T_g there is almost no molecular motion and the polymer has properties associated with organic glasses as well as hardness and stiffness. At T_m the crystals melt where a crystalline polymer resembles an amorphous polymer while above T_m no crystallization takes place. The maximum rate of crystallization occurs at a temperature of $\frac{1}{2}(T_m + T_g)$. Therefore the longer time the polymer stays between the T_m - T_g region the higher the degree of crystallization. For polypropylene and polycarbonate the crystallization parameters T_m and T_g are summarised in Table 4.1.

Crystallization Parameters	$T_g\,(°C)$	$T_m\,(°C)$	$\frac{1}{2}(T_m + T_g)$
Polypropylene, PP	5	150	77.5
Polycarbonate, PC	148	250	199

Table 4.1: Glass Transition Temperature and Crystalline Melting Point of PP and PC, from [92]

The commercial *iPP* polymer exhibits heterogeneous nucleation and is adequate described by a nucleation density which is temperature related. When the crystallization temperature drops or the cooling rate rises the nucleation density increases as well resulting in small size spherulites [85]. As the crystallinity reaches a critical value there is a sudden change in the viscosity. The high cooling rates at the skin layer do not have a quenching effect on the final part structure and most of the crystallization takes place during cooling or later on at mould temperature.

For the above reasons a good understanding of nucleation and growth in polymer processing is necessary in order to interpret accurately the relation between structure and properties. For example, if the number of formed nuclei is small the crystallite size increases considerably resulting usually in a brittle material. With reduced nucleation glass and amorphous regions are formed.

In the classical injection moulding process where a linear filling and packing profile is followed, the skin layer and subsequent layers close to the surface are highly oriented with a shish-kebab structure while at the centre a spherulitical structure is present due to the absence of shear [93].

4.3.2.1 Spherulites

Spherulites are formed when no strain is present. Normally the largest spherulites are found at the core (slow nucleation) of the part while they decrease in size as approaching the surface

(fast nucleation). This is attributed to the fact that spherulites near the skin layer have less time to grow due to the high cooling rates in the proximity of the mould wall [85]. As a result, the nucleation density increases considerably and the final spherulites stay small because of impingement. At that moment the crystal growth rate stops and secondary crystallization can follow. However large spherulites would grow near the skin layer if solidification occurs at high mould temperature [94]. At the region near the gate (where the melt temperature is higher), cooling takes place at a slower rate and spherulites have extra time to grow with low nucleation density before impingement occurs [85].

4.3.2.2 Shish-Kebab

A Shish-Kebab structure is formed under the presence of strain. In flow-induced crystallization the shear rate is the main influencing parameter. While the shearing takes place, thread-like nuclei (shish) are formed on which lamellae grows mostly in perpendicular direction (kebabs). Apart from the shish-kebab structure at the surface and a spherulitical at the center, a fine grained layer forms as an intermediate boundary [50]. Most likely this layer is composed of a thread-like structures perpendicular to the direction of flow.

4.3.2.3 Ways to Induce Nucleation

There are different ways to induce nucleation such as: flow, strain cooling and nucleation agents. The first developed nuclei form the basis for the crystallization process. The melt flow advances the crystallization which allows additional nucleation resulting in reduced spherulite size. High mould temperature favours large spherulites to form due to the extended relaxation of the molecules. The crystallization of the polymer during the process is affected by the thermo-mechanical history that the melt exhibits. The strain that the polymer liquid is subjected to accounts for the number and type of nuclei formed as well as for the final crystalline structure [93]. It has been suggested by [95], that in the event that the amount of strain during oscillating flow is equal (backward $\approx$ forward flow) then the number of nuclei could vary or minimise to zero.

A nucleation agent is a low molecular weight compound which is introduced into semi-crystalline polymers where acts as nucleating sites (substrate) for plastics molecules. This is the case of heterogeneous nucleation mentioned earlier where instantaneous growth of many crystallites takes place, increasing the crystallinity, modulus and tensile strength. The instantaneous growth of these crystallites contributes to the formation of many smaller size spherulites enhancing transparency, elongation and crystallization time.

4.3.3 Flow-induced Crystallization

The effect of flow-induced crystallization was first studied experimentally in the 1970s. It was found that a critical strain rate is necessary in order to initiate crystallization. During stretching, the distance between the cross-links is increased while the entropy of the polymer chain is reduced between the cross-links [89]. The material properties are effected as highly oriented structures are formed. Flow-induced crystallization can alter the final crystalline structure and mechanical properties of the semi-crystalline polymers within certain limits.

4.3.3.1 Effect of Cooling Rate & Pressure on Crystallization (no flow)

Effects of the cooling rate and pressure on iPP were investigated recently by [96] with the use of a custom-designed dilatometer . The cooling rates where varied from $0.1°\frac{C}{s}$ to $35°\frac{C}{s}$ and the pressure varied from 20MPa to 60MPa. Both the cooling rate and pressure were found to have a distinct effect on the crystallization temperature, T_m, and final specific volume (after cooling) of the melt.

Higher cooling rates shift T_m to lower temperatures and increases the specific volume. The transition due to crystallization is more gradual and widespread. Conversely high pressures shift T_m to higher temperatures and also increase the final specific volume after the pressure is released. In this study good homogeneity of samples was found up to cooling rates of $32.4°\frac{C}{s}$ and at pressure of $40 MPa$ [96].

4.3.3.2 Effect of Shear Rate on Crystallization

Further experimental findings of [96] have shown that the shear flow influences the crystallization kinetics. It was observed that a high shear rate applied to the under-cooled melt considerably reduced the transition to the semi-crystalline state. Consequently the crystallization occurred faster.

4.3.3.3 Effect of Pressure during Flow

In the same experimental research [96] the effect of pressure on crystallization was considered under flow conditions. A set of different pressure levels were applied, 20MPa, 40MPa and 60MPa. A fixed shear rate was applied to the under-cooled melt that was kept constant for all the tests. The crystallization temperature T_c marking the transition in specific volume was

elevated at higher temperatures (in all cases, with a maximum at $60MPa$). It was noted that the effect of pressure on flow increases the transition rate with respect to quiescent conditions by a factor of 1.4, 4.6 and 6 for the pressure levels of 20MPa, 40MPa and 60MPa, respectively. The effect of pressure on the specific volume of the solid state was insignificant which clearly shows that the degree of crystallinity is not affected (noticeably) [96].

4.4 Part Defects & Part Failure in Service Life

Quite often problems occur when producing parts of a desired quality where surface defects and geometry problems appear. The complex relationship between processing and in-mould parameters, makes it hard to detect the source of the problem and remedy it. Only modern control methods monitoring the melt polymer behaviour such as in-cavity pressure transducers, thermocouples, ultrasonic transducers and optical sensors can help to identify in-mould parameter changes that could initiate defects. Part defects can be classified in several categories such as:

- Surface defects (flow lines, jetting, poor gloss, surface ripples, gate blush-spay, etc.)
- Burning and Contamination problems (burn marks, degradation of melt, etc.)
- Physical problems (flash and short shots, sink marks, vacuum voids, etc.)
- Geometry problems (warpage, bowing, etc.)
- Structural defects (cracking, brittleness, etc.)

A review of the part defects and their relation to the process parameters is given in the following section.

4.4.1 Surface Defects

Various surface appearance problems of the parts can be attributed to high melt temperatures, shear heating of the melt and surface roughness of the mould. A good understanding of these factors is vital in order to adjust the processing conditions accordingly for each moulding case.

Surface irregularities occasionally appear in polymer blends with an elastomeric phase (ABS blends). In these cases the processing temperature can greatly affect the surface morphology of the parts up to a depth of 0.1mm. High melt temperatures form (stretches) the elastomeric

particles in ellipsoidal shape while low melt temperatures tend to deform the particles to result is a streaky morphology [97].

High injection rate (shear rate) can cause burn marks and cracks on the part surface while high shear stress particularly at the gates can increase the melt temperature and cause delamination [22]. As the burned material reaches the flow-front it can settle on the wall surface. It appears as *burn marks* and *flow lines* [20].

Jetting is another surface defect. It can be related to the injection rate as well as the viscosity of the material. To control the melt inertia and avoid jetting, the filling rate must be reduced as the polymer approaches the gate. The processing temperature is also important as low or high temperature increases or reduces the viscosity respectively [20].

The frozen skin thickness near the mould wall cavity is another parameter that effects to the formation of *sink marks*. Lower injection rate or lower mould temperature cause the melt near the wall to solidify faster (thick skin layer), reducing the molten core thickness (with spherulitic structure). This does not allow for an optimum packing to take place and sink marks form at the surface of the parts.

Flow Marks & Dull Surface can occur in parts moulded with polyethylenes. It was reported by [97] a case where the cavity used had one textured side with machined dots and lines, while the other side was polished. In the textured side a dull surface was formed near the gate while along the flow length, flow marks appeared with eventually no defects at the end of the part. Further investigation led to conclusions that the dull surfaces of the polymer were severely stretched and deformed parallel to the direction of flow. Less defects were found in the polished side as well as in parts moulded with low viscosity polyethylenes.

Some other surface defects are characterised by shiny and dull bands. These could be attributed to a flow instability that occurs near the free surface of the mould during the filling phase. These defects are usually perpendicular to the direction of flow and alternating on the upper and lower surfaces of the part. Often these are referred to as *flow marks*, or *ice lines* in polymers such as PP, PC and ABS. It has been proved in simulation by [98] that fountain flow front is subjected to viscoelastic instability (of an elastic nature) as seen in Figure 4.4. This instability can be delayed by increasing the degree of strain hardening of the specific fluid.

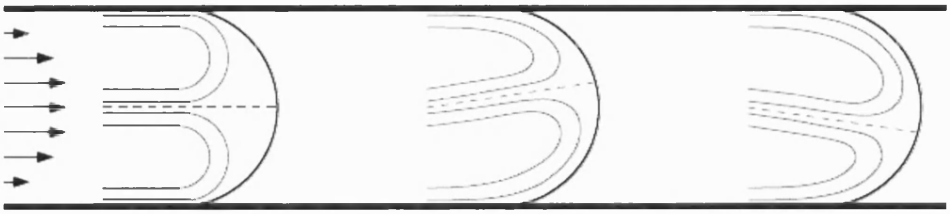

Figure 4.4: Polymer Flow Instability, from [98]

An example of flow instability applies for the case of polycarbonate where an injection speed higher than the recommended causes the shear and elongation stresses to reach excessive limits at the flow front and generate a failure in the superficial layer (layers of the substrate) of the polymer [97]. As a result defects start to form after the failure of the flow front envelope. Above the critical shear stress wall slip starts to occur on one side of the mould and the flow becomes unsteady with stick/slip flow introducing a vibration of the advancing flow front between the two walls of the cavity [97]. Alternatively low injection rates can cause premature solidification and formation of solid obstacles to the flow front. These can cause *micro flow marks* and defects at the part surface.

Grooved Surface Defects have been reported by [97] in parts moulded at low injection rates and/or low melt temperature. These defect were synchronous on both sides of the part. However the surface roughness was improved at higher filling rates.

From the results of the reported case studies, it is clear that increased mold temperature can improve the surface appearance of the part as it reduces the shear stress at the wall and secondary flows are decreased. In addition, possible defects that may form are allowed to relax for longer period reducing the residual stresses (assume uniform cooling).

4.4.2 Residual Stresses

Residual stresses are mechanical stresses present in the moulded part even without any external load. The level of these stresses is determined by the equilibrium positions of the atoms and the distortion of valence angles in the molecular chains as well as from changes in the distances between segments in the molecules [81]. Two types of residual stresses are present in the injection moulded parts: flow-induced and thermally-induced residual stresses. The flow-induced residual stresses are a result of shear & normal stresses during the injection of the polymer (fill - pack phase). Upon subsequent cooling some of these stresses are frozen in the part layers due to insufficient relaxation of the molecules. The thermally-induced residual stresses are

formed during the cooling phase due to asymmetric cooling in the thickness of the part. The layers closer to the surface and in direct contact with the mould wall solidify rapidly and are constrained from shrinkage. In addition, these layers restrain the subsequent layers towards the centre of the part from contracting, as solidification progresses. As a result the stresses are compressive near the surface layers and tensile at the core of the part. A typical case of residual stresses formed in an injection moulded part is presented in Figure 4.5.

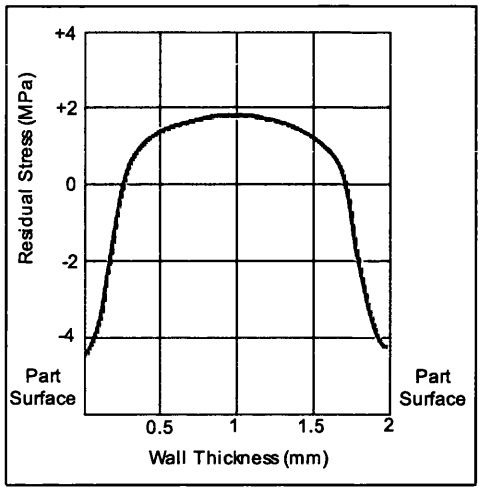

Figure 4.5: Residual Stress Distribution in a Typical Injection Moulded Part

In the cases where the cooling of the part is asymmetric the residual stresses are non-symmetric as well and may force the part to alter its shape by warping.

In an experimental study on residual stresses of thin-walled cavity it was reported by [99], that variations in the melt processing temperature and packing pressure have a small effect on the residual stresses. The packing pressure only influences residual stresses in the event that the cavity pressure will drop to zero prior to the complete glass transition. High mould temperature has the most significant effect and increases the tensile stress in the surface (skin layers) as the polymer is quenched at the mould temperature during the filling phase. In the rest of the part there were no obvious changes apart from the core region which was thicker. This advances stress relaxation and results in less residual stresses.

For the above reasons it is importance to control efficiently the mould temperature and the solidification process through T_g region, to allow the material to recover back to its equilibrium state when it is desirable (to have low residual stresses).

4.4.3 Part Shrinkage

A major factor that affects the shrinkage of the part is the type of material used. In crystalline polymer the phase transition in the crystalline regions of the material increases the shrinkage considerably, in contrast with amorphous polymers where shrinkage is less than 1%. There are two types of shrinkage; shrinkage related to pressure-temperature changes (for amorphous polymers) and crystallisation shrinkage (for crystalline polymers). Part shrinkage increases with increasing crystallinity as more crystals are formed (chains pack more efficiently) with volume changing. As mentioned in earlier sections (4.3.1) the specific volume of the polymer affects the degree of shrinkage. In amorphous polymers in contrast with semicrystalline, it is the pressure and temperature history that influences the specific volume rather than the degree of crystallinity. Therefore shrinkage is a more dominant factor in semicrystalline polymers and more attention is required. At higher crystallinity, shrinkage is higher and parts dimensions are smaller. The compressibility-temperature effects on shrinkage vary from polymer to polymer and a pvT diagram is necessary to identify volume changes during the injection cycle. The pvT diagram for polypropylene is shown in Figure 4.6.

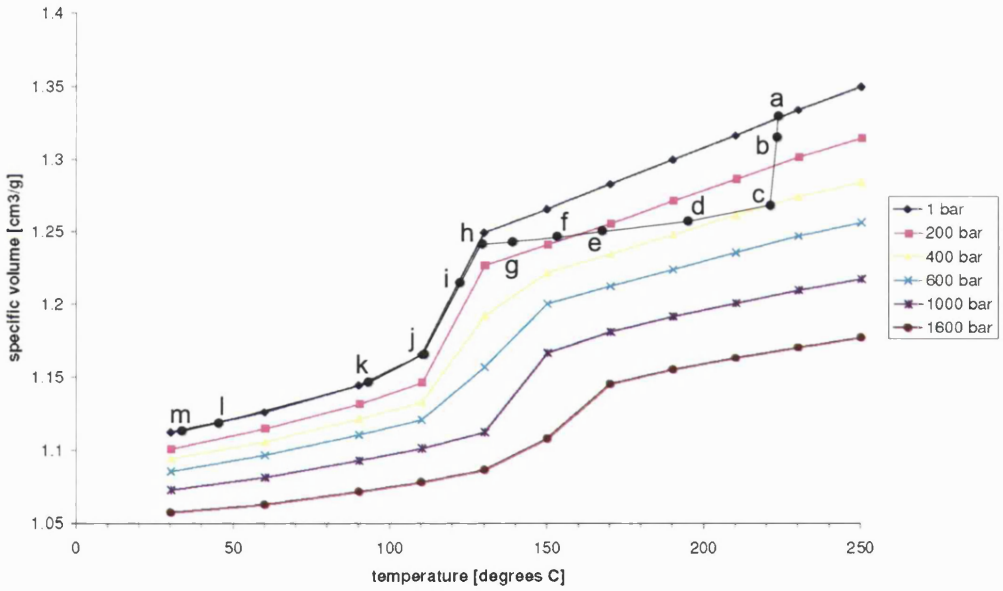

Figure 4.6: Pressure - Volume - Temperature Diagram of Polypropylene, from [14]

During the injection moulding cycle the following transitions can be identified on the pvT diagram (for isobaric cooling):

a. Beginning of the filling phase, the cavity gets gradually filled.

b. The cavity is 90% full, beginning of transition from filling to packing phase. The cavity pressure rises.

c. Beginning of the packing phase. The cavity pressure has reached its maximum level. The melt polymer is compressed.

d. The holding pressure it maintained constant for a small period of time.

e. The melt layers close to the cavity walls start to solidify and packing continues at the core of the part where the shearing reduces. The holding pressure pushes more polymer into the cavity as the existing volume contracts. An increase in the packing pressure at this stage would increase the onset temperature to crystallization as well.

f. The melt temperature drops below the crystalline melting point. Crystals start to form while the rate of crystallization depends on the cooling rate. Additional polymer is still injected as the core is packed further.

g. The cavity gate solidifies and no more material is injected. The cavity volume is constant.

h. The part continues to shrink and the cavity pressure drops further. Residual stresses start to form depending on the cavity pressure history and cooling rate throughout the part. There is a sharp decrease in the specific volume which corresponds to a sharp increase in the density of the polymer.

i. The cavity pressure drops to atmospheric level. The cooling phase continues.

j. The cooling continues at constant pressure.

k. Maximum rate of crystallization occurs at this temperature. The thermal conductivity of the polymer reaches its maximum value at this stage due to the degree of crystallization [100]. The solidification continues.

l. End of injection cycle, the part has solidified and is ejected from the mould cavity. Part warpage may occur if high residual stresses have formed.

m. Part reaches room temperature and crystallization has finished.

Generally shrinkage is more pronounced in parallel to the flow direction compared to that at right angles. This is attributed to the orientation of the molecular chains which are initially stretched and next relaxed during solidification. The importance of shrinkage could be seen in a case reported by [86]. Polypropylene caps where fracturing occurred when they were screwed on a tube as the dimensions were changed due to the pigment used to change the color. A rapidly cooled semicrystalline polymer in the mould might have a reduced crystallinity and continue to shrink long after it is removed from the mould. This illustrates the fact that a failure in the part might occur long after it is delivered to the customer. Process parameters

and mould design issues can have a major impact in the final dimensions of the part. Some of these are short-shots, flashing, gate size and final crystallinity of the polymer. If the degree of crystallinity and orientation of the part are efficiently controlled shrinkage can be reduced to eliminate warpage as well.

4.4.4 Short-Shot

The short-shot defect is a failure to fill the cavity, stemming either from inadequate amount of melt material prepared for the injection or from premature solidification of the flow front. This may occur at the gate or another flow channel where the cross section is critically small (due to poor design). For this reason the cavity is not properly filled and packed. To avoid short-shots the injection time should be increased up to the transition to the packing stage. If the short-shot is attributed to premature solidification either the injection speed or/and the melt temperature should be increased.

4.4.5 Flashing

Over-packing the mould cavity can lead to elastic deformation of the cavity. There is a strong link between the cavity pressure and the deflection of the cavity. Experimental results [23] have shown that the mould elastically deformed in all tests where sufficient internal pressure was present. In other words mould elasticity boosts the packing efficiency as energy is stored in the mould (wall) deformation and which is used subsequently to further pack the entrapped polymer (after the gate is frozen). However when the viscosity of polymer is low, part of the melt polymer may escape out of the mould during the deflection. In addition, over-packing leads to residual pressure at the end of the cycle. When the cavity opens, the part expands to its final dimensions which will be larger than that of cavity (negative shrinkage).

4.4.6 Gate Related Defects

Depending on the design of the gate and the injection rate, high shear rate through the gate can be developed and damages the polymer melt. This results in surface imperfection often as a splay mark near the gate (molecular stripping or gate blush). Polymer materials that are thermally sensitive need more attention as they can easily thermally degrade in this case. By profiling the filling rate this can be avoided [20].

Large gates create less pressure drop during the packing phase and greatly extend the time of

the compensating flow. This may result in flash either from low clamping force or deflection of the mould. For as long the internal pressure is present, the mould stays in the deflected shape [23] while varying the process parameters can have a small effect. At the end of packing the shrinkage (due to over-packing) is so small so that it only allows for partial relaxation of the deformed mould. This may result in a permanently deformed cavity or parts with high residual stress and non-uniform thickness. There is an additional time lag added in the solidification time of the gate.

On the other hand, *thin gates* provide a uniform packing pressure profiling (gates will freeze quicker and reduce the compensating flow) which can lead to low stress and uniform shrinkage parts [23]. Higher shrinkage will occur (because frozen skin is thinner with thin gates - molten core is greater) allowing for complete relaxation of the mould deformation. Fill rate has a stronger effect with small gates in the thickness of the part. A higher filling rate results in higher shrinkage with small gates. At low fill rates the frozen skin is thicker and results in heavier parts. This is mainly because frozen skin has a higher density than the melt. With viscous materials a direct sprue approach is preferable.

4.4.7 Warpage

Orientation of the part is one of the major parameters that cause the part to shrink by different percentage in the directions parallel and perpendicular direction to the flow direction. In the case of PP there is a high shrinkage parallel to the flow at low levels of orientation because the (shear) flow-induced crystallization is dominant. If orientation is higher, the shrinkage is higher perpendicular to the flow. Warpage usually appears due to variations in the shrinkage (non-uniform) throughout the part. In cases where shrinkage is uniform, the only downside effect will be smaller dimensions rather than warpage. The main effects of shrinkage that cause warpage can be categorised as follows [101]:

- orientation effects, due to the different shrinkage in parallel and perpendicular direction of flow (shrinkage within a region of the moulding)
- area shrinkage effects, which is the change in area that takes place due to parallel and perpendicular shrinkage (shrinkage between different regions of the moulding)
- differential cooling effects, in cases where there is uneven cooling on opposing mould faces. Once a flat part is removed from the cavity, cooling starts at a uniform temperature and the difference in contraction on each side of the part creates a bending moment that causes warping.

However sometimes parts may not warp because of the stiffness of the polymer but high internal stresses will be developed. This can occur from high packing pressure and low temperature moulding. If the part stiffness is reduced throughout the service life it is likely that the part will warp as the internal stresses are reduced. Two typical types of warpage are the dome & saddle shape as seen in Figure 4.7.

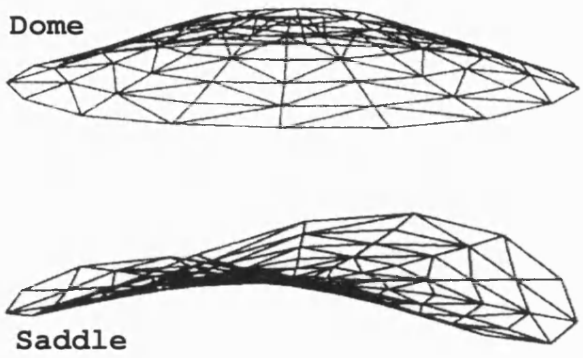

Figure 4.7: Dome & Saddle type of Warpage, from [101]

This usually appears in disk-shape parts, centre gated, that have a complicated way in which they shrink (more sensitive to shear stresses) compared with rectangular parts [102]. In the dome (or bowl shape) warpage, the shrinkage is higher in the transverse flow direction and less in the flow direction. This usually occurs with low shear stress conditions. In contrast with the dome case, in saddle warpage the shrinkage is higher in the flow direction [102]. To test products for warpage they can be submerged into boiling water for ten to fifteen minutes. If the dimensions remain the same there is little chance that they will warp afterwards. If the gate was located at the edge of the disk, the flow orientation would be completely different (a stream flow develops round the part perimeter) and the part would develop a dome warpage.

4.4.8 Part Failure in Service

4.4.8.1 Presence of Oxygen or Water

The presence of oxygen or water in very small concentrations during moulding can degrade the mechanical properties of polymers. For polycarbonate, water as low as 0.01% can cause hydrolysis and lower the molecular weight of the polymer. For polypropylene, the presence of oxygen in conditions of high temperature and melt shear can degrade the polymer during processing [86].

4.4.8.2 Variation of Molecular Weight during Processing

Molecular weight is an important property of polymers of a long chain nature. Mechanical properties of polymers such as strength, toughness and chemical resistance depend on the chain length and chain entanglement that take place during polymerization. The molecular weight is the product of monomer units in a chain and the molecular weight of each unit. It determines the processability of the polymer during the process. Small variations in the molecular weight can result in viscosity changes, affecting the flow orientation. In such conditions secondary flows form which could lead to surface defects. As the molecular weight deteriorates, the polymer mechanical properties start to degrade as well.

For failure to occur, a relatively high energy must be applied to the part to disrupt the entanglement of the molecules. For this reason the so called equivalent performance of short term properties cannot be guaranteed to predict the long term behaviour. If the material used is known to degrade in processing, then a grade with a higher molecular weight should be chosen to ensure that mechanical properties of the produced part will meet the specification throughout its service life expectancy. Two reported cases by [87] are presented to illustrate how some materials can degrade under non-optimised processing conditions.

- **PP case:** polypropylene caps used in a packaging application were designed to be constantly under a flexural load. However a wrong design in the caps had the gate placed at the top of the cap where the in-service stresses were greatest. In addition, inadequate antioxidant and the quantity of regrind used were the dominant factors of lowering the molecular weight below the acceptable limits. As a result fracture occurred with some of the cups due to the high flexural load and deformation.
- **PC case:** polycarbonate parts were secured to metal with screws at the corners. There was a direct contact of the metal screws with the part as well as being exposed to outdoors and to detergent washing. Finally fracture occurred in the polycarbonate plate as there was no rubber to moderate the stress from the tightened screws. It was also found that the moulded parts had a lower molecular weight from the initial pellets used. Although the variation in the molecular weight was very small it proved to be enough to cause fracture.

It is known that for relatively low molecular weight condensation polymers (nylon, PET, PC, PUR, etc...), a small reduction of the order of 5% for injection moulded parts can lead to a 50% part failure while 10% in molecular weight reduction in 100% failure [86]. Thus the resistance to fracture can be estimated by comparing the molecular weight of initial pellets with the lower molecular weight of the end product.

4.4.8.3 Post-Process Variations in Crystallinity

If an injection moulded part is not fully crystallised during injection it is likely that the part could continue to crystallize under specific service conditions. Two such cases are presented, reported by [86].

- **PBT case:** A glass-filled PBT part was moulded with a hole at the centre for a metal object to move through freely. As the part was tested at elevated temperature inside an oven, it continued to shrink. The tolerance between the part and the metal object reduced which wouldn't have happened if the part was fully crystallised during the moulding process. To avoid this incident a nucleating agent could have been used to fully crystallize the polymer during moulding.
- **Styrene Acrylonitrile:** In another case a piano key with a hook at the end was moulded with styrene polymer. After the part was moulded, heat reversion was used above the T_g. Due to the high level of shrinkage high levels of internal stresses developed at the hook which had shrink 50% more than normally. Solvent that was used to remove stains from the piano condensed on the hooks, causing environmental stress cracking of the hook. Consequently fracture occurred when the spring was attached on the hook.

Both reported cases demonstrate the fact that reduced crystallinity or unintentional intermolecular order can degrade the mechanical properties of the moulded parts to fail in their service life. Precise control of the process conditions during injection could aid the control of in-mould parameters such as molecular orientation, crystallization, shrinkage and warpage. The review of some advanced process control methods follows.

4.5 Injection Moulding of Enhanced Quality Parts Via Vibration Profiles

Modern hydraulic injection moulding machines rely on screw position, to control the process parameters and follow only approximately a pre-defined velocity and pressure profiles. Control of the process parameters during the injection cycle is important to ensure that parts are moulded under tight tolerances to meet service-life expectancy. During the moulding cycle, process conditions such as flow, pressure and temperature affect the viscosity of the polymer and degree of crystallinity; amount of crystalline and amorphous structures. The percentage of each type of structure present in the final product influences the physical and mechanical properties of parts. On the other hand, lowering the polymer's viscosity to fill and pack the

cavity during moulding is not always an easy task. Often excessive shear heating at the gate due to elevated processing temperature, can thermally degrade the polymer and cause surface defects. Processing methods by melt vibration which suggest that ease the processability of the polymer and improve the mechanical properties of the moulded parts are reviewed in the following sections.

4.5.1 Vibration of Polymers

An alternative method to lower the polymer's viscosity is to mechanically vibrate the melt polymer during moulding. The vibration of the melt during the process has been found [78] to lower the viscosity of the polymer, ease the processability (reduce the pressure drop at the gate), enhance the orientation of the molecules and reduce the amount of secondary flows. During the melt vibration the parameters pressure, temperature and cooling rate affect the shear-thinning behaviour of the melt. Some of the investigated [78] benefits of the vibration are: higher filling rates with prolonged duration and produced parts with lower shrinkage. These outcomes were attributed to the shear-heating effect that takes place near the gate allowing the solidification to proceed under continuous pulsating pressure. In general vibration is a dependent function of polymer viscosity where at low frequencies can affect the kinetics of nucleation and growth during the crystallization of the polymer. This eliminates the need of plasticizer (change T_g region) or nucleating agents that raise the cost of production.

Researchers in the past managed to reduce the melt viscosity of the polymer (by 50%) by vibrating the nozzle area at constant frequency. In the early 1980's a custom-built injection moulding device called *Rheomoulding*, moulded parts under vibrational conditions [79] which had improved mechanical properties such as flexural strength (35% increase) and ultimate strain (50% increase).

Other experimental results [103] have shown that vibration of the injection moulding screw at low frequency during the filling and packing phases, enhances the mechanical properties of the material, which can be improved up to 30%. In a similar study, again by using the injection screw (with open-loop control), melt vibration was applied. The frequency of vibration was set at 3Hz for the duration of 5 seconds. Vibration started 0.5 seconds after the start of injection. The parts produced had a 13.5% increase in ultimate tensile strength. However it was reported by [27] that extending the melt vibration to 10 seconds resulted in the formation of sink marks. It was suggested that the vibration should be stopped at some time in order to allow for a normal packing procedure.

Another approach, called *Scorim*, makes use of two additional live-feed injection pistons in front of the nozzle, that fill the cavity from two opposite directions. The moulding process

is separated in two-stages [78]. In this way a shear-controlled orientation is achieved at low temperatures. A considerable increase in the Young Modulus (80%) and tensile strength (60%) has been achieved, when compared with convectional moulding.

In another work reported by [104], a quadruple livefeed *Scorim* injection moulding machine was used to allow direction of the shear flows to be sequentially rotated by 90°, in order to produce a laminated structure with molecular orientation in the solid part that mirrors these flows. With the use of four gates injecting from different directions the tensile strength in the longitudinal and transverse direction were identical (normally in conventional moulding UTS is high only in the direction of flow). A high level of control in the microstructure and physical properties were achieved with this scheme.

Another modification of the injection moulding machine [105] called *Rheojector*, operates on the same principle as Scorim where researchers have shown that a considerable decrease in viscosity was achieved by the shear vibration of the polymer melt at low frequencies. In the case of semi-crystalline polymers such as polypropylene, it was found (experimentally) that melt vibration increases the Young Modulus and tensile strength of the polymer. Improves the crystallinity [105] up to 63%, which indicates that smaller and finer crystals are formed (especially at high processing temperatures). In other cases polypropylene polymer was softened to an extend that would not brake increasing the impact strength.

Vibration has also been used in polymer extrusion where different zones have been vibrated synchronously to increase the elasticity of the melt and the normal stresses, lowering the viscosity and increase both throughput and orientation. Others [27] have observed that applying vibrational forces to the melt plastic improves mechanical, thermal, optical and aesthetic properties of the parts. Manipulating the polymer rheology either by *shear* or *pressure* oscillations can have a significant influence on the viscosity during the cycle and on the final product morphology and structure.

The efficiency of pure hydrostatic (pressure) vibration to enhance the viscoelastic effects, either in a state of optimum orientation or optimum relaxation is much reduced compared with shear vibration and the best is often to combine pressure profiles with vibration patterns [78]. In addition, it must be taken into consideration that a certain amount of the vibrational force transmitted to the melt polymer (assuming the amplitude is constant) varies with the frequency. Part of the energy transmitted to the mould is dissipated to the rest of the components. Therefore the higher the vibrational frequency is (assuming constant amplitude) the more difficult it would be to transmit the vibrational energy to the polymer melt.

4.5.2 Shear Vibration Effects on Polymer Viscosity and Orientation

The effect of vibration in the polymer melt is determined to a great extent by the size of the gate plus the location at the cavity (side, top, at an angle, etc). At high oscillating frequencies the viscosity tends to reduce considerably and become less dependent on temperature [78]. The material viscosity during the moulding cycle can be reduced to improve the processability and then increased suddenly during cooling to achieve rapid solidification; fast quenching. In addition, the shear thinning of the melt can be achieved at a given temperature (above the T_g) by either increasing the shear rate or oscillation of the melt [78]. Therefore the mechanical properties of a polymer could be modified during the process by changing the frequency and amplitude of vibration. For example the viscosity of PMMA at $239°C$ was decreased from 130,000 Poises down to 20,000 Poises after oscillating the polymer melt at 16Hz. Further increase in the frequency from 16-80Hz did not have a significant effect [78]. This means that the melt vibration can be applied at low frequencies to lower the viscosity (by shear-thinning) of the melt to reduce the pressure drop at the gate and power consumption during fill-pack stage. For the case of a PET polymer processed at $275°C$ viscosity was reduced from 11,500 Poise down to 4,200 Poise at 16Hz. Further increase in the frequency up to 80Hz did indeed further reduce the viscosity down to 2,000 Poise.

Another example presented by [78] considered the vibration effect in the viscosity of polycarbonate (PC) when varying the melt temperature. At $200°C$ the viscosity of the PC decreases almost 10 times when the frequency of oscillation is increased from 0.16Hz to 80Hz. This rapid change in the viscosity of the melt can be applied at the time of cooling to quench the part fast and avoid crystallization of other phases. In addition, the viscosity has no temperature dependence at high oscillating frequencies [78]. This means that differences in the viscosity generated by local pressure and temperature gradients in the mould can be cancelled by maintaining a high frequency of oscillation during the filling-packing of the cavity.

4.5.3 Pressure Vibration Effects on Polymer Viscosity and Orientation

Pressure vibration has a different effect from shear vibration. In the static mode shear forces have the tendency to decrease the potential energy barrier of interaction of diffusion while hydrostatic pressure increases it [78]. In other words, shear vibration reduces the viscosity of the melt while pressure vibration has the opposite effect. Moreover the increase of the viscosity with pressure can be attributed to the decrease of free volume during the packing stage.

In general the viscosity strain-rate relationship is dependent on the relative melt temperature with respect to the glass transition temperature. Under the effect of pressure it could be assumed [78] that the same effect is valid for the relationship between the viscosity and frequency

of vibration. This means that when the melt polymer is under high pressure, shear-thinning occurs at lower frequency with constant temperature or with higher temperature and constant frequency [78]. Therefore hydrostatic pressure can shift the $T_g(P)$ to a higher temperature which in combination with vibration patterns, could alter the melt viscosity without the need of additives or the use of a different viscosity grade polymer. This applies to both amorphous and semi-crystalline polymers [78].

4.5.4 Viscoelastic Cooling Treatments Via Vibration

Application of vibration especially in amorphous polymers can greatly influence the glass transition temperature, T_g, region which occurs through a very sharp transition from the rubbery to the glassy state. For semicrystalline polymers vibration can also have an effect as it enhances orientation of the crystalline area and shifts the T_g to influence solidification of the amorphous region. To characterise the viscoelastic state of the polymer, two parameters must be specified: the melt temperature and the frequency of vibration (constant amplitude). In this way the T_g becomes a function of two parameters, $(T - T_g)$, and not only of temperature [79]. To initiate solidification of the melt, shifting of the $(T - T_g)$ parameter can be imposed either by cooling the mould at constant frequency (change T and keep T_g constant) or by increasing the vibration frequency at constant amplitude and temperature (change T_g and keep T constant) [79].

Different combinations of pressure vibrations and cooling rate profiles can be used during packing and cooling to induce solidification of the melt polymer. The most often used in industry are by isobaric or isothermal conditions however some more efficient combination could be used.

- In isobaric crystallization the pressure vibration is held constant while the temperature is reduced. This method is preferable in situations where low residual stresses are required in the final part [79]. Depending on the time given for relaxation, formation of residual stresses may vary.
- In isothermal crystallization the temperature of the mould is maintained constant while the pressure vibration is increased. The increase in pressure vibration, shifts the glass transition region at a higher temperature where there is a rapid transition (from rubbery to glassy state) and the cycle time can be reduced [79]. Orientation of the part is increased.
- A more efficient and faster way to reach the glassy state can be achieved by increasing the cooling rate while concurrently increase the pressure vibration [79]. In this way the melt temperature is decreased further before reaching the new transition region set by the shifted T_g at a higher temperature. These conditions favour orientation in the final

part where high internal stresses may be desirable to influence the shape and function of the moulded part [79].

- In contrast with the previous case both melt temperature and pressure vibration can be reduced at the same time. This is required when the final part is produced at high injection rates (to increase productivity) but prone to have high residual stresses which are not desirable. With this approach the T_g region is shifted to a lower temperature which allows more time for the relaxation process before the transition occurs [79]. The final orientation will vary depending on the cooling rate selected. Low cooling rate would reduce the orientation and residual stresses, but with a time penalty in production.

In general all cases mentioned above could be equally applied for the solidification of semicrystalline and amorphous polymers. The reviewed methods if successfully applied could advance solidification rates, reduce cycle times and enhance the molecular orientation of the moulded parts.

4.6 Concluding Remarks

A review of the factors affecting the injection moulding process assists in identifying critical parameters that influence part quality and production rate.

Depending on the processing conditions during moulding, orientation can be regarded as alignment of molecules in the flow direction under high shear stresses, followed by relaxation of this orientation. These parameters must be carefully controlled to predict the final material properties of the part. Along the thickness direction of moulded crystalline polymers, the following layers can be identified: a thin-oriented skin layer, a highly oriented sheared zone (non-spherulitic) and a spherulitic core with no preferred orientation. With conventional moulding, controlling the orientation of the molecules and especially at the core layers is not feasible, and surface defects, residual stresses and warpage are common problems that mould designers have to deal with.

Crystallinity is another important parameter of semi-crystalline parts. Crystallinity is the ability of the molecules to assemble into highly ordered arrays. Application of prolonged pressure during the packing phase increases the crystallinity which improves the chemical resistance, strength and toughness of the moulded parts. High degree of crystallinity enables the part to fully shrink during injection while it reduces the impact strength. Often nucleating agents are used to accelerate the crystallization process during the injection cycle. If a polymer does not crystallize in process, failure may occur in service-life.

Flow-induced crystallization can be used to modify the final crystalline structure and therefore the mechanical properties of semi-crystalline polymers. Melt flow advances crystallization where an instantaneous growth of many crystallites takes place which contributes to the formation of shish-kebab structures. In the presence of flow heterogeneous nucleation takes place which increases crystallinity, modulus and tensile strength. High pressures can shift the crystallization temperature, T_m, higher for nucleation and growth to occur faster.

Melt vibration is a method that influences the core orientation as shear takes place under pulsating flow. When vibration is applied during the filling phase, it can reduce differences in viscosity, generated by local pressure and temperature gradients in the cavity. Melt vibration can be applied at low frequencies (up to 20Hz) to lower the viscosity, improve the processability and reduce the hydraulic pressure drop. At high oscillating frequencies the viscosity has no dependence on temperature. Vibration has been applied with modified injection moulding machines (*Scorim*), where additional pistons are used to oscillate the polymer. A considerable increase in the Young Modulus (80%) and tensile strength (60%) has been achieved. Conventional moulding machines have also been used to apply melt vibration. An open-loop control system forces the screw to vibrate at low frequencies. Improvements in the mechanical properties of the parts up to 30% have been reported.

The combination of vibration and cooling can be applied to advance the solidification procedure, and therefore reduce the cycle time. The profile trajectories for each polymer should be designed according to pvT diagrams, in order to follow closely the required cooling rates. Melt vibration can be used to achieve fast quenching of the part when this is desirable without the limitations of the heat transfer solutions. However this approach must be imposed with care to avoid excessive shear heating and degradation (fatigue) effects.

Some of the reviewed strategies could be implemented to investigate further the effect of vibration on molecular orientation and crystallization during moulding. To set advance profiles (P-Q trajectories) for the screw to follow, a considerable modification in the hydraulic system of the current injection moulding machine would be required. Once completed it would be possible to implement modern control strategies in real time and investigate the effect of different vibrational profiles on part shrinkage, warpage and surface appearance. More details on the hydraulic circuit modification are given in Chapter 5.

Chapter 5

Enhancement of Hydraulic System and Controller Evaluation

5.1 Introduction

Recent advancements in injection moulding control have demonstrated that there is a great potential in enhancing the mechanical properties of moulded parts by implementing time varying flow and pressure (screw) profiles. However this was not possible under the original hydraulic circuit configuration as most of the processing parameters were preset and fixed throughout the cycle. In order to explore the effects of time varying profiles on the mechanical properties, surface appearance of the parts, hydraulic and cycle time efficiency, a new design to modify the original hydraulic circuit is proposed and assessed. A flow-pressure (P-Q) servo-proportional valve (supplied by Moog with integrated electronics) was used to replace the directional control valve which was mounted on the main manifold of the hydraulic circuit. This modification was aimed at simplifying the hydraulic circuit, reducing the pressure drop in the hydraulic flow lines and improving the dynamics of the injection unit (screw). It is described in detail in section 5.2. Therefore the side manifold (Figure 2.1) that originally regulated the flow and pressure characteristics during injection would not be required. In order to control the Moog valve effectively a PC based data acquisition system was build to enable real time control of the moulding machine via Matlab Simulink environment. Since operations such as the opening-closing of the mould, advance-retract of the injection unit and advance of the screw would be controlled independently by the user, safety interlocks need to be put in place to avoid any accidents. Such an incident could happen if the injection would start before a firm contact between the injection nozzle and mould sprue was granted (due to PC operator fault). As a result melt polymer could escape in the other compartments of the moulding machine creating a hazard. For the above reasons a separate unit with a programmable micro-controller was

used as the interface between the hardware controller of the moulding machine and the PC data acquisition system, as presented in section 5.3.1. All digital and analogue signals sent from the PC to drive different units of the moulding machine would pass through the micro-controller for a set of routine checks. If these are valid a relay would allow the control signal to drive the servo proportional valve. A threshold was put in place to avoid noise in the control (D/A) signals triggering the valve. This modification could be applied to any conventional or modern generation injection moulding machine to enhance its performance.

To implement the ultrasound monitoring method proposed in Chapter 3 for the solidification of the part during the process a second unit with a micro-controller was designed to process the ultrasound wave speed variation through the mould sections during injection. This is presented in section 5.3.2 including experimental validation.

For the control of the filling and packing phase a different approach from that traditionally used is also proposed here where vibration of the melt is used to lower the viscosity of the polymer. The advantages of this method are several as the orientation of the molecules can be enhanced to change the final structure of the part. A combination of shear and pressure vibration profiles can change the crystallization profile of the semi-crystalline polymers and influence the transition from rubbery to glassy state in amorphous polymers. At the same time the cooling profile of the part can be controlled by altering the frequency of vibration. Improvements in the mechanical properties of the parts have been reported as well by a few researchers [27, 78, 79].

A literature review of modern control methods (Robust Control, Neural Network, Fuzzy Logic, Learning Control and Adaptive Control) follows in section 5.6. The adaptive control Minimal Control Synthesis (MCS) algorithm was found to be the most suitable when plant uncertainties and unknown disturbances arise.

5.2 Modification of the Hydraulic Circuit

In order to replace the directional control valve the flow demand during injection should be derived to find the rated flow requirement for the new valve. According to the maximum injection speed during filling, the flow demand for the two actuators was estimated to be $51L/min$.

$$Q_{Fill} = 2 \times A_{an} \times u_{srew} = 51.1L/min \tag{5.1}$$

The closest P-Q valve size that could be supplied by Moog had a rated flow of $55L/min$ which

was within the required specification. The rated pressure drop at each spool land was 5bar. As the normal operating conditions (filling speed) for the tests were at 0.01m/s to 0.02m/s, the new valve would be operated at the lower region of its range (10-20% of control signal) where it has a faster response.

Another requirement for the new valve was to have an open centre spool to allow flow (when in centre) from port A to B during the plasticization. In this phase the screw rotates at a certain speed and the melt polymer is accumulated at the front part of the barrel. The screw should be allowed to move backward with the minimum pressure drop to the hydraulic system. Unfortunately the new valve did not have this feature and an additional cartridge valve was mounted on an extension manifold to provide the link between ports A and B during plasticization. A schematic illustration of the new modification is shown in Figure 5.1.

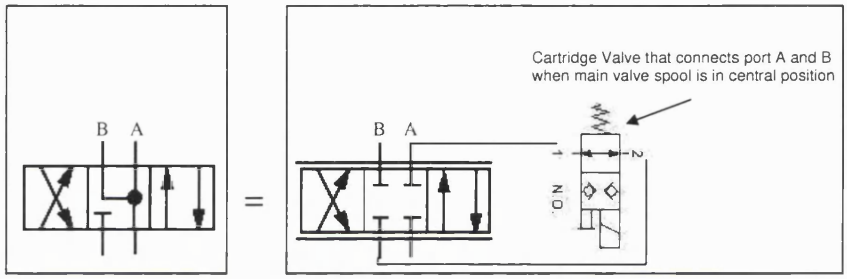

Figure 5.1: New Connection Arrangement of Moog Servo Proportional Valve with Cartridge Valve

The new cartridge valve is programmed to open only during plasticization to minimise cross port leakage. The extension manifold was added to accommodate properly the new valve and mate the hydraulic connections with the main manifold. The new arrangement with the Moog servo-proportional valve is shown in Figure 5.2. As required by the specification of the servo-proportional valve an oil filter of $10\mu m$ was installed in the pressure line before the valve to prevent contamination problems.

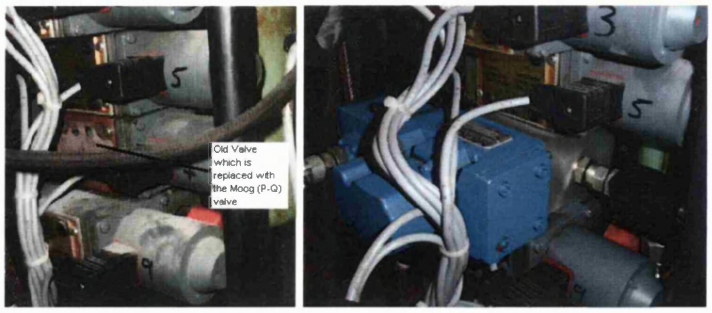

Figure 5.2: Moog Servo Proportional Valve

In order for the moulding machine to operate as a stand alone unit when not controlled by the PC, the new valve should be triggered to function from the signals driving the old valve solenoids (S6 & S7). An external potentiometer was mounted on the control panel of the moulding machine to preset the opening of the valve and control the flowrate when the machine is operated in manual or auto mode. Some further information about the electrical connections of the new valve is shown in Table 5.1.

Function	Voltage Command	Current Command
Supply	$\pm 15V\ VDC\ \pm 3\%$	
Input rated command valve flow	0 to $\pm 10V$ Input Resistance $100k\Omega$	0 to $\pm 10mA$ Load Resistance 400Ω

Table 5.1: Servo-proportional Valve Connection Specifications

5.3 Electrical Hardware

The electrical hardware that was used to drive the new valve was a PC based data acquisition board, connected in series with a separate micro-controller unit. For the monitoring of the rheological behaviour of the melt a 2nd micro-controller unit was used to process the ultrasound data during injection.

5.3.1 Data Acquisition Board

For the control of the injection molding machine a data acquisition card (DAC) was used (PCI-DAS1200 from Measurement Computing) with 16 A/D channels (for inputs from the temperature and pressure sensors), 2 D/A channels (for control of the new valve and one spare) and 24 digital I/O channels (for control of the main machine operations such as mould open-close, injection unit advance-retract, and screw rotation). The board was set to communicate with Matlab Simulink environment through Real Time Windows Target Toolbox. To control the operations of the moulding machine all the switches in the control cabinet (of the moulding machine) were wired up with the micro-controller and the digital output channels of the DAC. These switches are used in manual-mode to control the machine operations. When the moulding machine is in the manual mode a Simulink model is used to set all the cycle timings. The digital and analogue outputs from the DAC control the main operations of the machine and drive the Moog valve. During the injection cycle a watchdog in the Simulink programme sends a pulse to the micro-controller to verify that the Simulink real time model is running properly. In case of a computer crash as soon as the micro-controller detects that the watchdog is not active, all the operations are stopped (all the signals to the moulding machine are set low). A

block diagram with all the electrical wiring connections is presented in Figure 5.3.

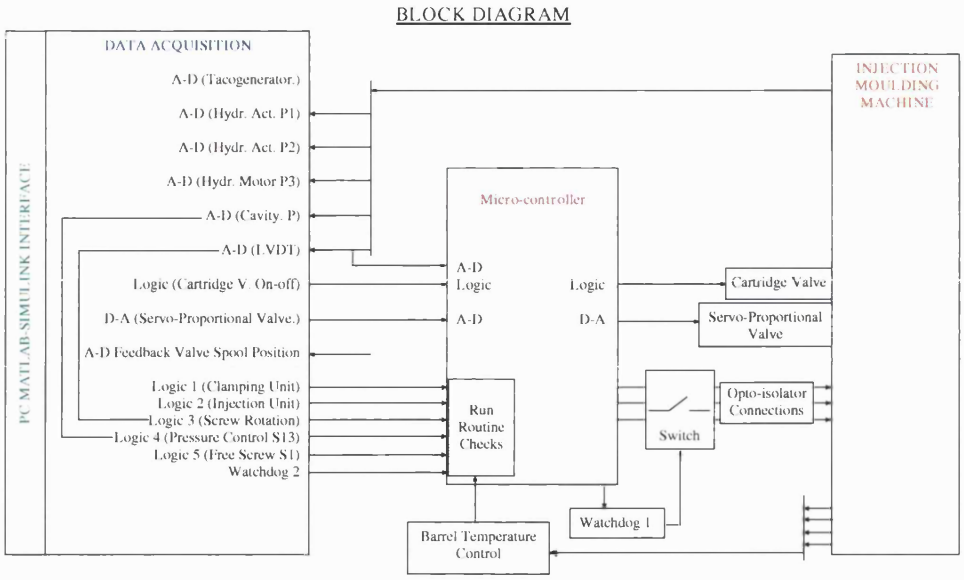

Figure 5.3: Wiring Connection Diagram of PC, Micro-controller and Injection Moulding Machine

5.3.2 Ultrasound Box

The ultrasound data acquisition box is a micro-controller based unit that was designed to detect the transmitted ultrasound wave through the mould and provide an accurate control feedback signal for fast process setup. As the wave speed variation is of the scale of micro seconds it would be very costly to have a PC based data acquisition system to detect and analyse the signal in real time. Therefore the time of only the first and last ultrasound transmissions through the cavity are captured and fed back to the Simulink model to:

- Initiate the transition to the packing phase (first transmission)
- Mark the end of part solidification and open the mould to eject the part (last transmission)

The advantage of this non-invasive method is that the equipment is portable and the ultrasound transducer can be attached at the external mould surface to detect the phase changes. Therefore the setting of the injection process parameters can be optimised very fast without the need of trial and error cycles to find the optimum transition and minimum solidification time.

5.3.2.1 Design Specification

The program embedded in the micro-controller detects if a valid transmitted ultrasound signal is present. The ultrasound signal consists of a reflected and a transmitted element which occurs at around 17 microseconds after the falling edge of the trigger. The circuit detects the falling trigger signal, introduces a delay, then reads in the ultrasound signal and generates a voltage reference signal. The significance of the delay is that the reflected part of the ultrasound signal is ignored. The ultrasound signal amplitude is then compared to that of the voltage reference and if the ultrasound signal amplitude is greater then the signal flag is set to signify that a valid signal is present.

5.3.2.2 Experimental Results

To test the design and functionality of the ultrasound data acquisition box a set of experiments were carried out. Initially a trial injection cycle was required to set up the micro-controller and adjust the signal's detection threshold. Once the unit was set-up the trigger from the Ultra-box was connected as a feedback signal to the Simulink model to initiate the transition to packing and mark the end of solidification during cooling. The ultrasound and Ultra-Box signals were monitored during the injection via a digital oscilloscope as presented in Figure 5.4. Starting from the top of the screen the signals are:

- Reflected ultrasound signal
- Transmitted ultrasound signal
- Voltage reference signal (VRS) from micro-controller
- Feedback signal acting as the trigger

The timescale of the display was set a 20 microseconds ($2\mu s/div$). At the beginning of the injection cycle (1s) the mould is open and the transmitted signal is reflected back, as seen in the left window of Figure 5.4.

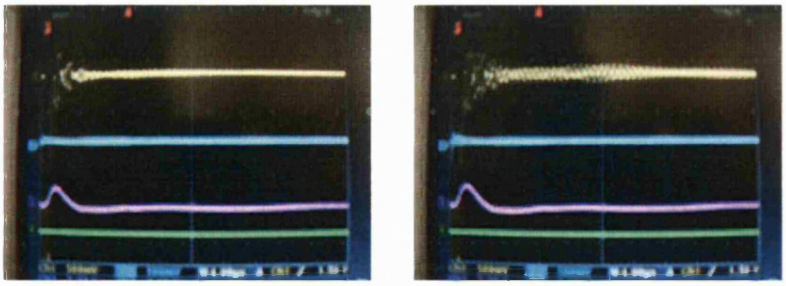

Cycle starts at 1s *Mould Close at 2s*

Figure 5.4: Ultrasound Signal at the Beginning of the Injection Cycle

Once the mould is closed (2s) the number of interfaces (that change the ultrasound coupling) in the mould increases and the amplitude of the reflected signal (top) changes as well as there are more reflections from the interfaces. As the cavity is partially filled there is no transmitted signal through because no coupling is created yet between the cavity walls.

After the closing of the mould the filling phase starts and after an interval of 4 seconds the cavity is almost full and a strong ultrasound coupling is created between the cavity walls by the melt polymer, left window of Figure 5.5. This enables the first transmitted signal to appear (at 6s) while after a programmed delay of half a second the trigger signal goes high (at 6.5s) and the screw motion control switches from flow to pressure. As the melt polymer comes in contact with the cold mould wall, continuous alternating interfaces of liquid to solid layers form, that gradually reduce the attenuation of the signal and increase the wave speed through the part.

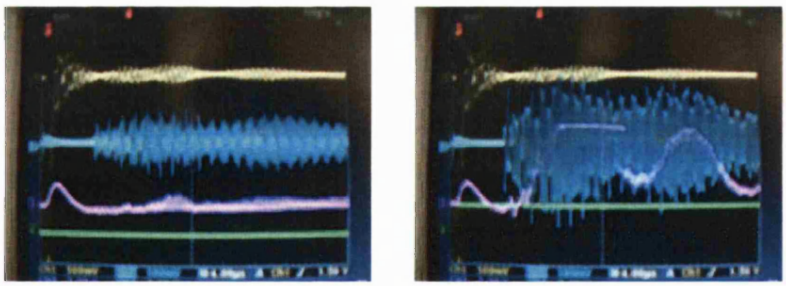

Filling at 6s *Packing at 6.5s*

Figure 5.5: Ultrasound Signal during the transition from Filling to the Packing Phase

During the packing phase the cavity pressure increases abruptly and the amplitude (at 7s) of the transmitted signal increases as well as shown in Figure 5.6 (left window). The increase in the amplitude of the signal is because cross sections of the part solidify during packing, therefore the signal is attenuated less as it propagates faster through the solid polymer interfaces. As the

packing phase progresses shearing of the melt continues (affecting molecular orientation) at the core of the part where a percentage of the polymer is still liquid.

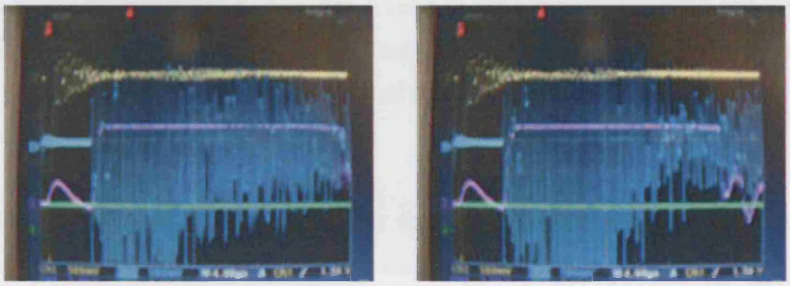

Packing at 7s *End of Packing at 9s*

Figure 5.6: Ultrasound Signal during the Packing Phase Period

Multiple reflections of the transmitted signal occur at the solid-melt and melt-solid interfaces of the part. These can be observed at the left window of Figure 5.6 where after the first transmission at around $7\mu s$, multiple transmissions (from reflections, since there is only one transmitted pulse, $f_{pulse} = 3Hz$) continue to appear with a decreasing amplitude up to $20\mu s$ period. At the end of packing (9s window) the transmitted signals from the reflections are less (in the second half of the right screen) as larger percentage of the part is now solid. In addition, during packing (7s window) the VRS (influenced by the power of the transmitted signal) is high as well during the $7\mu s$ to $20\mu s$ period.

In Figure 5.7, during the cooling phase the part continues to solidify (at 13s) and the time for the ultrasound to propagate through the part reduces.

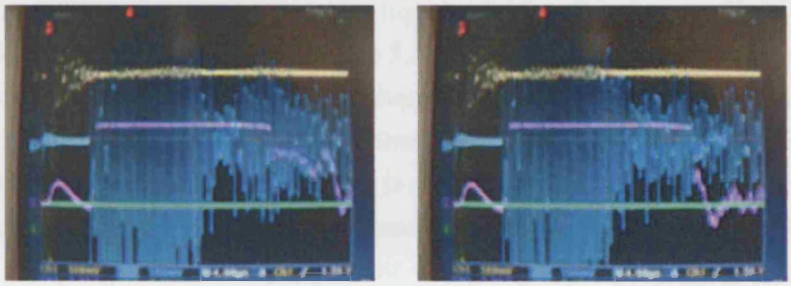

Cooling at 13s *Cooling at 14s*

Figure 5.7: Ultrasound Signal during the Cooling Phase

This was verified experimentally (Figure 3.27) by comparing data of the time of first arrival of the transmitted signal with successive ones. As a larger percentage of the part is solid, less liquid interfaces constitute the solidifying part. Therefore the fewer the reflections are at these interfaces, the fewer the successive transmitted signals through the mould. For this reason

most of the signal is transmitted through the part and a very small percentage is still reflected and transmitted again (which is highly attenuated). This is verified by the amplitude of the transmitted signal in the second half of the screen (14s) which is reduced considerably when compared with earlier screen shots captured during filling. In accordance with the reduction of the reflected signals the voltage reference signal started to decline as well after the $15\mu s$ period (13s window).

Finally in Figure 5.8 ultrasound screen shots from the end of the cooling phase are shown where the part shrinks considerably and the amplitude (at 15.7s) of the transmitted signal is attenuated as the ultrasound coupling strength between the part and cavity walls is less.

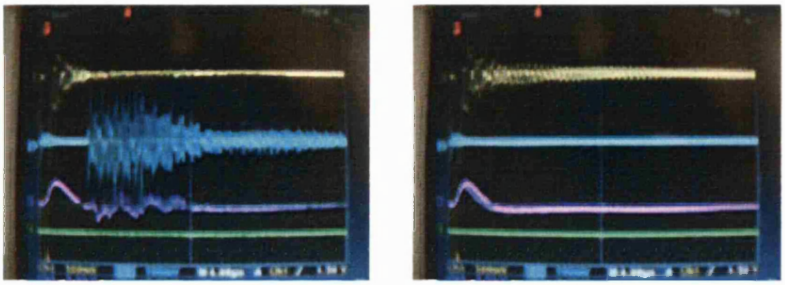

Cooling at 15.7s *End of Cooling at 15.8s*

Figure 5.8: Ultrasound Signal during the End of Part Solidification

The temperature gradient throughout the part is more uniform and there are no liquid layers present. This is verified by the nature of the transmitted signal which has no successive transmissions (in the second half of the screen, from $10\mu s$ to $20\mu s$ period) which were originating earlier (during filling and packing) from the liquid-solid interface layers. If the left window of Figure 5.8 is compared with that of Figure 5.5 it would be more clear for the reader to understand that at the beginning of the filling phase there are multiple reflections and therefore successive transmissions from the liquid and then liquid-solid layers of the part. At the end of the cooling time the part is solid and the wave is reflected only at the mould/polymer and at the polymer/mould interface. One tenth of a second later the part completely detaches from the mould walls and the ultrasound coupling is lost. All of the transmitted signal is reflected back (at 15.8s). The ultrasound data acquisition box sets the trigger signal (feedback to controller) low and the controller in the Simulink model initiates the opening of the mould to eject the solid part.

5.3.2.3 Discussion on Ultrasound Results

The application of the ultrasound data acquisition box for monitoring and as a control feedback for the injection moulding process was successful. The trigger signal generated by the micro-controller was sent as a feedback to the closed loop control algorithm (PID) to initiate the packing phase and later on mark the end of solidification. Apart from the trigger, the voltage reference signal (VRS) was seen to follow a varying profile throughout the cycle. During packing phase the VRS (influenced by the power of the transmitted signal) was high during the $7\mu s$ to $20\mu s$ period while at the end of the packing phase and during the solidification period, started to decline after $15\mu s$ period. This indicative profile of the VRS was verified as well by the transmitted signal the amplitude of which was reduced in the period $12\mu s$ - $20\mu s$ (Figure 5.7). Therefore in the presence of no scope to visually monitor the changes of the transmitted signal the profile of VRS could be processed within the micro-controller to provide more information, such as the end of the packing phase. However more tests are required to validate this proposal. Furthermore it was shown (experimentally) that the ultrasound can provide similar information as a cavity pressure transducer in the sense of identifying phase changes during the injection cycle. As the ultrasound method is cost effective, portable and non-invasive it would be more attractive for monitoring the moulding cycle when compared to a cavity pressure transducer.

5.4 Selected Flow and Pressure Profiles

Proper selection of (screw) flow and pressure profiles is required in order to influence the rheological properties of the melt during injection and control polymer orientation, surface appearance, part shrinkage and solidification rate. The proposed strategy of melt vibration during the filling and packing phase is believed to enhance mechanical properties such as strength, toughness and influence residual stresses (which cause warpage). Depending on the part final service environment some of these properties (e.g. crystallinity) might be desirable or not. With conventional moulding the orientation of the part molecular chains is maximum at the outer surfaces and minimum towards the core. The lack of orientation at the core is attributed to poor shear control of the melt (during packing) where the entangled molecular chains fail to untangle and become more oriented (due to low shear stresses). The molecular chains at the core are isolated (by above layers) and have the ability to relax more and become randomised. Part defects attributed to wrong mould design could be reduced (such as non-uniform cooling, etc) by improving the orientation in the part. Therefore a pressure trajectory can be combined with vibration enabling operation at lower frequencies (this applies to both semi-crystalline and amorphous polymers). However deformations in the molecules must be imposed with care to avoid excessive shear heating and degradation (fatigue) effects.

Although the effect of vibration has been investigated so far by a number of researchers little detailed information is available. Further investigation is required to evaluate the application of vibration in conventional moulding machines in a closed-loop control. To implement these strategies in an injection moulding machine a high level of control accuracy with fast acting screw dynamics is required. Some potential methods for the enhanced control of flow and pressure profiles during injection will be reviewed in the following sections.

5.5 Flow and Pressure Control

For the control of the injection moulding process both velocity and pressure profiles must be regulated during the filling and packing phase respectively. There are two types of controllers that could be used. First is the single controller were both velocity and pressure control are coupled within the same controller structure. There are two demand inputs and a single output for both velocity and pressure control. The second type has two separate controllers, one for velocity and one for pressure coupled together in a hybrid solution, as described earlier in section 2.4.2. A transfer algorithm is necessary in order to provide a smooth switch between the controllers and ensure a continuous command signal to avoid oscillatory behaviour in the system. The industry standard P-Q controller for injection moulding is a hybrid solution where a switch is used to change from an open-loop (or closed-loop) P velocity control to closed-loop PI pressure control [14]. There is a number of control methods that could be used for the moulding process and the most important are reviewed in section 5.6.

5.5.1 Main Problems with P-Q Controllers

The main problems associated with traditional P-Q controllers in injection moulding process are as follows [14]:

- The PID controller gains are tuned based on the experience of the commissioning engineer and remain fixed throughout the life of the moulding machine. However wear in the hydraulic valves controlling the motion of the screw can change the behaviour of the hydraulic response. In addition, if the operating conditions change (e.g. a different gate size in a new mould would change the pressure drop) the controller gains remain fixed which could have an effect in the efficiency of the injection cycle.
- The switching from velocity to pressure control is either time or position controlled. Therefore to achieve a smooth switch and maintain the command signal continuous relies on the experience of the commissioning engineer. In addition, the velocity controlled

phase is a low gain system compared to the pressure controlled phase which is a high gain system. Therefore improper adjustment of the settings may cause an oscillatory behaviour in the system which in turn may affect the viscosity of the material and mechanical properties in the final part.

- In the event that short hoses are used between the P-Q valve and the hydraulic actuator (due to the high bulk modulus) the PI pressure controller would be more tedious to tune properly for the whole bandwidth of operating conditions.

For the above reasons it would be a great advantage to use a hybrid controller with self-tuned gains to overcome these problems and also improve the productivity of the process.

5.6 Advanced Control Methods for Hydraulics

Nowadays more interest is drawn to modern control methods for hydraulic systems as the need for higher performance and efficiency is required. Moreover the huge progress in the speed of microprocessors allows implementation of such control methods in real time enabling nonlinear systems to be controlled faster with respect to parameter variations and show robustness to unknown disturbances. Although traditional control methods such as PID are widely used in industry, they are limited to certain operating conditions while their performance deteriorates with time as the controller gains remain fixed throughout the life-cycle of the plant. Therefore the trend is slowly changing towards advanced control methods as more and more demanding hydraulic applications arise. Some of these control methods which are applicable for flow and pressure control of the injection moulding process are reviewed in the sections 5.6.1-5.6.5.

5.6.1 Robust Control

With robust control the (nonlinear) plant is forced to follow a predefined control performance regardless the presence of unknown dynamics and disturbances. *Sliding mode control* (SLM) is a well known robust control technique where the system is forced to behave with dynamics of one dimension less than the real order of the plant dynamics. Therefore the system dynamics are governed by a user defined reduced order system. One drawback of this method is that it leads to control chattering which involves high control activity deteriorating the performance of the controller. In addition, there is a trade off between parametric uncertainty and tracking performance [106]. A good example of SLM for the position control of a hydraulic proportional spool valve is presented in [107] where the design of a sliding plane is presented. The SLM was found to be superior to PID with improved transient response. Recently a self-tuning

robust controller for an injection moulding application was tested in simulation for the velocity control of the filling phase [108]. A sliding surface was defined to achieve ram velocity tracking control. The chattering effect was reduced by smoothing out the control in a thin boundary layer adjacent to the switching surface. The control gains were tuned by an adaptive algorithm. The proposed adaptive controller maintained a good tracking performance in the presence of parameter variations (melt viscosity changes) and was capable of achieving tight set point regulation. However no experimental results were presented to back up the simulation findings. Although sliding mode control is an interesting option it was not chosen for the control of the injection moulding process as complete knowledge of the plant dynamics is necessary.

5.6.2 Neural Network Control

The artificial neural network (NN) is an interconnected group of artificial neurons that use a mathematical model or computational model for information processing. Usually an ANN is an adaptive system that regulates its structure according to external or internal information that flows through the network. The neural network model needs to be trained with existing data to represent an accurate model of the system to be controlled. Next the model is inverted and the optimum output profile of the plant is fed into the model. The neural network model generates an ideal input profile for the plant to be controlled [109]. In an injection moulding study an intelligent hybrid system [110], called HSIM was used to determine the initial process parameters based on artificial intelligent techniques (AI), case based reasoning (CBR), hybrid neural network (NN) and genetic algorithm (GA). The advantage of the proposed method was that it eliminates the need of expert personnel to set up the process. In another research study NNs were used to optimise the moulding parameters in order to improve the dimensional quality of moulded parts based on the concept of reverse process modelling [111]. The variation in injection time and cooling temperature were the process parameters used. In another study [112] a hybrid NN system which combined the training of NN with analytical knowledge of the moulding process was used to predict the injection pressure. It was found to be superior to a conventional NN requiring a minimum amount of process data for training. In general NNs are attractive as they simplify the need of a detailed mathematical model for the process, however issues of stability and performance robustness could arise [106]. On the other hand the injection moulding process involves changing of moulds and materials (with different properties) where a NN model would have to be retrained each time to maintain the same level of accuracy. This in turn would be time consuming in a process were cycle time is of prime importance. Therefore the use of NNs was not pursued further.

5.6.3 Fuzzy Logic

Fuzzy logic is applied in processes where an operator is usually required to control the system [113]. It is applicable in systems with time varying parameters [106] were a set of rules describes how the system input should be modified to give an optimum system output. The advantage of the fuzzy logic control is that no mathematical models are required. Fuzzy logic has been applied for the velocity control of the screw during filling [114]. A feedback and feedforward control system based on fuzzy logic was tested experimentally with a variety of moulds, materials and barrel temperatures. The experimental findings indicated that the fuzzy logic based controller outperformed the traditional PID controller. The work done by [115] details the implementation and testing of an incremental fuzzy control strategy with PI performance on an injection moulding machine for the control of screw velocity and nozzle pressure during the process. For the experimental part forty nine fuzzy rules were used to regulate velocity and pressure. Overall the controller maintained a constant velocity profile during filling (tested only for speeds up to 0.015m/s) while in packing phase could tolerate switching point variation and change of moulds. However during the switch, the controller (closed-loop fuzzy) was a little slower than the open-loop (fuzzy) controller but with less pressure overshoot. In general it would be feasible to construct a fuzzy P-Q controller although it could be complex while the analysis to guarantee global stability could be difficult.

5.6.4 Learning Control

Learning control is a method effective in processes with a repetitive nature. The learning controller monitors the plant's performance in each cycle and utilises this information to improve the performance in a subsequent cycle [116]. This type of controller is widely referred as *iterative learning controller* (ILC) as it reduces the tracking error of the plant in subsequent iterations. It was first introduced in the late seventies [117] but as it was originally published in Japanese became known later in the eighties when applied as a *betterness* process for the control of a robot arm [118]. In that work the ILC method was mathematically formulated; however all the published results were purely based on simulation. It was emphasised that the presence of noise in the feedback signal would be a disadvantage. The proper selection of the learning function (gain) would be a trade-off between fast learning and noise robustness. In a later study [119] an ILC structure was used for the control of a nonlinear system with minimum information required about the plant. However noise from the derivative of the error could imperil the stability of convergence. In another work [116] the application of ILC has been experimentally applied to the control of the injection moulding process. Good results were obtained as the error in the ram position and hydraulic pressure were successfully reduced within eight iterations. The author emphasised the need to generate an accurate trajectory output (of the controller) to achieve convergence. Combination of both ILC controllers in a hybrid scheme

was argued to be a trivial task in order to achieve a smooth fill-to-pack transition without the presence of pressure oscillations. In a later study [120] an *optimal* learning control structure (for batch processes with uncertain disturbances) with changing weighting matrices was applied successfully (experimentally) for the velocity control of an injection moulding machine. The system achieved convergence after eleven cycles. A specific condition was established to guarantee robust bounded-input-bounded-output stability of the iterative learning control system. Recently a hybrid ILC structure [121] for controlling flow and pressure in the injection moulding process was tested both in simulation and experimentally. This new scheme with the aid of a bumpless transfer algorithm (reference conditioning algorithm) achieved a smoother transition at the time of switching controllers which was a limitation in an earlier study [116]. The ILC (for load control) achieved good convergence after nine iterations. In a more recent study [122] for screw position control in the injection moulding filling phase, a hybrid controller was introduced with a PI feedback and a higher order ILC feed-forward loop. This new method was only tested in simulation showing robustness to parameter changes (polymer bulk modulus). Within five iteration the tracking error was reduced close to zero. One disadvantage of ILC when applied for the control of the packing phase is that the derivative of pressure is difficult to derive as noise from the hydraulic pump pressure ripple is likely to be present. When ILC was applied experimentally for both flow and pressure control it required a number of iterations to achieve convergence. In addition after convergence is achieved due to noise issues the learning process should be stopped and run the plant in open-loop. Moreover if process parameters are changed (material, mould) the identification of the plant would be again necessary to achieve convergence. For these reasons the ILC was discounted for further investigation.

5.6.5 Adaptive Control

Adaptive control is applicable to plants with dynamics that vary continuously due to the nature of the load acting on the system. In injection moulding this is mainly due to the nonlinear stiffness of the polymer during injection. Factors such as valve dynamics, unequal area actuator, bulk modulus, etc. may contribute as well to the nonlinearity of the system. Therefore the controller needs to adjust continuously and exhibit satisfactory performance throughout the cycle. The controller parameters are not fixed or predetermined as they update during the process depending on the plant error. There are two types of adaptive controllers, the *Gain Scheduled* and *Self Adaptive* controller.

In the *Gain Scheduled* type a priori information of the system dynamics is required as well as one or more measurable parameters with which the regulator is varied. Once a gain scheduling map is derived the system can exhibit enhanced performance [16]. Recently a *Gain Scheduled* controller was derived for the control of the hydraulic velocity and force in injection moulding

[123]. Reasonable control of velocity and pressure was achieved in simulation, however in experimental results problems in velocity tracking were observed to be due to unmodelled dynamics (dead time) in the design of the controller. Overall the tested operating range was not wide enough to justify the suitability of the proposed structure.

In contrast with the first type the *Self Adaptive* controller does not require a priori knowledge of the plant as it is designed to adapt regardless to parameter variations such as load changes and disturbances. Two general types fall in the second category; *Self Tuning Control* and *Model Reference Adaptive Control* (MRAC). A good introduction to these types is found in [124, 125].

For the Self Tuning approach an accurate mathematical model of the system is required for parameter identification. Upon successful identification the control parameters are regulated by a design procedure (such as pole placement) [16]. A self-tuning adaptive controller [126, 127] has been recently applied for the control of the (nozzle) packing pressure with different set points, moulds and barrel temperatures. Anti-windup, cycle to cycle adaptation and feedforward control were integrated to enhance the control of the nozzle pressure. To avoid the estimator windup the estimation was stopped when the error was small. Overall the controller exhibited superior performance compared with the PID which failed to provide satisfactory control.

On the other hand the *MRAC* approach first introduced by [128] has an advantage over *Self Tuning* as no precise identification of the plant is required. The MRAC scheme is comprised of the plant which has unknown parameters, the reference model (usually a 2nd order transfer function) that represents the desired performance of the plant and the feedback-feedforward controller which regulates the adjustable parameters according to the adaptation law. The reference signal is fed to the plant and the reference model while their output difference constitutes the *model following error* which is processed by the adaptive algorithm. This regulates the adaptive gains according to the amplitude of the error with the aim of reducing it to zero. The reference model is designed to represent the plant and with similar dynamic characteristics so that model tracking is feasible. By proper selection of the feedback and feedforward gains the poles of the plant are placed close to those of the model. Lately the MRAC structure was applied for the control of the injection moulding process [129]. A second order reference model was chosen for both the filling and packing process with a critical damping, $\zeta = 1$. The hybrid controller was tested with the hydraulic oil at room temperature and then at $40°C$. During the filling phase the response was equally good (0.015m/s) for both controllers whereas at the higher temperature the PI controller failed to track the reference signal and reduce the transient error. At the time of switching a bumpless transfer algorithm was utilised to ensure a smooth transition from flow to pressure control. Although no transients were present the tracking was poor with a large error. Overall the adaptive scheme achieved good tracking performance in both cases (of oil temp.) where again the PI controller experienced an oscillatory transition. Al-

though the MRAC exhibited good performance only one of experimental operating conditions set was tested.

An extension of the MRAC is the *Minimal Controller Synthesis* (MCS) first introduced in the 1990s [130, 131]. The advantage of MCS algorithm is that it is less complex and requires a minimal synthesis to build the control law. Not a priori knowledge of the plant is required (eliminating the need of plant identification) while the adaptive gains can start from zero initially. As long as the system parameters vary slower than the adaptive laws, the MCS can guarantee an asymptotically hyperstable closed-loop system. Therefore the MCS is robust to plant parameter variation, external disturbances and unmodelled plant dynamics. MCS has been successfully applied in the force control of a servo-hydraulic materials testing machine with good performance [132]. It has also been tested in a valve actuator system with a variable displacement pump [133]. The energy efficiency of the plant was improved by 44% for controlling a mass of 1000kg when compared to the linear control approach. The robustness of the MCS was investigated again in a material testing machine under cyclic load [134, 135]. A first order MCS was derived for load control of the plant with 2nd order dynamics. Specimens of different diameters and materials were used with the "Force MCS" exhibiting robust behaviour under all operating conditions. Lately an improved version of the MCS, the error based MCS with integral action (Er-MCSI) was presented [136] and tested both in simulation and experimentally. The standard MCS could exhibit a lack of explicit integral adaptation where gain wind-up problems could arise. This extension of MCS with integral action addresses this issue where the integral gain is driven by the error based feedback. The position control of a servo-hydraulic actuator model was tested in simulation, while experimentally the velocity control of a servomotor was successfully implemented. In both simulation and experimental studies the Er-MCSI outperformed the MCS controller under variable operating conditions and input disturbances.

Concluding the MCS algorithm shows advantages over the other possible control methods reviewed here. It has attracted the attention of a number of researchers and has been successfully applied on hydraulic valve actuator systems for position and load control. Due to the simplicity of building the control law as well as the robustness to model uncertainties and external disturbances, MCS was chosen for the hybrid P-Q controller.

5.7 Concluding Remarks

The hydraulic modification of the moulding machine was successfully undertaken enabling accurate P-Q control of the screw motion. This allowed different control strategies for the filling and packing phase to be applied via Matlab-Simulink environment to investigate their effectiveness and investigate the influence of vibration on part quality control. The installed

micro-controller serves as the interface between the PC and moulding machine which runs routine safety checks to monitor the validity and sequence of signals originated by the PC. It can prevent accidents caused either by the user or from a hardware failure. For optimising the injection cycle and reducing the number of trial and error cycles the proposed non-invasive method of ultrasound was implemented successfully via the ultrasound data acquisition box hardware (designed and build at the department). This analyses the process-critical information which is then fed back and processed by the closed-loop control of the injection moulding process. Following on the extensive literature review in Chapter 4, a different control approach for filling and packing (via melt vibration) is proposed using the current (screw) configuration of the injection moulding machine. Accurate control of the melt vibration with flow and pressure profiles could aid the processability of the polymer to obtain parts with different mechanical properties. Moreover the solidification of the part during cooling could be advanced by melt vibration to achieve fast quenching.

To successfully apply the proposed profiles, a controller capable of responding rapidly to non-linearities and parameter variation is essential. From all the control strategies reviewed the MCS adaptive controller seems to be the most promising for P-Q control. The MCS can be formulated in a hybrid scheme with a bumpless transfer algorithm to ensure a smooth switching between the phases. The main advantage of the MCS is that it requires no plant identification while the adaptive gains can start from the value of zero. There are issues with gain drift and amplification of noise during adaptation of the MCS but these will be addressed in Chapter 6 where a more extensive analysis of the approach is presented.

Chapter 6

MCS Flow & Force Control

6.1 Introduction

This chapter gives an outline of the *Minimal Control Synthesis* (MCS) theory and a detailed analysis of its application to the injection moulding process is presented. The adaptive MCS algorithm was initially proposed in the 1990s and successfully employed to cope with nonlinear problems in the field of robotics [137]. So far it has been successfully applied in certain hydraulic applications, mostly in research laboratories. The MCS algorithm can be used as stand alone or in parallel with a classical controller (PI - PID) to achieve consistent dynamic performance of the process (nonlinear) in real time without the need of detailed knowledge of the plant parameters.

This chapter starts with an initial analysis of the classical MCS structure and some extensions that can be used to enhance its performance, described in section 6.2. Continuing, the extension of classical MCS to Flow MCS and Force MCS are presented in sections 6.3 and 6.4 respectively. The order of the appropriate reference model for each case is estimated based on linearised models of the filling and packing phase of the injection cycle. Plant identification is carried out with the use of an MCS observer both in simulation and real time for an initial estimation of the adaptive gains of the flow control reference model. This is presented in section 6.5. Both MCS extensions are coupled in a Hybrid Scheme with the use of a bumpless transfer algorithm while their adaptation behaviour is tested in simulation, as described in detail in section 6.6. A development of the classic MCS algorithm that improves the efficiency and stability especially when a feedback state is corrupted (noisy) is tested in simulation and presented in section 6.7. Finally in section 6.8 the hybrid scheme of the proposed MCS structure is tested in real time in the injection moulding machine. Two viscosity grades of polypropylene material are used to test the robustness of the proposed controller at different operating conditions. The

chapter concludes (section 6.9) with a discussion on the results obtained both in simulation and real time, highlighting the advantages of the developed hybrid MCS. An area of potential where further work can be done is indicated.

6.2 MCS of MRAC

The minimal control synthesis (MCS) algorithm is a simplification of the model reference adaptive control (MRAC) first introduced by Landau [128]. Similarly to MRAC the MCS algorithm aims to achieve closed loop control regardless the presence of nonlinear plant parameters and external disturbances. It requires no plant model identification or linear controller synthesis and retains all the advantages of the MRAC structure. However in order to avoid transients during adaptation plant identification could be helpful for applications such as the injection moulding. In addition, the MCS simplifies the control system synthesis and implementation required, while remaining asymptotically hyperstable [130]. Unlike MRAC, MCS does not require the hyperstability check or the Lyapunov equation validation. Finally the main MCS parameters to be selected by the designer are the adaptive weights α and β and the error matrix C_e [138].

6.2.1 Advantages of the MCS Algorithm

The main advantages of the MCS algorithm for the control of the injection moulding cycle can be summarised as the following:

- It is not necessary to have a deep insight into the plant dynamics of the process. This is very useful in cases where uncertainties exist and it's difficult to derive a precise plant model. It is necessary to have a 1st and 2nd order model for pressure and flow control respectively (see sections 2.2.2.1, 2.2.2.2) to determine the MCS adaptation dynamics and ensure that the plant will follow sufficiently the trajectory of the reference model.
- MCS can adapt rapidly and yield high speeds to cancel out high bandwidth disturbances and internal parameter variations that occur in the system [139]. This is very critical at the beginning of the filling phase where the plant has to follow a specific velocity profile regardless to disturbances that may interrupt the injection cycle. Often variations can be related to the thermal history of the polymer and changes in the plasticization phase.
- MCS adaptive gains can start either from zero values or from estimates which have been derived from a system identification using an observer or from a previous injection cycle. In cases where predetermined values are used the initial transient period and error can be

significantly reduced. This is very critical in the filling stage that usually lasts for a very short period of time. Moreover once determined the MCS gains can also been locked during the cycle at a desired value resulting in a fixed gain controller.

- So far the stability and the robustness of the MCS algorithm have already been tested in demanding electro-hydraulic applications with promising results [139, 133].

6.2.2 Overview of Basic MCS Equations

The plant state-space equation is described as:

$$\dot{\underline{\mathbf{x}}}(t) = \mathbf{A}_p(t) \cdot \underline{\mathbf{x}}(t) + \mathbf{B}_p(t) \cdot u(t) + d(t) \tag{6.1}$$

where $d(t)$ is the disturbance vector.

The linear reference model state vector is defined as:

$$\dot{\underline{\mathbf{x}}}_m(t) = \mathbf{A}_m \cdot \underline{\mathbf{x}}_m(t) + \mathbf{B_m} \cdot r(t) \tag{6.2}$$

The MCS algorithm can be summarised in the following equations:

The control law equation is:

$$\underline{\mathbf{u}}(t) = \mathbf{K}(t) \cdot \underline{\mathbf{x}}(t) + K_R(t) \cdot r(t) \tag{6.3}$$

where $r(t)$ is the reference signal and $\mathbf{K}(t)$ and $\mathbf{K}_R(t)$ are the adaptive gains:

$$\mathbf{K}(t) = \int_0^t \alpha y_e(\tau) \underline{\mathbf{x}}^T(\tau) d\tau + \beta y_e(t) \underline{\mathbf{x}}^T(t) \tag{6.4}$$

$$\mathbf{K}_R(t) = \int_0^t \alpha y_e(\tau) r(\tau) d\tau + \beta y_e(t) r(t) \tag{6.5}$$

In equations 6.4 & 6.5 $\{\alpha, \beta > 0\}$ are the scalar adaptive weights of the integral (α) and pro-

portional (β) part of the adaptive gains $\mathbf{K}(t)$, $\mathbf{K}_R(t)$.

The output error $y_e(t)$ is:

$$y_e(t) = \mathbf{C}_e \underline{\mathbf{x}}_e(t) \tag{6.6}$$

and the state error is determined as

$$\underline{\mathbf{x}}_e(t) = \underline{\mathbf{x}}_m(t) - \underline{\mathbf{x}}(t) \tag{6.7}$$

To get a positive error matrix $\mathbf{C}_e$ the following condition must be valid:

$$\mathbf{C}_e = \mathbf{B}_e^T \mathbf{P} \tag{6.8}$$

where $\mathbf{P}$ is a positive-definite solution of the Lyapunov equation:

$$\mathbf{P}\mathbf{A}_m + \mathbf{A}_m^T P = -\mathbf{Q}, \;\; \mathbf{Q} > 0 \tag{6.9}$$

The input matrix $\mathbf{B}_e$ has the form of

$$\mathbf{B}_e = [0 \ldots 0\ 1]^T \tag{6.10}$$

The output error matrix $\mathbf{C}_e$ for the MCS algorithm is described as:

$$y_e = \mathbf{C}_e \underline{\mathbf{x}}_e = \mathbf{B}_e^T \mathbf{P} \underline{\mathbf{x}}_e \tag{6.11}$$

6.2.3 MCS with Integral Action

The integral action extension of the MCS algorithm has an additional term in the control signal, described by the following control law [140]:

$$\underline{\mathbf{u}}(t) = \mathbf{K}(t) \cdot \underline{\mathbf{x}}(t) + K_R(t) \cdot r(t) + K_i x_i(t) \tag{6.12}$$

The new integral adaptive gain $K_i(t)$ is given by:

$$K_i(t) = \int_0^t \alpha y_e(\tau) x_i^T(\tau)\, d\tau + \beta y_e(t) x_i^T(\tau) \tag{6.13}$$

where the integral state error $x_i(t)$ is:

$$x_i(t) = \int_0^t [r(\tau) - x(\tau)] d\tau \tag{6.14}$$

6.2.4 Magnitude Insensitive MCS

This extension to the MCS uses the sign function of the state vector [141]. This has a great advantage because the output value of the state vector is a function of the magnitude and the reference signal. If the states for a given system become very small or very large then the adaptive weights must be readjusted to provide a satisfactory adaptation rate. When the state values are removed, the sign function of the signal must remain to satisfy the Popov's hyperstability requirement. In this case the adaptive gains $\mathbf{K}(t)$ and $\mathbf{K}_R(t)$ are mainly error driven and can be rearranged as follows:

$$\mathbf{K}(t) = \int_0^t \alpha y_e(\tau)\, sgn\left(\underline{\mathbf{x}}^T(\tau)\right) d\tau + \beta y_e(t)\, sgn\left(\underline{\mathbf{x}}^T(\tau)\right) \tag{6.15}$$

$$\mathbf{K}_R(t) = \int_0^t \alpha y_e(\tau)\, sgn(r(\tau))\, d\tau + \beta y_e(t)\, sgn(r(\tau)) \tag{6.16}$$

The sign function can take the following values:

$$sgn(x(t)) = \left.\begin{array}{c} -1 \in x\langle 0 \\ 1 \in x\rangle 0 \\ 0, x = 0 \end{array}\right\} \tag{6.17}$$

To avoid the sharp switching action of the *sign,* a smooth switching function can be used

instead. By applying the following expression to the variable $x(t)$ it yields:

$$\tilde{x}(t) = \frac{x(t)}{|x(t)| + \varepsilon} \tag{6.18}$$

6.2.5 MCS Gain Locking

This is an extension of the MCS algorithm where the adaptive gains can be locked during the adaptation cycle [133]. It is necessary if the control signal reaches saturation where the adaptive gains can be locked until the signal comes out of saturation. In this case the MCS algorithm operates as a fixed gain controller.

There are two gain locking methods that can be applied; complete gain locking or integral gain locking. In the first case both the integral and proportional part of the gain is locked. This action can be dangerous as complete gain locking may result in instability of the system [133]. The second method is more safe to use since it locks the integral component that can cause gain "wind-up". As a result a smoother control signal is achieved as the system is left to partially adapt while it comes out of saturation.

6.2.6 2nd-order MCS

The typical application of the MCS algorithm is realised when the plant and the model have second order dynamics. In this case both of the feedback states are used. An illustration of the MCS control scheme is shown in Figure 6.1.

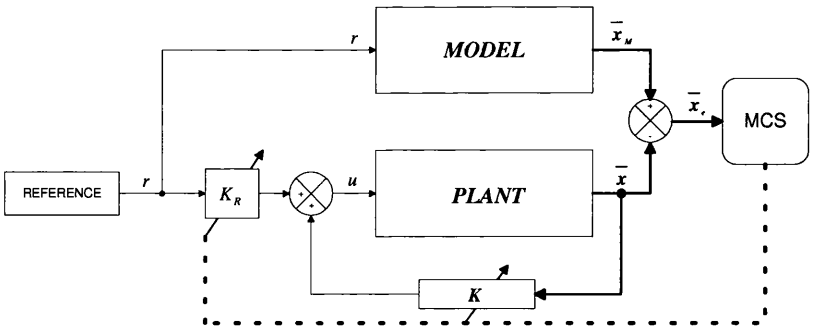

Figure 6.1: 2nd order MCS & Model

The MCS control signal is given by the following equations.

$$u(t) = \mathbf{K} \cdot \underline{\mathbf{x}}(t) + K_R(t) \cdot r(t) = [K_1(t) \quad K_2(t)] \cdot \begin{bmatrix} x(t) \\ \dot{x}(t) \end{bmatrix} + K_R(t) \cdot r(t) \tag{6.19}$$

The adaptive gains $\mathbf{K}(t)$ and $K_R(t)$ are given by:

$$\mathbf{K} = [K_1(t) \quad K_2(t)] = \int_0^t \alpha y_e(\tau) \cdot [\tilde{x}(\tau) \quad \tilde{\dot{x}}(\tau)] \, d\tau + \beta y_e(t) \cdot [\tilde{x}(t) \quad \tilde{\dot{x}}(t)] \tag{6.20}$$

$$K_R(t) = \int_0^t \alpha y_e(\tau) \cdot \tilde{r}(\tau) d\tau + \beta y_e(t) \cdot \tilde{r}(t) \tag{6.21}$$

The scalars α and β determine the adaptive effort of the MCS controller and on most occasions are tuned empirically. The output error signal $y_e(t)$ is:

$$y_e(t) = C_e \cdot x_e(t) \tag{6.22}$$

The matrix C_e must be pragmatically selected to satisfy the Lyapunov equation and for a second-order MCS algorithm is given by [133]:

$$C_e = [\omega_M \quad 1] \tag{6.23}$$

The vector of the generalised state error $\underline{\mathbf{x}}_e(t)$ is given by:

$$\underline{\mathbf{x}}_e(t) = \begin{bmatrix} x_M(t) - & x(t) \\ \dot{x}_M(t) - & \dot{x}(t) \end{bmatrix} \tag{6.24}$$

To minimise the steady-state error the integral action can be added in the original configuration of the MCS algorithm. An illustration of the MCSIA control scheme is shown in Figure 6.2.

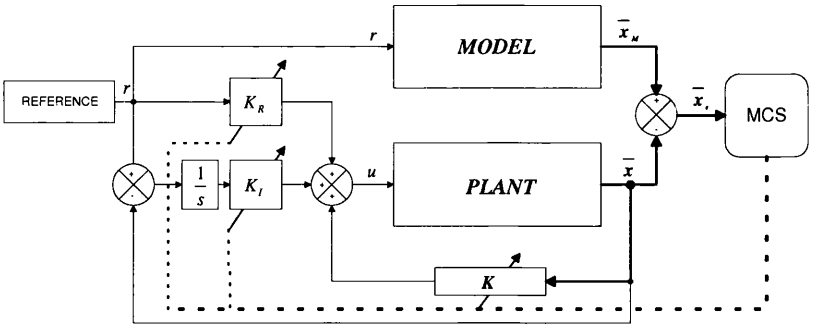

Figure 6.2: 2nd order MCSIA & Model

6.2.7 1st Order Model MCS

The 1st order model of the MCS can be applied in plants where only one feedback state is available. The second feedback state may be either not measurable or very noisy which can drive the controller unstable [133]. In this case the performance of the MCS is constrained to 1st order dynamics. An illustration of the MCS control scheme is shown in Figure 6.3.

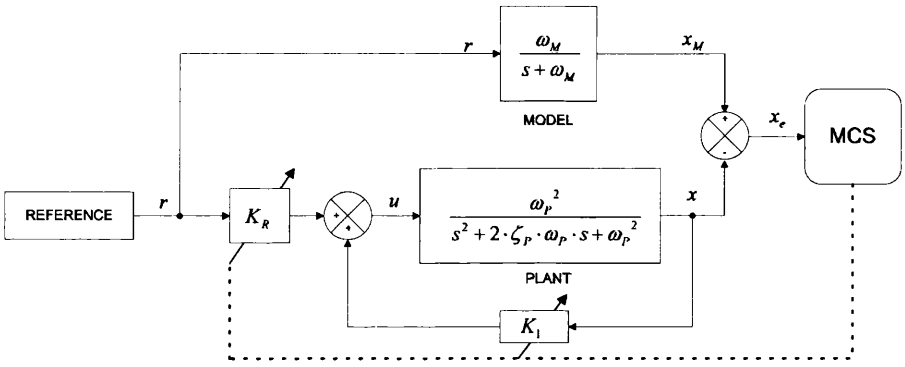

Figure 6.3: 1st order MCS & Model

Since only one state is used only one component of the feedback vector is active. Hence the 1st order MCS control law is given by:

$$u(t) = K(t) \cdot x(t) + K_R(t) \cdot r(t) \tag{6.25}$$

The adaptive gains $\mathbf{K}(t)$ and $K_R(t)$ are given by:

$$\mathbf{K} = [K_1 \;\; 0] = \int_0^t \alpha y_e(\tau) \cdot \tilde{x}(\tau)\, d\tau + \beta y_e(t) \cdot \tilde{x}(\tau) \tag{6.26}$$

$$K_R(t) = \int_0^t \alpha y_e(\tau) \cdot \tilde{r}(\tau)\, d\tau + \beta y_e(t) \cdot \tilde{r}(t) \tag{6.27}$$

In the output error signal $y_e(t)$ the coefficient C_e is scalar for a first order system:

$$C_e = 1 \tag{6.28}$$

6.3 MCS Flow Control

The first application of the MCS is "Flow MCS" which was used to control the actuator's velocity during the filling stage of the injection moulding cycle. This new scheme was initially tested in simulation using the non-linear model of the plant (described in Chapter 2).

The control of the ram's velocity is very challenging due to the non-linearities associated with the hydraulic system (unequal area actuator, unknown valve pressure and flow gain) and the polymer load dynamics (polymer viscous friction) during the mould filling. The filling stage typically lasts for a fraction of the injection cycle (5%) and an adaptive controller that would be able to accommodate these uncertainties and follow demanding (velocity) trajectories would be very attractive for the plastics industry.

In the modified hydraulic system a servo-proportional P-Q valve is used for the flow control of the (two) unequal area actuators. The valve has a very fast response compared with the actuator and hence the dynamics are neglected for the sake of simplicity. The overall dynamics of the hydraulic-mould system depends on the operating point and stage of the filling process. The linearised model (section 2.2.2.1) of the plant for velocity control, $\frac{\dot{y}(s)}{x(s)} = \frac{K \cdot s}{s^3 + a_2 \cdot s^2 + a_1 \cdot s + a_0}$, describes sufficiently the inertia load dynamics and has a relative degree of 2 (2^{nd} order dominant 3^{rd} order system). For this reason it is appropriate to use a model of the same order, "2nd order MCS", to control the plant and ascertain the appropriate rate of adaptation. The two "measurable" feedback states of the MCS loop are velocity and acceleration.

The control scheme for the velocity MCS of the plant is shown in Figure 6.4. It is desirable to set the behaviour of the (2nd order) model to have a rapid response with more damped dynamics than the plant. For the estimation of the model parameters an insight of the plant dynamics is required.

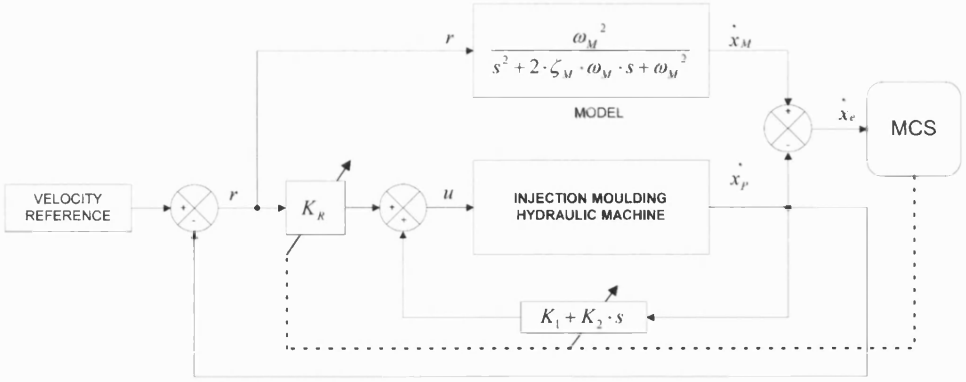

Figure 6.4: Velocity MCS & Model

Parameters from the linearised model or from system identification of the real plant can be used. It is anticipated that during the adaptation procedure the plant poles will move in the direction of the model poles improving the plant's behaviour.

By comparing the closed loop transfer function of the controlled plant,

$$G_P(s) = \frac{K_R \cdot \omega_P^2}{s^2 + \left(2 \cdot \zeta_P \cdot \omega_P - \omega_P^2 \cdot K_2\right) s + \omega_P^2 (1 - K_1)} \tag{6.29}$$

with that of the model,

$$G_M(s) = \frac{\omega_M^2}{s^2 + 2 \cdot \zeta_M \cdot \omega_M \cdot s + \omega_M^2} \tag{6.30}$$

an initial estimation of the model parameters, ω_M, ζ_M, can be realised. In this case (2^{nd} order model) the parameters matrices $\mathbf{A}_m$, $\mathbf{B}_m$ of the linear reference model,

$\dot{\underline{\mathbf{x}}}_m(t) = \mathbf{A}_m \cdot \underline{\mathbf{x}}_m(t) + \mathbf{B_m} \cdot r(t)$, can be set as:

$$\mathbf{A}_m = \begin{bmatrix} 0 & 1 \\ -\omega_n^2 & -2\zeta\omega_n \end{bmatrix}, \quad \mathbf{B}_m = \begin{bmatrix} 0 \\ \omega_n^2 \end{bmatrix} \tag{6.31}$$

The damping ratio for the second order model is usually, $0 < \zeta \leqslant 1$ and often set to 1. In this case the parameter matrices [139] are $\mathbf{A}_m = \begin{bmatrix} 0 & 1 \\ -\frac{16}{t_s^2} & -\frac{8}{t_s} \end{bmatrix}$, $\mathbf{B}_m = \begin{bmatrix} 0 \\ \frac{16}{t_s^2} \end{bmatrix}$, where t_s is the required step-response settling time for each case.

The adaptive weights of the controller can be set empirically starting from low values, $\alpha = 0.1$, $\beta = 0.01$, and increased to higher ones (by a factor of 10) if the adaptation is slow. It is reported [139], that suitable values for a servo-hydraulic test rig are $\alpha = 100$, $\beta = 10$. Keeping the weight ratio, $\frac{\alpha}{\beta} = 10$, usually ensures well damped error transients [130].

6.4 MCS Force Control

The second application of the MCS is the "Force MCS" used to control the hydraulic differential pressure (of the actuators) during the packing stage of the injection moulding cycle. This new scheme was initially tested in simulation using the non-linear model of the plant. A demanding task of this study was to avoid unwanted oscillations that can take place at the time of switching from "Flow to Force MCS" since the control signal should be continuous. Any fluctuations in the control signal could cause perturbations in the hydraulic pressure affecting the quality of the part, therefore a bumpless transfer algorithm was used for this task.

In the packing phase the plant has to follow a predefined pressure duty cycle from the start till the end of the packing phase. The initial condition for the reference model is determined at the time of the phase switch. The hydraulic differential pressure is monitored and the value during the phase switch is chosen. The maximum value of pressure that the reference model will reach is predetermined (depending on cavity size, clamping pressure, etc.). A servo-proportional P-Q valve with fast dynamics is used for the control of the hydraulic differential pressure. According to the linearised model (section 2.2.2.2) of the plant for pressure control, $\frac{p(s)}{x(s)} = \frac{K \cdot M}{A} \cdot \frac{s^2+b_1 \cdot s+b_0}{s^3+a_2 \cdot s^2+a_1 \cdot s+a_0}$, the model has a relative degree of 1 (1^{st}order dominant 3^{rd}order system). Following the assumption that a 1st order reference model can represent the plant pressure dynamics allowed a "1st order MCS" to be applied. It was expected that the 1st order model would sufficiently control the plant and ascertain the appropriate rate of adaptation. The "measurable" feedback state of the MCS loop is the hydraulic differential pressure.

The control scheme for the pressure MCS is shown in Figure 6.5. The reference model must be set to have faster dynamics than the plant with a damped behaviour (because of 1st order model). To determine the parameters of the model information is required about the response of the plant. Gain estimates from the linearised model for pressure control can be used, either the adaptive gains can be set to zero. To define how fast the plant should respond the model parameters should be adjusted accordingly. It is anticipated that during the adaptation procedure the plant poles will move in the direction of the model pole improving the response of the plant.

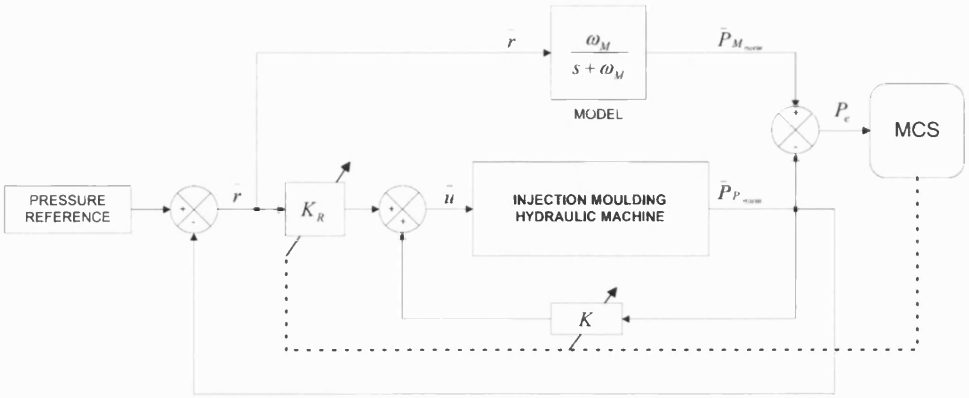

Figure 6.5: Pressure MCS & 1st order Model

By comparing the closed loop transfer function of the plant-controller for this case (1st order model) the parameters matrices A_m, B_m of the linear reference model,

$\dot{\underline{\mathbf{x}}}_m(t) = A_m \cdot \underline{\mathbf{x}}_m(t) + B_m \cdot r(t)$, can be set as:

$$A_m = -\omega_n, \quad B_m = -A_m \tag{6.32}$$

The adaptive weights of the controller α, β, can be set again empirically starting from low values, as described earlier on in this chapter.

6.5 Hydraulic Plant Identification

System identification is very useful in cases where plant uncertainties exist. The MCS identification algorithm ("MCS observer") allows the estimation of the plant parameter matrices $\{\mathbf{A}_p, \mathbf{B}_p\}$ and the unknown disturbance vector $\mathbf{d}$ (see eq.6.1) from the controller gains $\{K_R, \mathbf{K}\}$

where [142]

$$\mathbf{B}_p = \mathbf{B}_m \cdot \mathbf{K}_R^{-1} \tag{6.33}$$

$$\mathbf{A}_p = \mathbf{A}_m - \mathbf{B}_p \cdot \mathbf{K} \tag{6.34}$$

as long as,

- the reference signal is persistently exciting
- the controller gains have reached a steady-state condition
- the control signal is not saturated
- $\det(\mathbf{K}_R) \neq 0$.

Due to the nature of the injection moulding process at the start of the cycle a good tracking of the velocity reference model is required to keep the flow-front constant. This helps to maintain the mould filling uninterrupted without creating flow imbalances at the runners (multi cavity case). Since the filling phase usually last for a few seconds it would be an advantage to achieve fast adaptation of the MCS initially. In order to achieve that the adaptive gains should start from a predefined value be reduce the transient period. It has been reported in similar MCS applications (control of multi-axes tables) that a minimum time of 0.8-1s is required for the MCS to come near zero tracking error [133]. Although the injection moulding is a different application still fast adaptation from the beginning of the cycle would be an advantage especially in the case where the velocity reference would be more complex. Therefore it was decided that the "Flow MCS" could be tuned in advance for a range of velocities. To get the first estimate of the adaptive gains, the MCSIA observer was implemented in the injection moulding machine. The hydraulic system was excited using a velocity reference signal of 0.01m/s at a frequency of 10Hz.

For the case of the "Force MCS" no system identification was performed. During the packing phase the initial volume inside the cavity continuously changes giving rise to the cavity pressure. To run a system identification in this case, a very complex mould model would be required (in simulation) which would be very time consuming with no guaranteed result. For the above reasons it was decided that the "Force MCS" would be tested first in simulation with adaptation gains initially set to zero and if the behaviour was satisfactory then it would be implemented in real time.

6.5.1 Design of MCS Velocity Observer (Simulation)

The design of the MCS velocity observer was first implemented in simulation. A PID controller was used to control the velocity of the non-linear plant model (with no load) in parallel with PI position control. The latter was used to avoid position drift due to the unequal area actuator during the simulation and to maintain the same operating point. The command signal to the

plant was used as the reference model for the MCS Observer. The two measurable feedback states in the MCS observer's loop were plant velocity and acceleration. A schematic of the system identification is shown below in Figure 6.6.

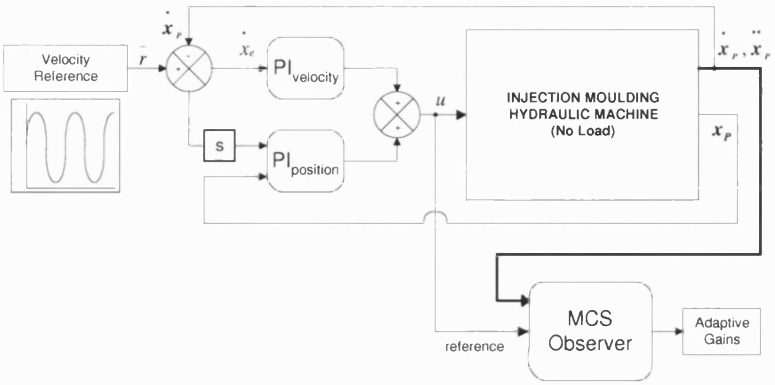

Figure 6.6: Schematic of Observer

The model of the observer is set to have very fast dynamics with a damped behaviour. Some more details are summarised below Table 6.1. The weighting parameters α, β are tuned empirically.

Natural Frequency (Hz)	Damping Ratio (ζ)	Model Gain	alpha	beta
150	0.9	1	0.015	0.0015

Table 6.1: MCS Observer Parameters

The first simulation results in Figure 6.7 show a good tracking of the model by the MCS observer. The gains of the MCS observer initially are initially set to zero and start immediately to evolve as soon as the system identification starts. By a closer inspection of Figures 6.7 & 6.8 it can be seen that after 14 iterations the error is minimum (at the -ve velocity) and the adaptive gains attain a steady state condition. However after the 15th iteration the observer's model starts to drift in contrast with the plant's output.

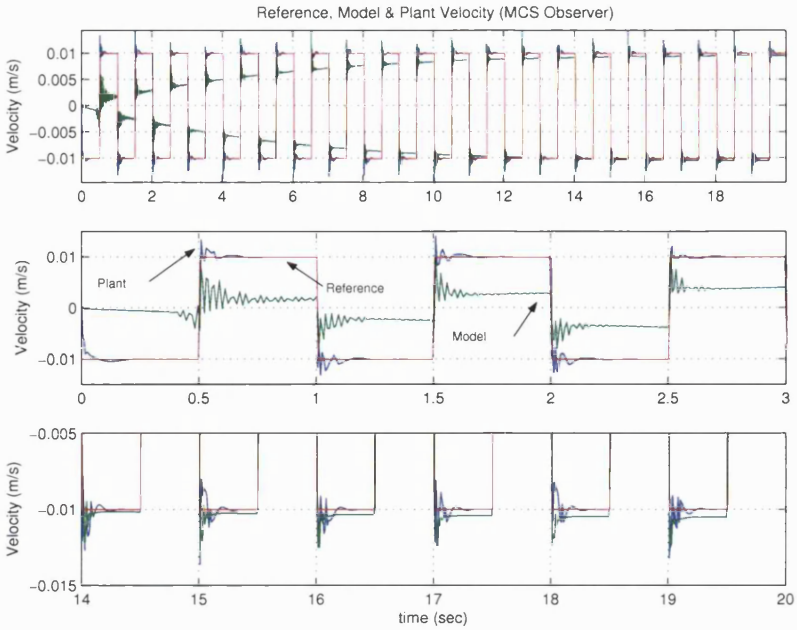

Figure 6.7: Reference, Model & Plant Velocity (MCS Observer)

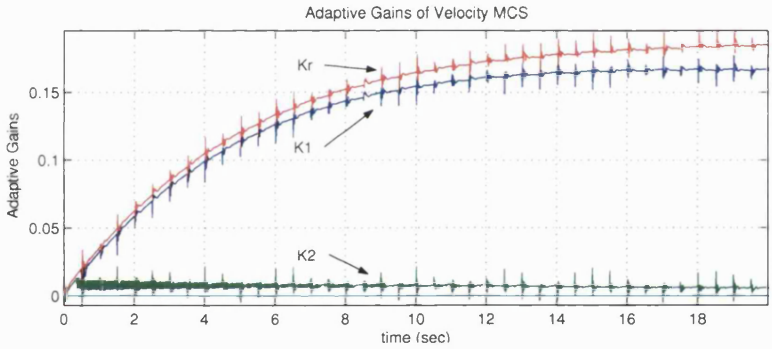

Figure 6.8: Adaptive Gains of Velocity MCS

To avoid the drift of the observer's adaptive gains that was experienced in the first simulation, an MCS with integral action (MCSIA) was used instead. In Figure 6.9 below it can be seen that the tracking error is minimum again after 14 iterations (on both +ve, -ve velocity reference) with no velocity drift as model reaches a steady-state condition.

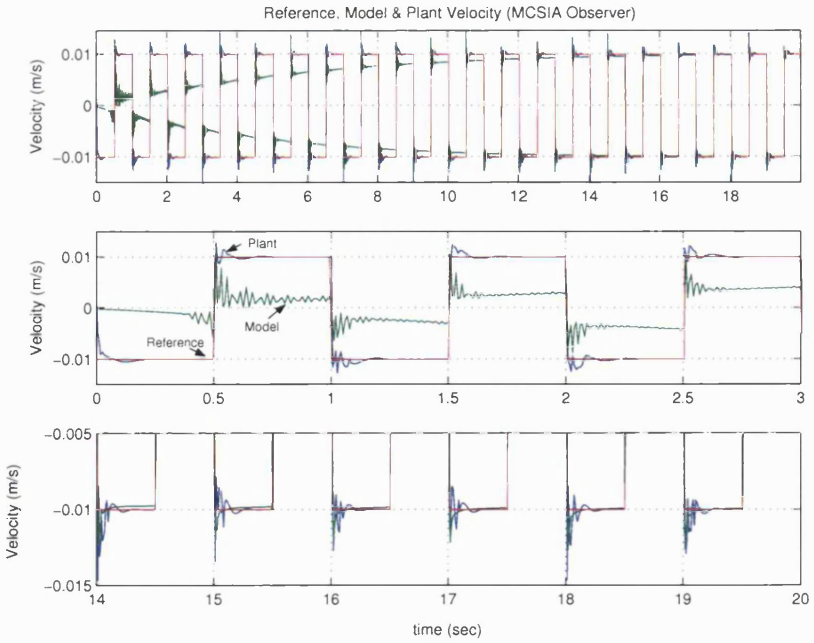

Figure 6.9: Reference, Model & Plant Velocity (MCSIA Observer)

The behavior of the adaptive gains with the MCSIA observer is shown in Figure 6.10. From the beginning of the identification the integral action reduces the error during the initial stage of the adaptation, part of which is due to the unequal area actuator.

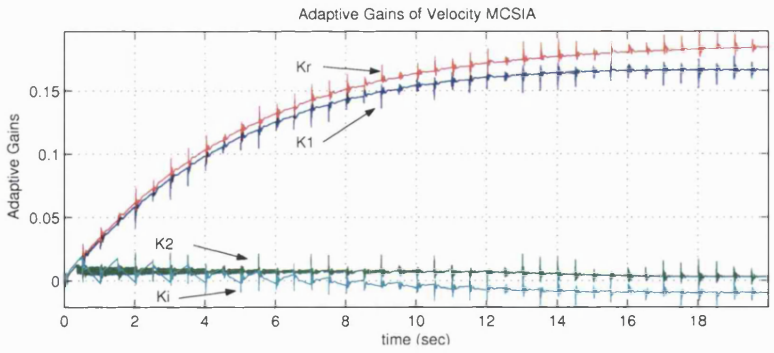

Figure 6.10: Adaptive Gains of Velocity MCSIA

6.5.2 Implementation of MCSIA Observer (Experimental)

A discrete PID controller was used to control the velocity of the screw during the identification stage. Again a PI position controller was connected in parallel to cancel out any position drift of the actuator. The injection barrel was kept empty at this stage (no load). The MCSIA

observer was connected again in the same configuration as in simulation. The adaptive gains were reset to zero and tuned for a range of velocity profiles (0.01 - 0.03 m/s). As previously performed in simulation the same reference signal (0.01m/s, 10Hz) was applied in the real plant and the identification procedure was monitored in real time. The MCSIA observer parameters were kept the same as in simulation. Some fine tuning in the PID and PI controller gains was performed. During the identification stage both the observer's model velocity and adaptive gains follow a similar pattern as previously predicted in the simulation. The MCSIA observer comes near to a zero tracking error after 14 iterations with no drift being noticed, as seen in Figure 6.11.

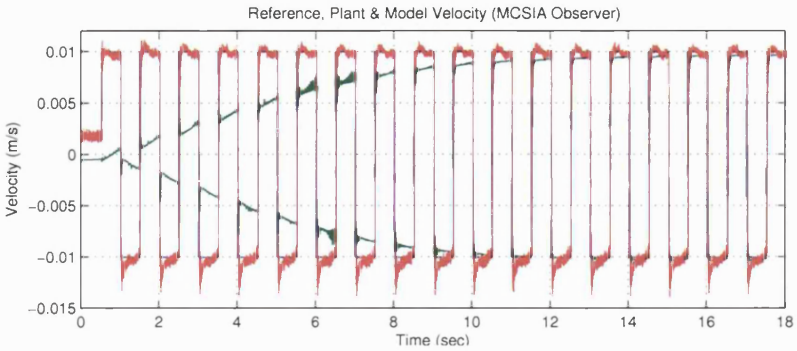

Figure 6.11: Velocity Tracking

In real time system identification an almost identical control response was achieved, however the adaptive gains as seen in Figure 6.12 were slightly higher. The difference in the adaptive effort reveals that there might be a small mismatch between the simulation and the real plant parameters or the fact that some non-linear effects may not have been included in simulation (actuator piston leakage, difference in bulk modulus, etc).

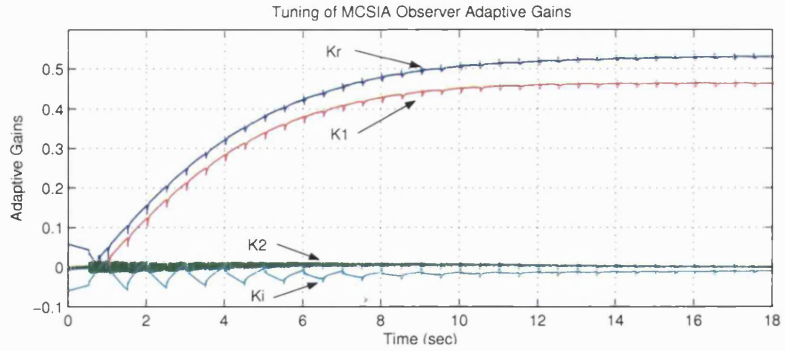

Figure 6.12: Tuning of MCSIA Observer Adaptive Gains

The hydraulic piston A_1 (low) and piston A_2 (high) pressures are shown in Figure 6.13. As it

can be seen from the graph the pressure signal is very clear with a minimum of noise. This is very important for the implementation of the " Force MCS" during the packing phase of the injection cycle.

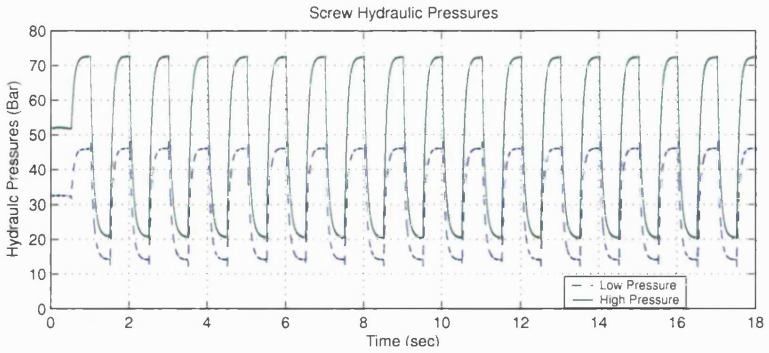

Figure 6.13: Screw Hydraulic Pressures

The command signal to the servo-proportional valve is shown below in Figure 6.14. The command signal includes the effort of both the PI and PID controller. The nature of the unequal area actuator of the injection moulding machine can be observed by the drive signal to the servo-proportional valve. On the extending of the ram the valve's spool supplies less flow to the annulus area of the actuator which is smaller than the annulus area when retracting.

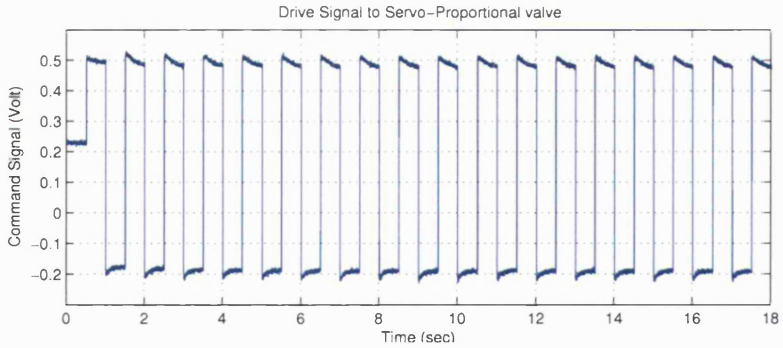

Figure 6.14: Command Signal to the Servo-Proportional Valve

6.5.3 Analysis of Velocity Identification Stage

A second order model was used in the identification stage of the MCS observer. The closed loop transfer function can be expressed as:

$$G_{M_{cl}}(s) = \frac{\frac{K_{R_{ID}} \cdot K_M}{1-K_{1_{ID}} \cdot K_M}}{\frac{T_M^2}{1-K_{1_{ID}} \cdot K_M} \cdot s^2 + \left(\frac{2 \cdot \zeta_M \cdot T_M - K_M \cdot K_{2_{ID}}}{1-K_{1_{ID}} \cdot K_M}\right) s + 1} \tag{6.35}$$

where, $T_M = \frac{1}{\omega_M}$. If the model parameters are compared with those of the linearised model of the plant (which has a relative degree of 2),

$$G_P(s) = \frac{K_{P_{est}}}{T_{P_{est}}^2 \cdot s^2 + 2 \cdot \zeta_{P_{est}} \cdot T_{P_{est}} \cdot s + 1} \tag{6.36}$$

it follows that:

$$K_{P_{est}} = \frac{K_{R_{ID}} \cdot K_M}{1 - K_{1_{ID}} \cdot K_M} \tag{6.37}$$

$$T_{P_{est}}^2 = \frac{T_M^2}{1 - K_{1_{ID}} \cdot K_M} \tag{6.38}$$

$$\zeta_{P_{est}} = \left(\frac{2 \cdot \zeta_M \cdot T_M - K_M \cdot K_{2_{ID}}}{1 - K_{1_{ID}} \cdot K_M}\right) \cdot \frac{1}{2 \cdot T_{P_{est}}} \tag{6.39}$$

6.5.4 Gain Estimation for "Flow MCS"

After the first system identification the reference model parameters can be estimated for the control of the plant. The MCS observer's adaptive gains that have attained steady-state condition during the identification can be used for the initial estimation of "Flow MCS" adaptive gains. During the plant identification there was no load (viscous friction during filling phase) considered. However it is expected that the MCS algorithm, with non-zero adaptive gains and appropriate weighting parameters set, will adapt rapidly to counteract this effect. Expressions for the calculation of the initial values for adaptive gains using steady values of adaptive parameters obtained from the identification stage are given in (eq: 6.40-6.42):

$$K_M = \frac{K_{R_e}^o \cdot K_{P_{est}}}{1 - K_{1_e}^o \cdot K_{P_{est}}} \Leftrightarrow \quad K_{R_e}^o = \frac{K_M}{K_{P_{est}}} \cdot \frac{T_{P_{est}}^2}{T_M^2} \tag{6.40}$$

$$T_M^2 = \frac{T_{P_{est}}^2}{1 - K_{1_e}^o \cdot K_{P_{est}}} \Leftrightarrow \quad K_{1_e}^o = \left(1 - \frac{T_{P_{est}}^2}{T_M^2}\right) \cdot \frac{1}{K_{P_{est}}} \tag{6.41}$$

$$\zeta_M = \left(\frac{2 \cdot \zeta_{P_{est}} \cdot T_{P_{est}} - K_{P_{est}} \cdot K_{2_e}^o}{2 \cdot T_{P_{est}} \cdot \sqrt{1 - K_{1_e}^o \cdot K_{P_{est}}}}\right) \Leftrightarrow \quad K_{2_e}^o = 2 \cdot \frac{T_{P_{est}}}{K_{P_{est}}} \cdot \left(\zeta_{P_{est}} - \zeta_M \cdot \frac{T_{P_{est}}}{T_M}\right) \tag{6.42}$$

The first estimated adaptive gains $K_{R_e}^o$, $K_{1_e}^o$, $K_{2_e}^o$ for studied model of the plant are summarised below in Table 6.2.

MCS Observer Gains			Estimated Adaptive Gains			
$K_{R_{ID}}$	$K_{1_{ID}}$	$K_{2_{ID}}$	$K_{R_e}^o$	$K_{1_e}^o$	$K_{2_e}^o$	$\zeta_{P_{est}}$
0.54	0.448	0.0005	2.231	-1.205	-0.011	0.55

Table 6.2: Estimated Adaptive Gains

6.6 Simulation of Hybrid MCS

The "Hybrid MCS" scheme was initially tested in simulation with the use of the non-linear model of the plant. Hybrid MCS was applied for the flow control of the filling phase and load control of the packing phase. The adaptive MCS algorithms were engaged successively at the start of each injection phase. This prevented the adaptive gains to drift and avoided parasitic effects from noise in the feedback states of the adaptive loop. The change of slope in the hydraulic or cavity pressure, was used to trigger the end of the filling and the commencement of the packing phase for which the duration was predetermined. During all other times (plasticization - cooling phase) a predefined $\simeq 0$ voltage was sent to the servo-proportional valve to offset any noise superimposed to the spool command signal. In this way the whole injection cycle was automated with the hybrid MCS scheme running in a sequence loop.

The "Flow MCS" algorithm was implemented using pre-estimated adaptive gains from system identification for the control of the filling phase. The "Force MCS" was realised with zero adaptive gains for the control of the packing phase. Both controllers were coupled in a "Hybrid MCS" scheme using a "Bumpless Transfer Algorithm" the objective of which was to match the adaptive drive signal during the phase change and suppress any oscillatory behavior of the feedback states.

6.6.1 Tuning of the "Flow MCS" Response

The standard form of the minimal controller synthesis algorithm was used with integral action and magnitude insensitivity (termed 'MCSIA'). The reason that the integral component used was because during the identification stage the MCSIA out-performed the traditional MCS. A second order reference model was used and a pragmatic choice of $C_E = [\omega_n \ \ 1]$ vector, while the adaptive gains (Table 6.2) were estimated from the system identification. The behaviour of the reference model was chosen to have fast dynamics coupled together with a damped behaviour ($\zeta = 0.9$). The model of the system given by a 2nd order transfer function (with servo-proportional valve drive as input and velocity as output) was approximated from real data obtained by feeding a chirp signal to the system. It should noted that identified natural frequency was estimated without the mould consequence. The natural frequency of the real plant according to a system identification procedure that was carried out using the "System Identification Toolbox in Matlab" was found to be 44Hz (section 2.2.2.3). The model's natural frequency was set at 150Hz which is about three times greater than the identified plant's natural frequency. This has the aim of achieving a system that adapts quickly to sudden disturbances and viscous load variations that occur during the filling phase. The adaptive weights α, β were tuned empirically. Parameters of the reference model and initial values for adaptive gains of Flow MCS selected on the basis of the identification stage are given below in Table 6.3.

Natural Frequency	Model Gain	Damping Ratio	alpha weight	beta weight
$\omega_M\,(Hz)$	K_M	ζ_M	α	β
150	1	0.9	0.015	0.0015

Forward Adaptive Gains	Feedback Adaptive Gains	
K_R	K_1	K_2
2.231	-1.2	-0.011

Table 6.3: Parameters of the Filling Reference Model

6.6.1.1 Simulation of Flow MCS

During the first simulation of the "Flow MCS" the plant exhibited an oscillatory behaviour during the filling phase. Since the main objective of the controller was to control the set-point velocity any changes to the stiffness of the mould would result in change in velocity, which would in turn be controlled by the "Flow MCS" scheme. This implies that for set-point flow control there is no need to use a higher order, 3^{rd} order MCS (more complex) which incorporates position feedback. Since the acceleration of the screw was measurable an additional acceleration feedback was initially considered in the MCS structure, which had 2^{nd} order model. Simulation studies showed that for the given controller arrangement that

included acceleration feedback, the set-point tracking was unstable. Presumably the reason for this instability originates from the mismatch between model (2^{nd} order) and the plant (3^{rd} order) due to the mould stiffness. In addition, different dynamics in the mould change the overall plant dynamics which does not always fit the model.

A solution to this problem was given by weighting the acceleration differently than the velocity feedback, a tactic which is closer to the MRAC approach. Stability over a wide range of operating conditions for the plant was guaranteed by setting the acceleration feedback to be 100 times smaller than that of the model. The weight ratio of the adaptive gains was initially set at, $\frac{\alpha}{\beta} = 10$. However it was observed that for higher values of the velocity demand, the plant exhibited more oscillatory behaviour during the transient period. The transients were improved by increasing the adaptive weight parameters ratio, $K_{\alpha,\beta}$, from 10 to 50 with a small compromise in the tracking error. The command signal to the plant was also filtered with a low pass filter (150 Hz) to smooth some sharp transients coming from the adaptive effort of the second state (acceleration feedback). This introduced a small time lag in the control loop, but with no serious consequences in the overall performance. The parameters used for the reference model are summarised in Table 6.4 below. The adaptive gains for the case with the weighted acceleration state were set to start from zero initial conditions.

Natural Frequency	Model Gain	Damping Ratio	alpha weight	beta weight
$\omega_M\,(Hz)$	K_M	ζ_M	α	β
150	1	0.9	0.05	0.001

Table 6.4: Filling Reference Model Parameters with Weighted Acceleration Feedback

With the new reference model parameters the response of the controlled system was significantly improved. Further simulation studies were also carried out with one state feedback (MCSIA with magnitude insensitivity). The reference model parameters are presented in the Table 6.5 The weighting parameters alpha and beta were tuned again empirically with the adaptive weight ratio, $K_{\alpha,\beta}$, set at 40.

Natural Frequency	Model Gain	Damping Ratio	alpha weight	beta weight
$\omega_M\,(Hz)$	K_M	ζ_M	α	β
150	1	0.9	20000	500

Forward Adaptive Gains	Feedback Adaptive Gains	
K_R	K_1	K_2
2.231	-1.2	-0.011

Table 6.5: Parameters of the Filling Reference Model with One Feedback State

In both situations the plant behaviour was similar, with the latter case being less oscillatory in the transient period. Robustness of the "Flow MCS" with single and dual state feedbacks were tested for a series of different velocity trajectories (0.01-0.02-0.03-0.04m/s) and found to have a very good adaptation behaviour. In Figure 6.15 the velocity transient response of the plant with the MCS with dual state feedback is presented. The filling velocity is set at 0.02 and 0.04m/s at the upper right and left windows respectively. At the lower windows velocity disturbances that occur due to the rise in the viscous friction (as the cavity is filled) are highlighted. After each disturbance the velocity error is quickly reduced to zero due to the adaptive effort of the MCS.

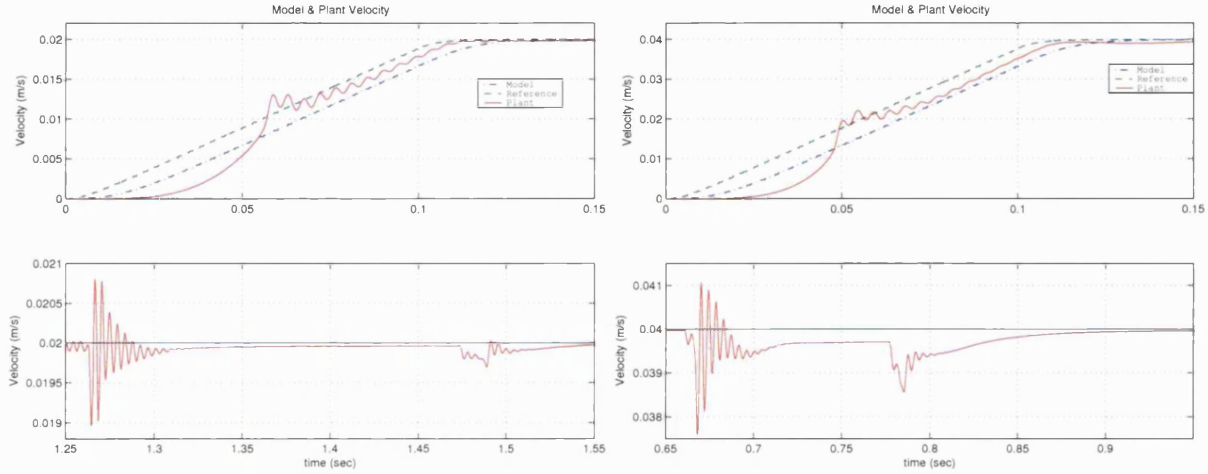

Figure 6.15: Model and Plant Velocity Response with Dual State Feedback MCS

In Figure 6.16 the same case as shown in Figure 6.15 is presented but now with the MCS with single state feedback.

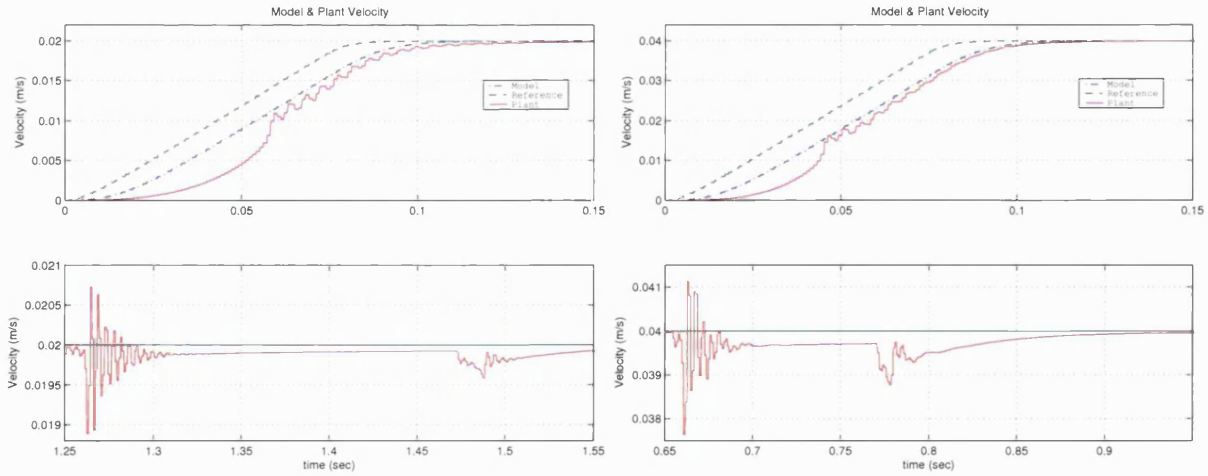

Figure 6.16: Model and Plant Velocity Response with Single State Feedback MCS

Due to the lack of the acceleration feedback the transients are less oscillatory however it takes longer for MCS to reduce the error back to zero. Overall the MCS with single state feedback provides a more stable plant behaviour when compared with the dual state feedback MCS case. Different model natural frequencies were also tried ($\omega_P = \frac{\omega_M}{2}$, $\omega_P = \omega_M$, $\omega_P = 2 \cdot \omega_M$) but the response of the plant in most situations became very sluggish and as a result the adaptive weights needed to be re-tuned. The adaptive gains in the case of MCS with single state feedback reached values of a steady-state condition which were higher than the initial estimate as can be seen in Figure 6.17 (in 0.02 & 0.04m/s case). These values can be used to replace the first estimation of gains and improve the adaptation dynamics of the MCS in the next cycle. In the second case where the velocity setpoint was higher (0.04m/s) the adaptive effort was greater as well.

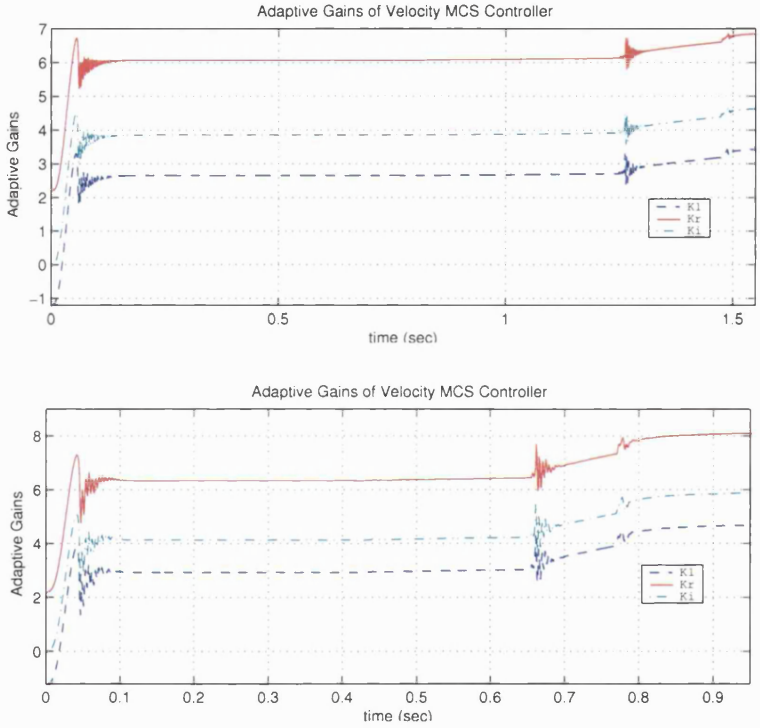

Figure 6.17: Adaptive Gains with Single State Feedback MCS

6.6.2 Tuning of "Force MCS" Response

For force control the standard form of the minimal controller synthesis algorithm with integral action was used. The normalised differential hydraulic pressure of the plant was used as the *scalar* feedback state. The second state (1st derivative of the plant ΔP pressure) of the plant, the unfiltered derivative of pressure was not suitable for control purposes in the real system, because of the pump's pressure ripple in the hydraulic line being superimposed on true signal.

For this reason and the fact that the linearised pressure model had relative degree of one, a first order reference model was used and a pragmatic choice of $C_E = [1]$ was selected. The adaptive gains were set to start from zero values. The behaviour of the adaptive model was chosen to have relatively fast dynamics coupled with a damped behaviour ($\zeta = 1$). The model natural frequency was set at 100Hz, which is almost twice the plant natural frequency during the filling phase. The parameters of the reference model and adaptive gain initial values are summarised below in Table 6.6.

Natural Frequency	Model Gain	Damping Ratio	alpha weight	beta weight
$\omega_M\,(Hz)$	K_M	ζ_M	α	β
100	1	1	100	10

Table 6.6: Parameters of the Packing Reference Model

6.6.2.1 Simulation of "Force MCS"

The first simulation of the "Force MCS" algorithm was performed using a simple design to change from one adaptive scheme to another (Flow to Force MCS). The hydraulic differential pressure was used as the trigger signal to switch to the packing phase. The reference model was set to have a first order exponential behaviour with a settling time of 4 seconds. The maximum differential pressure was set at 40bar. Reference model initial pressure condition was set to zero.

On the left hand side of Figure 6.18 the plant's (ΔP) hydraulic pressure tracked sufficiently well the reference model and eventually reduced the tracking error to zero over 0.2 seconds. However at the time of the switching (velocity to pressure control) there was an associated delay of 0.025s, for the reference model to reach the plant differential pressure. This occurred because the integrator of the reference model was set to start from zero bar pressure. Consequently there was a large (+ve) initial pressure error with a high adaptive effort required to improve the tracking.

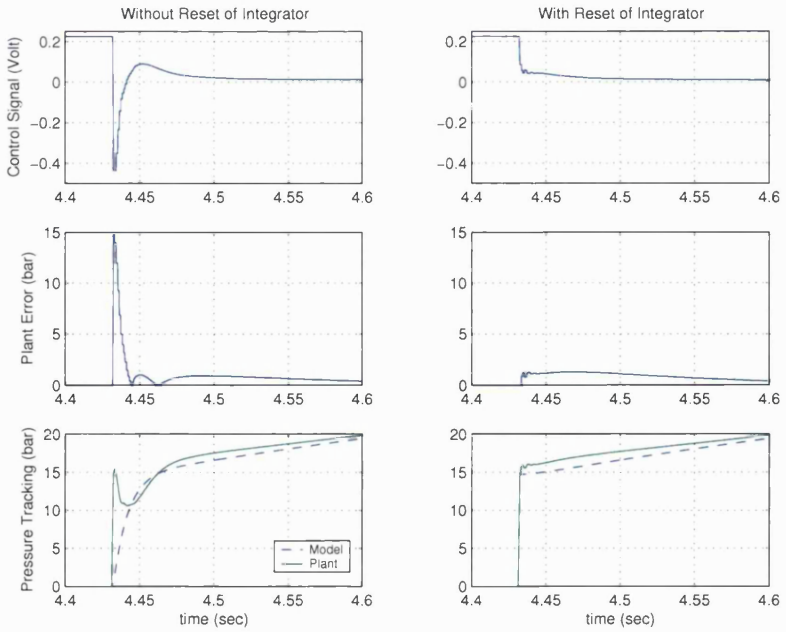

Figure 6.18: Reset of Discrete Model Integrator

To eliminate this transient, which potentially degrades the packing performance the discrete time integrator of the reference model was reset to the plant differential pressure at the time of switching. A schematic illustration of the 1st order model is shown in Figure 6.19.

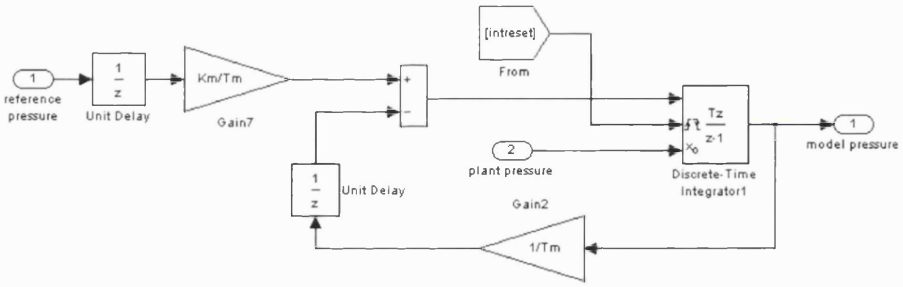

Figure 6.19: Reset of 1st Order Model Integrator

With the reset of the integrator during the switch, the tracking error was minimised. It was expected that less adaptive effort would be required and unwanted oscillations that occurred in the velocity of the plant would be considerably damped. With the integrator reset, the command signal after the switch decays gradually to zero controlling the pressure of the plant smoothly (R.H.S of Figure 6.18).

Overall the Force MCS algorithm was found to have robustness for a wide range of (ΔP) pressures from 20 to 60bar. Although the adaptive gains started from zero, then adapted sufficiently fast to minimise the tracking error. The adaptive weights were tuned empirically (first used in simulation).

6.6.2.2 Internal Monitoring of Velocity Control

Another important factor that must not be overlooked during packing is the screw velocity, regardless of the fact that the main controlled parameter is pressure. As the gate solidifies at the end of packing it is not possible to inject any further material inside the mould cavity, and the screw velocity decreases to a very low value close to zero. Before the screw stalls, the "Force MCS" must be stopped otherwise the pressure error will increase rapidly and the controller's effort will increase rapidly, driving the system unstable. In Figure 6.20 the packing phase takes place over the period of 8.28 to 10.5 seconds while the plant velocity becomes highly oscillatory as the "Force MCS" tries to minimise the tracking pressure error at the end.

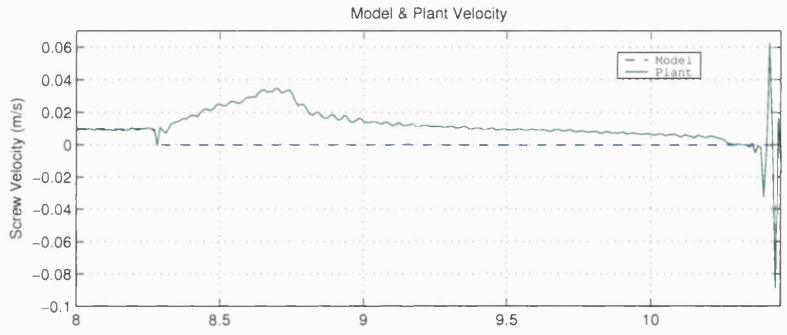

Figure 6.20: Oscillatory Behaviour of Velocity at the end of Packing Phase

The same situation might also occur if the initial material (shot) size during the plasticization phase is less than that required. Therefore the screw at the end of its travel will hit the nozzle and stall. This new extension of the MCS algorithm with internal monitoring of velocity will stop the adaptation on time and guarantee stability.

6.7 Improvements of Packing Phase & Associated Feedback Noise in the Force MCS

Resetting the integrator of the Force MCS proved to be an effective way for removing unwanted transients and ensuring a smooth transition between the injection phases. However noise can have a particularly damaging effects in the MCS because the algorithm tends to adapt to the noise present in the feedback signals. In addition, the pressure feedback has a bandwidth sufficiently high that it includes the noise coming from the hydraulic pump. Therefore the adaptive gains can drift which would not be the case if the system had no noise at all.

So, in order to enhance the bumpless transfer algorithm and improve the noise problem, a variation of the adaptive weights during the cycle would be beneficial. This means that the adaptive weights can increase or decrease the adaptive effort according to the requirements of the plant. To achieve this the adaptive effort of the MCS was mapped with the tracking error of the plant. This method was initially tested in simulation where the adaptive weights were set to start either from zero or from their maximum level. Results showed that the problem of feedback noise from the sensors to the MCS must be taken under consideration during initial design of the controller. Although the MCS performed really well with no noise, in the presence of noise it became unstable.

6.7.1 Fixed Weighting Parameters alpha and beta

In the first simulation the hybrid MCS was tested with the adaptive weights held constant during the packing phase. The adaptive gains were reset to higher ones after a few simulations to reduce the tracking error. White noise was superimposed on the pressure feedback to the MCS to match the level measured on the test rig. The adaptive weighting parameters alpha and beta were set to 100 and 10 respectively and kept constant. During the adaptation the tracking error reduced to zero withing 0.6 seconds and stayed low until the controller became unstable. The adaptive gains as seen in Figure 6.21 started picking up the noise from the feedback state immediately after the start of the adaptation.

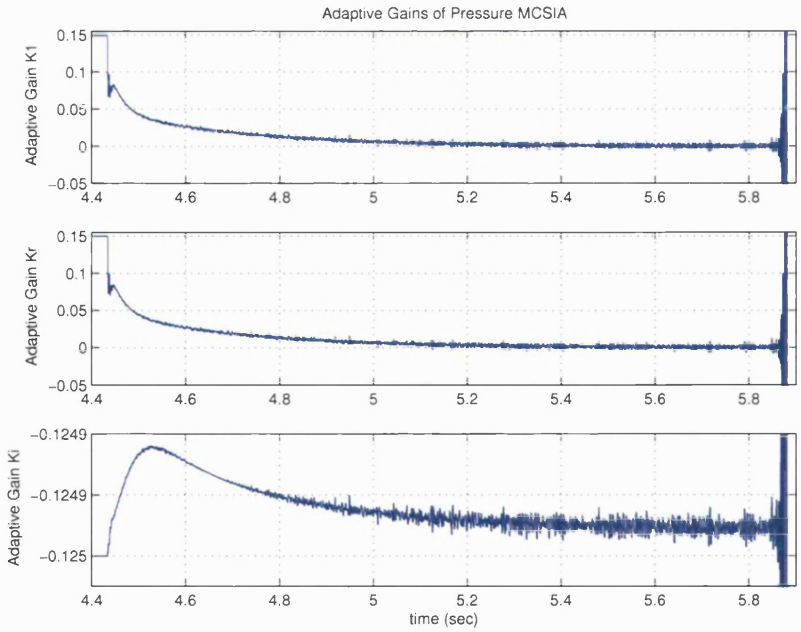

Figure 6.21: Adaptive Gains of MCSIA

At 5.9 seconds the tracking error increased considerably saturating the servo-valve drive signal as seen in Figure 6.22. Despite the instability occurrence, at the end of the packing phase it can be seen that the MCS algorithm tracked the pressure reference trajectory well.

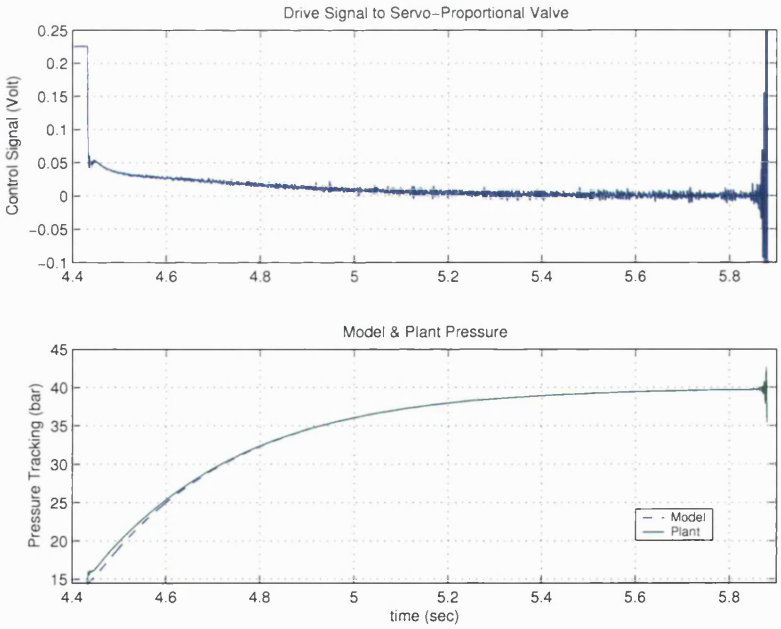

Figure 6.22: Command Signal and Pressure Tracking

6.7.2 Adaptive Weights Vs Error Rate

In next group of simulations the new method of variable adaptive weights was tested. It was clearly observed that the scheme produced better results over the fixed adaptive weight case. Adaptive coefficients, α, β, were proportional to the plant's tracking error and were set empirically. Two different cases are presented in the two following two subsections 6.7.2.1 and 6.7.2.2, with the adaptive weight initial conditions set to zero and high values respectively.

6.7.2.1 Zero Initial Adaptive Weights

The adaptive weights started from 0 with purpose to guarantee a smooth transition from one phase to the another and also to release the adaptive effort gradually. On the other hand because these factors were error dependent the values of alpha and beta could be set at very large values compared with the case where they were fixed. In Figure 6.23 the adaptive weights reached a high value of alpha (240) and beta (24) minimizing the tracking error. If the error is now compared with the previously presented case (with fixed alpha 100 and beta 10) it can be observed that although the error might be 40% higher for a fraction of time it reduced faster to zero, with the adaptive effort reducing to zero as well.

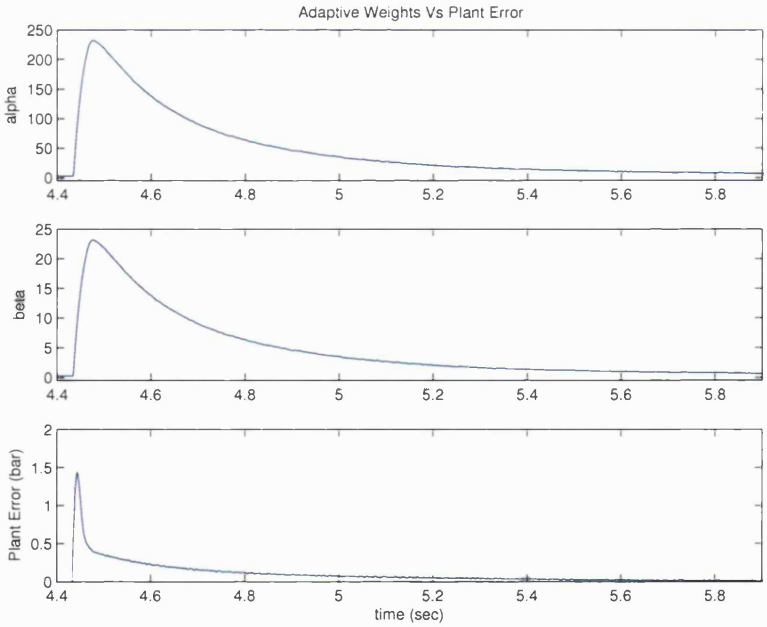

Figure 6.23: Variable Weighting Parameters

Since the adaptive effort is minimised gradually, the noise in the feedback states is not amplified

by the adaptive gains that decay (K_1 *and* K_R) back to zero (for K_r, K_1 case) as shown in Figure 6.24.

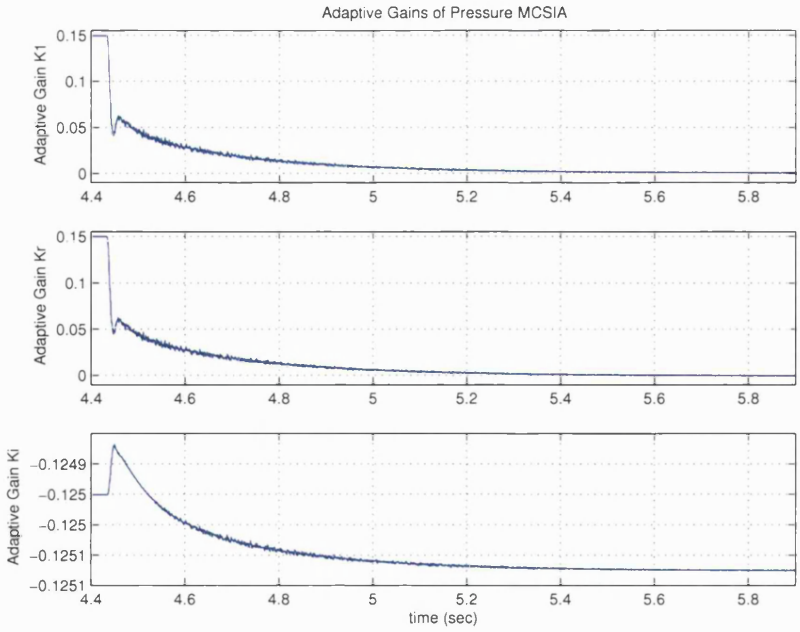

Figure 6.24: Adaptive Gains of MCSIA

As a result a smoother transition is achieved, without saturating the drive signal.

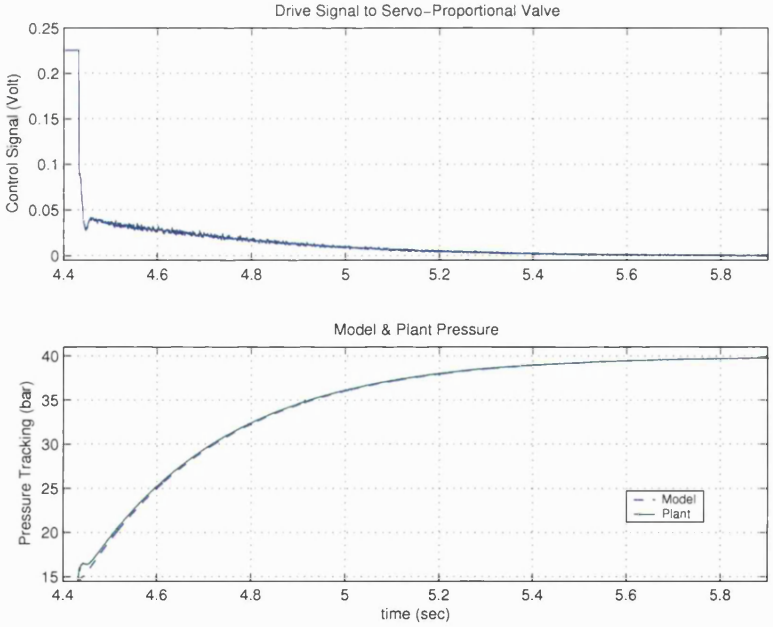

Figure 6.25: Command Signal and Pressure Tracking

In addition, if the pressure tracking in Figure 6.25 is compared with the previous case (Figure 6.22 $\alpha = 100$, $\beta = 10$) it can be seen that the plant achieves a better tracking of the reference model at the beginning (from 4.45s to 4.8s).

6.7.2.2 High Initial Adaptive Weights

In this case the adaptive weights were set to start from high values ($\alpha = 250$, $\beta = 25$, $K_{\alpha,\beta} = 10$) to examine the effect that they have during the transition and on the tracking error. In this case the plant error was substantially decreased, since the adaptive effort has a instant effect at the time of switching between phases. Again the high adaptive weights at the beginning of the packing phase, Figure 6.26, reduced rapidly the tracking error to zero while thereafter the adaptive effort of the MCS was set low as the error was considerably small.

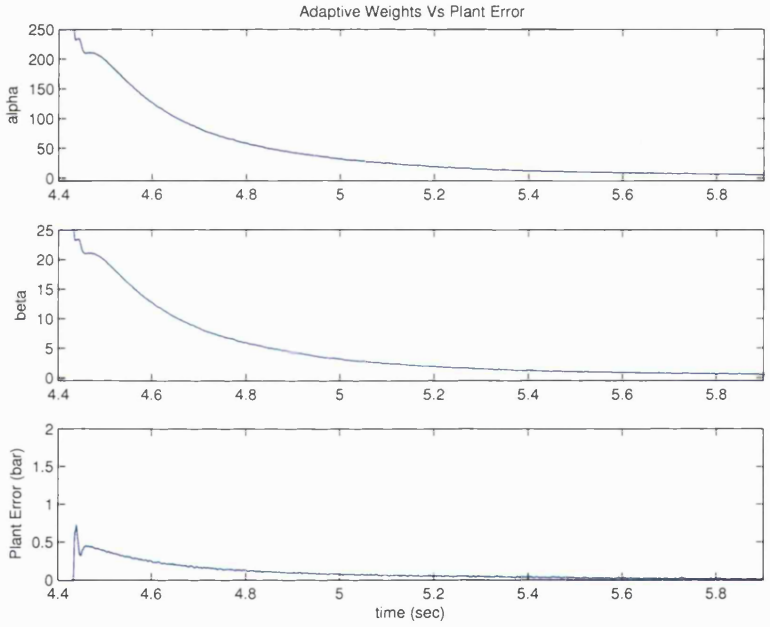

Figure 6.26: Variable Weighting Parameters

The adaptive gains for this case are presented in Figure 6.27. The downside of setting the adaptive weights high initially was that the adaptive gains (K_1 *and* K_R) undergo a large transient during the switching stage.

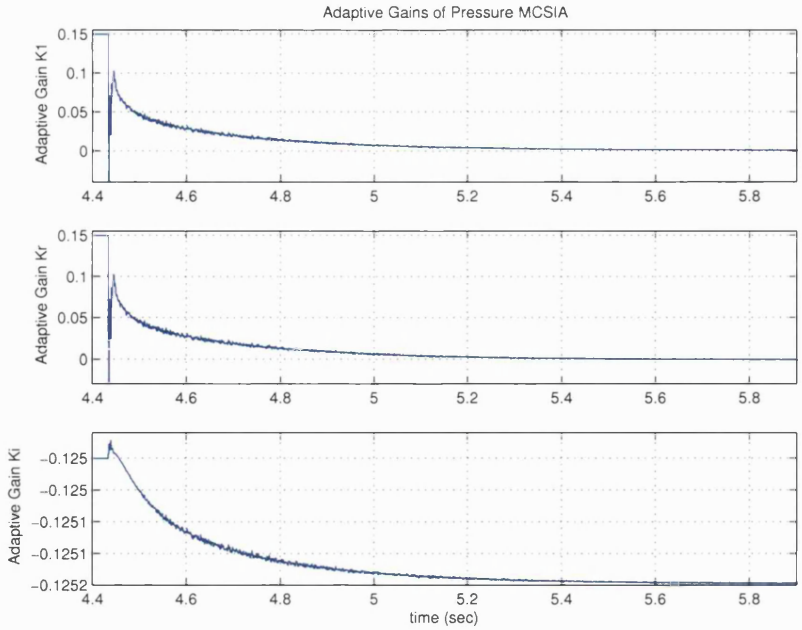

Figure 6.27: Adaptive Gains of MCSIA

Consequently these gain transients have a direct effect on the MCS control signal to the valve which value goes negative, as seen in Figure 6.28.

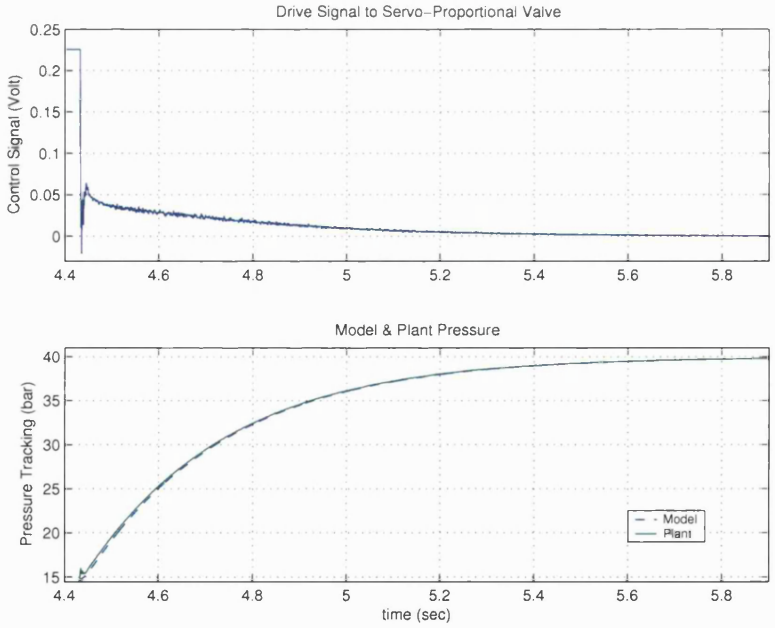

Figure 6.28: Command Signal and Pressure Tracking

This has a more dominant effect in the plant's velocity that may become oscillatory and drive the system unstable, when the plant is still under pressure control. Overall the tracking error was rapidly reduced (from 4.45s to 4.6s) to zero where the plant followed closely the reference signal. In the simulation studies it was shown that the variable adaptive weights, α, β, can dramatically reduce the noise sensitivity problem of the MCS scheme. The adaptive effort was safely increased (doubled) when the error was large and reduced to low levels when the error was small. The plant pressure error was efficiently reduced without saturating the drive signal since the higher adaptive effort was only available when the tracking error was large.

6.7.3 Adaptive Gains Safety Limit

In the presence of noise in the feedback signal it is likely that if the MCS algorithm is not properly tuned the system may become unstable. A quick modification in the MCS enabled accommodation of such cases where the adaptive gains reach excessive values. Such conditions were examined in simulation showing that this measure was very effective, especially in the initial stage where the MCS algorithm is being commissioned and tested for a new plant. Once a safety limit is reached the adaptive gains are reset to their initial conditions and adaptation can start again. The safety limit for this test was set empirically since from simulation the operating window of the adaptive gains was known. Two different cases are presented in the two following subsections 6.7.3.1 and 6.7.3.2 describing results obtained with and without the adaptive gain safety limit action.

6.7.3.1 Without Gain Limit

In Figure 6.29 the adaptive gains of the "Force MCS" started to become unstable around 4.7 seconds in the presence of noise in the feedback signal. In the controller's effort to reduce the plant's error the gains reached excessive limits, around 400% larger than usual.

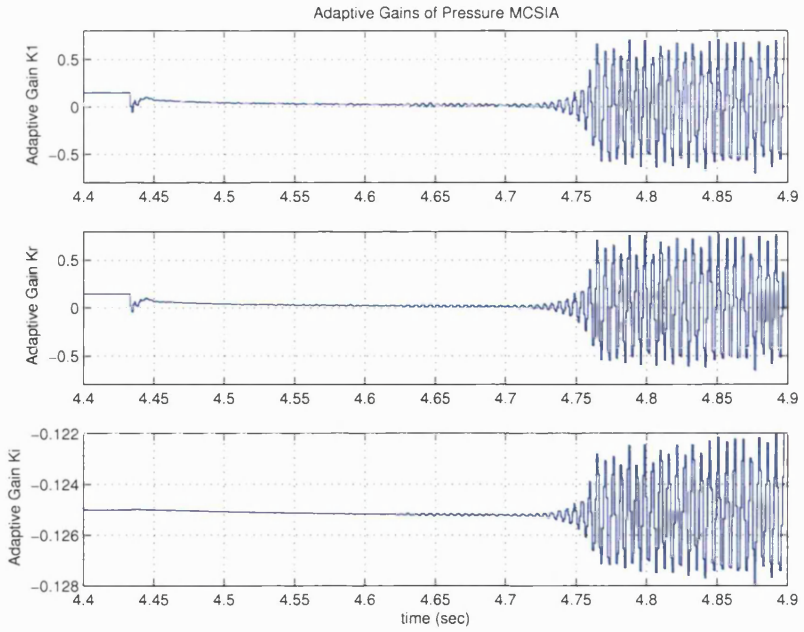

Figure 6.29: Adaptive Gains Case Without Gain Limit Safety

Consequently the MCS control signal became oscillatory driving unstable the system as it can be seen in Figure 6.30. This effect was more noticeable in the velocity profile of the plant rather than in the pressure which was the controlled parameter.

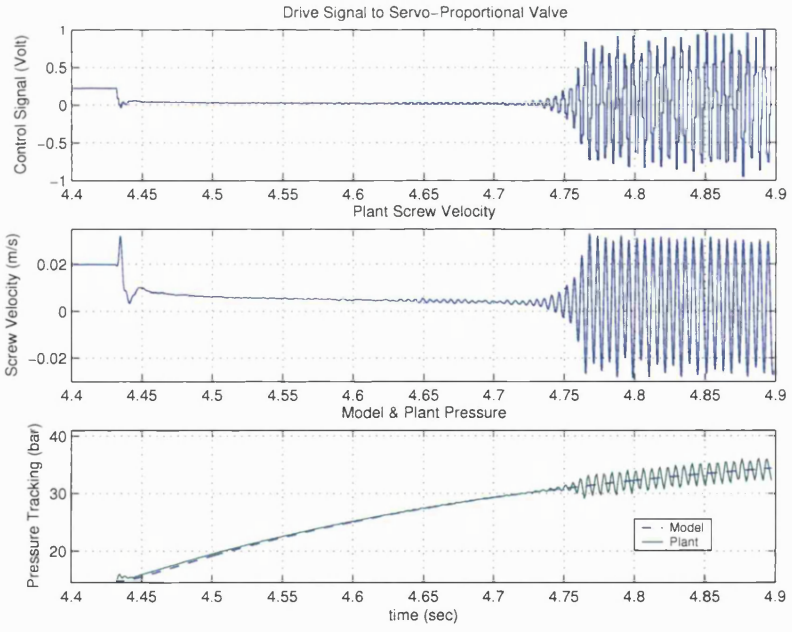

Figure 6.30: Drive Signal - Screw Velocity - Pressure Tracking

6.7.3.2 With Gain Limit

In this simulation the same operating plant conditions were used as in previous section, with the MCS safety limit action enabled. The maximum value of the adaptive gains was set. It can be seen in Figure 6.31 that the system becomes oscillatory around 4.7 seconds. However once the gains exceeded the permissible level they were reset back to zero to prevent valve saturation.

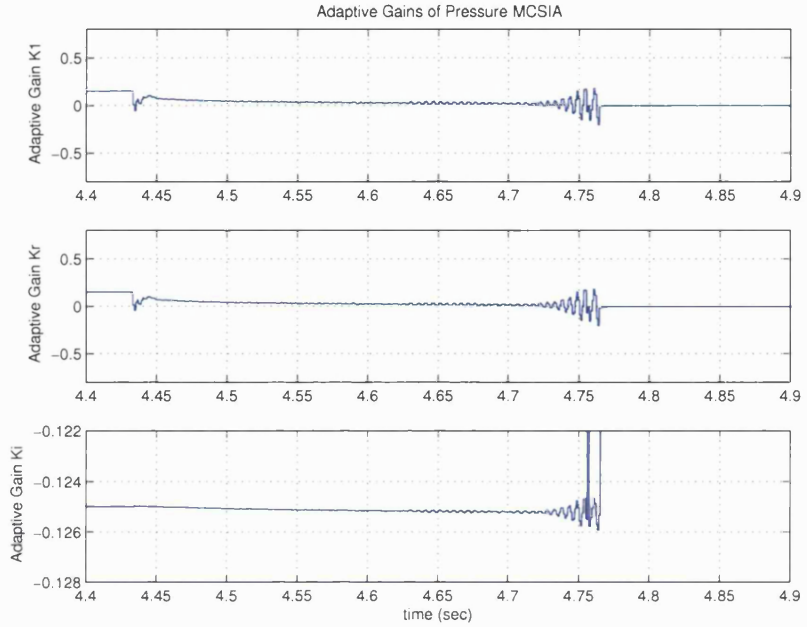

Figure 6.31: Adaptive Gains of Pressure MCSIA

Once the process is stopped the control engineer can identify the cause of instability and reevaluate the parameters of the MCS algorithm. In Figure 6.32 it can be observed that the velocity of the plant became zero while the trapped hydraulic pressure holds the plant pressure at 30bar.

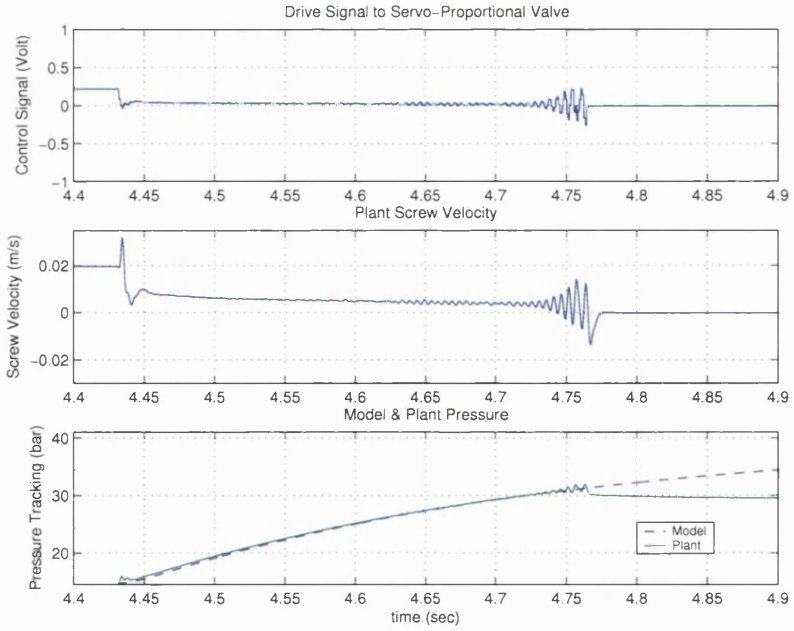

Figure 6.32: Drive Signal - Screw Velocity - Pressure Tracking

6.8 Implementation of Hybrid MCS

So far in simulation the hybrid MCS performed well with promising results for the control of the filling and packing phase of the injection moulding cycle. For this reason it was decided to verify the suitability of the proposed scheme in the real plant. The Simulink model of the hybrid MCS was implemented in the hydraulic plant of the injection moulding machine via Real Time Windows Target of Matlab.

The first experiment was performed with the same hybrid MCS parameters as used in simulation. The "Flow MCS" was used with a weighted acceleration feedback state (2nd order MCS with 2 feedback states, velocity and acceleration) while the "Force MCS" was used with one feedback state (pressure). In the experiments two different shape specimens (rectangular cavity shape in this chapter and tensile specimen cavity shape described in Chapter 7) were moulded with low and high viscosity polypropylene. A range of trigger signals (hydraulic pressure, cavity pressure, ultrasound) were used to initiate the start of the packing phase with the ultrasound trigger found to be the most accurate.

In section 6.8.1 the first experiment is described in which low viscosity polypropylene was used as the moulding material. A rectangular shape cavity was used with the gate at the centre of the part. This section also describes the initial tuning of the hybrid scheme by altering

the weighting parameters of the MCS. In section 6.8.2 the second experiment is described in which high viscosity polypropylene was used. This altered the viscous load conditions during the filling and packing phase of the cycle. To examine the robustness of the hybrid MCS algorithm a variety of reference setpoints and trajectories were used for the flow and pressure control of the plant. The more intelligent version of the "Force MCS" was implemented with variable adaptive weights dependent on the pressure error of the plant. The efficiency of this method and advantages that has in a real plant are justified. The overall performance of the hybrid MCS is summarised in the concluding section.

6.8.1 Moulding of Rectangular Part with Low Viscosity Polypropylene

To test the suitability of the proposed bumpless transfer in the real plant the adaptive weight parameters α, β of the force MCS were set to lower values ($\alpha = 15$, $\beta = 1.5$) than those used in simulation for safety reasons. In the first trial there was poor tracking of the velocity reference signal and the adaptive gains (of the Flow MCS) reached higher values than those initially predicted. This was anticipated since the first estimate of the adaptive gains was made without taking into account the materials viscous friction during the filling phase.

To reduce the transient error, the settled steady state adaptive gain values from the first test were used for the start of the next one. The response was greatly improved with good velocity tracking at the setpoint of 0.01m/s, as seen in Figure 6.33.

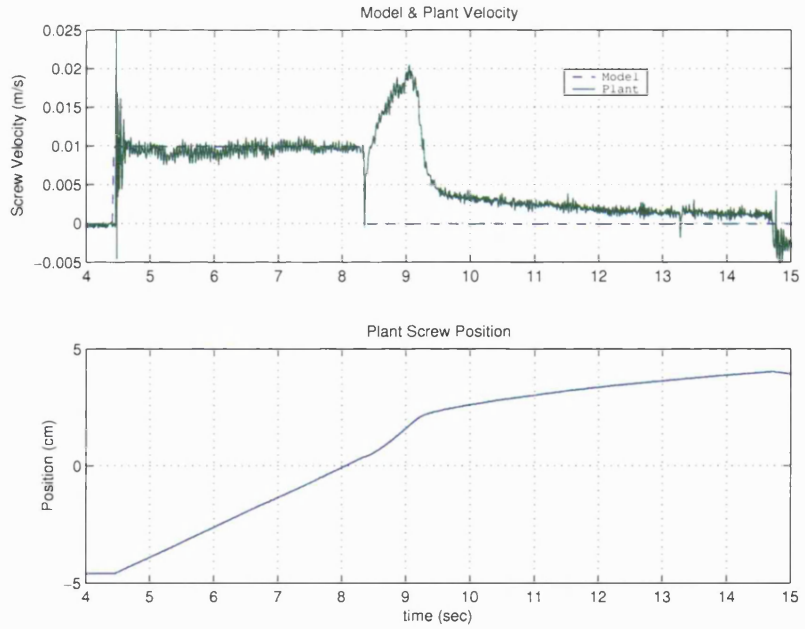

Figure 6.33: Model & Plant Velocity Response during the Injection Cycle

At the start of the injection there is an overshoot in the velocity of the screw which mainly comes from the adaptive effort of the acceleration feedback state. Similar behaviour was observed in simulation tests as well. However this transient settles fast (within 0.2s). The position of the screw, also shown in the figure, has a constant slope for the duration of the filling phase. During the packing phase the slope changes continuously as the velocity decays to zero.

The adaptive gains during the filling phase, Figure 6.34, change in order to maintain the velocity constant regardless the nonlinear behaviour of the viscous friction and stiffness of the polymer melt inside the injection barrel. The effort of the second state is less dominant because the acceleration state is weighted to guarantee stability.

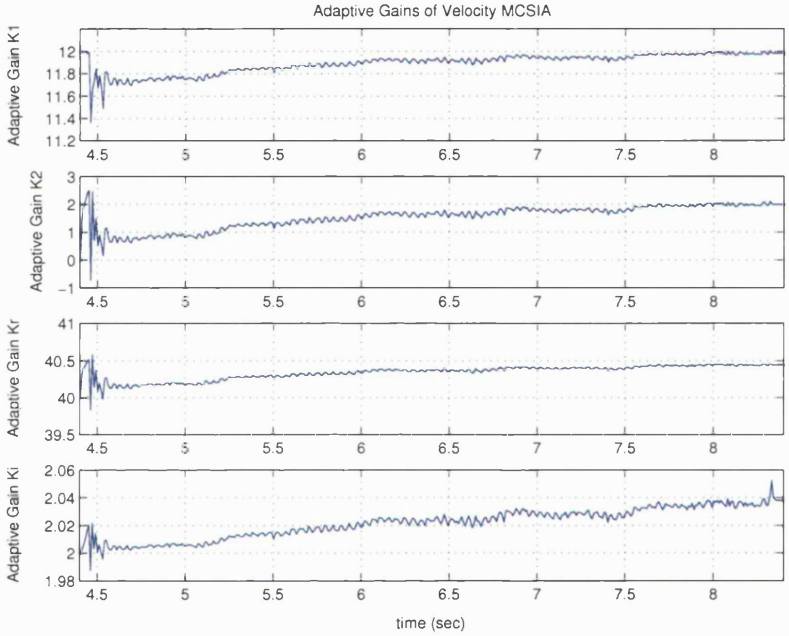

Figure 6.34: MCSIA Velocity Gains

The reference model for the packing phase was set to have a maximum value of 70bar with 4s settling time. As it can be seen in Figure 6.35 the tracking of the pressure reference signal was poor suggesting that higher values of the weight parameters, α and β, could be used (as in simulation, $\alpha = 100, \beta = 10$).

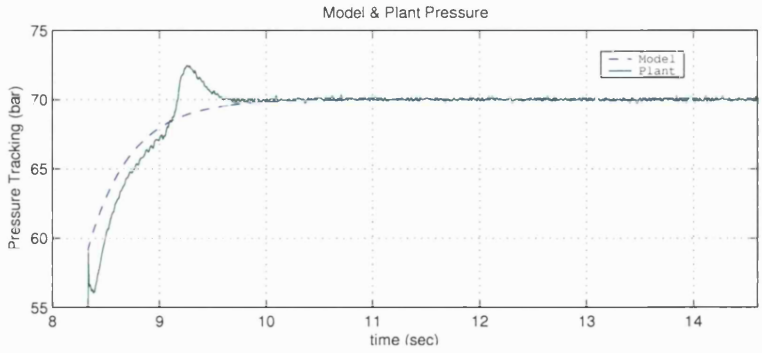

Figure 6.35: MCSIA Pressure Tracking

As shown in Figure 6.36 the adaptive gains K_I and K_R reached their maximum value of 0.37 and 0.51 respectively at the point where the pressure error was maximum. If these values were set as the initial conditions (for the adaptive gains), would help the MCS to adapt faster and reduce the transient error to zero.

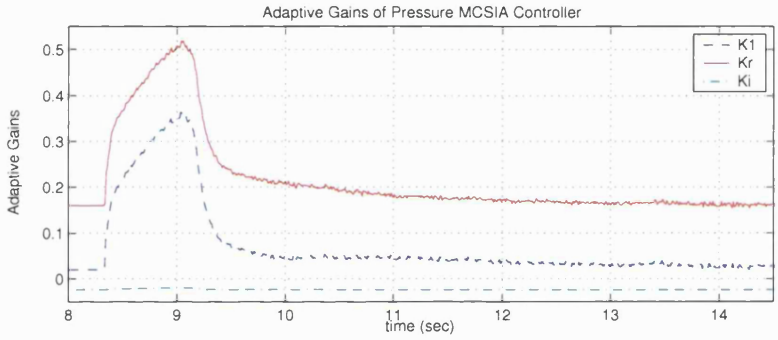

Figure 6.36: MCSIA Pressure Gains

The command signal to the servo proportional valve is shown in Figure 6.14. Higher adaptive weights of the "Force MCS" could possibly allow the control signal to develop faster and avoid the mismatch that takes place from 8.25s to 8.3 seconds. A smoother transition could be guaranteed in this case.

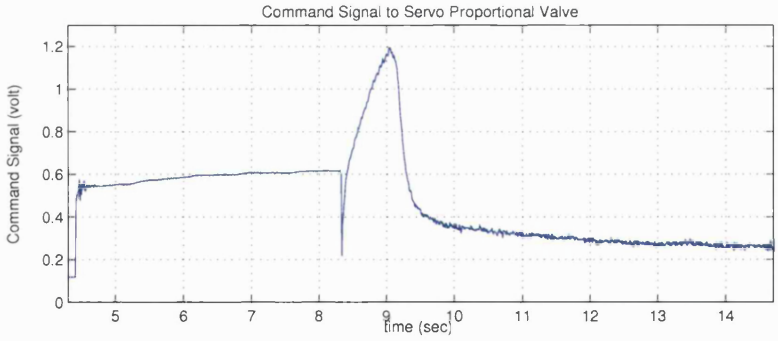

Figure 6.37: Command Signal to Servo-Proportional Valve

The results of the pressure control under hybrid MCS are shown in Figure 6.38. The hydraulic and cavity pressures during the injection moulding cycle can be clearly distinguished with the rise of the cavity pressure at the start of the packing phase. The ultrasound detects the pressure rise inside the cavity (around 8s) as well as the fall in pressure back to atmospheric level at the end of the injection cycle.

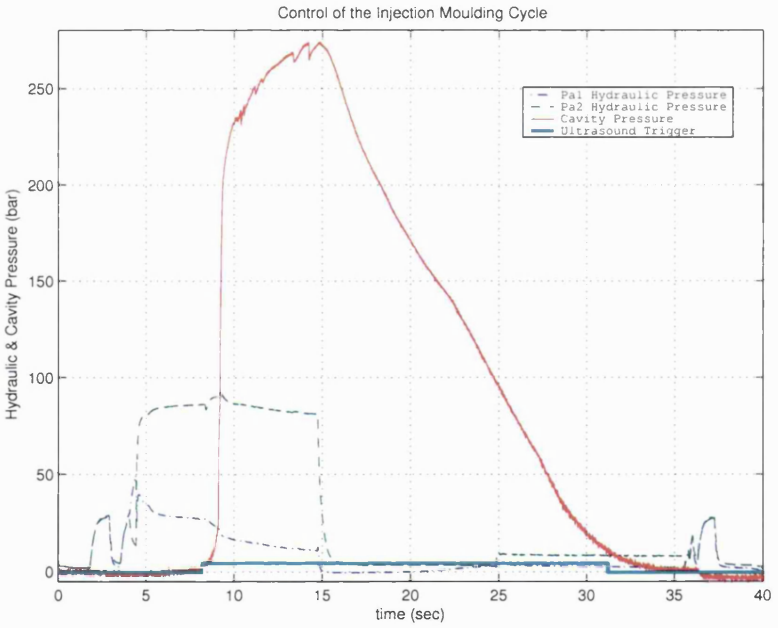

Figure 6.38: Control of the Injection Moulding Cycle with Hybrid MCS

6.8.2 Moulding of Rectangular Part with High Viscosity Polypropylene

To test the robustness of the hybrid scheme the second experiment was carried out with the same shape cavity but different moulding parameters. The material used this time was a high viscosity grade polypropylene with different viscous behaviour characteristics. The viscous friction and the damping effect on the screw motion during the filling and packing phase were both higher. The adaptive gains in both MCS schemes remained the same. The screw velocity shown in Figure 6.39 follows accurately the reference model which is set at 0.01m/s.

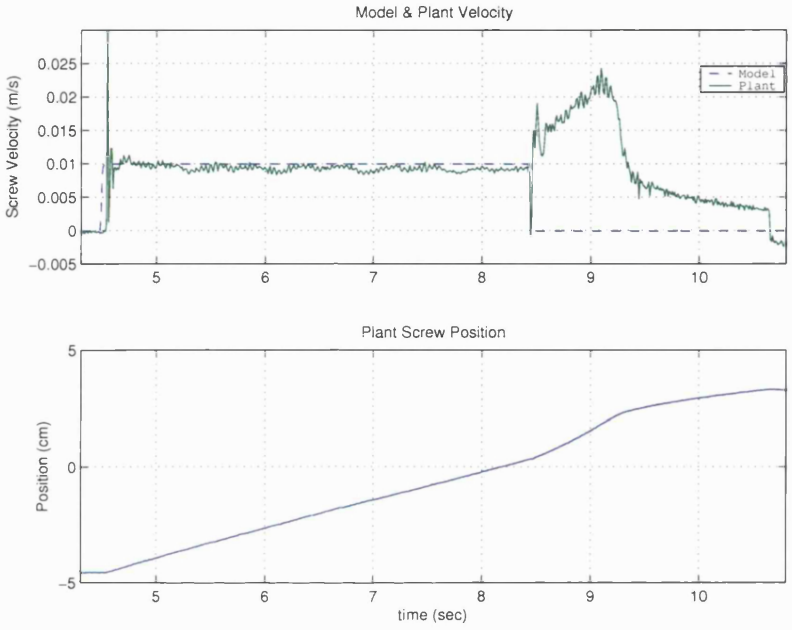

Figure 6.39: Model & Plant Velocity Response during the Injection Cycle

The switch from the filling phase to packing is initiated by the ultrasound trigger. The end of the packing phase was initiated by the screw velocity profile, with a saturating point being set at 0.003m/s. Overall the adaptive gains followed a similar behaviour as in the previously described case in section 6.8.1.

6.8.2.1 Adaptive Weights Vs Plant Pressure Error

In this experiment the new method with variable adaptive weights was applied. To achieve a smooth transition the weights started from zero and increased according with the plant pressure error. This was a very efficient approach as the MCS adapted less during periods were the plant error was small. The adaptive weights α and β were set higher than before where values of

$\alpha = 100$, $\beta = 10$ could be reached. In this case the adaptive weight ratio was set to, $K_{\alpha,\beta} = 10$. The adaptive weight, α, shown in Figure 6.40 (β is not shown since it is proportional to α) rose twice during this part of the cycle reaching a value peak of $\alpha = 68$ (and correspondingly $\beta = 6.8$) in order to minimise the error.

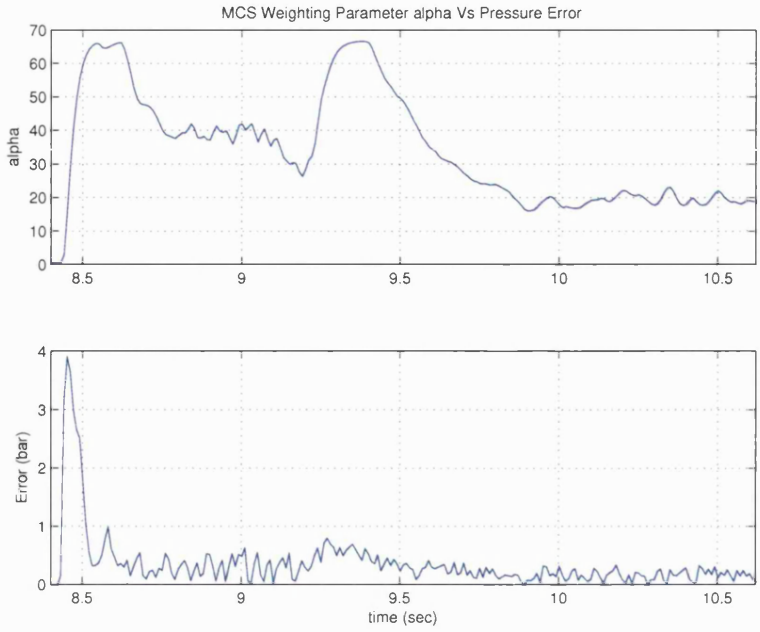

Figure 6.40: Adaptive Weight alpha and Corresponding Pressure Error

The adaptive gains were kept the same as in previous experiment (Figure 6.36) but faster adaptation was achieved as the weighting parameters were increased. In Figure 6.41 the adaptive gains start to settle after 9.5s and the weighting parameters α and β drop to the values of 20 and 2 respectively.

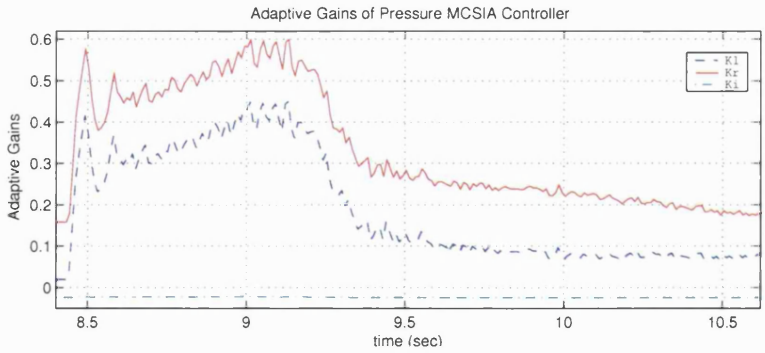

Figure 6.41: MCSIA Pressure Gains with Variable Adaptive Weights Scheme

At the time of the switching (phase change) the hydraulic plant pressure (ΔP) was 53bar as it can be seen in Figure 6.42. The plant pressure exhibited very good tracking of the pressure reference model which was set to reach a maximum pressure of 70bar with 4s settling time. Control of the packing phase stops as soon as the pressure reference setpoint is reached (70 bar) and/or the velocity drops to a value below 0.003m/s. This stops the MCS adaption process before the screw stalls. Otherwise the adaptive effort would increase enormously (and saturate the servovalve) as the MCS would try to control the pressure of the screw which would not physically move (screw would have reached the end of its travel, hits the nozzle).

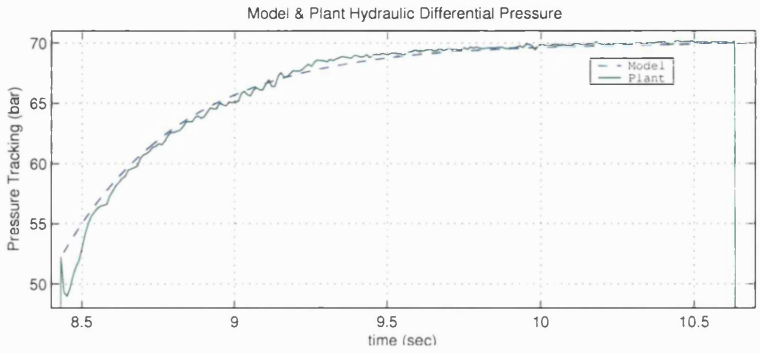

Figure 6.42: MCSIA Pressure Tracking

The command signal to the plant during the packing phase was a bit noisy due to the continuous variation of the adaptive effort as seen in Figure 6.43. Filtering of the command signal or the plant error would be an appropriate action to smooth the control signal.

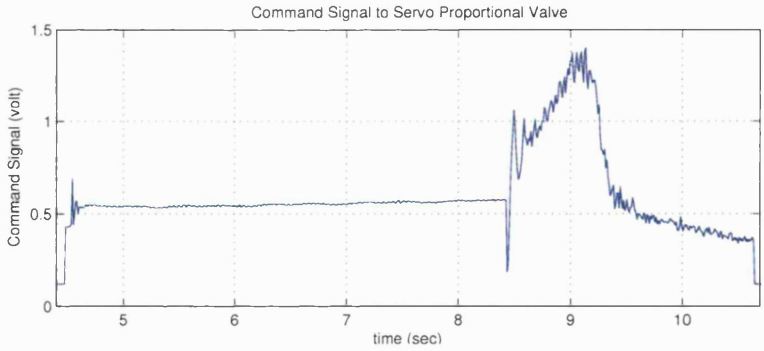

Figure 6.43: Command Signal to Servo-Proportional Valve

In Figure 6.44 the results of the pressure control under hybrid MCS are shown. The cavity pressure does not reach as high a level as in the previous case where low viscosity polypropylene was used. This happened because higher local pressures could be reached near the cavity pressure transducer diaphragm when low viscosity polypropylene is used.

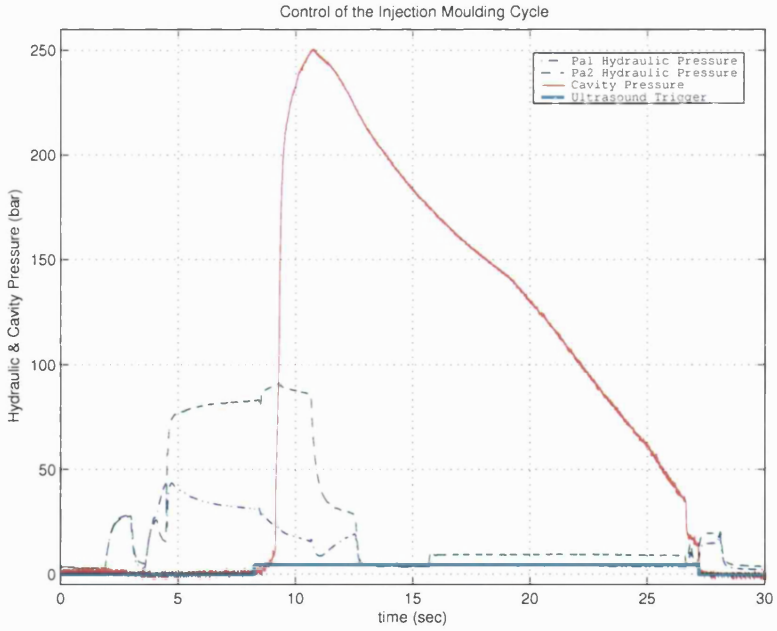

Figure 6.44: Control of the Injection Moulding Cycle

6.8.2.2 2nd Order "Flow MCS" with One State Feedback

The second order "Flow MCS" exhibited a robust behaviour for the control of the filling phase in both cases where two different viscosity grades of polypropylene were used. Both of the feedback states were used, velocity and acceleration, with the latter been weighted less to optimise the performance of the controller. Previously tested in simulation, with the 2^{nd} order MCS utilising a single feedback state achieved a similar behaviour with that of dual feedback states. For this reason it was decided to test the suitability of the 2^{nd} order MCS (no integral action but with magnitude insensitivity) with single feedback state (velocity) for the cases were the acceleration of the plant is not measurable. The model reference parameters summarised in Table 6.7 were used in the experiment. Most of these values are the same as those used in the simulation studies.

Natural Frequency	Model Gain	Damping Ratio	alpha weight	beta weight
$\omega_M\,(Hz)$	K_M	ζ_M	α	β
150	1	0.9	20000	500

Forward Adaptive Gains	Feedback Adaptive Gains
K_R	K_1
42	12

Table 6.7: Parameters of the Filling Reference Model with Single Feedback State

The proposed MCS scheme was tested for a set of different velocity setpoints (0.01 to 0.03m/s). All exhibited a stable behaviour with very good tracking of the reference setpoint. Two of these cases are shown in Figures 6.45 and 6.46 with the response of the adaptive gains being similar.

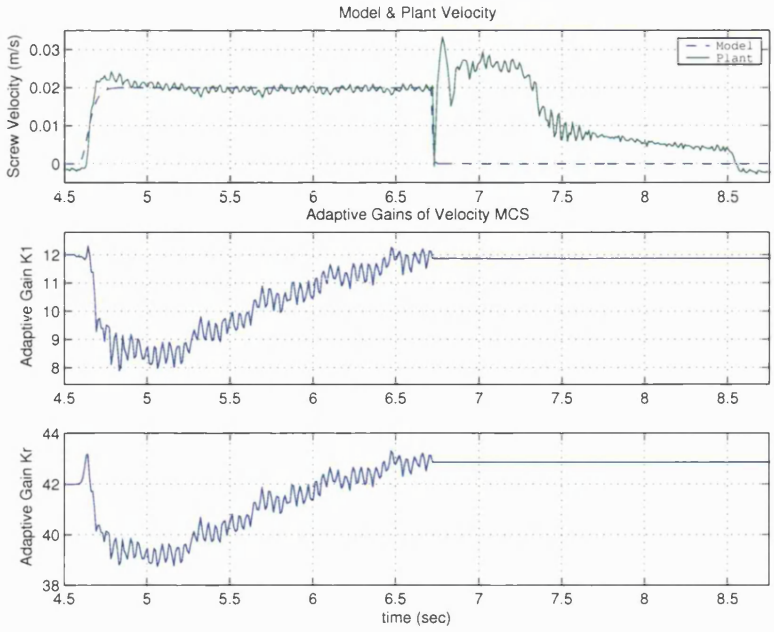

Figure 6.45: Velocity Tracking at 0.02m/s and Adaptive Gains

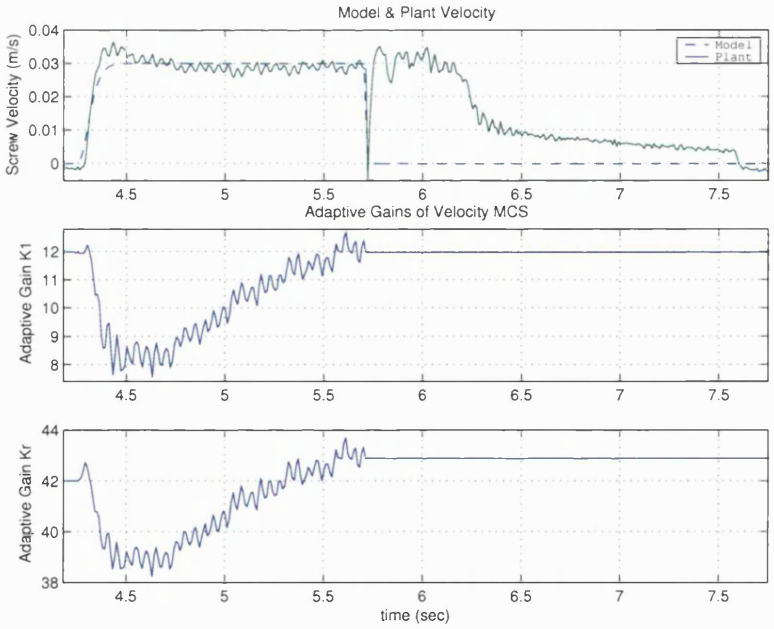

Figure 6.46: Velocity Tracking at 0.03m/s and Adaptive Gains

It should be noted that a smooth ramped reference model was used. Good tracking of the reference was achieved in both cases while the overshoot at the beginning was reduced compared with cases described in sections 6.8.1 and 6.8.2 (Figures 6.33 & 6.39).

6.8.2.3 Change from High to Low Pressure Reference Profile

In some cases due to the design of the runner-gate path in a mould, the gate does not solidify completely at the end of the packing phase. As a result, a small quantity of material comes out of the pressurised cavity affecting the dimensional properties of the part. Provision for such behaviour can be taken if the pressure reference model switches to a lower level to 'stop' gradually the packing phase while allowing more time for the gate to solidify (2-3). This new pressure reference trajectory was successfully tested in one of the experiments as seen in Figure 6.47. A high adaptive effort was provided to maintain stability while at the same time following closely the reference model.

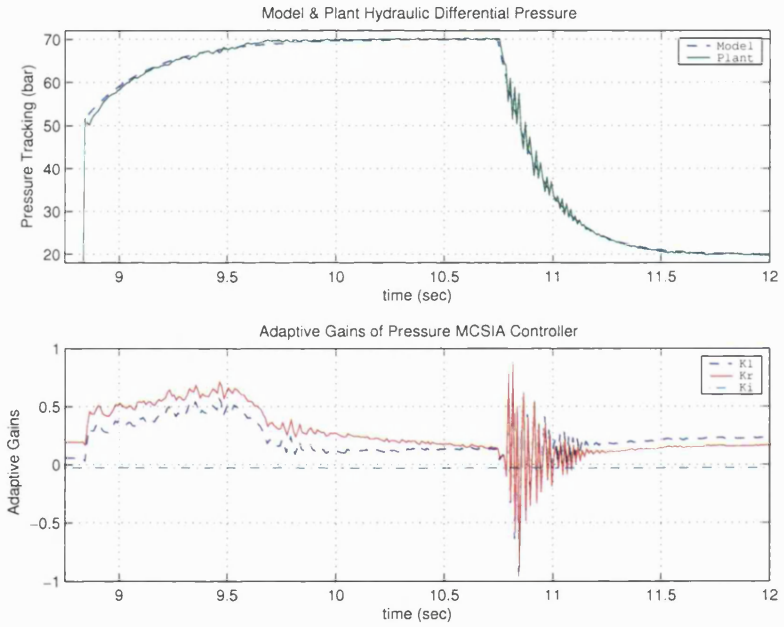

Figure 6.47: Low Pressure Reference Model at the end of Packing Phase

On this occasion the adaptive gains go very high and low at the same time, as there is a large step change in the pressure reference. The adaptive gains try to respond to the plant parameter changes as some high frequency pressure perturbation occur during this transition. As the hydraulic pressure reduces at the same time the large pressurised volume in the cavity tries to expand as the gate has not solidified yet. Therefore an interaction between the two systems (mould dynamics and hydraulics with injection barrel bulk modulus) takes place during the

step change which justifies the intense adaptive effort of the MCS to maintain close tracking of the pressure reference.

6.9 Concluding Remarks

In this chapter two extensions of the MCS algorithm were presented, the "Flow MCS" and "Force MCS" for the closed loop control of the injection moulding cycle. A bumpless transfer scheme was integrated within the hybrid MCS to match the adaptive effort of the two controllers and ease the adaptation during the switching between filling and packing. The selection of the reference model in the two MCS algorithms proved to be critical as the stability of the adaptation is guaranteed. The adaptation behaviour is mainly dependent on the adaptive weights (α, β) and the selection of the adaptive weight ratio ($K_{\alpha,\beta}$). The former affects the speed of adaptation while the latter determines the relative effort of the proportional and integral parts of the adaptive gains.

An initial estimation of the reference model parameters for the Flow MCS enabled the controller to start with predetermined gains. This effectively reduced the transient velocity error while the adaptive gains quickly developed to counteract the disturbance of the nonlinear viscous load (both in simulation & experimental). The 2nd order model MCS used for the filling phase was tested with both dual and single feedback states exhibited a robust behaviour (less overshoot in 2nd case) for different operating conditions and viscosity grades of polypropylene used. An initial tuning of the adaptive weights improved the adaptation performance. For the second phase (packing) the 1^{st} order MCS with one feedback state and zero adaptive gains, followed sufficiently well (starting with zero gains) a variety of reference models with the adaptive weights been adjusted according to the plant error. This allowed larger adaptive weights to be selected without compromising the stability. The overall efficiency of the MCS was improved and the algorithm became less sensitive to noise. An extension of the MCS scheme which would have both the adaptive weights and adaptive weight ratio variable is an area where further investigation should be conducted.

Chapter 7

Melt Polymer Vibration Control

7.1 Introduction

In this Chapter the effect of melt vibration in the injection moulding process has been investigated experimentally. As previously reported in Chapter 4, vibration can lower the viscosity of the polymer to improve processability, enhance orientation and reduce surface defects. The aim of the these experiments was to investigate the feasibility of applying melt vibration on semi-crystalline polypropylene with a conventional injection moulding machine controlled by the adaptive MCS algorithm. A one-stage injection moulding machine was used with no other components interfering between the nozzle and the mould, such as in *Scorim* and *Rheojector* [105]. A variety of flow and pressure profiles were applied during the filling and packing phase, where the screw vibrates (at different frequencies and amplitudes) and transmits the energy into the melt polymer to lower its viscosity. The hybrid MCS algorithm was used for the closed loop control of the screw motion, as presented in detail in Chapter 6. The mould temperature was kept constant during the experiments and no cooling profiles were investigated with the melt vibration during injection. The parts produced under vibration were examined for improvements in dimensional capability and part warpage (caused by asymmetric distribution of residual stresses). The parts were then tested with an *Instron* tensile test machine to estimate their tensile modulus. The mechanical properties of these parts were compared with parts produced with conventional moulding and showed significant improvements.

7.2 Experimental Setup

For the vibration of the melt polymer the screw motion during injection was controlled (only) by the P-Q servo-proportional valve (*Moog*). The screw flow and pressure profiles were set to follow a predetermined trajectory (reference signal) where a sinusoidal signal was superimposed on the reference signal to force the screw to vibrate. The screw was set to oscillate at frequencies ranging from 8Hz to 20Hz with different amplitudes for the filling (0.01m/s to 0.04m/s) and packing phase (5bar to 10bar). For the switching from flow to pressure control the cavity pressure was used and different switching levels (5, 10, 45, 80, 90bar) were chosen to test the robustness of the MCS controller. In each experiment the prepared shot size was kept small in order to transmit efficiently the vibration force field in the polymer inside the cavity. As reported in the literature [78], low frequencies of shear vibration (5-20Hz) can reduce the viscosity of the melt and ease the processability of the melt, resulting in a better orientation-morphology at the core of the part. Once the viscosity is lowered via vibration, faster filling and packing can be achieved improving the power consumption and cycle time. The average processing temperature of polypropylene was set to $220°C$ while the mould temperature was maintained constant at $50°C$.

Due to time constraints it was not possible to develop closed loop cooling control for the mould, to combine rapid cooling with vibrational profiles that could further enhance the mechanical properties of the parts (Section 4.5.4). An advantage in the experimental setup would be to have an injection screw with a check valve (ring) which would reduce the leakage past the screw during injection and improve the transmission of vibration to the melt polymer.

7.2.1 Warpage Measurement

To investigate the influence of melt vibration in the stress distribution in the parts, warpage was measured in each moulded specimen 24-hours after the end of the process. This time was allowed since the shrinkage of the part may continue outside the mould in semi-crystalline PP for a few hours at room temperature. To measure warpage the one side of the part was fixed while the difference in hight with the other side was measured with a digital caliper. To know exactly the moment when the tip of the caliper would touch the tested part an analogue micrometer was set to sense any minor part movement. The experimental arrangement is shown in Figure 7.1.

Figure 7.1: Warpage Measurement Experimental Setup

The same procedure was followed for all the parts tested for warpage to avoid any discrepancy in the measurement. The rest of the dimensions (length, width, thickness) in the parts were measured as well with a micrometer for later comparison.

7.2.2 Tensile Modulus Measurement

To estimate the Tensile Modulus of the parts an *Instron 4303* (25kN) series testing machine was used. The polymer specimens were placed between the two clamps of the *Instron*. The upper jaw moves upward and applies an increasing stress onto the specimen, which is recorded as a function of time on the PC. As the crosshead speed is known (10mm/min) the program estimates the elongation from the time measurement. The distance between the clamps was the same for all the tests. After each run the upper clamp was lowered for the next specimen to be tested. The tensile test method (No. 83) used was Instron's standard for polymer plastics. At the end of the test all the data were processed by *Instron's* software as presented in Figure 7.2.

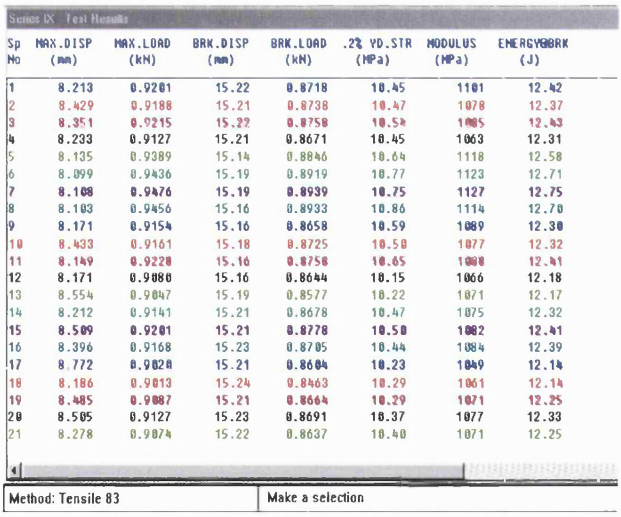

Series IX Test Results

Sp No	MAX.DISP (mm)	MAX.LOAD (kN)	BRK.DISP (mm)	BRK.LOAD (kN)	.2% YD.STR (MPa)	MODULUS (MPa)	ENERGY@BRK (J)
1	8.213	0.9201	15.22	0.8718	10.45	1101	12.42
2	8.429	0.9188	15.21	0.8738	10.47	1078	12.37
3	8.351	0.9215	15.22	0.8758	10.5x	1085	12.43
4	8.233	0.9127	15.21	0.8671	10.45	1063	12.31
5	8.135	0.9389	15.14	0.8846	10.64	1118	12.58
6	8.099	0.9436	15.19	0.8919	10.77	1123	12.71
7	8.108	0.9476	15.19	0.8939	10.75	1127	12.75
8	8.103	0.9456	15.16	0.8933	10.86	1114	12.78
9	8.171	0.9154	15.16	0.8658	10.59	1089	12.30
10	8.433	0.9161	15.18	0.8725	10.58	1077	12.32
11	8.149	0.9228	15.16	0.8758	10.65	1088	12.41
12	8.171	0.9080	15.16	0.8644	10.15	1066	12.18
13	8.554	0.9047	15.19	0.8577	10.22	1071	12.17
14	8.212	0.9141	15.21	0.8678	10.47	1075	12.32
15	8.509	0.9201	15.21	0.8778	10.58	1082	12.41
16	8.396	0.9168	15.23	0.8705	10.44	1084	12.39
17	8.772	0.9028	15.21	0.8604	10.23	1049	12.14
18	8.186	0.9013	15.24	0.8463	10.29	1061	12.14
19	8.485	0.9087	15.21	0.8664	10.29	1071	12.25
20	8.505	0.9127	15.23	0.8691	10.37	1077	12.33
21	8.278	0.9074	15.22	0.8637	10.40	1071	12.25

Method: Tensile 83 | Make a selection

Figure 7.2: Analysed Data of Plastic Specimens from Instron's Software

7.3 Melt Vibration during the Packing Phase

For the first experiment the vibration of the melt polymer was only applied during the packing phase where the mould rectangular cavity was used. No cavity insert was used at this point to change the shape of the moulded part. During the filling phase the velocity of the screw was maintained constant at 0.02m/s. For the control of the pressure profile a reference signal at 80bar with a sine-wave of 5bar amplitude and 8Hz frequency were used. The results of the pressure vibration control under the hybrid MCS controller are shown in Figure 7.3. The start of the packing phase can be clearly distinguished with the rise in the cavity pressure that reached a level of 250bar. By observation of the right window (magnification) it can be seen that a smooth transition was achieved between the two phases. The vibration had a small effect on the cavity pressure which exhibited low oscillatory behaviour from the period of 7.5s to 8.6s. It was clear that vibration with a larger sine amplitude would have a more pronounced effect in the vibration of the screw and cavity pressure which reflects the state of the melt polymer inside the cavity.

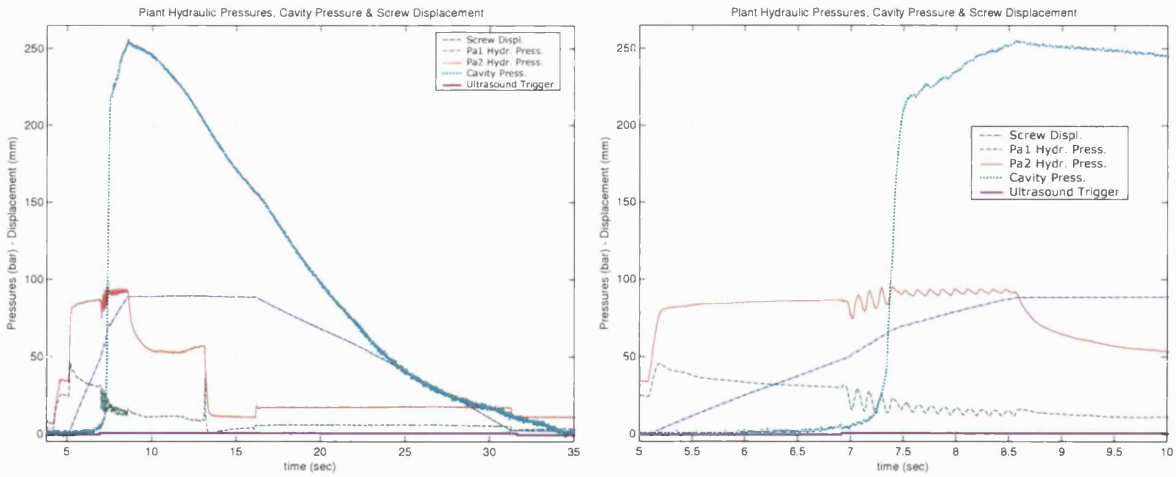

Figure 7.3: Melt Vibration at 8Hz during the Packing Phase, 80bar

During the injection cycle the MCS controller performed well and good tracking of the reference signal was achieved for both velocity and pressure (vibrational) profile. At the beginning of the filling phase there was a small overshoot above the 0.02m/s setpoint, Figure 7.4, however the tracking error was quickly reduced to zero. A smooth transition to the packing phase followed with the screw following closely the reference signal (left window). Due to the nonlinear load effect of the melt polymer that solidifies continuously during injection, a small pressure (tracking) error occurred in the beginning which was quickly reduced to zero.

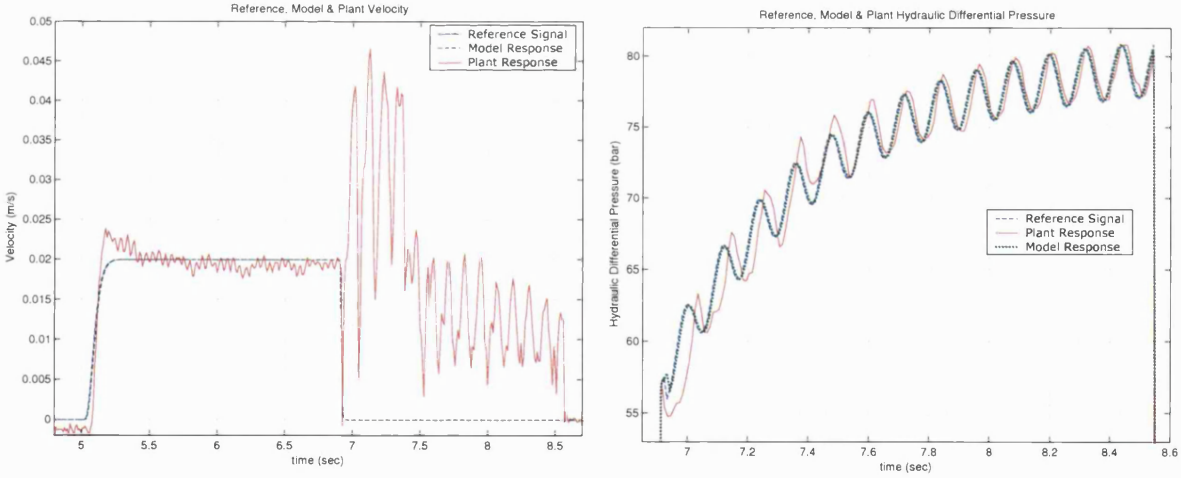

Figure 7.4: Reference Velocity and Pressure Models for Melt Vibration at 8Hz during the Packing Phase

On the other hand the adaptive weights of the Force MCS were adjusted according to the

pressure error to allow larger values to be selected without compromising the stability. It is of great importance to achieve close tracking of the reference trajectories to distinguish the effect that different vibrational profiles have on the mechanical properties of the parts.

7.4 Melt Vibration during Filling and Packing Phase

Following a stable and satisfactory performance of the Force MCS in controlling the vibrational pressure profile during packing the same method was extended for the filling phase where shear vibration was applied in the melt polymer. For these experiments the rectangular cavity with a special insert was used to mould tensile specimen parts (gate at the side of the specimen) which could be tested afterwards for their mechanical properties. As investigated in section (Section 7.3) a larger amplitude of sine-wave would have a more significant effect on the melt vibration, therefore an amplitude of 10bar was used for the pressure profile. A series of experiments with different frequencies (8-20Hz) and amplitudes (fill velocity 0.01m/s to 0.04m/s and pack pressure 5bar to 10bar) were carried out with satisfactory tracking performance for both filling and packing phase. For one of these experiments the following amplitude and frequency were used as presented in Table 7.1.

Vibration Parameters	Filling Phase	Packing Phase
Control Setpoint	0.02m/s	100bar
Switching at P_{cav}	90bar	
Frequency of Vibration	20Hz	20Hz
Amplitude of Vibration	0.025m/s	10bar

Table 7.1: Vibration Parameter Settings during Injection

The effect of shear vibration during filling is very important as it can influence the orientation of the solidifying layers as well as the thickness of the skin and subsequent layers in the part. The excessive shear that takes place does not allow the part layers below the skin to solidify under isothermal conditions and therefore the crystallinity in the part can be greatly influenced. Additionally melt shear vibration could reduce mould filling imbalances that have been reported to occur due to non-symmetrical shear distribution of the melt as it travels through the runner flow paths [143]. It is expected that shear vibration during filling would reduce variation in the melt viscosity inside the runners which can increase shear heating of the melt and result in high flow rates (may result in jetting) in multi cavity moulds.

The results of both shear and pressure vibration applied during injection are presented in Figure 7.5. The applied vibration in both phases had a significant effect on the viscosity of the melt polymer as the cavity pressure reached the level of 540bar. Without vibration the max-

imum cavity pressure reached (for 100bar reference signal) under same operating conditions was 440bar. This clearly indicates that the melt viscosity was lowered during vibration due to the extensive shearing that took place in both the filling and packing phases. The extensive shearing of the melt increased the melt temperature in the cavity (due to shear heating) which delayed the solidification of the skin and subsequent layers towards the core. Therefore the melt polymer at the core of the part was more time under pulsating flow which improved the molecular orientation in the part. However more extensive experimental analysis (with optical microscopy) would be required to verify this changes in the morphology of the parts. In the right window of Figure 7.5 it can be observed that the frequency of oscillation of the screw position is reflected on the cavity pressure which perturbed at the same frequency. This indicates that the melt polymer was vibrated during injection (5.6s to 6.5s) with the cavity pressure oscillating at the frequency of 20Hz with an amplitude varying from 5bar to 25bar. This favours the reduction of warpage which is dependent on the cavity pressure variations prior to the glass transition period, T_g [144]. In addition, the duration and level of the cavity pressure reached improves the stress distribution in the part and reduces the stresses [145]. Therefore with melt vibration such processing conditions can be attained more efficiently without the need to process the material at high temperatures. All the above findings indicate that the polymer could be processed at a lower temperature as the viscosity could be regulated according to the frequency of vibration. That would be of great significance in polymers that are more prone to degrade at high processing temperatures (at the gate entrance due to shear heating).

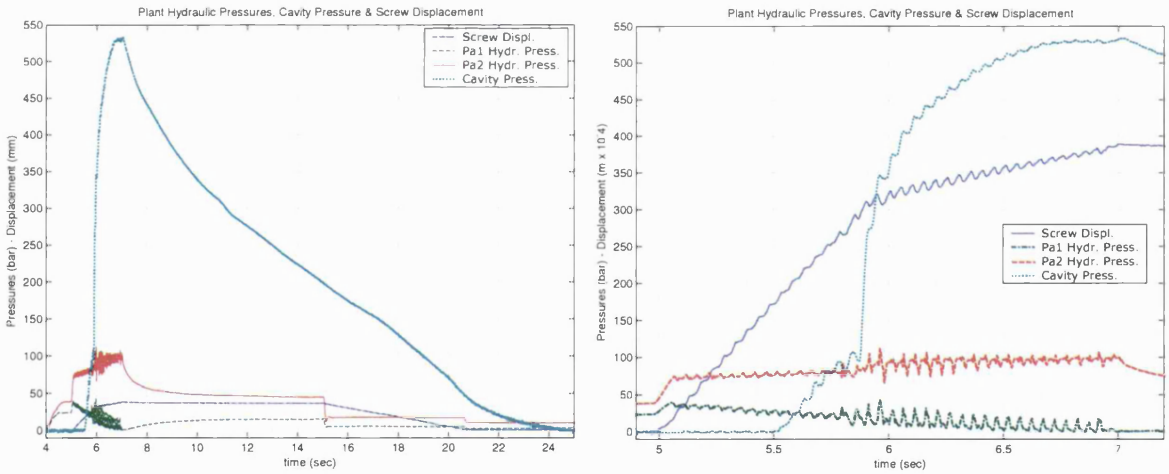

Figure 7.5: Melt Vibration at 20Hz during Filling and Packing Phase, 100bar

The tracking performance of the Flow MCS and Force MCS controller is shown in Figure 7.6. During the filling phase the screw followed closely the model response which deviated slightly from the reference. Better tuning of the MCS controller adaptive weights could improve the performance and reduce the error. For the packing phase satisfactory tracking of the model response was achieved (by the screw with a phase lag) if it was considered that there was a

big change in the melt stiffness due to the smaller cavity (with insert) used. In addition, at the end of the packing phase a big percentage of the part had already solidified which made the control of the pressure in the cavity more difficult. This effect resulted in saturation of the servo-proportional valve. It is considered that a smaller vibration amplitude would improve the tracking response of the plant without saturating the valve.

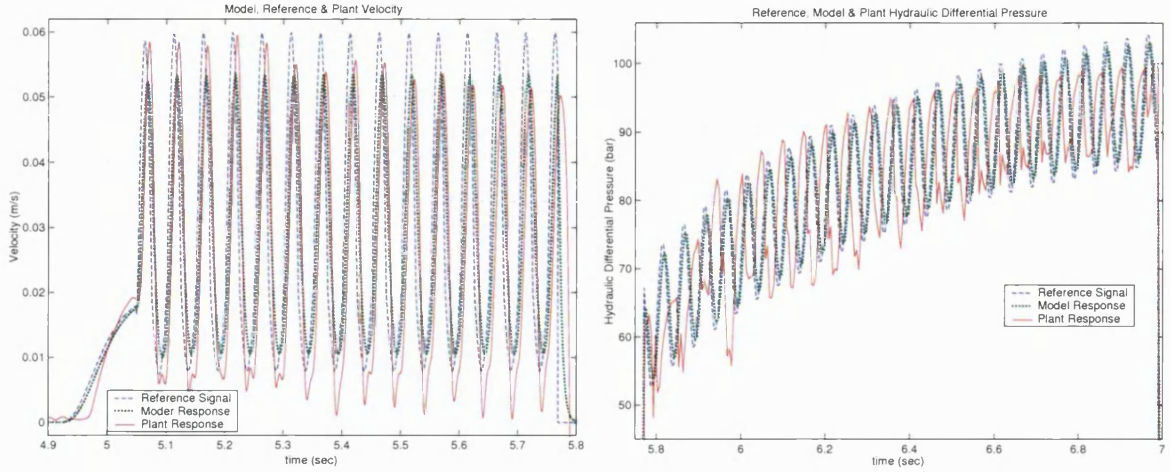

Figure 7.6: Reference Velocity and Pressure Models for Melt Vibration at 20Hz during Filling and Packing Phase

7.4.1 Effect of Vibration on Viscosity

From the presented experimental data presented so far it has been clear that vibration reduces the apparent viscosity and improves the processability of the polymer, especially during the packing phase. A closer inspection of the experimental data during the filling phase shows that shear vibration also influences the viscosity of the polymer. A comparison of the hydraulic pressures during the filling phase with and without vibration is shown in Figure 7.7. In the left window of the Figure where no vibration was applied the hydraulic pressure, Pa2 rises from 42bar to 88bar (Pa1 from 25bar to 26bar) at the end of filling phase, while in the case with vibration Pa2 rises from 42bar to 80bar (Pa1 from 24bar to 25bar). Therefore there is a reduction in the hydraulic pressure drop from 62bar without vibration to 55bar with vibration to fill the mould. The melt viscosity could have been reduced further if the leakage past the screw was less (if screw was equipped with a check valve).

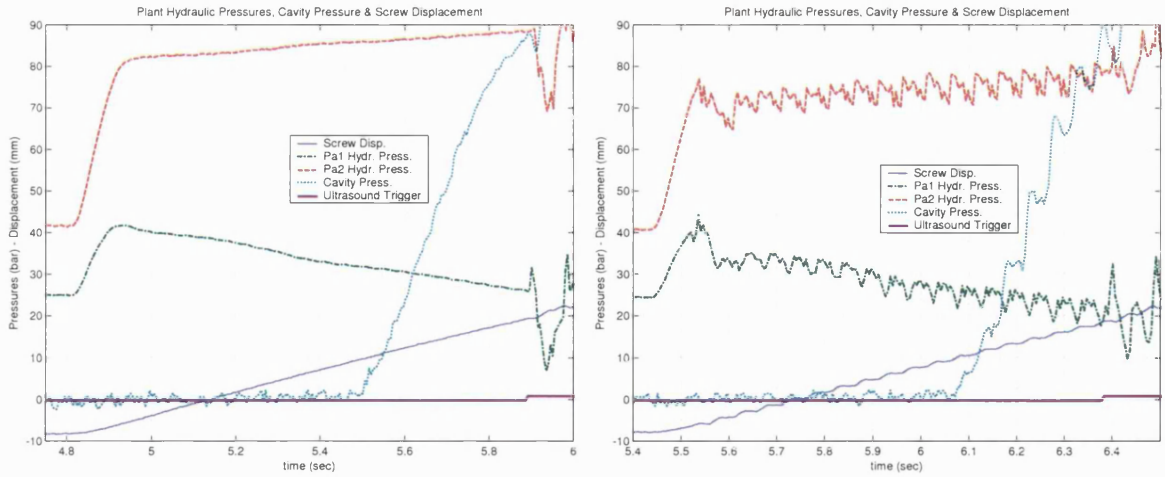

a. Conventional Moulding *b. Vibrational Moulding*

Figure 7.7: Reduction in Hydraulic Differential Pressure due to Melt Vibration at 20Hz during Filling, Switch at $P_{cav} = 90bar$

7.5 Effects of Vibration on Part Quality & Mechanical Properties

To investigate further the effect of vibration on part quality and mechanical properties two more sets of experiments were carried out. In the first test arbitrary vibrational settings were chosen and the parts produced were tested for dimensional tolerance and warpage. It should be noted that long parts as the one used for the experiments have a higher tendency to warp as they have no other surfaces at right angles (ribs) to restrict warpage. The settings used for each test are presented in Table 7.2. The switching point was set at different levels of cavity pressure such as at 5bar, 10bar, 45bar and 90bar. In all tests a smooth transition during the switching was obtained with stable plant behaviour.

Vibration Parameters	*1*	*2*	*3*	*4*	*5*	*6*	*7*	*8*
Frequency, f_{fill} (Hz)	-	-	-	-	20	20	20	20
Amplitude, A_{fill} (m/s)	-	-	-	-	0.01	0.03	0.04	0.04
Frequency, f_{pack} (Hz)	10	12.5	20	20	20	20	20	20
Amplitude, A_{pack}(bar)	5	5	5	5	5	5	6.5	8
Maximum, P_{pack} (bar)	80	80	90	90	90	90	90	90
Duration, T_{pack} (s)	2	2	3	3	3	3	3	3
Switch P-Q at P_{cav} (bar)	5	80	90	45	10	45	90	90

Table 7.2: Frequency and Amplitude of Vibration during Injection

The analysis of the experimental results is presented in Figure 7.8.

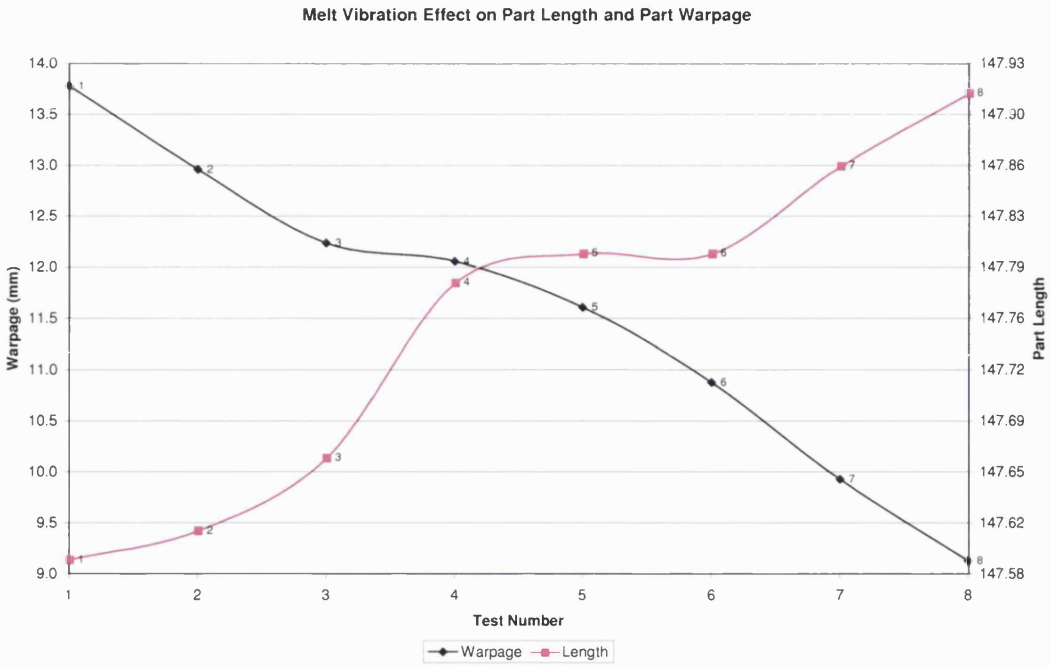

Figure 7.8: Melt Vibration during Filling and/or Packing

As it was anticipated warpage decreased (from 13.78mm down to 9.13mm) with vibration, as the residual stress distribution is more uniform throughout the part. This is attributed as well to the lowered viscosity during processing which allows extensive shearing of the melt especially at the core layers. Part shrinkage was also reduced due to the improved orientation of the molecules (results in more uniform shrinkage throughout the part) with the length of the part having a smaller deviation (from 147.59mm to 147.91mm) from the cavity dimension ($L_{cav} = 148mm$).

Although there are clear benefits from melt vibration at the same time there is a variety of settings to select. It is not straightforward to identify the effect of each individual parameter on the mechanical properties and quality of the part especially when several process parameters change at the same time (e.g. cooling profiles). However the trend in those preliminary tests shows that when vibration is applied both at filling and packing the dimensional capability is increased and warpage is reduced. It is important for vibration to be applied before and during the transition through the T_g as afterwards would have no effect. The switching point also seems to play a key role since the transition to packing must not be early (extensive shrinkage, part with poor dimensional tolerances) neither be delayed (results in excessive cavity pressure, part flashing). Also improvements in the surface appearance of polypropylene (PP) moulded under vibration, have been reported [146] were failure cracks of the impact surface of PP were denser and more homogeneous when compared with conventional moulded parts.

7.5.1 Further Experimentation with Melt Vibration and Analysis of Experimental Data

In the first part of the experiments it was found that application of melt vibration at high frequency in both filling and packing phase reduces shrinkage and warpage. Based on these conclusions it was decided to further investigate the effect of vibration with varying only the reference pressure level and cooling time. The filling vibration amplitude and P-Q switching level ($P_{cav} = C$) were kept constant for all tests. The packing pressure was changed at increments of 10bar from 80bar to 100bar. The cooling time of the parts was varied from half to three minutes (0.5, 1, 2, 3min). To compare the "with" vibration parts with those produced by conventional moulding, a set of conventional parts was produced with varying packing pressure and packing time and with a constant cooling time of 1min. The process parameter settings used in both tests are presented in Table 7.3.

Conventional Moulding	Filling Phase	Packing Phase
Control Setpoint	0.02m/s	80bar-100bar
Switching at P_{cav}	90bar	
Duration of Packing	2s-4s	

Vibrational Moulding	Filling Phase	Packing Phase
Control Setpoint	0.02m/s	80bar-100bar
Switching at P_{cav}	90bar	
Frequency of Vibration	20Hz	20Hz
Amplitude of Vibration	0.025m/s	10bar

Table 7.3: Process Parameter Settings for Conventional and Vibrational Moulding

A comparison between parts moulded with vibration and conventionally follows where all the moulded tensile specimens were tested for dimensional accuracy, Young's Modulus and warpage. The analysis of the first experimental set is presented in Figure 7.9. In the left window, the results from conventional moulding are presented while in the right window the ones with vibrational moulding.

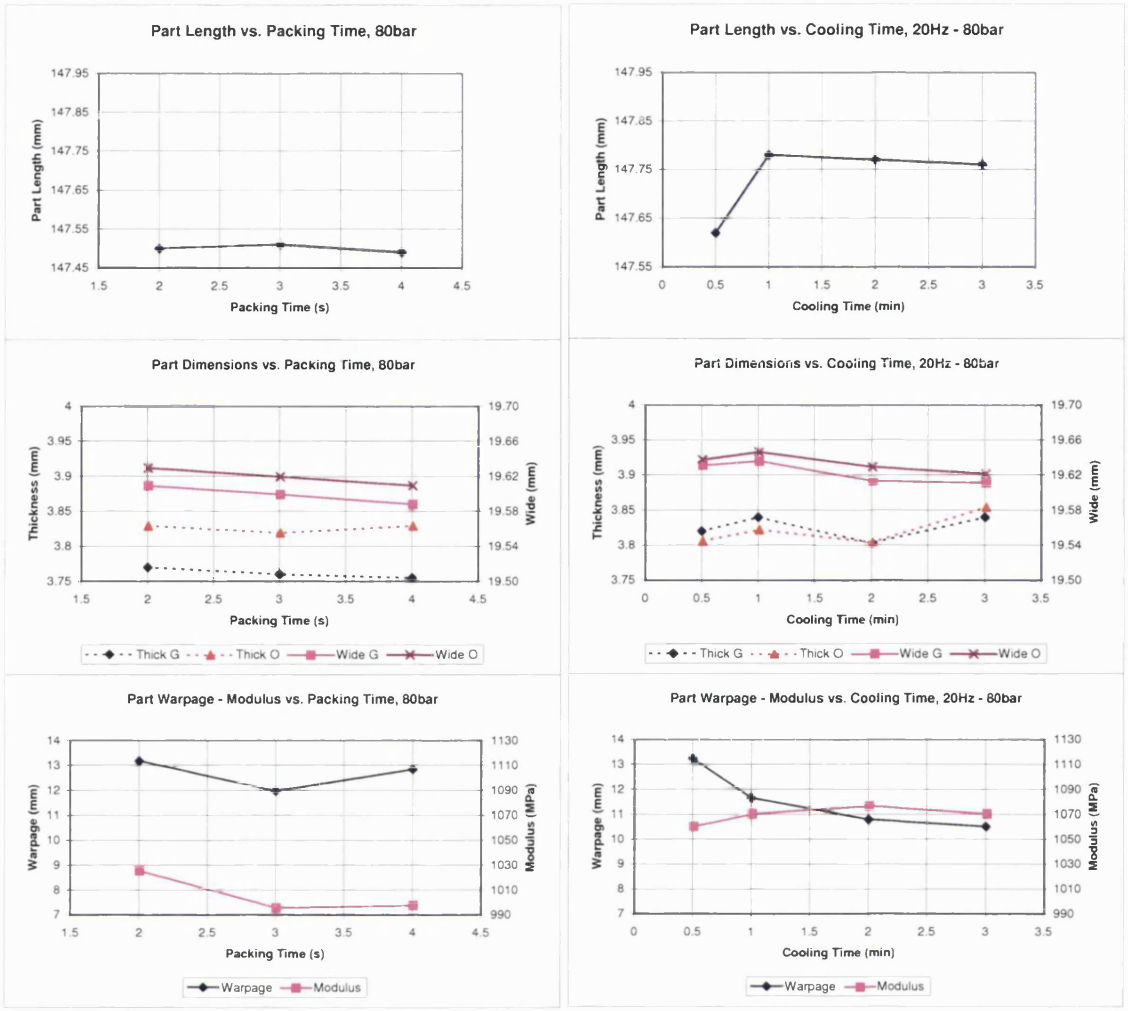

a. Conventional *b. Vibrational*

Figure 7.9: Conventional and Vibrational Moulding at 80bar

By comparison of the results it can be seen that with vibration the parts have a better dimensional capability and improved mechanical properties. This is apparent in the thickness dimension where with vibration small deviation ($\pm 0.015mm$) exist between measurements near the gate (Thick G) and the other side of the part (Thick O). The same applies also for the width dimension which was close (deviation of 0.38mm in worst case) to the nominal value (20mm). It should be noted as well that shrinkage for polypropylene in the across flow direction is slightly greater that the shrinkage in the flow direction [60]. The part length is also increased as the shrinkage is reduced. This is attributed to the enhanced orientation of the crystalline area by vibration which also shifts the glass transition to a higher temperature to advance the crystallization of the amorphous region. As a result most of the part crystallizes during the process and a small percentage after being ejected. On the other hand, parts moulded without vibration are more prone to crystallise for several hours after ejection being free to shrink further as they

are not restricted any more by the cavity form. There is an improvement in the modulus by 7.4% and a more significant improvement in warpage by 11% with vibration.

In the next Figure 7.10 the tests are identical with the previous apart from the packing pressure which was increased to 90bar.

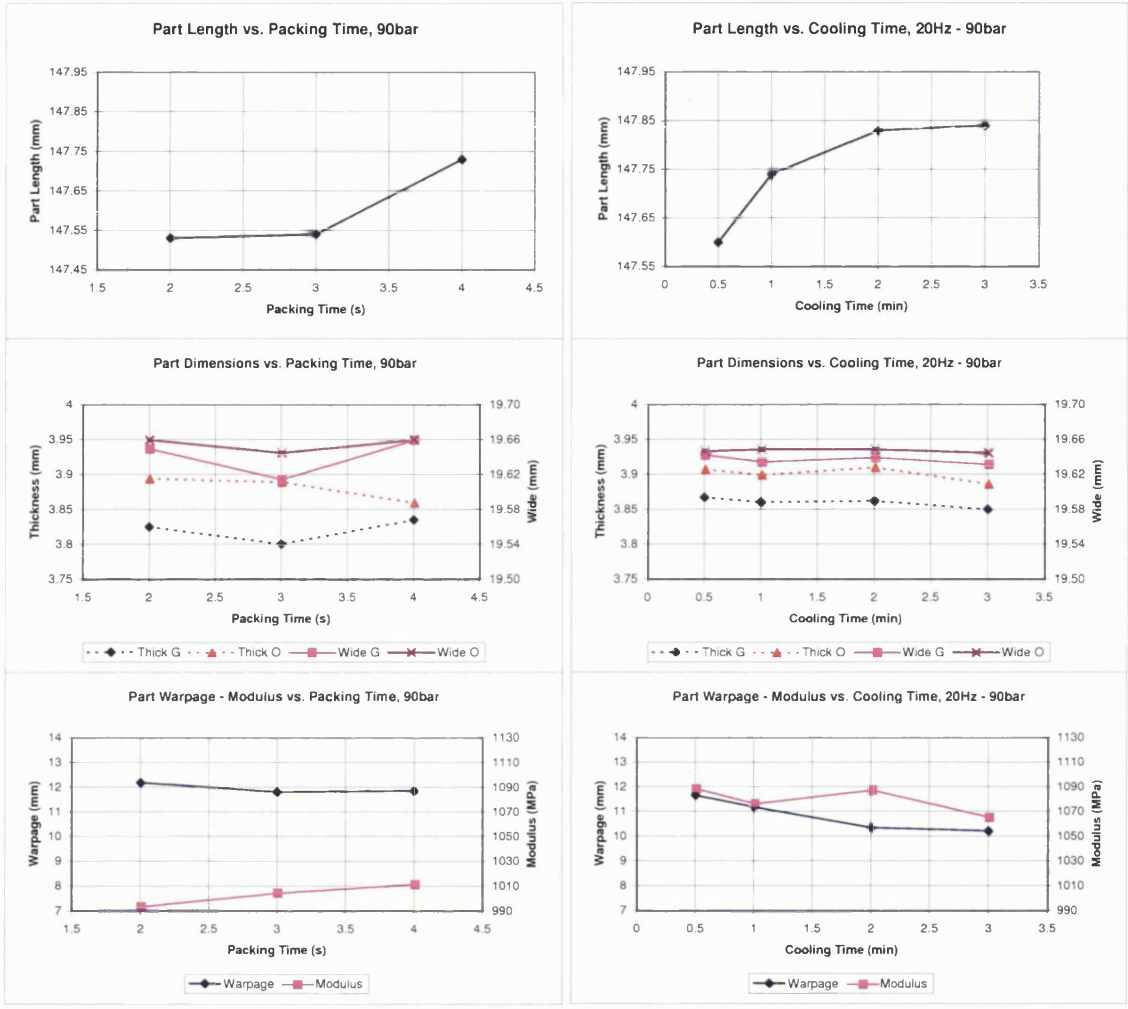

a. Conventional *b. Vibrational*

Figure 7.10: Conventional and Vibrational Moulding at 90bar

For both tests the increase in the packing pressure to 90bar improved the dimensions of the parts (Length, Thickness, Width). The 10bar increase in the packing pressure improved the ("with" vibration) part modulus by 1% and reduced the warpage by 3%. In addition, the parts moulded with vibration had an increase in the modulus by 9% and reduction in part warpage by 13%, when compared with the conventional moulded parts. In addition, the part length was further increased by 1% as pressure advances crystallization and reduces shrinkage. In both the previous case (vibration-80bar) and now the modulus of the part was reduced with extensive

cooling time (when comparing cooling case from 2min to 3min) as the molecules have more time to relax and become randomised (reduces warpage). Depending on the application of the part this might be desirable or not, for example shorter cooling time results in higher residual stresses, higher modulus but low level of environmental stress crack resistance (low impact resistance as well).

In the last test the hydraulic pressure reference was increased to 100bar. The analysis of the results is presented in Figure 7.11 which shows that the higher hydraulic pressure especially in the vibration case improved the mechanical properties and quality of the parts.

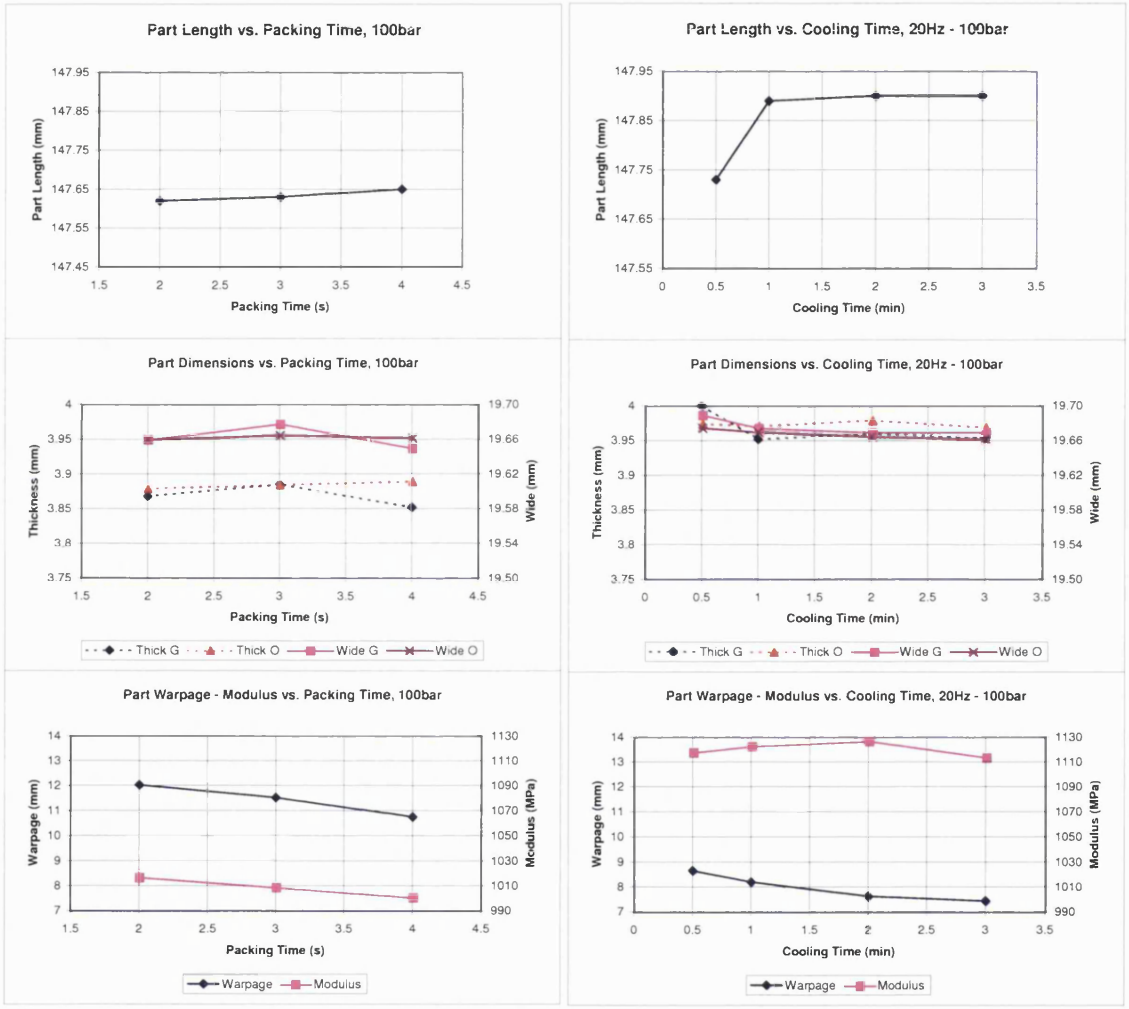

a. Conventional *b. Vibrational*

Figure 7.11: Conventional and Vibrational Moulding, at 100bar

All the dimensions ($L \times W \times T$) of the specimens moulded under vibration were within $\pm 0.03\%$, $\pm 1.7\%$ and $\pm 0.75\%$ tolerance of the nominal dimensions (148mm x 10mm-20mm x 4mm) for

the length, width and thickness respectively. It should also be noted that polypropylene has a higher tendency for shrinkage in contrast with amorphous polymers. Compared with conventional moulding (last case, 100bar) melt vibration reduced part warpage by 30% and increased the tensile modulus by 10%. In addition, the higher modulus indicates that the parts moulded under vibration crystallised much faster. Improvements in the Young's modulus of polypropylene parts due to the effect of vibration amplitude have also been reported in a recent study using a custom made vibration injection moulding machine [147].

Melt vibration was successfully applied in a conventional injection moulding machine where parts properties were enhanced. It was verified that with melt vibration, parts can be moulded at lower temperature and/or hydraulic pressure, retaining the same properties as with parts moulded with conventional method at higher processing hydraulic pressure. Therefore a new generation of injection moulding machines could be easily modified to apply vibration to the melt polymer for parts where high dimensional tolerances are required. Moreover the efficiency of the melt vibration in conventional moulding machines could be improved with different screw designs.

7.6 Concluding Remarks

The application of melt vibration was investigated in the injection moulding process using a modified conventional moulding machine. The adaptive MCS algorithm was used to control flow and pressure during the cycle with very good adaptation and reference model tracking. A smooth transition between the phases was achieved at different cavity pressure switching levels (10bar, 45bar, 90bar) used to change from flow to pressure control. Unlike other proposed vibration assisted injection moulding methods [105] which are open-loop controlled, the flow and pressure profiles of the screw were controlled in a closed-loop system. Although no simulation was performed to test the suitability of the MCS algorithm under such advanced P-Q profiles where the load exhibits a nonlinear nature (load stiffness changes continuously), the hydraulic screw in most experiments exhibited good tracking of the reference profiles.

The application of melt shear vibration was tested with a variety of flow and pressure profiles and found to have a profound influence on the viscosity of the polymer which favours the mechanical properties (modulus, warpage, dimensional capability) of the parts. All tests were carried out with constant mould temperature, although it would be an advantage in the future to test different cooling profiles with vibration profiles. In addition, melt vibration could also be applied during plasticization to further reduce the viscosity of the melt and improve moulding machine efficiency and reduce cycle times.

Chapter 8

Conclusions

In this work the moulding control of high quality parts with new methods to enhance their mechanical properties were the main goals. In order to achieve this, the monitoring and identification of the process parameters that cause quality variations was of prime importance. The polymer materials used in the experimental part were: semi-crystalline polypropylene and amorphous polycarbonate. Two non-invasive monitoring methods were set in place in order to provide critical information in real time about the melt polymer behaviour. Simulation studies of the filling and packing phase, alongside experiments undertaken on an *Arburg* 25-tonne injection moulding machine, provided the experience for a good understanding of the relation between the machine process parameters and the in-mould parameters. This knowledge led to the design of portable non-invasive monitoring equipment which makes use of ultrasound waves. Information provided by this monitoring system enabled the fast set up of the controller to estimate the duration of the injection phases in real time. No need of intervention by an operator would be necessary even if a new mould is to be used. The majority of the control methods found in the literature generally necessitate a complex mathematical model to describe the process. Often the derivation of such models is tedious; moreover they need revising every time process parameters change (mould, material, processing conditions). In this work an adaptive controller based upon *minimal control synthesis* (MCS) was used and applied to the injection moulding process. The use the adaptive MCS controller, in combination with the modification of the hydraulic system, enhanced the performance of the injection moulding machine. This modification allowed the screw to follow demanding flow and pressure trajectories and to vibrate the melt polymer in order to enhance the mechanical and physical properties of the moulded parts. Parts produced with the vibration method had improved dimensional accuracy, tensile modulus and reduced warpage, when compared with conventional moulded parts.
The development and completion of this complex monitoring and control system involved addressing a number of tasks. Key aspects, contributions, and findings of the work are as follows:

- **Preliminary testing to understand and identify the phases of the injection moulding process**. The departmental *Arburg* 25-tonne injection moulding machine was used for this purpose. The control limitations of the moulding machine were identified, where the duration of the injection phases (filling , packing and cooling) was preset before the start of the injection. In addition, the velocity and pressure setpoints to be reached during filling and packing respectively, could not be altered during the process. Available moulds were used at this preliminary stage, until a new mould was designed and manufactured. Alongside the experimental studies, a detail model of the hydraulic circuit and mould flow paths was used in the simulation of the injection filling and packing phase. For the simulation, rheological data for isotactic polypropylene were used in order to estimate parameters such as: maximum injection pressure, filling time, hydraulic pressure, cavity pressure, leakage past the screw, etc.

- **Insights into the injection process in respect of the effect of the processing parameters** (melt temperature, injection rate & pressure, cooling time, etc.) **on the in-mould parameters** (cavity pressure, solidification time, part weight, dimensional capabilities, skin thickness, warpage, etc.). These were gained through simulation and experimentation. It was found that accurate estimation of the transition time from filling to packing phase and prediction of part solidification were parameters of utmost importance in order to control part quality. Therefore two non-invasive methods were proposed and designed. The first method used a pair of thermocouples embedded close to the cavity surface to estimate the extent of solidification in real time. This approach does not require a complex heat transfer model because real time temperature data are used to estimate the heat transfered from the melt part to the mould. The second method uses ultrasound waves that propagate through the melt polymer in order to identify phase changes, determine the extent of solidification of the part (in real time) while also measure the part thickness (off-line) before part ejection.

- **The concept of a new mould which allowed parts with different shapes** (tensile specimens and rectangular parts) **to be moulded with the proper cavity insert**. The gate position could be changed from the centre to the side, to test the effect of flow orientation in the mechanical properties of the parts. In addition, a transparent polymer was used with color additives to visualise the flow orientation in the parts. The mould was manufactured from a tough aluminium alloy with a high thermal conductivity, to minimise the heating-up time and to allow thermocouples to detect the heat transients during injection. The thermocouples and ultrasound transducers were embedded at the mould while the cavity pressure transducer (tip) was positioned flush to the cavity surface. The instrumented mould enabled testing of the functionality of the two proposed methods for monitoring the melt behaviour and verification of the hypotheses made. From the solidification rate (both thermocouple & ultrasound methods had similar results) it was estimated that nearly 50% of the part had solidified by the end of the filling phase (with no cooling). This makes the shearing of the melt at the core (of the part) more difficult

because the molecular chains get isolated from the above layers and have more time to relax and become randomised. These results led to the publication (Appendix A.6) of a journal paper published at the IMechE Journal of Engineering Manufacture, Part B [148].

- **The modification of the hydraulic circuit in order to enhance the controllability of the moulding machine and change the processing parameters during the injection.** A servo-proportional flow and pressure control valve was used to bypass the side manifold of the original hydraulic circuit which was used to preset the hydraulic flowrate and pressure during injection. In order to control the new valve (the screw motion) and the other operations (mould open-close, injection unit forward-retract) of the moulding machine via a PC, the electrical circuit of the machine was bypassed by safety hardware to prevent any hazardous situation. All the signal information (temperature, pressures, propagation time of ultrasound waves) from the instrumented mould and hydraulic circuit (screw position, velocity and hydraulic pressure) were processed by the closed-loop control system.

- **The development of a hybrid MCS adaptive controller with a bumpless transfer scheme for the control of the filling and packing phases**. The hybrid MCS was first tested in simulation using a nonlinear model of the plant. Robustness to a range of operating conditions validated the performance of the hybrid MCS which was next implemented experimentally. Dual (velocity & acceleration) and single (velocity only) feedback signals were tested with the "Flow MCS" controller. A system identification allowed the estimation of the initial adaptive gains which considerably improved the transient response (enhanced adaptation) at the start of the filling phase. The adaptive weight ratio was changed from the generally accepted value to improve the performance and stability of the control scheme. In the case of the "Force MCS" controller the adaptation effort was modified such that it was proportional to the plant's pressure error. This permitted high adaptive weights to be safely used at the beginning of the packing to reduce the error rapidly, as well as to reduce the sensitivity of the MCS to noise in the feedback states which could result in gain drift or saturation of the adaptive gains. A bumpless transfer algorithm was developed to avoid discontinuity in the control signal during the switching from flow to pressure control. Otherwise pressure perturbations could occur during the transition which would disrupt the flow orientation (in the cavity) and possibly result in part surface defects and poor dimensional capability. Overall the hybrid MCS controller exhibited a robust behaviour to all operating conditions during the experiments which included changing of the mould cavity and polymer material.

- **A good understanding of the melt polymer flow orientation during injection and the influence of injection velocity and pressure on the formation of the part layers.** It is well known that conventional injection moulded part consists of: a thin oriented skin layer at the surface, a second layer which is highly oriented and the core layer which has

no preferred orientation. To influence the molecular orientation at the core layers, a new method was proposed where melt vibration was applied by vibrating the screw during the filling and packing phases. To achieve this a sinusoidal reference signal with varying amplitude and frequency was superimposed on the control signal that drives the servo-proportional valve to force the screw to oscillate. The vibrational energy is transferred to the melt polymer lowering the viscosity and improving the molecular orientation as filling and packing proceed under continuous pulsating shear flow. This hypothesis was supported by the profile of the cavity pressure which was increased exponentially with time while at the same time was oscillated at a frequency of 20Hz with an amplitude varying from 5bar to 25bar. In addition, higher cavity pressures were achieved during vibration which exceeded nominal values (with conventional moulding) by 100bar. The duration and level that the cavity pressure reached during vibration, improves the stress distribution in the part and reduces the stresses, therefore it reduces part warpage. Compared with conventional moulding, polypropylene parts (tensile specimens) moulded under melt vibration had a reduction in part warpage by 30% and increased tensile modulus by 10%. The higher modulus is also an indication that the parts, during vibration moulding, crystallised faster as vibration shifts the glass transition temperature higher. Moreover sensitive polymers (which degrade at high temperatures) could be processed at low temperatures where melt vibration would be used to lower the viscosity and ease the processability. This method could be easily applied to modern conventional injection moulding machines without the need of additional components to initiate melt vibration as others methods have proposed (such as Scorim, etc.).

8.1 Future Work

This work has identified new directions for the monitoring and control of the injection moulding process as well as new methods to enhance the mechanical and physical properties of the parts. Suitable area for further work include:

- **Experiments with melt vibration to investigate further the effect of frequency and amplitude of vibration in the shear thinning behaviour of polymers**. Vibration in conjunction with variable cooling profiles could control efficiently the melt viscosity during moulding, degree of crystallinity and size of spherulites to produce parts with different mechanical properties according to the application. In addition, vibration could be also applied during the plasticization phase to further reduce the viscosity of the polymer. Multi gate cavities should be also tested (with vibration profiles) to investigate the effects in part orientation. The parts produced should be tested with Optical Microscopy and other advanced methods (SEM, WAXD, DSC) to elucidate further the impact of

vibration frequency and amplitude on the degree of crystallinity, morphology and orientation in the parts. Parameters such as density and molecular weight of parts should also be measured and compared with the initial values to avoid vibration settings that could degrade the melt polymer.

- **Use of the proposed melt vibration method for applications of micro-moulding.** Lowering the viscosity of the melt during injection could allow to fill and pack cavities with thicknesses less that a millimetre. As melt vibration shifts the glass transition temperature higher and advances nucleation, the parts moulded could be compared with conventional moulded parts with and without nucleating agents. In particular, when using metallic pigments to colour the polymer, vibration could overcome current problems of surface defects and differential cooling. Melt vibration would be beneficial when additives are required to be mixed with polymers during the process, resulting in a better blending. However experimental testing is required to verify these hypotheses.

- **Carry out further tests with the hybrid MCS controller with a range of polymers and cavity sizes to validate the robustness of the proposed strategy.** A self-commissioning procedure could be designed where the hybrid MCS would automatically tune the initial adaptive gains (to improve the transient response). This information could be provided from plant identification procedure running in parallel with the MCS during the injection moulding cycle (when necessary). In addition, a mechanism that could adjust automatically the adaptive weights ratio, would be an advantage in cases where the load conditions change considerably to improve performance and guarantee stability.

- **Commercialise the ultrasound monitoring kit to be used with the moulding machine controller to estimate the duration of the injection phases in real time.** This would considerably reduce the setup time for a new mould (only one cycle is necessary) and the information could be used for real time quality control and for statistical process control analysis. Moreover ultrasound could be used to extract information such as melt temperature and pressure [149] as well as the degree of crystallinity. At the moment the two leader companies in instrumentation, Dynisco and Kistler do not have such a kit and rely completely to cavity pressure transducers (which are very costly) to switch from filling to packing phase. In addition, if a miniature version of the ultrasound transducer is used, new moulds could be manufactured with ready-embedded ultrasound sensors to monitor a number of in-mould parameters in real time. Such an approach could lead to all-phase control (Section 1.3.1) of the injection moulding process.

Thus there seems to be a great potential to control the melt polymer behaviour with melt vibration in order to enhance the quality of the parts and improve the injection cycle (time) efficiency. The use of the ultrasound is very promising and could be used in the future for rapid optimisation of the process settings.

Bibliography

[1] Tadmor, Z., and Gogos, C., 1979. *Principles of polymer processing, SPE textbook.* John Wiley and Sons.

[2] Ernest, C., 1960. *Processing of Thermoplastic Materials.* SPE, Reinhold Publishing Corporation, New York.

[3] Osswald, T., 1998. *Polymer Processing Fundamentals.* Munich: Hanser.

[4] Rosato, D., and Rosato, D., 1995. *Injection Molding Handbook.* Chapman and Hall.

[5] Kazmer, D., and Hatch, D., 1999. "Towards Controllability of Injection Moulding". *ASME, IMECE, Nashville.*

[6] Mann, J.", 1974.". *Plastics Engineering and Science*, p. 25.

[7] Agrawal, A., Pandelidis, I., and Pecht, M., 1987. "Injection Moulding Control: A Review". *Polymer Engineering and Science,* **27(18)**, pp. 1345–1357.

[8] Kazmer, D., and Speight, R., 1997. "Polymer Injection Moulding Technology for the Next Millennium: A Vision to the Future". *Journal of Injection Moulding Technology,* **1(2)**, pp. 81–90.

[9] Rafizadeh, M., Patterson, W. I., and Kamal, M. R., 1996. "Physically-Based Model of Thermoplastics Injection Moulding for Control Applications". *International Polymer Processing,* **11**, pp. 352–362.

[10] Shankar, A., and Paul, F., 1982. "A Mathematical Model for the Evaluation of Injection Molding Machine Control". *Transactions of the ASME 104,* **104**, pp. 86–92.

[11] Chiu, C., Shih, M., and Wei, J., 1991. "Dynamic Modelling of the Mould Filling Process in an Injection Moulding Machine". *Polymer Engineering and Science,* **31**, pp. 1417–1425.

[12] Havlicsek, H., 1998. "Iterative Learning Control of Injection Molding". Master's thesis, University of Illinois Urbana-Champaign, U.S.A.

[13] Zheng, D., and Alleyne, A., 2000. "Modelling and learning Control of an Electro-Hydraulic Injection Moulding Machine With Smoothed Fill-to-Pack Transition". *Japan USA Vietnam RESCCE Workshop, Ho Chi Minh City, June 6-9.*

[14] Guerrier, P., 2001. "Hydraulic Pressure & Flow Control of Injection Moulding". PhD thesis, University of Bath, Department of Mechanical Engineering.

[15] Mok, S., and Kwong, C., 1999. "Review of Research in the Determination of Process Parameters for Plastic Injection Moulding". *Advances in Polymer Technology,* **18(3)**, pp. 225–236.

[16] Edge, K., 1997. "The Control of Fluid Power Systems - Responding to the Challenges". *Proc. IMechE,* **211(1)**, pp. 91–110.

[17] Zheng, D., and Alleyne, A., 2000. "Control-Oriented of an Injection Moulding Machine including the Fill-to-Pack Transition". *Proceedings of the ASME, Dynamic Systems and Control, Orlando,* **69(1)**, pp. 345–352.

[18] Potsch, G., and Michaeli, W., 1995. *Injection Molding An Introduction.* Hanser Publishers, Munich.

[19] Tian, Y.C., . G. F., 1999. "Injection Velocity Control of Thermoplastic Injection Moulding Via A Double Controller Scheme". *Ind. Eng. Chem. Res.,* **38(9)**, pp. 3396–3406.

[20] Speight, R., Monro, A., and Khassapov, A., 1998. "Benefits of Velocity Phase Pprofiles for Injection Moulding". *ANTEC.*

[21] Gurhan, K., and Bevis, M., 1997. "Processing and Physical Property Relationships in Injection-Molded Isostatic Polypropylene. 1. Mechanical Properties". *Journal of Polymer Science,* **35**, pp. 241–263.

[22] Astbury, D., Bakharev, A., and Speight, R., 2003. "Automatic injection velocity initialization for computer-assisted injection molding setup". *ANTEC*, pp. 576–580.

[23] Leo, V., and Cuvelliez, G., 1996. "Effect of packing parameters, gate geometry and mould elasticity on the final dimensions of a molded part". *Polymer Engineering and Science,* **36**(15), Mid-August, pp. 1961–1971.

[24] Dontula, N., Sukanek, P., Devanathan, H., and Campbell, G.", 1991.". *Polymer Engineering and Science,* **31**.

[25] Coates, P., and Speight, R., 1995. "Towards Intelligent Process Control of Injection Moulding of Polymers". *Proc. IMechE Journal of Engineering Manufacture,* **209**, pp. 357–367.

[26] Mamat, A., Trochu, F., and Sanschagrin, B., 1995. "Shrinkage Analysis of Injection Polypropylene Parts". *Polymer Engineering and Science,* **35(19)**, pp. 1511–1520.

[27] Coulter, J., Tom, A., and Kikuchi, A., 1999. "An experimental evaluation of vibration-assisted injection molding during manufacturing". *Journal of Materials Processing and Manufacturing Science,* **8(2)**, pp. 141–153.

[28] Christopher, C., 1999. "Monitor Cavity Pressure Perfects Injection Moulding". *Journal of Assembly Automation,* **19(3)**, pp. 197–202.

[29] Gao, F., Paterson, W., and Kamal, M., 1996. "Cavity Pressure Dynamics and Self-Tuning Control for Filling and Packing Phases of Thermoplastics Injection Moulding". *Polymer Engineering and Science,* **36(9)**, pp. 1272–1285.

[30] Kamal, M., Varela, A., and Paterson, W., 1999. "Control of Part Weight in Injection Moulding of Amorphous Thermoplastics". *Polymer Engineering and Science,* **39(5)**, pp. 940–952.

[31] Gao, F., Paterson, W., and Kamal, M., 1996. "Cavity Pressure Control During the Cooling Stage in Thermoplastic Injection Moulding". *Polymer Engineering and Science,* **36(19)**, pp. 2467–2476.

[32] Long, A., 2002. Polymer Engineering Course Notes (H3CPOE). Tech. rep., University of Nottingham.

[33] Gao, F., Paterson, W., and Kamal, M., 1993. "Dynamics and Control of Surface and mould Temperatures in Injection Moulding". *Intern. Polymer Processing,* **VIII (2)**, pp. 147–157.

[34] Varela, A., Kamal, M., and Paterson, W., 1996. "A Method for Estimating Bulk Melt Temperature and Part Weight in Injection Moulding of Amorphous Thermoplastics". *Advances in Polymer Technology,* **15(1)**, pp. 17–28.

[35] Chen, S., and Chung, Y., 1992. "Simulations of Cyclic Transient Mould Cavity Surface Temperature in Injection Mould Cooling Process". *Int. Comm. Heat Mass Transfer,* **19**, pp. 559–568.

[36] Xia, Z., and Mallick, P., 1997. "Control of Dimensional Variability in Injection Moulded Plastic Parts". *ANTEC.*

[37] Beard, R., 1999. "Process Validation Considerations for Injection Molding". *Journal of Validation Technology,* **5(2)**.

[38] Wenskus, J., 1997. "Part Weight as a Control Metric for Injection Molding". *Journal of Injection Moulding Technology,* **1(3)**.

[39] Garvey, E., 1997. "On-line Quality Control of Injection Molding Using Neural Networks". Master's thesis, Department of Computer Science, Royal Melbourne Institute of Technology, Melbourne, Victoria, Australia.

[40] Petrova, T., and Kazmer, D., 1999. "Incorporation of Phenomenological Models in a Hybrid Neural Network for Quality Control of Injection Moulding". *Plastics Technology and Engineering,* **38(1)**.

[41] Wen, S.-S., Jen, C., and Nguyen, K., 1999. "Advances in On-line Monitoring of the Injection Moulding Process Using Ultrasonic Techniques". *Inter. Polymer Processing,* **XIV(2)**, pp. 175–182.

[42] Nishiwaki, N., and Hori, S., 1998. "Measurement of Injection Moulding and Machine Process Using Ultrasonic Technique". *IEEE Ultrasonic Symposium,* **2**, pp. 755–758.

[43] Nishiwaki, N., Hori, S., Orita, H., Cui, A., and Konno, M., 1990. "A New Ultrasonic Method for Measurement the Crystallinity of Thermoplastics Used in Injection Molding Products". *The International Conference on Manufacturing Systems and Environment, Tokyo, Japan*, pp. 217–222.

[44] Brown, E., Olley, P., and Coates, P., 2000. "In line melt temperature during real time ultrasound monitoring of single screw extrusion". *Plastics, Rubber and Composites,* **29(1)**, pp. 3–13.

[45] Rawabdeh, I., 2001. "Ultrasonic Measurements of Polymer Density Variation in Plastic Injection Moulding Process". *XII ADM International Conference.*

[46] Wang, H., Cao, B., Jen, C., and Nguyen, K., 1997. "On-line Monitoring of the Injection Moulding Process". *Polymer Engineering and Science,* **37(2)**, pp. 363–376.

[47] Ballman, R., and Shusman, T., 1959. "Easy Way to Calculate Injection Moulding Set-up Time". *Modern Plastics*, p. 126.

[48] Dietzel, H., Hamburg, Schumann, J., Chemnitz, and Muller, K., 1991. "Calculating the Cooling and Sealling Times Analytically". *Kunststoffe German Plastics,* **81(12)**, pp. 32–33.

[49] Stelson, K. Estimating the extent of solidification for Polymer Injection Moulding. Bath University Int. Report, 2001, 17, pp. 1-11,.

[50] Zuidema, H., 2000. "Flow induced crystallization of polymers". PhD thesis, Eindhoven University of Technology, Netherlands.

[51] Kikuchi, A., Coulter, J., and Angstadt, D., 2002. "Polymer Melt Manipulation and In-Process Morphology Control During Molding Processes: A Review". *Journal of Injection Molding Technology,* **6(2)**, pp. 91–106.

[52] Rawabdeh, I., 1999. "In-line Monitoring of Injection Moulding Operations: A Literature Review". *Journal of Injection Molding Technology,* **3(2)**, pp. 47–53.

[53] *Fluid Power Courses, FP4 Lecture Notes 2000.* Centre for Power Transmission and Motion Control (PTMC), University of Bath.

[54] Merrit, H., 1967, New York. *Hydraulic Control Systems.* John Willey and Sons.

[55] Karnopp, D., 1985. "Computer Simulation of Stick-Slip Friction in Mechanical Dynamic Systems". *ASME Journal of Dynamic Systems Measurements and Control,* **107**, pp. 100–103.

[56] Brydson, J., 1981. *Flow Properties of Polymer Melts.* Godwin in association with the Plastics and Rubber Institute.

[57] Lenk, R., 1978. *Polymer Rheology.* Applied Science publishers LTD, England.

[58] Nielsen, L., 1977. *Polymer Rheology.* Dekker, New York.

[59] Cross, M. M., 1979. "Relation between viscoelasticity and shear-thinning behaviour in liquids". *Rheologica Acta,* **18(5)**, pp. 609–614.

[60] Pontes, A. J. V., 2002. "Shrinkage and ejection forces in injection moulding products". PhD thesis, University of Minho, Portugal.

[61] Woll, S., and Cooper, D., 1997. "A dynamic injection-moulding process model for simulating mould cavity pressure patterns". *Polym. Plast. Technol. Eng.,* **36(5)**, pp. 809–840.

[62] Ieremias, A., 2002. "Modelling of the performance of an injection moulding machine". Master's thesis, University of Bath.

[63] Edwards, C., and Postlethwaite, I., 1998. "Anti-windup and bumpless transfer schemes". *Automatica,* **34(2)**, pp. 199–210.

[64] Han Wee, N., 1999. "Iterative learning control and bumpless transfer for an electro-pneumatic servo system". Master's thesis, University of Illinois.

[65] Paxman, J., and Vinnicombe, G., December 2000. "Optimal Transfer Schemes for Switching Controllers". *Proceedings of the 38th IEEE,* pp. 1093–1098.

[66] Astrom, K., and Hagglund, T., 1988. *Automatic Tuning of PID Controllers.* Instrument Society of America.

[67] Stelson, K. A., 2003. "Calculating Cooling Times for Polymer Injection Moulding". *Part B: Journal of Engineering Manufacture,* **217**, pp. 709–713.

[68] Arburg Manufactures Handbook, Manual of the Injection Moulding Machine.

[69] MatWeb, material property data, http://www.matweb.com.

[70] RTP, material property database, http://www.rtpcompany.com.

[71] Tennalum, A Division of Kaiser Aluminium, Kaiser Aluminum Technical Reference Library No.1011, Specifications of Aluminium Alloy 7075, http://tennalum.com/td7075.htm.

[72] Holman, J., 1997. *Heat Transfer.* McGraw-Hill 8th Edition.

[73] Bayplastics, Properties of Insulation Material, Grade 10G/40 Epoxy Glass Fabric, http://www.bayplastics.co.uk/datahtm.

[74] Zhang, X., Voller, V. R., Stelson, K. A., Bhattacharya, M., Cheng, X., and Sen, A., 2002. "An approximate model of tThermal residual stress in an injection molded part". *Journal of Thermal Stresses,* **25**, pp. 523–538.

[75] Krautkramer, J., and Krautkramer, H., 1983. *Ultrasonic Testing of Materials.* Springer, Verlag Berlin Heidelberg.

[76] Selfridge, A., 1985. "Plastic Materials Acoustic Properties". *IEEE Transactions On Sonics and Ultrasonics,* **SU-32(3)**, pp. 381–394. NDTnet, http://www.ndt.net/links/proper.htm.

[77] Ultrasound Theory on the Web, http://freespace.virgin.net/mark.davidson3/ reflection/reflection.html.

[78] Ibar, J., 1997. "Smart Processing of Plastics through Vibration Controlled Shear Thinning and Orientation". *CAE and Intelligent Processing of Polymeric Materials ASME,* **79**, pp. 223–248.

[79] Ibar, J., 1981. "Rheomolding: A new process to mould polymeric materials". *Polymer Plastic Technology Engineering,* **17(1)**, pp. 11–44.

[80] Humbeec, E., 2002. "Polypropylene A Material of Choice for Medical and Pharmaceutical Application, Technical Service and Material Development Engineer, ATOFINA Polypropylene Business Unit - ATOFINA Research". *Medical Device Manufacturing & Technology 2002.*

[81] Daly, H., Nguyen, K., Sanschagrin, B., and Cole, K., 1998. "The Build-Up and Measurement of Molecular Orientation, Crystalline Morphology, and Residual Stresses in Injection Molded Parts: A Review". *Journal of Injection Molding Technology,* **2(2)**, pp. 59–85.

[82] Keller, A., and Kolnaar, J., 1997. "Flow-induced orientation and structure formation". *Processing of Polymers, Material Science and Technology,* **18**, pp. 189–268.

[83] Cakmak, M., 2001. "Structure development in injection molding of fast and slowly crystallizing semicrystalline polymers". In FLOW INDUCED CRYSTALLIZATION OF POLYMERS, Salerno, Italy.

[84] Jerschow, P., and Janeschitz-Kriegl, H., 1997. "The role of long molecules and nucleating agents in shear induced crystallization of isotactic polypropylenes". *International Polymer Processing XII,* **1**, pp. 72–77.

[85] Pantani, R., Coccorullo, I., Speranza, V., and Titomanlio, G., 2005. "Modeling of morphology evolution in the injection molding process of thermoplastic polymers". *Progress In Polymer Science,* **30**, pp. 1185–1222.

[86] Ezrin, M., 2002. "The role of fundamentals, visual observation and state-of-the-art instrumental methods in solving plastics failures". *ANTEC*, pp. 3062–3066.

[87] Ezrin, M., Lavigne, G., Dudley, M., and Pinatti, L., 2005. "Case studies of plastics failure related to molecular weight or chemical composition". *ANTEC*, pp. 3469–3474.

[88] J.N., H., 1995. "The physical ageing of amorphous and crystalline polymers". *Pure and Applied Chemistry,* **67(11)**, pp. 1855–1858.

[89] ir. J. van Meerveld. Flow-induced crystallization, Thermodynamically consistent modelling approach. Institute of Polymers, Polymer Physics, ETH Zurich.

[90] Swartjes, F., 2001. "Stress induced crystallization in elongation flow". PhD thesis, Eindhoven University of Technology, Netherlands.

[91] Lauritzen, J., and Hoffman, J., 1960. "Theory of formation of polymer crystals with folded chains in dilute solution". *J. Res. Natl. Bur. Stand.,* **64**, pp. 73–102.

[92] Ltd., T. T. Shrinkage in Plastics Processing, http://www.tangram.co.uk. Tech. rep.

[93] Zuidema, H., Peters, G., and Meijer, H., 2001. "Development and validation of a recoverable strain based model for flow-induced crystallization of polymers". *Macromolecular Theory and Simulations,* **10(5)**, pp. 447–460.

[94] Cermak, R., Obadal, M., Ponizil, P., and Stoklasa, K. "Injection Moulidng of a- AND b-Polypropylenes: Morphology Consequences". *ANTEC 2005*, pp. 2163–2167.

[95] H. Itoh, K. M., 1996. "Effect of pressure and shear stress on crystallization behaviors in injection molding". *International Polymer Processing,* **11(4)**, pp. 363–368.

[96] Beek, M. v. d., 2005. "Specific volume of polymers, Influence of the thermomechanical history". PhD thesis, Eindhoven University of Technology, Netherlands.

[97] Lacrampe, M., and Pabiot, J., 2000. "Defects in surface appearance of injection moulded thermoplastic parts - A review of some problems in surface gloss distribution". *Journal of Injection Molding Technology,* **4**(4), December, pp. 167–176.

[98] Arjen, C., Bogaerds Martien, A., and Hulsen Gerrit, W., 2004. "Stability Analysis of Injection Molding Flows". *Journal of Rheology,* **48**, pp. 765–785.

[99] Wang, T., and Young, W., 2005. "Study on Residual Stresses of Thin-Walled Injection Moulding". *European Polymer Journal,* **41**, pp. 2511–2517.

[100] Dawson, A., Rides, M., and Nottay, J., 2005. "The Effect of Pressure on the Thermal Conductivity of Polymer Melts". *Polymer Testing*, pp. 1–8.

[101] Moldflow, 1991. Warpage Design Principles, Making Accurate Plastic Parts.

[102] Timm, M., and Couts, M. "Relationship of Predicted Shear Stress to Molded Plastic Parts". *ANTEC 2003*, pp. 3373–3376.

[103] Kikuchi, A., and Coulter, P., 2000. "Improved Processing of New and Recycled Material Blends through Vibration-Assisted Injection Moulding". *Journal of Materials and Manufacturing Science,* **8**, pp. 273–289.

[104] Wang, L., Allan, P., and Bevis, M., 1997. "Application of shear controlled orientation in injection moulding for in situ formation of 0-90 degrees laminates in moulded thermotropic liquid crystalline polymers". *Plastics, Rubber and Composites Processing and Applications,* **26(8)**, pp. 351–359.

[105] Ibar, J., 1998. "Control of Polymer Properties by Melt Vibration Technology: A Review". *Polymer Engineering and Science,* **38(1)**, pp. 1–20.

[106] Edge, K., 2003. "On the control of electrohydraulic systems - some recent research contribution". *The Eight Scandinavian International Conference on Fluid Power, Tampere, Finland.*

[107] Gamble, J. B., and Vaughan, N. D., 1996. "Comparison of sliding mode control with state feedback and PID control applied to a proportional solenoid valve". *Trans. ASME, Journal of Dynamic Systems, Measurement and Control,* **118(3)**, pp. 434–438.

[108] Tan, K., Huang, S., and Jiang, X., 2001. "Adaptive Control of Ram Velocity for the Injection Moulding Machine". *IEEE Transactions on Control Systems Technology,* **9(4)**, pp. 663–671.

[109] Suykens, A., Vanderwalle, J., and De Moor, B., 1996. *Artificial Neural Networks for Modelling and Control of Non-Linear Systems*. Kluwer Academic Publishers.

[110] Mok, S., Kwong, C., and Lau, W., 2000. "An Intelligent Hybrid System for Initial Process Parameter Setting of Injection Moulding". *INT. J.PROD.RES.,* **38(17)**, pp. 4565–4576.

[111] Lau, H., Ning, A., Pun, K., and Chin, K., 2001. "Neural Networks for the Dimensional Control of Moulded Parts based on a Reverse Process Model". *Journal of Materials Processing Technology,* **117**, pp. 89–96.

[112] Petrova, T., and Kazmer, D., 1999. "Hybrid Neural Models for Pressure Control in Injection Molding". *Advances in Polymer Technology,* **18(1)**, pp. 19–31.

[113] Pedrycz, W., 1983. *Fuzzy Control and Fuzzy Systems.* Research Studies Press.

[114] Tsoi, H., and Gao, F., 1999. "Control of injection velocity using a fuzzy logic rule-based controller for thermoplastics injection moulding". *Polymer Engineering and Science,* **39(1)**, pp. 3–17.

[115] Huang, S., and Lee, T., 2000. "Fuzzy Logic Controller for a Retrofitted Closed-loop Injection Moulding Machine". *IMechE, Proc Instn Mech Engrs,* **214(1)**, pp. 9–21.

[116] Havlicsek, H., and Alleyne, A., 1999. "Nonlinear control of an electrohydraulic injection molding machine via iterative adaptive learning". *IEEE/ASME Transactions on Mechatronics,* **4(3)**, pp. 312–323.

[117] Uchiyama, M., 1978. "Formation of a High-Speed Motion Patern of a Mechanical Arm by Trial". *Transactions of Society for Implementation and Control Engineers,* **14**, pp. 706–712.

[118] Arimoto, S., Kawamura, S., and Miyazaki, F., 1984. "Bettering Operation of Robots by Learning". *Journal of Robotic Systems,* **1(2)**, pp. 123–140.

[119] Sugie, T., and Ono, T., 1991. "An Iterative Learning Control Law for Dynamical Systems". *Automatica,* **27(4)**, pp. 729–732.

[120] Gao, F., Yang, Y., and Shao, C., 2001. "Robust Iterative Learning Control with Applications to Injection Moulding Process". *Chemical Engineering Science,* **56**, pp. 7025–7034.

[121] Zheng, D., and Alleyne, A., 2003. "Modeling and Control of an Electro-hydraulic Injection Molding Machine With Smoothed Fill-to-Pack Transition". *Transactions of the ASME,* **125**, pp. 154–163.

[122] Li, X., Ouyang, G., Guan, X., and Du, R., 2006. "Ram Position Control in Plastic Injection Molding Machines with Higher Order Iterative Learning". *Control and Intelligent Systems,* **34(1)**, pp. 64–72.

[123] Sugiyama, T., and Uchida, K., 2002. "Gain Scheduled Velocity and Force Controllers for the Electro-hydraulic Servosystem". *Proceedings of the American Control Conference, Anchorage*, pp. 4433–4438.

[124] Astrom, K., 1983. "Theory and Applications of Adaptive Control - A Survay". *Automatica,* **19(5)**, pp. 471–486.

[125] Isermann, R., 1992. *Adaptive control systems.* Prentice Hall.

[126] Yang, Y., and Gao, F., 1998. "Adaptive Control of Nozzle Melt Packing Pressure". *Journal of Intelligent Materials System and Structures,* **9**, pp. 1046–1050.

[127] Yang, Y., and Gao, F., 1999. "Cycle-to-cycle and within-cycle adaptive control of nozzle pressure during packing-holding for thermoplastic injection molding". *Polymer Engineering & Science,* **39(10)**, pp. 2042–2063.

[128] Landau, Y., 1979. *Adaptive control, the model reference approach.* New York and Basel: Marcel Dekker, INC.

[129] Ito, K., Yokota, K., and Ikeo, S., 2006. "Adaptive Control for Injection Molding Machines". In 5th International Fluid Power Conference.

[130] Stoten, D., and Benchoubane, H., 1990. "Robustness of a Minimal Control Synthesis Algorithm". *International Journal of Control,* **51(4)**, pp. 851–861.

[131] Stoten, D., and Benchoubane, H., 1990. "Empirical studies of an MRAC algorithm with minimal controller synthesis". *International Journal of Control,* **51(4)**, pp. 823–849.

[132] Stoten, D. P., 1992. "Implementation of minimal control synthesis on a servo-hydraulic testing machine.". *Proc. IMEchE Part I, Journal of Systems and Control Engineering,* **206(13)**, pp. 189–194.

[133] Beard, G., 1998. "Adaptive control of energy efficient hydraulic systems". PhD thesis, Department of Mechanical Engineering, University of Bristol, Bristol.

[134] Bulut, S., 2000. "The Robustness of Reduced Order Minimal Controller Synthesis Control in the Plastic Region". *Proceedings of the I MECH E Part I, Journal of Systems & Control Engineering,* **214(3)**, pp. 185–195.

[135] Bulut, S., 2006. "Strain Measurement Under the Minimal Controller Synthesis (MCS) Algorithm and a Extensometer Design". In Proceedings of the 5th International Symposium on Intelligent Manufacturing Systems.

[136] Stoten, D., and Neild, S., 2003. "The error-based minimal control synthesis algorithm with integral action". *Proc. IMEchE Part I, Journal of Systems and Control Engineering,* **217**, pp. 187–201.

[137] Stoten, D. P., and Gomez, E. G., 2001. "Adaptive Ccontrol of Sshaking Tables using the Minimal Control Synthesis Algorithm". *Phil. Trans. R. Soc. Lond. A.,* **359**, pp. 1697–1723.

[138] Gomez, E., 1999. "Application of the MCS algorithm to the control system of the Bristol shaking table". PhD thesis, University of Bristol, Bristol.

[139] Stoten, D., and Bulut, S., 1994. "Application of the MCS Aalgorithm to the Control of an Electrohydraulic System". *IEEE.*

[140] Stoten, D., 1995. "The Adaptive Minimal Control Synthesis Algorithm With Integral Action". *IEEE*, pp. 1646–1651.

[141] Bernardo, M., and Stoten, D., Dec 1997. "A New Extended Minimal Control Synthesis Algorithm with an Application to the Control of Chaotic Systems". *Proceedings of the 36th Conference on Decision & Control, San Diego, California USA*, pp. 1902–1907.

[142] Stoten, D., 1993. "An overview of the minimal control synthesis algorithm". *MechE Conference on Aerospace Hydraulics and Systems, C474-033, London.*, pp. 1494–1516.

[143] Beaumont, J., and Young, J., 1997. "Mold Filling Imbalances in Geometrically Balanced Runner Systems". *Journal of Injection Moulding Technology,* **1(3)**, pp. 133–143.

[144] Bushko, W., and Stokes, V., 1996. "Solidification of Thermoviscoelastic Melts. Part 3: Effects of Mould Surface Temperature Differences on Warpage and Residual Stresses". *Polymer Engineering and Science,* **36(3)**, pp. 322–335.

[145] Kamal, M., Lai-Fook, R., and Hernandez-Aguilar, J., 2002. "Residual Thermal Stresses in Injection Mouldings of Thermoplastics: A Theoretical and Experimental Study". *Polymer Engineering and Science,* **42(5)**, pp. 1098–1114.

[146] Xiangfang, P., Chao, X., Fengling, Z., Yiquan, L., and Nanqiao, Z., 2005. "Effects of Vibrating Injection on Structure and Property of Polymer Produce". *ANTEC Proceedings*, pp. 456–459.

[147] Hongwu, W., and Jinping, Z., 2005. "Processing and Properties Optimization of Dynamic Injection Molded PP". *ANTEC Proceedings*, pp. 884–888.

[148] Fronimidis, D., 2004. "Use of Non-Invasive Measurement Methods to aid the Control of Part Quality in the Injection Moulding Process". *Proc. IMechE Journal of Engineering Manufacture, Part B,* **218**, pp. 1195–1201.

[149] Zhaoyan, F., and Gao, R., 2006. "A Dual Sensing Approach to Silultaneous Temperature and Pressure Measurement from Injection Mold Cavity". *Proceedings of ASME, IMECE, Chicago, Illinois, USA*, pp. 1–7.

[150] Middleman, S., 1977. *Fundamentals of Polymer Processing*. McGraw-Hill.

Appendix A

Appendix

A.1 Material Dosage Shot Size

The material dosage shot size must be set according to the volume of the cavity neglecting any compressibility effects. An excess volume of material must be included to account for the leakage past the screw and additional volume required for the packing phase.

$$V_{cav} = A_{cav} \times h_{cav} = 7.04 \cdot 10^{-3} \times 4 \cdot 10^{-3} = 2.82 \cdot 10^{-5} m^3$$

If 10% is allowed for the excess volume required during packing the new required cavity volume will be:

$$V_{cav+ex.vol} = 1.1 \times 2.82 \cdot 10^{-5} = 3.1 \cdot 10^{-5} m^3$$

To define the dosage shot scale (active range of the screw) of the injection moulding machine a set of experiments was carried out with different shot sizes. In Figure A.1, the experimental results of the screw stroke versus the dosage shot are plotted. A 20% of leakage flow is included.

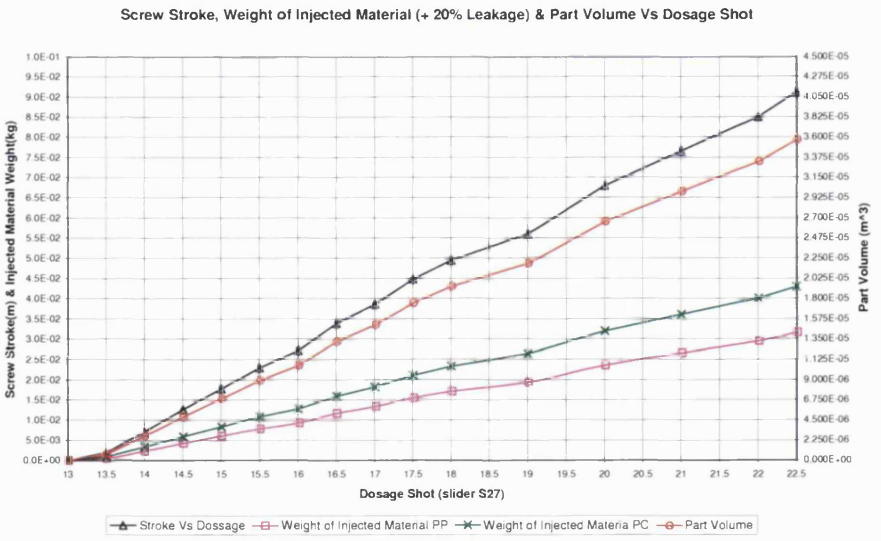

Figure A.1: Polymer Dosage Shot Size Vs Screw Stroke

According to the required volume of the new moulds cavity, the slider setting must be set to 21.

A.2 Cavity Pressure Profile

A typical cavity pressure profile is shown in Figure A.2.

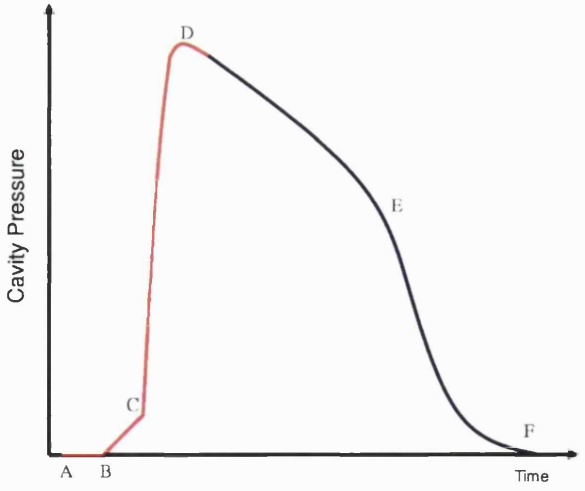

Figure A.2: Typical Cavity Pressure Profile during the Injection Moulding Cycle

During the injection moulding cycle the following stages can be identified from the cavity pressure profile:

a. Beginning of the injection phase, mould is closed and the filling of the cavity starts.

b. Polymer is injected at constant screw velocity. Melt material touches the pressure sensor.

c. Cavity is 95% full. Transition from filling to packing phase.

c-d. Pressure is regulated and the melt material starts to get pressurised inside the cavity.

d. Maximum cavity pressure according to the packing pressure control.

d-e. Reduction in cavity pressure due to volumetric shrinkage. Additional melt polymer is injected to compensate for changes in volume. Profile of cavity pressure depends on the profile of the holding pressure.

e. Sealing of the gate, constant volume in the cavity.

e-f. Pressure slowly drops to atmospheric level.

f. Shrinkage of the part inside the cavity, any changes in pressure are related to dimensional changes of the part.

A.3 Properties of Aluminium Alloy 7075 T6

The material that has been selected for the manufacture of the mould is a high strength Aluminium Alloy (7075_T6) that is used in the industry for plastic injection moulds. It provides very good machinability and hardness. The key feature of using this Aluminium Alloy is the advantage of high strength (similar to steel) and high thermal conductivity (6.5 times higher of steel). Some important mechanical and physical properties compared with those of steel are provided in Table A.1 below.

Material	Steel (mild)	Aluminium 7075-T6
Tensile Strength (MPa)	480	570
Shear Strength (MPa)	350	330
Modulus of Elasticity (GPa)	207	72
Thermal Conductivity (W/mK)	20	130

Table A.1: Mechanical Properties of Steel and Aluminium, from [71]

A.4 Heat Transfer Constants

The free convection constants for isothermal surfaces are presented in Figure A.3.

346 7-4 Free Convection from Vertical Planes and Cylinders

TABLE 7-1
Constants for use with Eq. (7-25) for isothermal surfaces

Geometry	$Gr_f Pr_f$	C	m	Ref(s).
Vertical planes and cylinders	10^{-1}–10^{4}	Use Fig. 7-7	Use Fig. 7-7	4
	10^{4}–10^{9}	0.59	$\frac{1}{4}$	4
	10^{9}–10^{13}	0.021	$\frac{2}{5}$	30
	10^{9}–10^{13}	0.10	$\frac{1}{3}$	22, 16†
Horizontal cylinders	0–10^{-5}	0.4	0	4
	10^{-5}–10^{4}	Use Fig. 7-8	Use Fig. 7-8	4
	10^{4}–10^{9}	0.53	$\frac{1}{4}$	4
	10^{9}–10^{12}	0.13	$\frac{1}{3}$	4
	10^{-10}–10^{-2}	0.675	0.058	76†
	10^{-2}–10^{2}	1.02	0.148	76†
	10^{2}–10^{4}	0.850	0.188	76
	10^{4}–10^{7}	0.480	$\frac{1}{4}$	76
	10^{7}–10^{12}	0.125	$\frac{1}{3}$	76
Upper surface of heated plates or lower surface of cooled plates	2×10^{4}–8×10^{6}	0.54	$\frac{1}{4}$	44, 52
Upper surface of heated plates or lower surface of cooled plates	8×10^{6}–10^{11}	0.15	$\frac{1}{3}$	44, 52
Lower surface of heated plates or upper surface of cooled plates	10^{5}–10^{11}	0.27	$\frac{1}{4}$	44, 37, 75
Vertical cylinder, height = diameter Characteristic length = diameter	10^{4}–10^{6}	0.775	0.21	77
Irregular solids, characteristic length = distance fluid particle travels in boundary layer	10^{4}–10^{9}	0.52	$\frac{1}{4}$	78

† Preferred.

Figure A.3: Free Convection Constants for Isothermal surfaces, from [72]

A.5 Density Variation of Polypropylene Vs Temperature

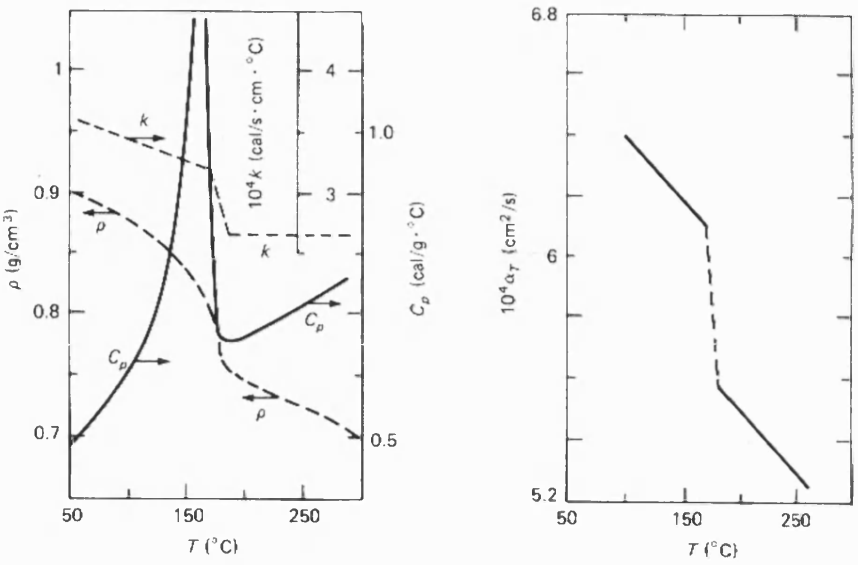

Figure A.4: Density Variation of Polypropylene Vs Temperature, from [150]

A.6 Related Publication

Use of non-invasive measurement methods to aid the control of part quality in the injection moulding process

D Fronimidis[1]*, K A Edge[2], K A Stelson[3], A R Mileham[1] and M A Sokola[2]
[1]Department of Mechanical Engineering, University of Bath, Bath, UK
[2]Centre for Power Transmission and Motion Control, University of Bath, Bath, UK
[3]Department of Mechanical Engineering, University of Minnesota, Minneapolis, Minnesota, USA

Abstract: The ability to monitor and detect changes in the morphology of injection moulded parts during the manufacturing cycle is a key issue for improving the process. Knowledge of the extent of solidification of the part during the packing and cooling phase enables better control of the process and good repetition of product quality. A novel way of extracting process information from two existing non-invasive methods is presented here. One method uses piezoelectric transducers generating/recording ultrasound waves that propagate through the polymer melt, while the other utilizes fast-response thermocouples embedded close to the mould cavity. The ultrasound wave speed variation and amplitude attenuation are monitored. These are then utilized with the aid of an off-line data processing algorithm to identify phase changes during the injection cycle (instead of monitoring variations in cavity pressure), as well as to predict accurately the extent of solidification of the produced part. The extent of solidification is also predicted with the thermocouple method. The results of both methods can be used to improve the control of product quality, with the ultrasound method providing significant additional information.

Keywords: injection moulding, polymer solidification, ultrasound wave

NOTATION

A	area of the mould cavity
b	half-thickness of the moulded part
c	specific heat of the polymer
c_{av}	average ultrasound velocity through the mould cavity
c_l	ultrasound velocity through the liquid polymer
c_s	ultrasound velocity through the solid polymer
C	thermal capacitance of the thermal section
L	latent heat of crystalline polymers (for amorphous polymer is zero)
q	heat flux
R_c	thermal convective resistance at the mould–polymer interface
T_m	temperature of the mould
T_s	temperature of the solidified polymer
T_1	temperature from the thermocouple close (5 mm depth) to the cavity surface
T_2	temperature from the thermocouple close (15 mm depth) to the cavity surface
U_T	total internal energy of the moulded part
z_s	thickness of the solidified layer of the polymer
ρ	density of polymer

The MS was received on 5 April 2004 and was accepted after revision for publication on 28 May 2004.
**Corresponding author: Department of Mechanical Engineering, University of Bath, 8E-2.8, Claverton Down, Bath BA2 7AY, UK.*

1 INTRODUCTION

Injection moulding is a widely used process for the manufacturing of complex shape products. Every time a new mould is used, expert knowledge is required to finely tune the injection moulding machine. To reduce the initial set-up time and predict physical and anisotropic properties (related to the oriented structure) of the moulded part accurately, non-invasive monitoring techniques are preferred. Previous researchers have used ultrasound sensors to describe the polymer's behaviour during extrusion and injection moulding [1, 2]. Some other groups have used ultrasound to describe the influence of blowing agents and fillers on the rheology of the polymer [3, 4].

SC01804 © IMechE 2004

In this research study the attenuation and speed variation of the longitudinal ultrasound wave propagating through the mould cavity are shown to have a strong relationship with the temperature and pressure variation of the molten polymer. In addition, the injection phases can be accurately identified as well as the moment during cooling where the part detaches from the wall. This is used as an initial indication of the extent of solidification of the part.

The results are validated using a previously developed thermal-based method [5], which processes real-time data from fast-reacting thermocouples. This enables the thermal change that occurs inside the mould during injection to be monitored, assuming perfect coupling between the part and the cavity and with no loss of energy being transferred to the environment. The extent of solidification of the moulded part was determined in real time. Alternatively, a theoretical method for calculation of the extent of solidification has been reviewed in reference [6].

2 EXPERIMENTAL SET-UP

For the monitoring of the in-mould parameters a special-purpose aluminium mould was designed with a rectangular cavity (160 mm × 44 mm × 4 mm). This makes the geometry simple and facilitates understanding the behaviour of the polymer melt during the injection cycle. An insert was used to produce tensile testing specimens [7]. The mould was instrumented with temperature, cavity pressure and ultrasound sensors (Fig. 1). Insulation between the mould and the injection moulding platens was used to reduce the heat loss to the surroundings and stabilize the cooling phase of the moulded part. Two polymeric materials were used for the experiments: amorphous polycarbonate (PC) and semi-crystalline polypropylene (PP).

2.1 Thermocouple monitoring of solidification

The first technique makes use of real-time temperature measurements at two different depths close to the cavity wall. The high thermal conductivity of aluminium helps the transient temperature effects to be transferred rapidly. The sensors are assumed to be in the centre of a thermal section. An algorithm takes into account the heat conducted from the first thermal section to the second section and relates that to the growth of solid layers within the molten part (Fig. 2). Information about the polymer properties and dimensions of the cavity are used to estimate the reduction in the internal energy and solidification rate of the part. A perfect thermal contact is assumed at the polymer–mould interface and the thermal convective resistance is neglected.

The heat flowrate into the mould $q(t)$ is proportional to the extent of the solidified layers of the polymer [5]:

$$q(t) = -\frac{\mathrm{d}U}{\mathrm{d}t} = \rho A\left(c\frac{T_\mathrm{s} - T_\mathrm{w}}{2} + L\right)\frac{\mathrm{d}z_\mathrm{s}}{\mathrm{d}t} = w\frac{\mathrm{d}z_\mathrm{s}}{\mathrm{d}t} \qquad (1)$$

Upon integration of the above equation the solidified layer profile z_s is expressed by [5]

$$z_\mathrm{s}(t) = \frac{C}{w}T_1(t) + \frac{1}{wR_\mathrm{c}}\int_0^t [T_1(\tau) - T_2(\tau)]\,\mathrm{d}\tau \qquad (2)$$

2.2 Ultrasound monitoring of solidification

The second technique makes use of ultrasound waves generated by piezoelectric transducers operating at high frequency (4 MHz). These waves propagate through the mould sections and polymer melt in the cavity. As the state of the polymer changes from liquid to solid an increase in the wave speed and attenuation in the amplitude is observed. These real-time data are captured and

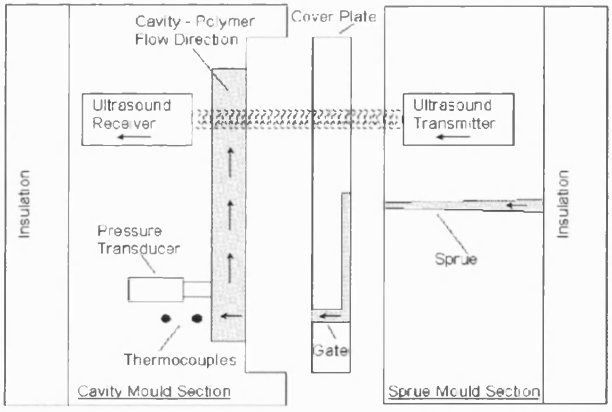

Fig. 1 Position of thermocouples and ultrasound sensors in the mould

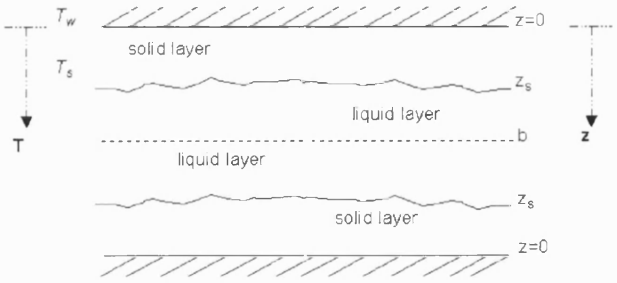

Fig. 2 Solid–liquid layers of the cavity model

analysed to identify the trajectories and transitions of the phases, variation in process parameters and solidification rate of the part. The extent of solidification is defined by the average wave speed through the thickness of the cavity [5]:

$$z_s(t) = b\frac{c_l/c_{av}(t) - 1}{c_l/c_s - 1} \tag{3}$$

Data for the ultrasound wave speed through the liquid layers have been obtained experimentally.

3 EXPERIMENTAL RESULTS AND DISCUSSION

For the experimental work the injection moulding machine was carefully set up to produce tensile testing specimens with appropriate dimensional accuracy. Physical properties will change due to the variation in mould and processing temperature. The filling, packing and cooling times for the moulding of the parts (PP) were 1.5, 15 and 25 s respectively.

3.1 Ultrasound data analysis

The ultrasound waves that propagate through the cavity show a variation in the propagation period and amplitude during the injection cycle. In Fig. 3 the variation of the received signal during the injection of PP is shown for different mould temperatures.

Parameters such as mould temperature and pressure affect the crystallization kinetics and consequently the way that the polymer chains are formed. Unsurprisingly the higher the temperature of the mould the longer it takes for the part to solidify and detach from the mould wall. The sudden change in sound delay at the beginning of the injection (falling from 7.3 to 6.6 μs) cycle indicates that nearly half of the part solidifies when the polymer comes in contact with the mould

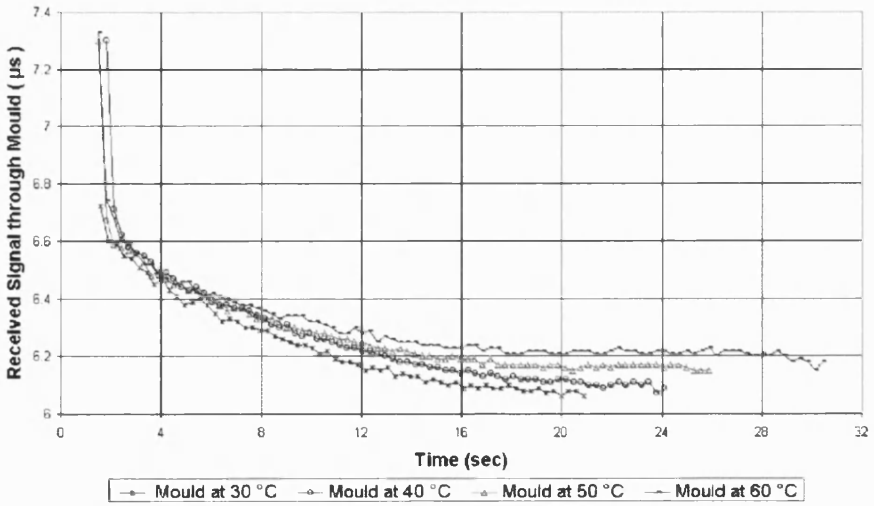

Fig. 3 Received ultrasound signal through the mould cavity during the injection of PP at 200 °C

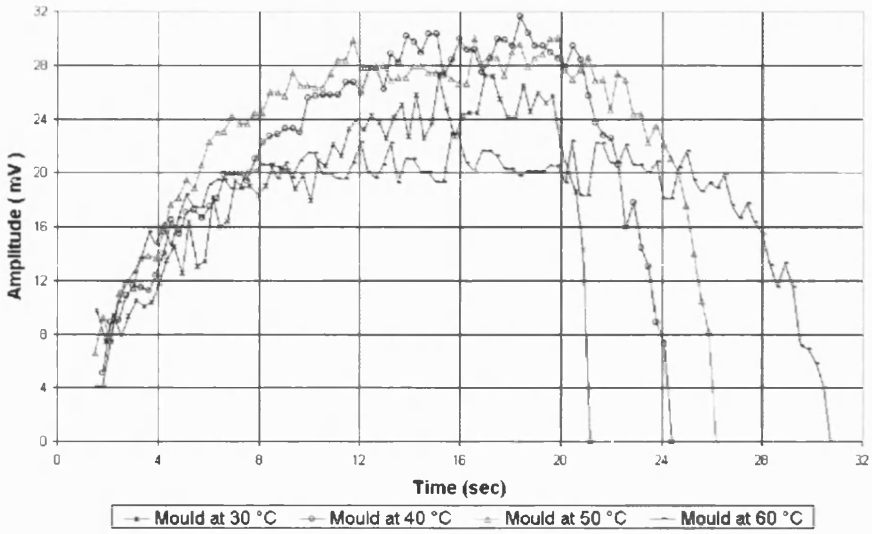

Fig. 4 Amplitude of the received ultrasound signal through the mould cavity during the injection of PP at 200 °C

wall. The core solidifies less rapidly and during this phase the packing pressure plays an important role in the core orientation of the produced part. The differences in sound delay were also correlated with the measured thickness of the produced parts. For a mould temperature varying from 30 to 60 °C the increase in thickness ranged from 4.00 to 4.01 mm.

In Fig. 4 the amplitude of the received ultrasound signal from the start of the filling phase exhibits a near linear rise for the first 5 s. It then approaches a steady state level immediately after the packing phase and remains roughly constant for most of the cooling phase. During the cooling phase small changes occur in the molecular properties of the polymer. At the end of that phase the sudden attenuation of the received signal indicates that the part has detached from the mould wall as the amplitude decays to zero.

Similar behaviour in the sound delay and amplitude variation was also observed in the moulding of PC. However, changes in sound delay were less observable (<0.015 μs compared with those for PP moulding, which were around 0.05 μs) at mould temperatures of 80 up to 110 °C. The amplitude of the received signal follows a different pattern during solidification, which reflects the cooling behaviour of amorphous materials. Cooling time is much shorter compared with moulding of PP since no crystal formation takes place in amorphous polymers.

In Fig. 5 the correlation coefficient between successive reflected signals during the injection cycle of PC is plotted alongside the cavity pressure profile.

Major variations in the correlation coefficient that occur during the injection cycle characterize most of the phases, such as:

(a) mould closing (first peak: interfaces change);
(b) end of filling and transition to packing phase (2nd peak);
(c) packing phase (coefficient decays to 1);
(d) end of cooling and part detachment from the wall (3rd peak).

The major changes in the reflected signals are due to the molecular changes that take place early in the packing phase.

3.2 Temperature data analysis

In the filling stage the molten plastic enters the cavity and a thermal shock is created at the mould walls. Both thermocouples embedded close to the cavity wall accurately track this transient, as shown in Fig. 6. At the same time as the internal energy of the mould increases, the heat conducted from the first to the second thermal section decreases.

The first thermocouple, which is closer to the interface (wall/PP), receives the thermal flow transient first. These experimental temperature data are processed in real time and the extent of solidification is predicted. The model given by equation (2) assumes that both thermocouple readings start from the same set point.

In Fig. 7 the extent of solidification for the injection moulding of PP is shown for different mould temperatures. The pattern of the extent of solidification for most cases (mould at 30 up to 60 °C) is mainly the same since no external cooling is used for the mould. Given that the

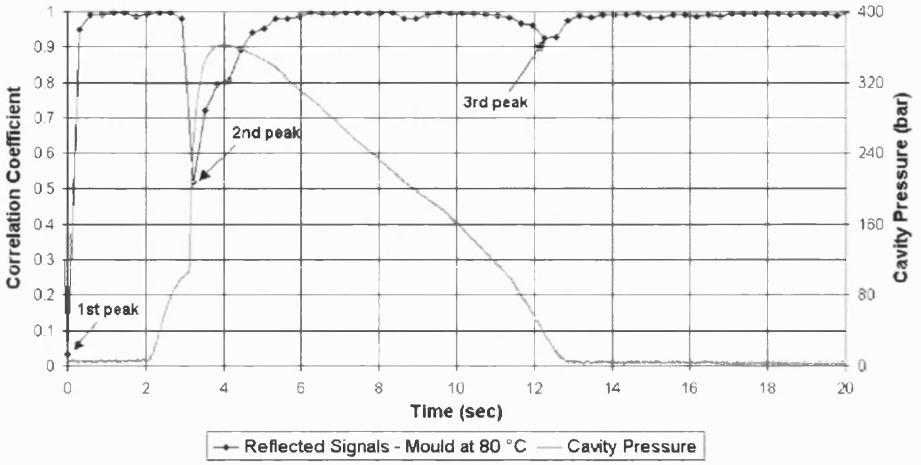

Fig. 5 Correlation coefficient between successive reflected signals during the moulding of PC at 290 °C

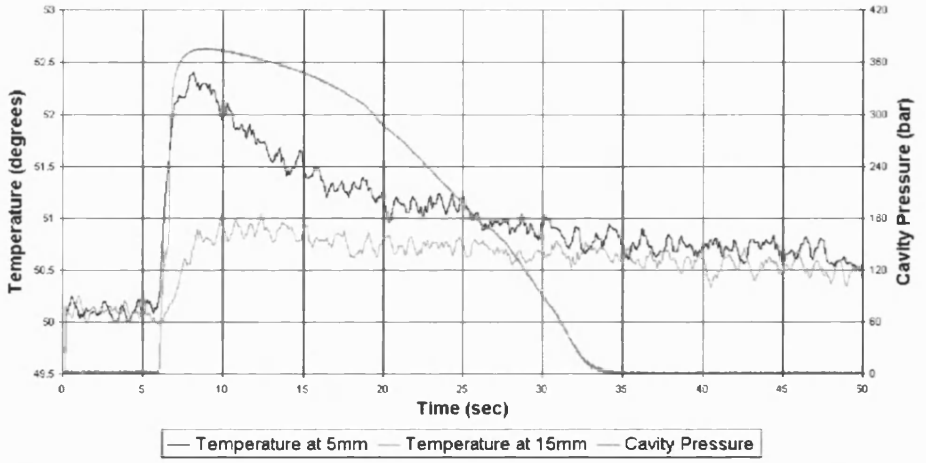

Fig. 6 Thermal transients near the cavity wall during the injection of PP at 200 °C versus cavity pressure

mould is symmetrical, the model predicts the solidification of the half-part (2 mm). The part can be safely ejected when:

(a) the extent of solidification reaches 100 per cent of the part thickness;
(b) the temperature gradient of the mould reaches the steady state condition of the preset temperature level (30 up to 60 °C).

3.3 Comparison of the two methods

The ultrasound and thermocouple methods used to monitor the in-mould parameters and track the phase changes were very reliable. In Fig. 8 the extent of solidification [see equations (2) and (3)] of the produced part (PP at 200 °C and mould at 50 °C) is estimated using (a) the average ultrasound speed and (b) thermal changes that predict the heat being transferred to the mould.

The solidification results of two predictions show a small disparity due to the position of the sensors (Fig. 1) in each method. The thermocouples were placed near the gate at the injection point while the ultrasound sensors were on the other side. Consequently, the part side, which is near the hot gate, takes longer to cool compared with the other side, which has no thermal influence.

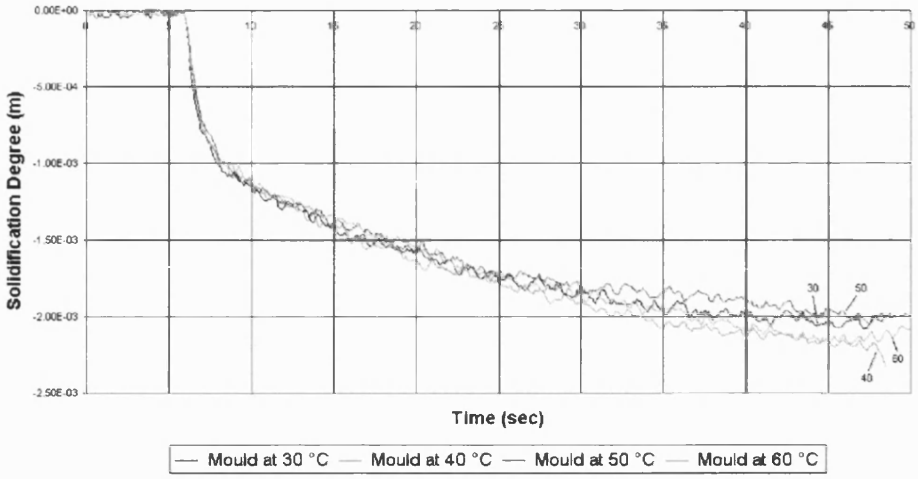

Fig. 7 Extent of solidification for the produced parts during the injection moulding of PP at 200 °C

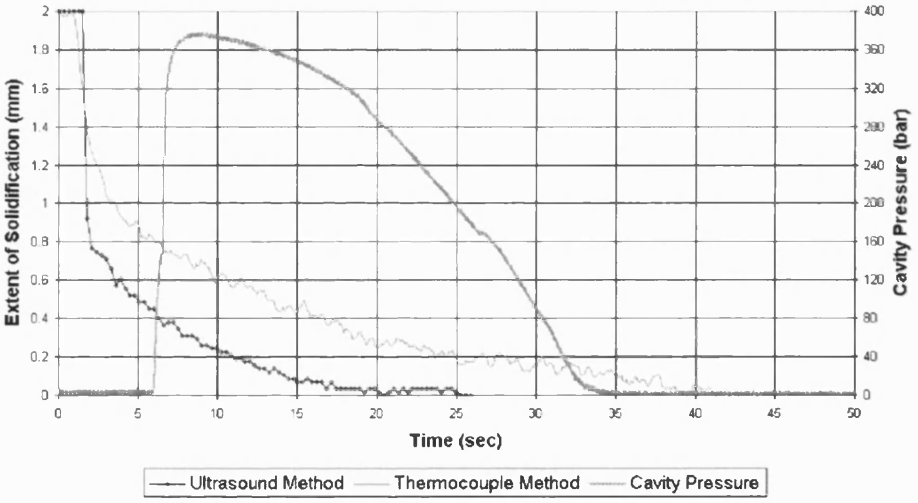

Fig. 8 Extent of solidification of the part—comparison of the two methods

4 CONCLUSIONS

The polymer molten behaviour during the injection cycle has been evaluated based on real-time ultrasound and temperature data.

Ultrasound measurement has proved to be a powerful method used to characterize the polymer rheological behaviour and the physical dimensions of the produced part. The development of an off-line data processing algorithm helped to process the data efficiently and produce meaningful results. Trajectories and transition of phases that can be used for control purposes were precisely identified (Fig. 5) and compared with cavity-based pressure profiles. Ultrasound sensors can be easily placed in any mould position to extract information about cycle changes, especially in complex shape cavities. Overall they have an advantage in moulds where cavity pressure sensors are not desirable for aesthetic reasons.

On the other hand, the use of thermocouples is an economic and reliable method, which provides sufficient information for determining the extent of solidification

of the produced part (in real time, see Fig. 7), thus reducing the cycle time. They can also be used for control of the packing pressure, if it is desired to control packing pressure as a function of the degree of solidification.

ACKNOWLEDGEMENTS

The authors would like to acknowledge Dr Victor Humphrey in the Department of Physics at the University of Bath for his input in the experimental design of the ultrasonic measurement system.

REFERENCES

1 **Wang, H., Cao, B., Jen, C. K.** and **Nguyen, K. T.** On-line monitoring of the injection moulding process. *Polym. Engng Sci.*, 1997, **37**(2), 363–376.

2 **Edwards, R., Thomas, C. L.** and **Bur, A. J.** On-line monitoring of polymer orientation during injection moulding. *Polym. Engng Sci.*, 2001, **41**(9), 1644–1653.

3 **Sahnoune, A., Hamel, A.** and **Piche, L.** Ultrasonic characterization and rheology of polymer foams. In Proceedings of ANTEC Annual Technical Conference, 1998, Vol. 2, pp. 1927–1930.

4 **Brown, E. C., Collins, T. L. D., Dawson, P. O.** and **Coates, P. D.** Ultrasound: a virtual instrument approach for monitoring of polymer melt variables. *J. Reinforced Plastics and Composites*, 1999, **18**(4), 331–338.

5 **Stelson, K. A.** Estimating the extent of solidification for polymer injection moulding. University of Bath Internal Report 17, 2001, pp. 1–14.

6 **Stelson, K. A.** Calculating cooling times for polymer injection moulding. *Proc. Instn Mech. Engrs, Part B: J. Engineering Manufacture*, 2003, **217**(B5), 709–713.

7 BS EN ISO 527-2, 1996 *Plastics—Determination of Tensile Properties—Part 2: Test Conditions for Moulding and Extrusion Plastics*, 1996 (British Standards Institution, London).